Graph theoretical analysis of braided rivers

Gabriel Connor-Streich

Submitted in partial fulfilment of the requirements of the Degree of Doctor of Philosophy

School of Geography, Queen Mary University of London

Statement of originality

I, Gabriel Max Connor Streich, confirm that the research included within this thesis is my own work or that where it has been carried out in collaboration with, or supported by others, that this is duly acknowledged below and my contribution indicated. Previously published material is also acknowledged below.

I attest that I have exercised reasonable care to ensure that the work is original, and does not to the best of my knowledge break any UK law, infringe any third party's copyright or other Intellectual Property Right, or contain any confidential material.

I accept that the College has the right to use plagiarism detection software to check the electronic version of the thesis.

I confirm that this thesis has not been previously submitted for the award of a degree by this or any other university.

The copyright of this thesis rests with the author and no quotation from it or information derived from it may be published without the prior written consent of the author.

Signature:

Date:

25/02/2019

Details of collaboration and publications:

Connor-Streich, G., Henshaw, A.J., Brasington, J., Bertoldi, W. and Harvey, G.L., 2018. Let's get connected: A new graph theory-based approach and toolbox for understanding braided river morphodynamics. Wiley Interdisciplinary Reviews: Water, 5(5), e1296.

Abstract

Braided rivers are one of the most complex and unpredictable natural systems on Earth. Found worldwide, they are easily identified from above by their distinctive morphology (a large network of interlinked channels divided by interspersed sedimentary deposits). Their propensity to dramatically adjust their form during flood events impacts upon millions of people who interact with them. However, their size and the intensity of processes that are active during these episodes of morphological change have presented considerable barriers to the measurement, understanding, prediction and management of braided river behaviour. This research has begun to resolve these issues through the successful development of a new theoretical framework for the study of braided river evolution based on graph theory (a branch of mathematics concerned with network structure and function). Leveraging a recent upsurge in open-access Earth observation data provision, it is now possible to extract network representations of braided rivers globally from satellite imagery. A workflow for the extraction of braided river networks from multi-spectral remotely sensed imagery is described herein, with these networks providing the basis for graph analysis. A key question in network research is how to define functional units, which in the context of braided rivers are reaches. Defining reaches has previously been done arbitrarily, which likely negates key controls that determine the spatial scales over which braided river morphologies evolve. This research proposes a new, physically-based approach to defining reaches in braided rivers that accounts for spatial scaling and network structure. Evolution of braided river morphologies at the reach-scale or greater occurs over timescales that range from event-based change to long-term trajectories of change in the whole braided channel network. Analysis of the topological evolution of a braided channel network is presented to show spatio-temporal variation in connectivity and how this relates to braided river morphodynamics.

Acknowledgements

I would first and foremost like to thank my supervisors, Dr Alex Henshaw and Dr Gemma Harvey, for giving me the opportunity to complete this PhD and for their mentoring and support throughout the process, and throughout my higher educational career. Thanks to Dr Walter Bertoldi and Professor James Brasington for their constructive input to various elements of this PhD, as well as to the first publication to come from it. And I'd also like to thank Shazia Sadiq for her administrative assistance, even in the face of my occasional lack of organisational ability. I should also mention my office mates, who provided light relief when it was needed, and sometimes when it wasn't.

A shout out has to go to my big bro, Kim, for constantly telling me to get a real job and thus redoubling my efforts to continue in education till its logical conclusion. My parents, Lori and Jude, thanks for the continued support and always telling me that I could do this; and Jude, thank you for so much for proofreading and catching the bits where all I could see was trees. Voland the cat deserves some credit for giving me some perspective; as important as I may have thought writing-up was, his dinner was consistently a much bigger concern. I owe the largest debt of gratitude to my partner, Lauren, for her support, the pizzas and keeping me sane throughout the process of writing this thesis. And a final mention will be given to Douglas J. Adams and The Hitchhikers Guide to The Galaxy, which provided a healthy dose of surreality at the end of a long day's reality.

Table of Contents

Table of Figures

List of Tables

List of Abbreviations

BI	Channel-count braiding index
E_{glob}	Global efficiency
CP	Central pathway
CPS	Central pathway sinuosity
m	Number of edges in network
BC	Betweenness centrality
eBC	Edge betweenness centrality
nBC	Node betweenness centrality
neBC	Normalised edge betweenness centrality
nnBC	Normalised node betweenness centrality
$C^s(i)$	Straightness centrality
AWW	Average wetted width at channel forming flow
AW	Active width
WW	Wetted width
BW	Braid wavelength
Q	Discharge
CV	Coefficient of variation
ABMs	Agent-based models
OBIA	Object-Based Image Analysis
MLC	Maximum likelihood classification
MNDWI	Modified Normalised Difference Water Index
NDVI	Normalised Difference Vegetation Index
SWIR	Shortwave infrared
NIR	Near-infrared
AWEI	Automated Water Extraction Index
D_{50}	Sediment particle diameter representing the 50% cumulative percentile of a sediment sample, e.g. 50% of sediment grains in a sample are smaller than D_{50}.
AOI	Area of interest

1. Introduction

1.1 Braided rivers and their associated management problems

Braided rivers are one of the most dynamic Earth surface systems, representing an end member on the continuum of river channel patterns (Kleinhans, 2010) that is prone to rapid and often high magnitude morphological change (Ashmore, 2013). The largest of these systems, such as the Jamuna River, Bangladesh, can span hundreds of kilometres in length, be over 10 km wide and erode thousands of hectares of floodplain on an annual basis, impacting tens of thousands of people (Sarker *et al.*, 2014). Exceptional rates of erosion and deposition creates significant problems for the engineering of bridges and other braided river floodplain infrastructure (Bristow & Best, 1993). A lack of understanding of braided river processes has often led to their mismanagement, with varying effects. On the River Waiho, New Zealand, river training works are responsible for exacerbating aggradation, resulting in super-elevation of the Waiho's bed to more than 10 m above its floodplain in some locations and causing a significant flood risk (Davies *et al.*, 2013). This risk came to fruition in 2016, when the Waiho temporarily avulsed and severely flooded the tourist town of Franz Josef.[1] Combinations of channel- and catchment-scale anthropogenic activity resulting in changes to sediment supply and transport regimes have also caused many European braided rivers to reduce their braiding intensity significantly or even transition to wandering or meandering planforms, resulting in the loss of rare and diverse ecological habitats (Surian, 1999; Surian & Rinaldi, 2003; Gurnell *et al.*, 2009; Belletti *et al.*, 2015; Kidová *et al.*, 2016).

The rarity of braided rivers is due to the conditions under which they form, requiring unconfined valleys with large inputs of unconsolidated sediment to streams that have an excess of stream power capable of supporting significant sediment transport (Ashmore, 2013). These conditions are found largely in Alpine and Piedmont environments, restricting the geography of braided rivers. Catchment-scale controls on sediment supply, the input of organic matter and discharge have marked influences on fluvial morphodynamics (Gurnell *et al.*, 2009; Charlton, 2010). In braided rivers, discharge variability is not a prerequisite of braiding (e.g. Egozi & Ashmore 2009; Murray & Paola 1994), but the general geography of braided rivers often results in flashy

---

[1] Current reporting of this incident is limited to media stories, e.g. https://www.nzherald.co.nz/nz/news/article.cfm?c_id=1&objectid=11611183.

hydrographs and a considerable influence of flood flows on morphodynamics (e.g. Bertoldi, Gurnell *et al.*, 2009). These factors combine in highly dynamic systems where the emergent geomorphic properties are characterised by an ephemeral ensemble of channels and bars that evolve due to interactions between the aforementioned allogenic controls and an array of autogenic processes (Bristow & Best, 1993; Ferguson, 1993; Ashmore, 2013).

1.2   The complexities of controls on braided rivers morphodynamics

The emergent form of braiding results from interactions in processes from the particle- to the catchment-scale. It has been shown how hydrodynamics can impact the hydraulics of sediment transport, causing the deposition of mid-channel bars and channel bifurcation (Engelund & Skovgaard, 1973; Richardson & Thorne, 2001).   Field studies and hydraulic and numerical modelling have been used to show how the dynamics of bifurcations and confluences are linked to the geometries and bed topography of their upstream and downstream channels, as well as the migration of alternate bars and unit bars (Best & Roy, 1991; Bolla Pittaluga *et al.*, 2003; Bertoldi & Tubino, 2007; Kleinhans *et al.*, 2008; Szupiany *et al.*, 2009; Hardy *et al.*, 2011; Thomas *et al.*, 2011; Bertoldi, 2012; Marra *et al.*, 2014). This research has shown that bifurcations and confluences are fundamentally unstable and contribute to the continuous evolution of the braided channel network. Bifurcations and confluences are often linked through confluence-bifurcation units, which show typical length scaling in a similar manner to the bars around which these units form (Ashmore, 2009; Hundey & Ashmore, 2009). Bifurcation-confluence units link the dynamics of confluences and bifurcations such that the attendant morphodynamic processes occurring at the scale of single bifurcations and confluences result in the spatially variable patterns of erosion and deposition that drive reach-scale braided river morphodynamics (Ashworth & Ferguson, 1986; Kollmann *et al.*, 1999; Bertoldi *et al.*, 2010; Ashworth *et al.*, 2011; Welber *et al.*, 2012; Wheaton *et al.*, 2013).

In braided rivers that support the establishment of vegetation on bars, reach-scale morphodynamics can also be heavily influenced by the accretionary and stabilising effect of vegetation (Gurnell *et al.*, 2001; Zanoni *et al.*, 2008; Bertoldi, Drake *et al.*, 2011). The conditions that support the establishment of vegetation on exposed surfaces in braided rivers are heavily impacted by local groundwater hydrology, such that different locations along the course of a braided river may support different levels of vegetation growth (Gurnell *et al.*, 2001; Corenblit *et al.*, 2014). This emphasises the spatial heterogeneity of certain factors that influence braided river morphodynamics at larger than reach-scales.   Indeed, it is longer-term changes in

catchment land use, sediment supply, river training works and variable discharge regimes that provide overarching controls and determine the system-scale evolution of braided rivers (Ferguson, 1993; Belletti *et al.*, 2015).

1.3 Current approaches and new opportunities for the study of braided rivers

Our understanding of braided river morphodynamics comes from a large body of field and modelling studies. Controlled experiments using hydraulic (aka physical) models have elucidated various aspects of braiding processes, including fundamental mechanisms that result in braided planforms (e.g. Ashmore, 1991b). Different styles of hydraulic model include single bifurcations or confluences with fixed banks and bed (e.g. Best & Roy, 1991; Thomas *et al.,* 2011) and large flumes with unconstrained and fully mobile beds from which braided channel networks can develop (e.g. Bertoldi *et al*. 2014; Garcia Lugo *et al*. 2015). These experiments with hydraulic models have been used to probe an array of braided river processes, from hydrodynamics in bifurcations and confluences to the storage and remobilisation of large woody debris. Advances in process knowledge of braided river morphodynamics has, to a lesser extent, also been provided by numerical modelling (Ashmore, 2013). The most commonly used numerical models are reduced complexity models (RCMs; Brasington & Richards, 2007) and physics-based models (PBMs; Williams *et al.*, 2016). RCMs can replicate reach-scale statistical properties of braiding over spatio-temporal scales relevant to the large scale evolution of braided networks (Murray & Paola, 1994; Doeschl-Wilson & Ashmore, 2005; Brasington & Richards, 2007; Ziliani *et al.*, 2013). PBMs can simulate extremely detailed hydrodynamic and hydraulic processes and their impact on braided morphologies, but are somewhat limited by computational demand (Crosato & Saleh, 2011; Williams *et al.*, 2016). Field surveys provide the other main approach to braided river research and have been instrumental in developing our understanding of reach-scale morphodynamics. Particular attention should be paid to the considerable advances in 3-D survey techniques such as terrestrial laser scanning (Brasington *et al.*, 2012), structure-from-motion photogrammetry (Westoby *et al.*, 2012) and the fusion of 3-D sub-aerial surveys with bathymetric mapping to derive surface models covering both wet and dry surfaces in braided reaches (Williams *et al.*, 2015).

Field and modelling studies may have provided major advances in our knowledge of braided river processes, but these methods are all limited to some degree by spatial and temporal scaling. Hydraulic models would need to be unfeasibly large to model prototype rivers at the

scale of the whole braided channel network (Young & Warburton, 1996). Field surveys are limited either by spatial scale for ground-based approaches or often by cost for airborne survey techniques and in both cases, temporal limitations are presented by the need for repeat surveys. Numerical models may overcome the limitations of hydraulic models and field surveys, but are limited by our a lack of datasets for validating their results (Williams *et al.*, 2016), especially at larger scales. The recent release of NASA's Landsat archive (Woodcock *et al.*, 2008) and the launch of ESA's Sentinel missions (Berger *et al.*, 2012), as well as other higher spatial resolution proprietary datasets, now provide a possible solution to the problem of spatial and temporal coverage.

The Landsat missions provide near-continuous global coverage on a 16-day repeat cycle from the 1980s (Henshaw *et al.*, 2013) and with a 30 m spatial resolution, the imagery is detailed enough to resolve channel networks in medium to large braided rivers. A few recent studies have used the Landsat archive for geomorphic analyses of braided rivers at large (10s km) spatial scales (Takagi *et al.*, 2007; Henshaw *et al.*, 2013; Marra *et al.*, 2013; Ashraf *et al.*, 2016), though these studies were limited in their temporal depth, resolution or both and they applied traditional, per-pixel image classification methods to extract channel networks and other landcovers of interest. It has been suggested that Object-Based Image Analysis (OBIA) approaches to image classification may provide a significant advance on per-pixel methods (Blaschke *et al.*, 2014), however applications of OBIA to braided rivers have thus far been limited (e.g. Belletti *et al.*, 2015). Rapid, accurate classification procedures are key to unlocking the potential of satellite data archives and enabling multi-spatial and multi-temporal analysis of braided river geomorphology, globally. There is also a need, however, for an analytical framework to maximise the information that can be extracted from these new datasets.

1.4 Connecting the dots: the emergence of connectivity research in the geosciences and its potential for braided river research

Research has shown that changes in the spatial locations of erosion and deposition can be connected to changes in braided river morphology at proximal locations (Ashworth *et al.*, 2000) and that these linked changes can cascade downstream (Takagi *et al.*, 2007; Schuurman *et al.*, 2016). An emerging body of work is emphasising that this connectivity is key to understanding the way Earth surface systems behave (Bracken *et al.*, 2013; Heckmann *et al.*, 2015; Phillips *et al.*, 2015; Passalacqua, 2017; Wohl *et al.*, 2017, 2019; Rinderer *et al.*, 2018; Turnbull *et al.*, 2018). Key questions in the study of connectivity in complex systems are how to define fundamental

units within a system and how to measure connectivity between these units (Turnbull *et al.*, 2018). In braided rivers, the structure of the network lends itself intuitively to analysis using graph theory (Figure 1.1), the branch of mathematics concerned with quantifying the structure of networks and that intrinsically captures various aspects of a system's connectivity.

Graph theory represents networked systems as a collection of nodes, which are some element of the system, and edges, the connections between the elements (Newman, 2010). In multi-channel river systems, bifurcations and confluences represent the nodes and their connecting channels are edges. This analytical framework has seen numerous recent applications to river deltas for the quantification of network structure and function (Tejedor *et al.*, 2015a, 2015b, 2017, 2018; Passalacqua, 2017; Sendrowski & Passalacqua, 2017). Applications of the graph theory framework to braided rivers have been less numerous, with studies by Howard *et al.*, (1970) and Webb (1995) using topological metrics to describe global properties of network structure that provide similar data to traditional braiding indices. Lehotský *et al.*, (2018) took a graph theory approach to quantify sediment connectivity between bars in a wandering-braided river, though their approach provides a reach-averaged index of connectivity at best. Marra *et al.*, (2013) present the only study, thus far, to have combined satellite image processing with graph theory to analyse braided channel network structure using a fully distributed, channel-scale metric of connectivity, at the scale of the whole channel network. This study was innovative and highlighted the potential of graph analysis for braided river research. However, their work was temporally limited to a short time period that did not capture any large floods, provided limited assessment of the range of available metrics, applied only one suitable graph theory metric and performed little analysis on the spatial distribution of this metric across the channel network. There is clearly considerable room for development of graph theory and its application to braided rivers, both in terms of methods for extracting networks from satellite imagery and in the development of a set of analytical tools drawn from the wide array of different metrics available within the graph theory framework.

1.5 Thesis aims and objectives

The spatial and temporal limitations inherent in present approaches to braided river research means that significant gaps in our understanding of braided river processes exist. These gaps are particularly evident in our capacity to predict the evolution of natural braided rivers, presenting considerable problems for river management and conservation. As such, the core aim of this thesis is to:

Address the spatio-temporal limitations of current approaches to studying braided rivers through the development and application of a novel toolbox of metrics for quantifying braided river network structure and function based on graph theory.

This core aim has been broken down into the following goals:

1. Identify a toolbox of graph theory metrics relevant to braided river morphodynamics based on critical, inter-disciplinary analysis of network research across a range of sciences.

2. Test the utility of OBIA for image classification of braided channel networks to support the extraction of braided river network graphs from satellite imagery.

3. Address a key question in connectivity-based research: how to define fundamental units at different hierarchical levels of system organisation? Or in the case of braided rivers, how should we define a reach when working at the scale of the whole channel network?

4. Apply graph theory-based analysis to a multi-spatial, multi-temporal dataset encompassing a range of different flood magnitudes known to cause varying levels of morphological change in a braided river.

To address these goals, the following objectives were set:

Goal 1:

- Complete a critical survey of network science literature to identify metrics from graph theory with possible relevance to braided rivers;

- Synthesise this survey with research on braided river geomorphology to provide recommendations for the possible applications of graph theory to braided river research.

Goal 2:

- Develop image classification routines using OBIA for rapid extraction of braided river channel networks from satellite imagery;

- Test the accuracy of the OBIA classifications against traditional, per-pixel methods of image classification;

- Develop a workflow to enable the extraction of graph representations of braided channel networks from classified satellite imagery.

Goal 3:

- Define different spatial frameworks for the delineation of braided river reaches, based on traditional, arbitrary reach lengths, reach lengths scaled on channel geometry and reach lengths defined by network topology;

- Test the impact of the different spatial frameworks on the quantification of braiding using a simple channel-count braiding index and assessing change in the braiding index over different magnitudes of flood event;

- Assess the strength of relationships between braiding intensity and physical controls on braiding under each of the reach frameworks.
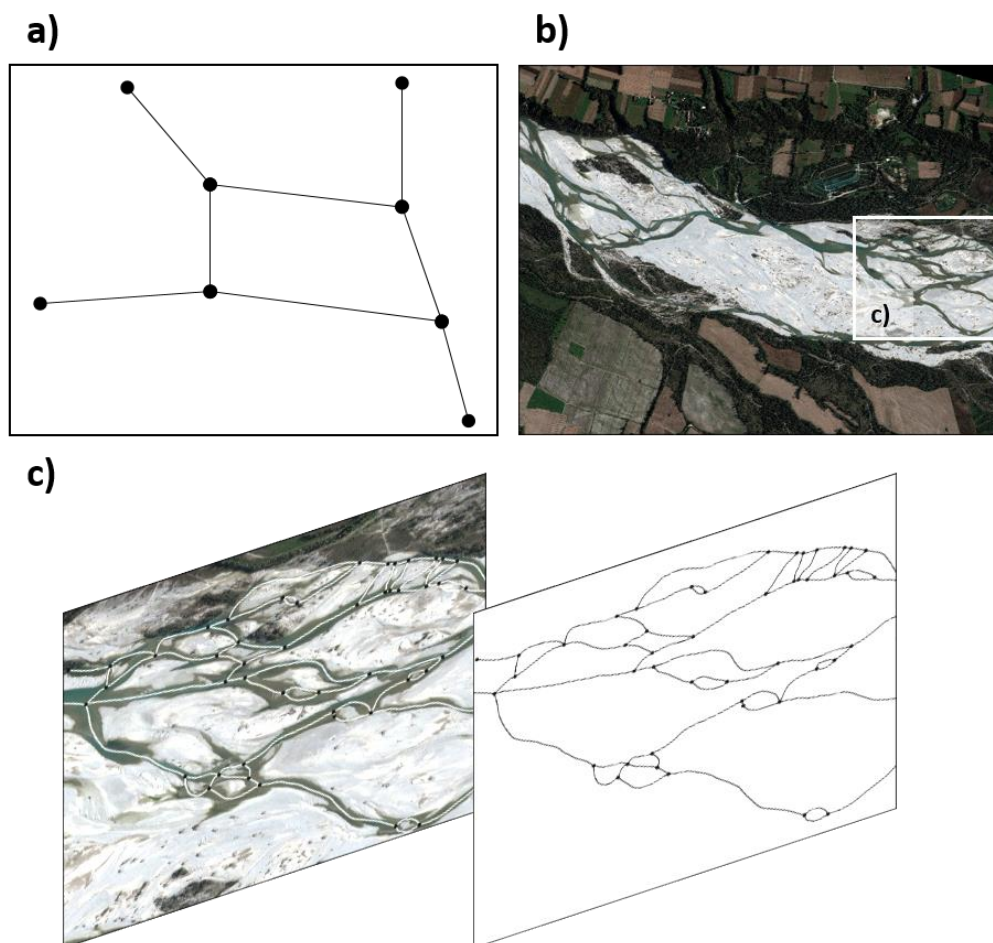
Figure 1.1: a) hypothetical example of a network graph; b) a braided section of the Fiume Tagliamento, Italy with the area in the square expanded in c) an intense area of braiding and its associated network graph.

Goal 4:

- Derive a series of braided river graphs covering a period of decades and multiple flood events of varying magnitude;

- Assess the spatial and temporal variation in graph theory metrics in response to different magnitude flood events.

1.6 Thesis structure

The overall thesis structure is presented in (Figure 1.2). This shows how the different chapters and the work associated with them feed into each other. A brief synopsis of each chapter and its relation to the rest of the thesis is given below.

Chapter 2 – Past, present and future developments in fluvial and braided river geomorphology

This chapter is based on a wide-ranging literature review that begins with the development of quantitative methods and the reductionist paradigm in geomorphology. These developments set the context for a summary of our understanding of braided river processes at multiple scales, from the scale of interactions between hydrodynamic and hydraulic processes that can initiate bar deposition and braiding, to the controls on morphodynamics at the system-scale. A review of methods for the study of braided rivers highlights deficiencies in our current array of tools for the study of braiding, which feeds into chapter 4's analysis of techniques for the extraction of graph representations of braided rivers.

Chapter 3 – Let's get connected: A new graph theory-based approach and toolbox for understanding braided river morphodynamics

This chapter presents an edited version of Connor-Streich *et al*. (2018), which makes the case for the application of graph theory to braided river research. Founded on inter-disciplinary reading across fields of network science from neuroscience to transportation, analogies between the properties of various networks and braided rivers are used to highlight the potential of graph theory for braided river research. A critical analysis of different metrics was conducted to determine a graph theory-based toolbox that can be applied to the quantification of braided river network structure across multiple scales. Synthesising this critical analysis with current knowledge of braided river morphodynamics, suggestions are given as to possible

applications of graph theory to braided river research. This chapter provides the theoretical backbone to applications of graph theory in chapters 5 & 6.
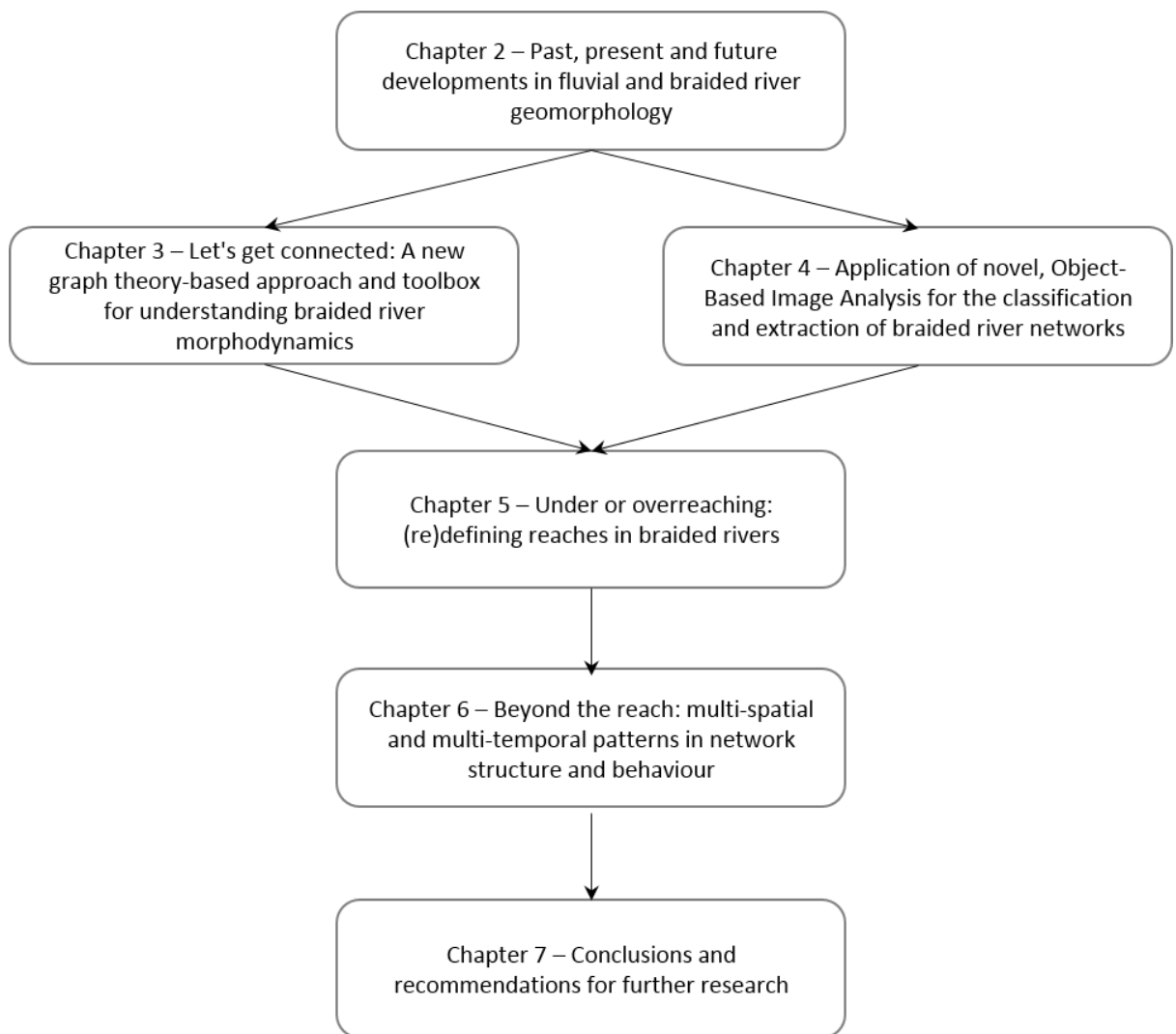
Figure 1.2: Thesis structure diagram

Chapter 4 – Application of novel image classification techniques to support braided river network extraction

The application of graph theory to braided rivers requires the extraction of network graphs of their channel networks. Satellite image archives provide a data source from which braided channel networks can be extracted, however this requires a geoprocessing workflow combining raster image classification and vectorisation procedures. Raster image classification has traditionally been done using "per-pixel" methods, but a potentially more powerful, object-based approach is increasing in usage within GIScience (Blaschke *et al.*, 2014). The performance

of OBIA is tested against per-pixel methods for the classification of braided channel networks, bare gravel and vegetation. A semi-automated workflow is then developed, detailing the vectorisation of the channel network and extraction of information on the connectivity of network elements (channels, bifurcations and confluences). The extracted channel network is evaluated against the geometrical properties of a reference dataset. Outputs from this chapter provide the data inputs to chapters 5 & 6.

Chapter 5 – Under or overreaching: (re)defining reaches in braided rivers

Reaches are the most ubiquitous spatial units in fluvial geomorphology, used as a means to divide a largely continuous system into more manageable chunks from which aggregate geomorphic properties can be derived. In most cases, reach lengths are defined arbitrarily and thus may neglect some nuance of the spatial configuration of a river that does not conform to an arbitrary reach length. This chapter seeks to define a new approach to delineating reaches in braided rivers, based on properties of the system rather than an arbitrary length designation. A traditional, arbitrary 1 km reach framework is tested against reach lengths determined by scaling the average wetted width of the channel network at two channel forming flows, and variable reach lengths that are set by the underlying topology of the network using a graph theory-based algorithm designed to determine network community structure. The performance of these different reach frameworks was tested by assessing the spatial variation in a channel-count braiding index in networks separated by varying magnitudes of flood events and in bivariate relationships between the braiding index and reach-scale physical variables. Recommendations are provided in terms of future approaches to reach definition in braided rivers and the findings feed into the multi-spatial analysis of braided river structure presented in chapter 6.

Chapter 6 – Beyond the reach: flood driven responses in braided river network structure and behaviour at multiple scales

The dynamics of braided rivers are determined by complex interactions between processes acting at micro- to catchment-scales. Previous studies of braided river morphodynamics tend to focus on one spatial scale, e.g. single bifurcations or confluences, bars or the reach. Graph representations of braided rivers allow analysis at nearly any scale, from single bifurcations to the whole channel network. Using this unrestricted spatial framework, a series of networks from the Fiume Tagliamento, Italy, that are separated from one another by a range of different magnitude flood events, are analysed to assess patterning in the spatial distribution of a

normalised edge betweenness centrality (*neBC*), which measures the connectivity of single channels. Changes in the spatial distribution of *neBC* in response to different magnitude flood events are also analysed and linked to planform dynamics. Finally, two new metrics not previously applied to braided river research are tested. These metrics quantify network scale change in the sinuosity of the most highly connected pathway through the network and provide a new measure of global network structure based on the network's topology. The findings from this chapter highlight key flaws in the traditional braiding indices used for planform analysis and the need for a spatially distributed approach to studies of braiding.

Chapter 7 – Conclusions and recommendations for further research

Key findings from this thesis are presented in the context of both the core aim and research goals that underpinned this work. These findings highlight the potential of graph theory for braided river research but also underline the significant amount of further research that is required. Some suggestions for further research have been provided.

1.7 The Fiume Tagliamento: a natural laboratory for the study of braiding

1.7.1 Physical and biogeomorphological characteristics of the Fiume Tagliamento

The primary study site for the research presented herein is the Fiume Tagliamento, Italy (Figure 1.3). Standing against the declining trend in Europe's braided rivers (Gurnell *et al.*, 2009), the Tagliamento has remained largely free of intensive management (Gurnell *et al.*, 2000). Anthropogenic activities on the river include minor water diversions for hydropower generation, some river training works and gravel mining (Bertoldi *et al.*, 2010), the latter activity having likely the greatest effect on the rivers morphology (Ziliani & Surian, 2012). However, anthropogenic impacts on the Tagliamento are minor and it supports a floodplain woodland riparian zone along the majority of its 170 km length, has seen no significant variation in flows resulting from regulation or abstraction and, despite some check dams on steeper tributaries to manage sediment inputs, is largely in good connectivity with catchment sediment sources (Gurnell *et al.*, 2000). As such, the Tagliamento presents one of the few near-pristine examples of a medium-sized braided river left in Europe, providing a rare fluvial environment and natural "laboratory" for the study of braided river morphodynamics (Bertoldi, Gurnell *et al.*, 2009).

With a main stem rising at approximately 1200 m a.s.l., the Tagliamento's funnel shaped catchment covers an area of about 2580 km^2 (Bertoldi, Gurnell *et al.*, 2009). The morphologically active area of the river's main stem covers an area of ~150 km^2 (Bertoldi *et al.*, 2010) and it follows a stepped profile with bedrock narrows separating wide, gravel filled basins in the upper to middle course, before flowing over a wide plain between Pinzano Gorge and the coast (Figure 1.3; Henshaw *et al.*, 2013). Width variation of the active braidplain is significant, varying from ~150 m to 1.5 km (Welber *et al.*, 2012; Henshaw *et al.*, 2013) due to bedrock constrictions, the influence of vegetation and floodplain topography. The Tagliamento is classed as a gravel-bed river and shows marked downstream sediment fining (Petts *et al.*, 2000). Over the 72 km stretch of the Tagliamento that is the focus of this research (Figure 1.3), D_{50} is in the range of cobbles to medium gravel, with most reaches having D_{50} in the very coarse to coarse gravel categories. Sediment entrainment shows high local variability due to the complex topography of the braidplain that causes low elevation areas to experience much greater flood disturbance (Mao & Surian, 2010). This topography is also heavily impacted by vegetation, with the active channel network variously flowing around exposed gravel bars and vegetated islands and reaches being classified as bar- or island-braided, dependent on vegetation densities (e.g. Van Der Nat *et al*. 2002).

1.7.2 An overview of the Fiume Tagliamento's hydrology

There is a strong climatic gradient across the 170 km length of the river, transitioning from alpine to Mediterranean, which results in a flashy, pluvio-nival flow regime (Figure 1.3; Gurnell *et al.*, 2001). Discharge is highest in spring and autumn, with low flow periods from December to February and in August (Gurnell *et al.*, 2001). Average discharge estimated from stage records at the Venzone hydrometric station (Figure 1.3) is approximately 90 m^3 s^{-1}, with the 2, 5 and 10 year floods estimated at 1100, 1600 and 2150 m^3 s^{-1}, respectively (Bertoldi, Gurnell *et al.*, 2009). Despite estimates of these key discharge statistics, no accurate stage-discharge relationship exists for the Tagliamento and thus most studies on the impact of flow on morphodynamics rely on a stage record from the Venzone hydrometer (e.g. Van Der Nat *et al.*, 2002, 2003; Bertoldi, Gurnell *et al.*, 2009; Bertoldi *et al.*, 2010; Welber *et al.*, 2012), which provides an extensive dataset of daily mean and maximum stage from 1986. Certain benchmark stages have been identified as corresponding to different levels of morphological change. Stage of ~0.65 m corresponds roughly to a discharge of 150 m^3 s^{-1}, which can cause shear stress to exceed the threshold for sediment movement (Bertoldi, Ashmore *et al.*, 2009; Bertoldi *et al.*, 2010). At stages between 1-2 m, lower amplitude bars are inundated, sediment turnover is initiated in

some inundated areas and disconnected channels and ponds begin to connect (Bertoldi, Gurnell *et al.*, 2009). Between 2-3 m stage, non-vegetated bars are inundated and connection of channels occurs across the braidplain, leaving only higher vegetated surfaces exposed and inducing large scale morphological change (Bertoldi, Gurnell *et al.*, 2009). ~3 m stage at Venzone represents bankfull conditions, with an estimated discharge of 1700 $m^3 s^{-1}$ (Bertoldi *et al.*, 2010) and a return period of 2 years (Welber *et al.*, 2012). Flows > ~3.5 m have return periods of 10 years or more and cause large scale turnover of bars and vegetated islands (Bertoldi, Gurnell *et al.*, 2009). These stage ranges will be referred to throughout this thesis in relation to analysis of flow on morphodynamics.
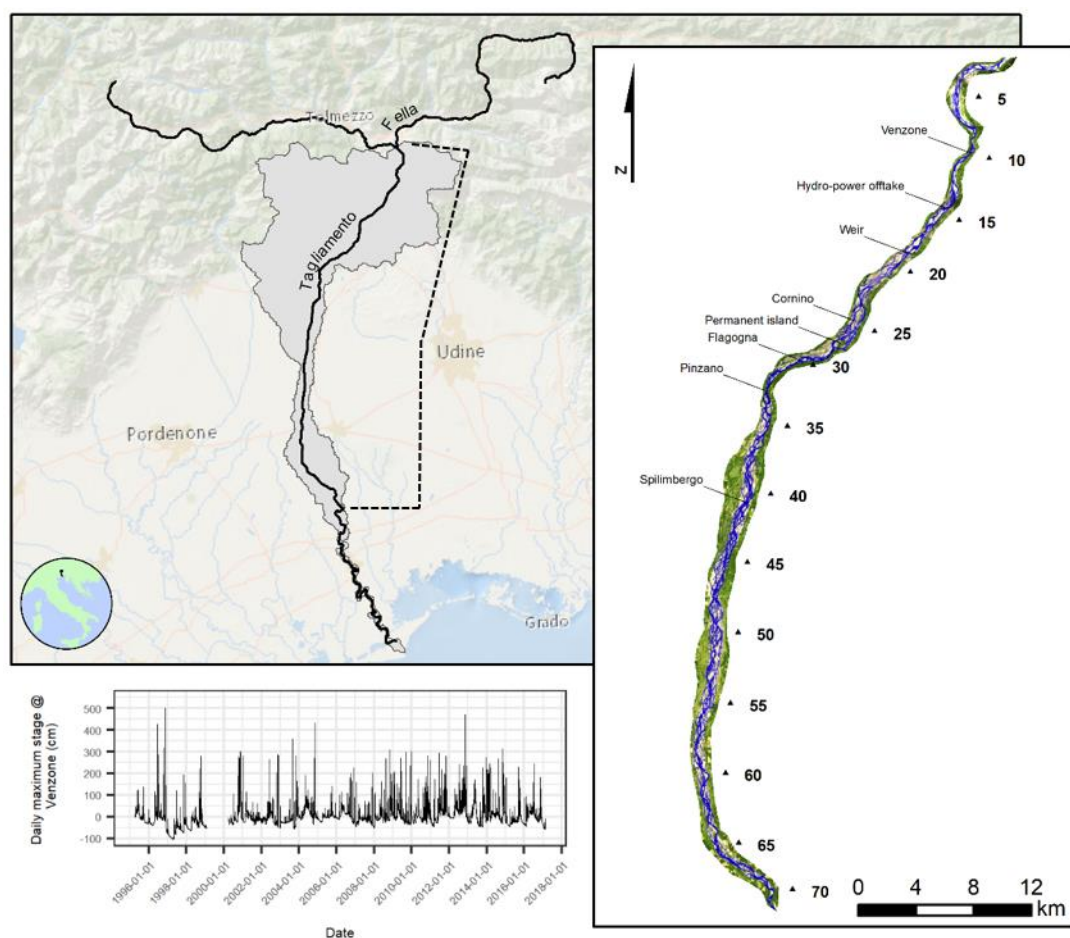
Figure 1.3: Location of the Fiume Tagliamento and Fella tributary (left). The dashed line indicates the study reach used in this research, which is enlarged in a Landsat false-colour composite that also shows the downstream positions of morphodynamically significant locations and 5 km intervals moving downstream (right). A hydrograph of daily maximum stage from the Venzone hydrometric station shows the Tagliamento's flood record over the past ~20 years (bottom left).

Whilst the stage record for Venzone is extensive, it is not complete for the whole period of study used in this research. Gaps were filled where possible by interpolating stage at Venzone from a

second stage record recorded at the Villuzza hydrometric station ~20 km downstream of Venzone. Three gaps in the Venzone record are present between 1999-2003, whilst data from Villuzza is available from early 2000, leaving a period of ~1 year with no stage data. To test the accuracy of the interpolation, the Venzone record was also interpolated for dates where Venzone has recorded data. Correlation analysis (Spearman's rank correlation as data are highly positively skewed) of the interpolated stage at Venzone with the actual stage at Venzone indicates that the interpolation is fairly accurate across the range of recorded stages (r = 0.6, p << 0.0001, n = 5477). The relationship between the interpolated and actual stage values increases in strength considerably for higher stage, with r of 0.78, 0.78, 0.85 and 0.98 (p << 0.0001, n = 117, 59, 30 and 9) for stages > 1.5, 2, 2.5 and 3 m, respectively. This indicates that the interpolated record, whilst not necessarily that accurate at lower stages, is sufficient for highlighting floods of a higher magnitude. The issues associated with the stage record at low flows stem from the consistently changing morphology of the bed at the Venzone gauge relative to the local datum against which stage is recorded and can cause negative stages to be recorded over certain periods of low flow.

Spatial and temporal variability in the presence of surface flow on the Tagliamento is strongly impacted by connectivity with its alluvial aquifer, especially at times of low flow when various stretches of the river see no surface flow at certain locations and certain times over most summers (Gurnell & Petts, 2006; Henshaw *et al.*, 2013). The presence of exposed bedrock at Pinzano Gorge and a band of silt and clay towards the downstream limit of the Tagliamento's braided section create local controls on the water table, forcing water to the surface with concomitant effects on the availability of water to support vegetation growth and on the presence of surface flow (Henshaw *et al.*, 2013; Surian *et al.*, 2015). The impact of these spatial patterns in water table depth can often be seen in satellite imagery of the whole braided channel network, where decreases in channel width and braiding intensity tend to be associated with areas where the river loses most water to its alluvial aquifer.

1.7.3 Morphodynamically significant locations on the Fiume Tagliamento

There are various specific locations along the length of the Fiume Tagliamento that exert significant local control on morphodynamics. Some of these locations are also sites that have attracted considerable research interest with a wide body of literature dedicated to understanding the morphodynamics of contrasting reaches. The 72 km reach of the braided Tagliamento that forms the primary study site for this research (Figure 1.3) incorporates these

significant locations and begins slightly upstream of the confluence between the Tagliamento and Fella Rivers. This confluence results in an increase in braiding intensity as flow increases, followed by a decrease in braiding as the river flows through a bedrock constriction at around 10 km downstream of the start of the study reach. The bedrock constriction provides a relatively stable cross-section for the location of the Venzone hydrometer (Bertoldi, Drake *et al.*, 2011). Downstream of the bedrock constriction, the braidplain widens slightly and the river begins to braid again. At around 15 km, a hydropower offtake diverts some of the river's flow and results in a relatively fixed position of the main channel against the left bank of the braidplain (left and right on the braidplain are referred to looking downstream throughout this thesis). A bridge and weir span the river just upstream of 20 km (Figure 1.3). The weir is the only significant flow control structure within the study reach and, due to its ponding effect, often appears as a wide channel orthogonal to the main flow direction. Downstream of the weir, the braidplain widens as the river flows into Cornino, the first of two heavily studied reaches. Cornino centres at around 25 km (Figure 1.3) and is described as bar-braided, with low density vegetation and high braiding intensity that peaks at intermediate flow stage (Bertoldi, Drake *et al.*, 2011; Welber *et al.*, 2012). This reach is highly dynamic, seeing significant removal of vegetation, planform change and turnover of up 45% of aquatic habitats during high flow events (Van Der Nat *et al.*, 2002; Bertoldi, Drake *et al.*, 2011; Welber *et al.*, 2012). However, based on average measurements of properties such as shoreline length and braiding indices, there is often little difference in the reach averaged composition of the active braidplain in Cornino post-flood events (Van Der Nat *et al.*, 2002).

The downstream limit of the Cornino reach is marked by a permanent bedrock island in the middle of the braidplain between 25-35 km (Figure 1.3), which exerts strong control on planform, forcing the channel network to divide around it into two parallel and close to single-thread branches. This island marks the transition into another heavily studied reach known as Flagogna, which centres around 30 km downstream (Figure 1.3). Flagogna is described as island-braided, due to groundwater hydrology that supports considerable vegetation growth and the establishment of large vegetated islands that have concomitant impacts on channel pattern and morphodynamics (Gurnell *et al.*, 2001). Vegetation turnover due to flood disturbance in the Flagogna reach is high, but the recruitment of freshly eroded trees and quick regrowth results in the vegetated percentage of the braidplain area remaining remarkably stable (Kollmann *et al.*, 1999; Zanoni *et al.*, 2008). It is this propensity to supporting higher proportions of vegetation that results in the "topographic signature" of a second peak at higher elevations in the bed elevation frequency distributions of more densely vegetated reaches (Bertoldi, Gurnell *et al.*,

2011). However, as in the case of Cornino, flood flows result in significant turnover of habitats and associated morphological change in Flagogna, though again the reach-averaged planform characteristics are relatively constant and largely dependent on stage (Van Der Nat *et al.*, 2002, 2003; Welber *et al.*, 2012).

Pinzano Gorge at around 32 km marks the downstream limit of the Flagogna reach and also the position of the Villuzza hydrometer (Figure 1.3). It is the second bedrock constrained section that forces the river to become single-thread. The unconstrained plain over which the river flows downstream of Pinzano Gorge (Henshaw *et al.*, 2013) allows the braidplain to widen, supporting high braiding intensity over the ensuing 25-30 km. This reach is less well studied, although Bertoldi *et al.,* (2011) found that their topographic signature of vegetation was also observed in the 5 km downstream of Pinzano Gorge. At around 40 km and adjacent to the town of Spilimbergo (Figure 1.3), there is an area of floodplain woodland of quite variable density due to significant signs of erosion and dissection by flood flows. This area is also often associated with larger vegetated islands in the middle of the braidplain that can influence channel planform. Between 40-60 km, periodic narrowing of the Tagliamento's active tract and the presence of bridges may have some impact on braiding intensity. From 60 km onwards braiding intensity begins to decrease systematically as the river begins its transition through a wandering to single-thread style (Ziliani & Surian, 2012). A final interjection of groundwater hydrology with its effects on the establishment of vegetation is observed downstream of around 60 km, where silt and clay deposits raise the water table and improve conditions for vegetation growth, resulting in higher vegetation densities and the associated impact on planform and morphology (Henshaw *et al.*, 2013).

2. Past, present and future developments in fluvial and braided river geomorphology

Chapter synopsis

The core aim of this thesis is to explore the potential of graph theory for the analysis of braided river morphodynamics. In the following literature review, our present understanding of braided river morphodynamics is summarised in the context of historical developments of reductionist methods in geomorphology. Braided river processes are discussed based on a hierarchy of scale, from particle-scale interactions to catchment-scale controlling variables. This discussion of process prefaces an overview of the dominant methodological approaches to braided river investigations, highlighting their deficiencies in resolving braided behaviour at larger spatial and temporal scales. The review of methods for the study of braided rivers includes a more detailed assessment of applications of satellite remote sensing to fluvial geomorphology, with a focus on studies of braiding.

2.1   Conceptualisation of systems in (fluvial) geomorphology

Approaches to geomorphology have, like landscapes themselves, evolved over time. The origins of geomorphology in some form or other may date back to antiquity, though some credit its modern origin to the works of G.K. Gilbert and W.M. Davis in the late 19th century (Sack, 2002; Church, 2010). The importance of these two workers stems, in part, from their approaches to geomorphology. Gilbert's early work, whilst being highly descriptive, incorporated quantitative, inductive methods to analyse the origins of landforms and sedimentary deposits (Gilbert, 1877, 1895). Davis (1899) applied purely qualitative methods to describe his theory of "The Geographical Cycle", through which landscapes evolve within a closed system to a peneplain through the action (largely) of fluvial erosion, with cyclicity introduced to the system by periodic uplift. Davis' reliance on qualitative enquiry meant his methods were purely deductive, and geomorphology remained in this mould until near the mid-20th century when workers such as Bagnold (1935), Horton (1945) and, in particular, Strahler (1952a) brought quantitative, inductive methods to the fore.

Whilst various workers presaged the wider adoption of quantitative methods in geography and geomorphology during the "quantitative revolution" of the late 1950s, the contributions of Arthur Strahler stand out (Burton, 1963). Davis (1899, p. 482) stated:

"The forces by which structures and attitudes have been determined do not come within the scope of geographical inquiry, but the structures acquired by the action of these forces serve as the essential basis for the genetic classification of geographical forms."

Strahler (1950) offered a stern rebuke of Davis' aversion to the forces governing process-form interactions which shape landforms; and in his seminal paper, *Dynamic Basis for Geomorphology*, Strahler (1952a, p. 923) states that geomorphic processes should be treated as:

"…manifestations of various types of shear stresses, both gravitational and molecular, acting upon any type of earth material to produce the varieties of strain, or failure, which we recognise as the manifold processes of weathering, erosion, transportation and deposition."

These papers embedded the drive for reduction in both temporal and spatial scales of enquiry within geomorphology, with the goal to understand landscape evolution based on the quantification of physical processes that define landscapes and the development of general laws to describe these processes.

Moves to quantify process-form interactions in geomorphology arose from the engineering tradition. For example Bagnold (1935),[2] studying desert dune formation, looked first at forces/processes and then at form; though ultimately he was concerned with the system that gave rise to varying dune forms. In his seminal paper on stream erosion, Horton (1945)[3] began with the quantification of infiltration, deriving a series of analytical and empirical general laws which result in the principle erosive processes that form drainage networks. The majority of Horton's (1945) thesis was focussed on hydrophysical processes up to the channel-scale. He did, however, also provide a range of indices based on physiographic factors. These indices describe characteristics of the drainage network, but in contrast to Davis (1899), quantification allowed for the establishment of general laws that were transferable between systems. Further advocating the potential application of general laws in geomorphology, Strahler (1952a) suggested that research should incorporate mathematical modelling of geomorphic processes, conducted on the basis of empirical statistical or rational deductive methods. These new quantitative approaches to geomorphology spawned huge advances in our understanding of geomorphic systems.

---

[2] R.A. Bagnold was an officer in the British Army, Royal Engineers (Throrne & Soar, 1996).
[3] R.E. Horton was a hydraulic engineer (Strahler, 1950),

Strahler's own, early applications of his principles used rational and empirical methods to derive relationships between hypsometric curves and transitions between stages of landscape evolution (Strahler, 1952b); and statistical relationships between physiographic factors of drainage basins to develop general laws describing properties of drainage networks (Strahler, 1957). Pioneering work using empirical methods developed hydraulic geometry relationships that quantified the variables responsible for the self-formed geometries of river channels and relationships between these variables (Leopold & Maddock, 1953). Empirical methods also began to elucidate the factors that determine why river channel patterns vary on a continuum from straight to braided (Leopold & Wolman, 1957). Attempts to apply general physical laws to understand landscape evolution were also applied at the scale of whole systems, such as Leopold & Langbein (1962) who used probabilistic concepts of entropy to predict the distribution of energy in a fluvial system, from which geometric properties of the system could be deduced. A key aspect of the application of concepts of entropy to river systems was the acknowledgement that these are open systems in dynamic equilibrium, ideas which were central to the new, "dynamic basis" of geomorphology.

Theoretical discussions, influenced heavily by the concepts of General System Theory (Von Bertalanffy, 1950), suggested that the attainment of steady states in geomorphic systems that are subject to unsteady fluxes of matter and energy indicate the presence of dynamic equilibrium in emergent properties of a system (Chorley, 1962). Dynamic equilibrium means that the landscape units of a system in steady state may show some mean conditions, definable statistically, but that fluctuations around these mean conditions will occur over time (Chorley, 1962). A consequence of this view was a shift away from Davis' conception that geomorphic information is "timebound", to the dynamic view that processes are "timeless", though not without recognising that a systems history will affect the processes shaping its future. This was conceptualized by Schumm & Lichty (1965) in a time-based scheme of changing spatial dependence, independence, relevance and indeterminism between variables affecting river morphology. Time-scales represented geological ($1 \cdot 10^6$ yrs. BP to present), modern ($1 \cdot 10^3$ yrs. BP to present) and present (1 yr. or less) time. They hypothesized that variables operating at the catchment scale or below may switch between being dependent on extraneous factors (time, geology, climate) over geologic time to independent during modern and present time. At the smallest spatial scales, factors such as river discharge, flow characteristics and sediment transport switch from being indeterminate over geological time to dependent on larger scale variables. However, this spatially hierarchical treatment of the key variables affecting river morphology is simplistic, lacking acknowledgment of interdependencies between spatial scales

whereby small-scale processes can manifest as large-scale changes, owing to oft non-linear interactions between variables (Lane & Richards, 1997).

Non-linear dynamics, chaotic dynamics and historical contingency resulting in both probabilistic and deterministic responses to forcing (Huggett, 1988; Phillips, 1992) are indicative of the inherent complexity of geomorphic systems. Such complexity means that whilst reductionism and the application of (often empirical) general laws with the eventual goal of predicting the behaviour of geomorphic systems has hugely expanded our knowledge of geomorphology (Church, 2010), we are still quite far from models that can accurately predict geomorphic evolution, especially in more dynamic systems. There is also a risk that theories developed on solely empirical grounds can be flawed, especially when the guiding assumptions of a theory were also developed by an empirical methodology (Brown, 1996), which may underpin recent calls to deepen physics-based modelling in fluvial geomorphology (e.g. Church & Ferguson, 2015). However, the physics of sediment transport and the hydrodynamic interactions between flows over vegetation and sediments of different roughness, which vary markedly in both space and time in natural environments, makes this an exceptionally difficult task. Indeed, it was the complexity of natural systems that spurred on the development of General Systems Theory.

General Systems Theory describes a trans-disciplinary approach for systems where reduction to physico-chemical or purely physical processes increases complexity to unmanageable levels (Von Bertalanffy 1950). By abstracting complex systems to interacting units that incorporate physical processes, general laws can be deduced that describe interactions between these units, thus describing the behaviour of a given system. Despite the influence that General Systems Theory had on Strahler's Dynamic Basis for Geomorphology (Huggett 1988), his principle of also taking a rational deductive approach to geomorphology gained less traction. More recently, there have been calls to embrace both the empirical and rational tenets of Strahler's dynamic geomorphology, especially in light of the non-linearities that often underpin geomorphic system behaviours (Lane & Richards 1997). Rhoads (2006) espouses a more holistic approach, or "process-philosophy", that recognises landforms as amalgamations of processes, with dynamics resulting from the interconnection of internal and external forcing. Recent work has begun to emphasise this, with increasing attention being paid to connectivity within geomorphology and related disciplines (Bracken & Croke, 2007; Bracken *et al.*, 2013; Wohl *et al.*, 2017, 2019). Our knowledge of interconnections within geomorphic systems, along with our capacity to quantify these connections and the resultant system behaviour is underdeveloped. Reduction to small-scale processes often increases complexity to unmanageable levels and so abstraction of a

system to fundamental units that incorporate manifold processes may help develop understanding of the emergent phenomena that build landscapes.

2.2 Braided river processes and behaviours from micro- to system-scales

Braided rivers have a highly distinctive morphology that, when viewed from the air, appears as a complex network of interconnected channels that divide and converge around bars composed of sand or gravel (Figure 2.1). They are typically found in unconfined valley settings where the prevailing local geological, hydrological and geomorphological conditions result in large volumes of unconsolidated sediment, high stream powers that are capable of sustaining intense levels of bedload transport, and channel boundaries that are susceptible to erosion relative to the energy of the stream (Ashmore 2013). These factors combine to make braided rivers one of the most dynamic and unpredictable Earth surface features, varying their morphology rapidly and dramatically via a suite of depositional (bar development) and erosional (bar dissection) processes that are most active under high flow conditions (Ashmore, 1991b; Ferguson, 1993).

These processes and their attendant variables are active across a huge range of spatio-temporal scales, which will be discussed in the following sections. Discussion is structured around the spatial scale at which processes are active and how these scales interact to develop and determine braided river morphologies.

2.2.1 Micro-scale interactions with meso-scale results

At the smallest scales, fluid dynamics and the mechanics of sediment entrainment, transport and deposition determine the patterns of erosion and deposition that ultimately result in braided river morphologies (Knighton, 1998; Charlton, 2010). It has been shown in a large, sand-bed braided river that single-thread flows, with a single high velocity core, can separate into two flow threads with independent high velocity cores, subsequently causing sediment deposition in the slower flow between the two threads (Richardson & Thorne 2001). A positive feedback effect was observed, whereby scour beneath the high velocity cores accentuated deposition in the region of slower flow, resulting in the growth of a mid-channel bar. Whilst Richardson & Thorne (2001) note that this behaviour was dependent on energy conditions, with high flows potentially causing reverse behaviour, their study confirms that micro-scale hydrodynamic effects play a large role in the instigation of braiding. However, if depositional processes may

be responsible for the initiation of braiding, the maintenance and evolution of braided rivers morphologies is highly dependent on erosive processes (Ashmore, 1991b; Ferguson, 1993).

The 'braiding mechanisms' defined by Ashmore (1991b) include both purely depositional processes ('central bar initiation'), a combination of erosion and deposition ('transverse unit bar conversion' and 'multiple bar braiding') and purely erosive processes ('chute cutoff'). Other studies have emphasised the importance of avulsion as another mechanism by which rivers attain/maintain a braided planform (Ferguson, 1993; Kleinhans et al., 2013). Regardless of the mechanism, the effect of these processes is to create the fundamental geomorphic unit in braided rivers: the bifurcation-confluence unit, which is intrinsically unstable and evolves in response to interacting hydrodynamic and channel geometry variables (Ashworth, 1996; Thomas et al., 2011; Bertoldi, 2012; Kleinhans et al., 2013; Marra et al., 2014; Schuurman & Kleinhans, 2015).

Figure 2.1: The Waimakariri River, New Zealand; a textbook example of the complex channel network of a braided river. Flow is from top to bottom. (Source: McSaveney, 2015)

Confluences exhibit typical flow structures, such as a strong shear layer towards the confluence centre, secondary circulation that moves downward in the shear zone and obliquely outward at the bed, stagnant flow in the area around the bar tail where the tributary channels meet and

flow acceleration where the upstream flows converge (Szupiany *et al.*, 2009; Ashmore, 2013). These flow structures are often reflected in key morphological features, including a scour zone in the area directly downstream of the confluent channels, avalanche faces dipping into the scour zone from the mouth of each tributary, sediment deposition at the bar tail around which channels converge and lateral bars formed adjacent to the scour zone, or a mid-channel bar deposited downstream in the post-confluence channel (Szupiany *et al.,* 2009). Various factors may control the flow structures and channel morphology within confluences, with particular importance given to the confluence angle, flow and sediment discharge ratios between the upstream channels and discordance in the bed elevations of the confluent channels (Szupiany *et al.,* 2009; Ashmore 2013). In particular, differences in upstream bed elevations of the confluent channels, affecting flow depth, can have a large impact on the location of sediment transport and deposition downstream of the confluence, which will tend towards the shallower tributary's side of the downstream channel (Best & Roy, 1991). This effect will diminish when the tributaries have concordant bed elevations at which point scour hole position and secondary circulation in smaller channels and the position of high velocity flow threads in larger channels may become dominant (Szupiany *et al.*, 2009). In both cases, the orientation of the confluence is responding to the geometry of the upstream channels, with confluence orientation subsequently affecting the location of upstream erosion and of downstream deposition, the combination of which results in a bifurcation and establishment of a confluence-bifurcation unit (Ashmore 2013).

As in the case of confluences, bifurcation dynamics reflect complex interrelationships between hydrodynamics, the hydraulics of sediment transport and channel morphology. Transverse bed slopes at bifurcation entrances, water level in respective channel mouths and the geometric properties of the upstream channel impact, and are impacted by, flow separation and the associated variability in transversal velocity (Kleinhans *et al.*, 2008, 2013). These interrelationships effect the distribution of discharge into the bifurcates and subsequent secondary circulation patterns, affecting downstream patterns of sedimentation. Bar dynamics are also intrinsically linked to bifurcations, both in the sense of bifurcation initiation through, for example, flow expansion and central bar deposition (Federici & Paola, 2003) and through the migration of bars that can block channels and close bifurcations (Schuurman & Kleinhans, 2015). Bifurcations are inherently unstable (Kleinhans *et al.*, 2013) and their stability is heavily related to Shields stress, with bifurcations found to be unstable at low Shields stress both in physical and theoretical models (Bolla Pittaluga *et al.*, 2003; Federici & Paola, 2003). This characteristic

fits with the hydraulic properties of braided rivers which, especially in the case of gravel bed rivers, have low Shields stress (Ashmore 2013).

General hydraulic properties of braided rivers may provide information on the general dynamics of bifurcations, but local geometric properties, which effect local hydraulic properties, mean the specific behaviours of bifurcations vary markedly within one river. Transverse bed slopes at the head of a bifurcation are strongly associated with topographic steering of flow and sediment transport into the channel with lower inlet bed elevations, the direction of the transverse bed slope being affected by the migration of alternate bars (Bolla Pittaluga *et al.*, 2003; Bertoldi & Tubino, 2007). These analyses, which were on theoretical and idealised channels, suggest that channel dominance may oscillate between channels at a bifurcation with the passage of alternate bars, however in natural systems it has been shown that subordinate channels are more susceptible to instability and closure than dominant channels (Bertoldi 2012; Marra *et al.*, 2013). Channel dominance can be caused by various factors. Increased water surface slope in one bifurcate, resulting from either greater bed slope or a difference in bed elevation at the downstream end of the channel, can cause the channel with greater water surface slope to capture more discharge and thus have more capacity for erosion (Thomas *et al.*, 2011). However, Marra *et al.*, (2014) suggest that the effect of increased discharge to a dominant channel at the bifurcation also results in large increases in the near-bed flow entering this channel, with concomitant effects on sediment transport. They propose that the dominant channel may capture so much sediment that it aggrades, reducing the water surface slope advantage and moving the bifurcation back towards stability. Complicating matters further, numerical modelling by Hardy *et al.*, (2011) suggests that upstream curvature of the pre-bifurcation channel may have a flow steering effect, resulting in capture of flow and sediment discharge in the channel on the outer bend of the upstream curve that is sufficient to override a slope advantage on the inner bend channel. Theoretical, numerical and laboratory modelling and a more limited array of field studies have elucidated many of the factors that impact bifurcation stability and evolution, though their exact behaviour remains elusive. Bifurcations are, however, unified by what divides them: bars.

In braided rivers, bars are broadly categorised as unit and compound. Unit bars are characteristically lobate in planform, with downstream avalanche faces, and may show significant rates of downstream migration (Sambrook Smith *et al.*, 2006). Compound bars form from the coalescence of unit bars and may initially show common planform features, such as elongated downstream "limbs", but will develop heterogeneous planforms as they grow, evolve

and migrate slowly downstream (Sambrook Smith *et al.*, 2006; Schuurman & Kleinhans, 2015). Depositional models for bars in both gravel and sand-bed rivers show common features, with initial growth of bars resulting from stalling of bedload sheets or migrating bedforms and subsequent accretion caused by a positive feedback as local decreases in competency are accentuated by the growing bar (Ashworth *et al.*, 2000; Best *et al.*, 2003; Lunt *et al.*, 2004). Once formed, certain types of bars have been found to act as preferential sites of further sediment deposition, with compound, diagonal unit and point bars accumulating 80% of deposits on existing bars in a flume study (Kasprak *et al.*, 2015). This research also found that 70% of deposition was on bar heads and margins, a finding mirrored in a flume study on the loci of large wood deposition (Bertoldi *et al.*, 2014). In braided rivers supporting vegetation growth within the active tract, vegetation has a huge impact on the evolution of bars, stabilising them against erosion and significantly increasing their capacity for sediment accretion during flood events due to the increase in surface roughness (Gurnell *et al.*, 2001; Rodrigues *et al.*, 2007; Corenblit *et al.*, 2014).

The dynamics of bar initiation and migration is a major control on braided river planform evolution. Mid-channel bar growth can impact the cross-sectional geometry of single channels, not only due to aggradation in the channel centre, but also through channel widening as flow is deflected to the outer margins (Ashworth 1996). Chronicling the evolution of an anabranch around a compound bar in the sand-bed, South Saskatchewan River, Canada, Ashworth *et al.*, (2011) show the impact of multiple bar migration and evolution processes on local planform. Over a four-year study period, the channel narrowed, closed, reopened and finally closed, with this sequence resulting variously from unit bars stalling at the compound bar head, bedform migration reducing channel slope, variability in flow conditions and reorientation of the main channel thalweg increasing the bifurcation angle. These last two factors evidence the impact of processes occurring at larger than the meso-scale of bars, bifurcations and confluences, such that bars in different reaches of the same river may show considerable differences in response to the same forcing, such as floods of the same magnitude (e.g. Reid *et al.*, 2018).

2.2.2 From meso to macro: competing influences that shape reach-scale braided morphologies

The assemblage of bars and predominantly asymmetric bifurcations and confluences results in the reach-scale configurations of braided channel networks, whereby multiple parallel channels exist in a hierarchy, from the main, first-order channels to higher order branching channels (Bristow & Best, 1993). Empirical models explain the emergence of braided channel patterns as

a function of stream power relative to median grain size (van den Berg, 1995; Kleinhans & van den Berg, 2011), with recent work suggesting sediment supply may actually be the defining factor for the emergence of braiding (Mueller & Pitlick, 2014). Whilst these efforts provide useful data on key controls of the transition from single-thread to braided channels, questions have been raised about the utility of such a reduced-complexity approach (Lewin & Brewer, 2001). This criticism reflects the complex nature of braided river planforms and morphology, which may see considerable change within a single reach of one river in response to floods of different magnitude (e.g. Bertoldi *et al.*, 2010; Picco *et al.*, 2013), whilst essentially retaining the same channel pattern (Van Der Nat *et al.*, 2002). This behaviour has been observed for both gross scale planform characteristics of bars and islands (Zanoni *et al.*, 2008), and in channel pattern quantified using a channel count braiding index (BI) in laboratory and natural braided rivers (Egozi & Ashmore 2009; Wheaton *et al.*, 2013). Adding to the complexity of braided river planform behaviour is variation with stage, such that BI may be highest at intermediate stages when the channel network is fully connected but a large proportion of bars are still exposed, reducing to minima (one, or essentially a single thread river) at bankfull flows (Welber *et al.*, 2012). Inter-reach variation in vegetation may cause further planform variability within the same river, as vegetated bars and islands promote accretion and thus may remain exposed during a bankfull flood, maintaining a local multi-thread character (Welber *et al.*, 2012).

The impact of vegetation on reach-scale braided river morphologies can be significant. Vegetation stabilises bars and other floodplain surfaces against erosion and enhances deposition, affecting reach-scale topography (Gran & Paola, 2001; Rodrigues *et al.*, 2007; Gurnell *et al.*, 2008; Bertoldi, Drake *et al.*, 2011; Bertoldi, Gurnell *et al.*, 2011; Welber *et al.*, 2012; Corenblit *et al.*, 2014; Mardhiah *et al.*, 2015). Where vegetation density is high enough, this effect can be so significant as to impart a 'topographic signature' on bed elevation frequency distributions which tend towards negative skew and secondary peaks above the mean reach bed elevation (Bertoldi, Gurnell *et al.*, 2011). The size of vegetated patches also affects channel planform, with many smaller patches associated with divergent flow pathways and a more complex channel network as flow is forced around local obstacles that are resistant to erosion, whereas larger vegetated islands may focus flow into larger central channels from which smaller channels branch (Gran & Paola, 2001; Murray & Paola, 2003; Coulthard, 2005; Henshaw *et al.*, 2013). Flow also plays a large role in the longer-term evolution of reach-scale vegetation patterns. Cyclic patterns of vegetation establishment, growth and persistence linked to the spacing of high magnitude flood events are indicative of a strong temporal component in the evolution of reach-scale braided morphologies (Kollmann *et al.*, 1999; Zanoni *et al.*, 2008;

Bertoldi, Gurnell *et al.*, 2009). The resulting interplay between flows, sediment and vegetation result in reaches with higher vegetation densities being characterised as a complex, shifting 'habitat mosaic' (Van Der Nat *et al.*, 2002, 2003; Mardhiah *et al.*, 2015), emphasising the spatially heterogeneous nature of braided river morphologies.

The spatio-temporal heterogeneity of braided morphologies is, of course, not limited to reaches with higher densities of vegetation. Complex feedback processes are at play in braided reaches, where heterogeneous topography steers flow and results in spatio-temporally variable sediment transport pathways that, in turn, re-sculpt reach-scale topography (Ashmore *et al.*, 2011; Wheaton *et al.*, 2013). Field research has shown that the mechanisms causing the majority (61% of the volumetric difference in sediment in a Scottish braided reach) of this topographic change matches Ashmore's (1991b) proposed braiding mechanisms (Wheaton *et al.*, 2013). Secondary, sub-bar-scale erosional and depositional processes (e.g. bank erosion, channel incision) accounted for the remainder. Another pertinent observation from Wheaton *et al.'s* (2013) data relates to the locations of erosion and deposition which, while being centred around the main channel, show significant spatial variation around the reach over the three years of their study. Observations in both flume and field studies have shown large variations in both active width (the width over which bed morphology is observed to change; Ashmore *et al.*, 2011; Peirce *et al.*, 2018) and active braiding index (the number of channels actively transporting sediment; Egozi & Ashmore 2009). These findings match those of Reitz *et al.* (2014), who have also reported this mode of diffusive evolution of a laboratory braided river, suggesting morphological activity migrates around the network. Spatially variable patterns of erosion and deposition have been reported in flume environments with constant (Reitz *et al.,* 2014) or stepped increases (Egozi & Ashmore 2009) in discharge, and in pro-glacial rivers where diurnal cycling dampens discharge fluctuations (Ashworth & Ferguson, 1986; Ashmore *et al.*, 2011). However, in rivers with variable discharge regimes, high magnitude flood events can cause widespread alteration of channel network structure, at the reach- and larger scales, when the river is at or above bankfull and sediment transport and erosion may be occurring across the wetted width of the channel, as seen in European braided rivers where the magnitude of morphological change often correlates with flood magnitude (Bertoldi *et al.*, 2010; Belletti *et al.*, 2015). This is indicative of larger, catchment-scale controls on braided river morphodynamics.

2.2.3 Reaching out to the scale of full braided river networks

A suite of catchment-scale variables provides overriding control on the morphodynamics in braided rivers. Given the importance of stream power on the emergence of braiding, valley slope is a key factor in ensuring energy conditions are capable of supporting high rates of sediment transport (van den Berg, 1995; Kleinhans & van den Berg, 2011). Width constraints can have a considerable effect on braided planforms, with channel narrowing often causing a reduction in braiding intensity, a decrease in width/depth ratios and potentially forcing a braided channel to transition to single-thread or wandering (Fotherby, 2009; Mueller & Pitlick, 2014; Garcia Lugo *et al.*, 2015; Reid *et al.*, 2018). Whether banks can constrain the active area of a braided river relates to the balance between stream power and bank resistive strength, which can vary longitudinally due to bedrock constrictions and the presence of vegetation that increases sediment cohesion (Gurnell & Petts, 2006; Corenblit *et al.*, 2014). Establishment of vegetation is linked to conditions conducive to vegetation growth, which can be discontinuous along the length of a braided river (Gurnell *et al.*, 2001), further emphasising the contrasting controls on reach-scale morphodynamics that exist within a single braided river network. Longitudinal variation in grain size is also a notable control, as material that is too large relative to stream power, or too small and thus cohesive, can retard the capacity for erosion, deposition and the onset of braiding (Ashmore, 2013).

Whilst the aforementioned controls have considerable impact on the spatially varying nature of braided river morphodynamics, likely the most important factors over non-geological timescales are sediment supply and discharge regime. Numerous studies from rivers across a wide geographic distribution have cited variation to sediment supply as the overriding factor in long-term evolution of braided river morphologies (Surian, 1999; Ashworth *et al.*, 2007; Bravard, 2010; Liébault *et al.*, 2013; Mueller & Pitlick, 2013; Kidová *et al.*, 2016). Where sediment supply is not limiting, variable discharge regimes will provide the overarching control on braided river network dynamics, with small (less then bankfull) floods causing more localised erosion and deposition, whilst bankfull and larger events have the capacity to thoroughly rearrange network structure and braidplain morphology (Bertoldi *et al.*, 2010; Belletti *et al.*, 2015). Anthropogenic activity, either within catchments, for example through land use change or hydropower developments, or direct alterations to channels such as gravel mining or river training structures can also impact the evolution of braided river morphologies (Gurnell *et al.*, 2009).

Morphodynamic responses of geomorphic systems result from the present dynamics of variables that drive a system's evolution, which are imposed onto antecedent conditions (Lane & Richards, 1997; Phillips, 2015). Kidová *et al.*, (2016) provide a modern case study of this phenomenon on the Bela River, Slovakia. Here, afforestation, river training works and gravel mining has reduced sediment supply, while a decreasing trend in flood magnitude has reduced the capacity for floods to remove vegetation, which is now stabilising floodplain surfaces and reducing sediment erosion and supply from within the river. The combination of antecedent conditions that have reduced sediment supply and the present flow dynamics that are no longer sufficient to counteract the lack of sediment has reduced the capacity of the Bela River to support a braided planform. A similar story has been documented on the Piave River, Italy by Surian (1999), though without a changing trend in discharge regime.

Key to the analyses of historical channel evolution by Kidová *et al.* (2016) and Surian (1999) is the availability of time series' of aerial photographs and/or maps showing changes in channel planform over time. Similar data sources and analyses have also been applied to study the long-term evolution of alpine braided rivers in France (Belletti *et al.*, 2015) and the River Tagliamento, Italy (Ziliani & Surian, 2012). Studies are also beginning to utilise the increasing availability of satellite imagery for long-term analyses of braided rivers with relatively high temporal resolution (at least annual or better), as well as being able to characterise changes in key parameters such as vegetation along a whole braided river network (e.g. Henshaw *et al*. 2013). Analysis of patterns of channel change over large time and space scales also point to the migratory nature of perturbations in braided rivers (Takagi *et al.*, 2007). This study used satellite remote sensing to analyse destabilisation of different land cover classes along a near-200 km long section of the Brahmaputra River, Bangladesh. They found migratory behaviour of regions of destabilisation, which suggests that the links between bank erosion and bar building in a proximal downstream area observed by Ashworth *et al.* (2000) on the same river may be playing out across this braided network. This downstream propagation of a perturbation has also been seen in network-scale analysis of a numerical model that approximates the Brahmaputra, such that a perturbation destabilises bifurcations and asymmetrically reshapes bars in its vicinity, with this destabilisation then propagating downstream (Schuurman *et al.*, 2016). Clearly there is a need to account for the connectivity between different areas of a braided network and how this connectivity may affect morphodynamics in the context of changes to the variables that drive braided river evolution at the network scale.

2.3 Methods for the investigation of braided river behaviour

Methods employed to investigate braided rivers can be broadly divided into two categories: 1) field-based, 2) modelling. A third category of remote sensing-based studies of natural systems could be argued, though this is deemed more a very distinct sub-category of field investigation. Within modelling, the two types of model applied most widely in braided river research are hydraulic and numerical. Hydraulic models have a long history in studies analysing braiding (e.g. Leopold & Wolman 1957) and have led to fundamental developments in braided river process understanding, e.g. Ashmore's (1991b) braiding mechanisms. Small scale models with immobile beds have been applied to the analysis of hydrodynamics in idealised bifurcations and confluences (e.g. Best & Roy 1991; Thomas *et al.*, 2011; Marra *et al.*, 2014), or bifurcation evolution and bar building processes in flumes with moveable bed sediments (e.g. Ashworth 1996; Federici & Paola 2003; Bertoldi & Tubino 2007). Larger scale models in less laterally confined flumes with fully mobile beds provide the opportunity to model the responses of reach-scale morphodynamics to forcing under completely controlled conditions (e.g. Ashmore 1987; Ashmore 1991a).

Hydraulic models of braided rivers can replicate the processes and behaviours of field prototypes by relaxing the similarity of the grain Reynolds number to natural rivers, whilst ensuring that flows are fully turbulent and sediment transport is not impeded by near-bed viscous forces, as well having Froude numbers of around 1, such that flows can be both sub- and super-critical (Ashworth *et al.*, 1994). In meeting these conditions, hydraulic models have been used to study a wide array of braided river processes and dynamics, including the impact of lateral confinement on braiding intensity and bed topography (Garcia Lugo *et al.*, 2015); sediment transport path lengths and deposition locations (Kasprak *et al.*, 2015); applying DEMs of difference (DODs) to assess the vertical and lateral extent of scour and deposition under conditions of constant discharge and slope (Leduc *et al.*, 2015) or varying slope to increase stream power (Peirce *et al.*, 2018). Other studies have utilised hydraulic models to assess the impacts of vegetation on planform (Gran & Paola, 2001; Coulthard, 2005) and how woody debris is stored and remobilised (Bertoldi *et al.*, 2014).

However, despite this broad range of applications, there are limitations, especially in scale, to the scope of hydraulic modelling studies. The limits placed on length and width scaling mean that hydraulic models can only really scale to the size of reaches in natural, prototype rivers before size requirements of the flume and the volumes of sediment involved defy logistical

considerations (Young & Warburton, 1996). Scaling down sediment size also means truncating grain size distributions to avoid inclusion of cohesive particle sizes that would affect the cohesionless properties of most braided river bed sediments, a problem especially true of gravel-bed rivers (Young & Warburton, 1996), though fine scale non-cohesive substances have been employed to represent the finest fractions in some studies (Kleinhans *et al.*, 2015). When designing a hydraulic modelling study to replicate a specific prototype river, there is also the need to have good field data on the prototype (Young & Warburton, 1996), which limits the number of real rivers that can be studied using this approach.

The difficulties inherent in field studies of braided rivers has, in part, spurred on research into the development and application of numerical models of braided river morphodynamics (Williams *et al.*, 2016). Numerical models provide complete control of parameter space and the opportunity to output detailed morphometric and hydraulic data, enabling analysis of braided river evolution that is as detailed as the numerical scheme. Williams *et al*. (2016) provide a taxonomy and critique of different types of numerical models, which include purely analytical models and 1- to 3-D numerical models. Analytical and 1-D numerical models are limited by their requirement to average out the significant topographical, depth and shear stress variations that are seen in braided rivers. Of the 2-D approaches, reduced-complexity models (RCMs) stemming from Murray & Paola's (1994) seminal cellular automata approach have seen the widest application. This model showed the emergence of braiding as the default channel pattern in unconstrained and non-transport limited rivers, however subsequent research has highlighted that Murray & Paola's (1994) model struggles to replicate detailed, channel scale processes and scaling (Doeschl-Wilson & Ashmore, 2005). Thus, RCMs are seen as useful tools for probing the evolution of braided rivers based on replication of reach-scale statistical properties of channel geometry and topography under given boundary conditions (Brasington & Richards, 2007). Furthermore, due to relatively low computational demand, they can be applied to modelling at meso-scale spatial and temporal resolutions (10-100 km, 10-100 years), as was recently shown by Ziliani *et al.* (2013) using the Cellular Automaton Evolutionary Slope and River (CAESAR) RCM to model the evolution of the River Tagliamento over a 33 km reach and an 8 year time period. By tuning model parameters in a sensitivity analysis, Ziliani *et al.* (2013) achieved run times of 6 hours on standard desktop computers, indicating that large time and space scale modelling of braided rivers is possible without specialist computing resources.

More detailed, 2- and 3-D numerical models of braided rivers, classed as 'physics-based' (PBMs; e.g. Delft3D, HSTAR, MIKE21C and others), are capable of simulating micro-scale hydrodynamic

and sediment transport processes and their effect on the evolution of braided river topography (Williams *et al.*, 2016). Despite certain simplifications, such as decoupling processes of flow and sediment transport (Williams *et al.*, 2016) and applying uniform roughness coefficients to the model domain (Church & Ferguson, 2015), PBMs do provide an unrivalled ability to study the micro-scale hydrodynamic and sediment transport processes that ultimately determine change in braided river morphologies. Applications of PBMs have allowed detailed analysis of the processes of bar formation, subsequent dissection and associated bifurcation evolution (Schuurman & Kleinhans, 2015). Delft3D, parameterised to replicate an 80 km reach of the Brahmaputra River, Bangladesh, has been applied to model the effects of perturbations on bar morphology and discharge distributions at bifurcations (Schuurman *et al.*, 2016), evidencing the potential for PBMs to represent network-scale dynamics in braided rivers. Studies are also now including vegetation effects in PBMs (e.g. Crosato & Saleh 2011), albeit with highly simplified representations of vegetation that only represent the hydraulic effect of slowing and deflecting flow. There is clearly huge potential for the use of PBMs in furthering our understanding of braided river morphodynamics and potentially providing tools for the prediction of morphological evolution, however they are not without limitations. Although modern computing continues to lower the barrier of computational demand, it is still relevant to running PBMs over large spatial and temporal scales (Crosato & Saleh, 2011; Ziliani *et al.*, 2013; Williams *et al.*, 2016), which places limitations on the application of PBMs to studying the evolution of medium to large braided rivers. Further issues exist in the acquisition of field data to calibrate and validate numerical models, especially at the small scales at which PBMs can reproduce braided river topography.

Field survey techniques have developed markedly in recent years and it is now possible to obtain cm- to mm-scale topographic data using modern surveying techniques, such as terrestrial laser scanning (e.g. Reid *et al*. 2018) and Structure-from-Motion photogrammetry (Westoby *et al.*, 2012). Innovative solutions fusing bathymetry with sub-aerial topographic mapping are also providing a means to create DEMs that cover the full extent of braidplain morphology (e.g. including inundated areas), which has previously been a limitation of 3-D topographic methods (Williams *et al.*, 2015). However, capturing these data still requires significant field campaigns that severely limit temporal scale, whilst spatial coverage of such studies rarely extend beyond the reach-scale (or even bar-scale in mega rivers; e.g. Ashworth *et al*. 2000). It is possible to increase the spatial coverage of 3-D surveys using aerial LiDAR (Bertoldi, Gurnell *et al.*, 2011) or photogrammetry techniques, but these are costly approaches to gathering data.

The problems of limited spatial coverage, temporal resolution and high survey costs associated with field studies can be circumvented with 2-D remote sensing, especially utilising satellite data. Dating back to 1972, NASA's Landsat programme provides the World's longest and most comprehensive Earth observation dataset, and was recently made available for free by the U.S. Geological Survey (Woodcock *et al.*, 2008). Applications of Landsat data in studies of fluvial geomorphology are not new (e.g. Bristow, 1987) and it has proved a valuable tool in the analysis of properties of fluvial landscapes and the dynamics of flood inundation (Smith, 1997; Mertes, 2002). Trigg *et al.* (2012) used Landsat imagery to map floodplain channels along a 285 km reach of the River Amazon and 107 km of one of its tributaries, the Purus. They showed that in larger river basins, Landsat's 30 m (15 m if using pan-sharpening) spatial resolution is sufficient to resolve numerous fluvial features, developing an understanding of floodplain hydrology and its associated morphology at large spatial scales. At smaller scales, Landsat data has been used to understand the dynamics of important fluvial forms, showing the evolution of confluences and their associated impact on river planform over multi-decadal timescales (Dixon *et al.*, 2018). This capacity for planform analysis across a range of spatial and temporal scales highlights the utility of Landsat data, and satellite remote sensing more generally, for tackling the problems inherent in field-based approaches to fluvial geomorphology.

Planform analysis of rivers using satellite imagery tends to focus on classification of fluvial forms, e.g. bars, and spatial patterns of erosion and deposition over time. Largely qualitative studies using Landsat and other sensors have shown how data from satellite remote sensing can be used to study the dynamics of mega rivers, such as the River Ganga and the braided River Brahmaputra (Bristow, 1987; Gupta *et al.*, 2013). These studies have highlighted processes occurring at single locations, such as meander evolution and bar erosion and deposition, and broader patterns of geomorphic change through the movement of bank lines that highlight the spatial distribution of bank erosion and accretion. However, whilst satellite remote sensing may show geomorphic change across multiple spatial and temporal scales, studies by Baki & Gan (2012) and Dewan *et al.* (2017) highlight that unpicking the drivers of, for example, large-scale bank erosion can be difficult and thus there is a need for contextual information on what may be driving change within a fluvial system.

Where clear drivers of geomorphic change are known, Landsat has been proven as a useful tool, even in rivers with complex morphologies. Following damming of the Lhasa River, Tibet, Landsat data was used to show how disruption of sediment supply by the dam resulted in changes to downstream bar assemblages as the river adjusted to a new regime of erosion and deposition

(Wu *et al.*, 2018). In braided rivers where vegetation is important for determining planform and morphology, the multi-spectral sensors onboard many satellites provide a means to manipulate the reflectance characteristics of vegetation and map its area and areal change over time in response to controlling variables. Studies of the River Tagliamento using Landsat and ASTER data have applied the Normalised Difference Vegetation Index (NDVI), which manipulates vegetation's high reflectance in the infrared wavelengths to discriminate vegetation from other landcovers (Bertoldi, Drake *et al.*, 2011; Henshaw *et al.*, 2013). These studies related change in vegetation area to other variables such as flood disturbance and moisture availability, highlighting reaches on the Tagliamento where vegetation establishment is more, or less, likely. This shows locations with greater probability of supporting biogeomorphic feedbacks between vegetation and braidplain morphology, whereby vegetation establishment promotes bar and island accretion which in turn supports vegetation growth (Corenblit *et al.*, 2014).

The majority of the studies detailed above have used satellite remote sensing data to relate areal changes in river planform to morphodynamics, however 2-D representations captured by satellite also lend themselves to analysis using planform metrics designed to capture the complexity of a braided channel network. Planform metrics provide useful and (relatively) easily attainable measures of the 2-D evolution of braided channels. These metrics, often termed braiding indices, are used to measure the intensity of braiding, predominantly at the reach-scale. Egozi & Ashmore's (2008) review of braiding indices categorised them as channel count-, bar- and sinuosity-based. They highlighted several practical limitations to braiding indices. With all indices stage variation will influence index values, leading to an as yet unstandardised sampling strategy for use across different rivers. There is also no direct equivalence between two of the most widely used indices: channel count index and total sinuosity and the inherent natural variability in braided river planforms prohibits measuring braiding indices with a coefficient of variation ≤ 20% (Egozi & Ashmore 2008). Despite these limitations braiding indices have been widely applied to laboratory (e.g. Gran & Paola, 2001; Coulthard, 2005; Egozi & Ashmore, 2009; Garcia Lugo *et al.*, 2015) and field studies (e.g. Fotherby 2009; Ashmore *et al.*, 2011; Welber *et al.*, 2012) of braided rivers, where they provide spatially averaged data on fluctuations in certain aspects of network complexity and geometry. However, by using spatially averaged metrics it is not possible to see where within a braided river network morphological changes are active, thus neglecting the nuances of braided network evolution. There is clearly a methodological gap in our capabilities to utilise 2-D planform data on braided rivers, which is also the data that gives the most comprehensive spatio-temporal coverage of these systems.

In attempt to bridge this gap, an innovative study by Marra *et al.* (2013) applied graph theory to the channel network of the Jamuna River. Graph theory is the mathematics of networks (Newman, 2010) that allows quantification of properties of networks from the level of single network elements, e.g. channels, bifurcations, confluences and bars in the case of braided rivers, up to patterns of connectivity at the scale of the whole river network. To the author's knowledge, this study presents the only in-depth analysis of braided river morphodynamics using graph theory, which may provide a flexible new framework for the multi-spatial and multi-temporal analysis of braided river networks. Furthermore, Marra *et al*'s. (2013) graph representations of the Jamuna River's channel network were derived from Landsat imagery. There has been a recent drive to adopt connectivity-based approaches within geomorphology and the geosciences (e.g. Heckmann *et al.*, 2015, 2018; Phillips *et al.*, 2015; Wohl, Magilligan *et al.*, 2017; Rinderer *et al.*, 2018; Turnbull *et al.*, 2018; Wohl *et al.*, 2019). With the recent increase in availability of satellite remote sensing data from sensors such as Landsat (Woodcock *et al.*, 2008) and the European Space Agency's Sentinel programme (Berger *et al.*, 2012), there is now an exciting possibility to use these datasets to enable graph theoretical analysis of braided rivers, incorporating the physical properties and underlying connectivity that determine how braided river networks evolve across multiple scales.

2.4 Conclusion

Current approaches to the study of braiding are, in most cases, built on the foundations of reductionist empiricism laid by Arthur Strahler at the start of the quantitative revolution in geomorphology. These approaches have driven huge advances in our knowledge of braided river morphodynamics and evolution at micro- to meso-spatial scales. However, current field and modelling methods for investigating braided river morphodynamics struggle to resolve the linkages between scales and to quantify the evolution of braided river networks over modern timescales (1-100 years). These shortcomings in braided river research place limits on our ability to predict braided river behaviour. Satellite remote sensing, notably the Landsat programme, has provided various insights into the behaviour of braided and other fluvial systems, though we lack an analytical framework that allows us to maximise the information that can be gleaned from remotely sensed datasets at the scale of whole braided river networks. The recent upsurge in connectivity research in the geosciences is a clear recognition that prediction of change in Earth surface systems must recognise the structural and process connections that drive their dynamics. Braided river planforms intuitively lend themselves to analysis using graph theory, providing a framework for connectivity-based research which has seen a paucity of applications

to questions on braided river morphodynamics. As network research develops across multiple disciplines and methods for analyses of dynamic networks evolve (currently an open area of research, e.g. Barrat *et al.,* 2013), so too will opportunities for novel analyses of problems in braided river research. Special attention should be paid to research on spatial networks, a category of networks to which braided rivers belong that has certain implications for their topology and analysis (see chapter 3; Barthélemy (2011) provides a treatise on the subject of spatial networks). The proceeding chapters present the first thorough application of graph theory to the study of braided river morphodynamics and demonstrate the huge potential of this new framework. What is presented here is likely the tip of the iceberg and it is hoped that the outputs from this thesis will stimulate widespread adoption of graph theory into the lexicon of braided river research.

3. Let's get connected: A new graph theory-based approach and toolbox for understanding braided river morphodynamics

Chapter synopsis

Our understanding of braided river morphodynamics has improved significantly in recent years, however, there are still large knowledge gaps relating to both long-term and event-based change in braided river morphologies. Furthermore, we still lack methods that can take full advantage of the increasing availability of remotely sensed datasets that are well suited to braided river research. Network analysis based on graph theory, the mathematics of networks, offers a largely unexplored toolbox that can be applied to remotely sensed data, quantifying the structure and function of braided rivers across nearly the full range of spatiotemporal scales relevant to their evolution. This chapter identifies important commonalities between braided rivers and other types of complex network, providing a compelling argument for the wider uptake of complex network analysis methods in the study of braided rivers. Applications of these metrics as new tools for multiscale characterization of braided river planforms that improve upon traditional, spatially averaged approaches are discussed and potential approaches to network-based analysis of braided river dynamics are proposed, drawing on a range of different concepts from braided river research and other network sciences. Finally, the potential for using graph theory metrics to validate numerical models of braided rivers is assessed.

n.b. This chapter is an edited version of Connor-Streich, G., Henshaw, A.J., Brasington, J., Bertoldi, W. and Harvey, G.L., 2018. Let's get connected: A new graph theory-based approach and toolbox for understanding braided river morphodynamics. Wiley Interdisciplinary Reviews: Water, 5, e1296.

3.1 Introduction

The complex, ever-changing planform and morphology of braided rivers (Figure 3.1) present particular challenges to the study of their morphodynamics. Existing tools for studying braided river morphological structure and behaviour through planform analysis do not account for the complex nature of these systems. Traditional approaches to quantifying changes in braided river morphology at the scale of the channel network often utilise oblique/aerial photos or satellite images. Through-time and between-reach differences in braiding intensity have been

investigated through the computation of indices based on the average number of individual channels across the river (e.g. Ashmore, 1991a; Howard *et al.*, 1970; Luchi *et al.*, 2007; Sarker & Thorne, 2006; Surian, 1999) or the total length of individual channels in a given reach length (e.g. Hong & Davies, 1979; Robertson-Rintoul & Richards, 1993). Relative levels of planform activity have been assessed through reach-averaged planimetric measurements of bank erosion and lateral shifts in the position of dominant channels (e.g. Bertoldi *et al.*, 2010).

Figure 3.1: Looking upstream at the complex channel network of the braided Tagliamento River, Italy.

The deployment of these methods in studies of natural and experimental rivers has greatly enhanced our understanding of the control exerted by discharge and stream power on braiding intensity (Robertson-Rintoul & Richards, 1993; Bertoldi, Gurnell *et al.*, 2009; Egozi & Ashmore, 2009) and the morphological significance of floods of different magnitudes in braided rivers (Bertoldi *et al.*, 2010), but they have several limitations. In addition to commonly reported issues such as their sensitivity to river stage and a lack of equivalence between different index types (Egozi & Ashmore, 2008), it is important to note that indices of braiding intensity only provide an aggregate measure of channel complexity, not morphological activity *per se*. As a result, they cannot be used to discriminate, for example, between braided reaches that experience no change between two points in time from those which are reconfigured extensively yet maintain the same number or length of channels. Similarly, reach-averaged values of channel migration obscure important geographical aspects of morphological change in braided rivers. Qualitative observations have demonstrated the importance of bifurcation evolution and avulsions as

critical controls on the spatial configuration of braided channel networks (e.g. Bertoldi *et al.*, 2010; Egozi & Ashmore, 2009) but these cause-effect linkages cannot be captured using existing planimetric methods.

Advances in geomatics and the development of methods for quantifying morphological change in three dimensions have partially addressed these issues. Modern techniques have eased the large-scale acquisition and processing of data for production of high-resolution digital elevation models (DEMs) of braided rivers with high accuracy (e.g. Brasington *et al.*, 2012; Westoby *et al.*, 2012; Williams *et al.*, 2013), allowing identification of spatial patterns of post-flood erosion and deposition through DEM-differencing techniques capable of accounting for uncertainty (Brasington *et al.*, 2003; Lane *et al.*, 2003; Wheaton *et al.*, 2010). The causal mechanisms of observed channel changes can then either be inferred through the identification of unique morphodynamic signatures, such as Ashmore's (1991b) "braiding mechanisms" and bank erosion (Wheaton *et al.*, 2013), or field observations of bedload transport pathways and flow patterns (Williams *et al.*, 2015). Nevertheless, the effort of field surveying means geographical and temporal coverage of existing models of morphological change in braided rivers are restricted.

The potential for new insights into the controls on braided river behaviour over broader spatial scales and longer time periods has been increased substantially by the recent revolution in Earth observation data. The public release of NASA's Landsat satellite image archive (Woodcock *et al.*, 2008) and the launch of ESA's Sentinel missions (Berger *et al.*, 2012) have provided scientists with a freely-accessible, global-scale dataset of multispectral satellite imagery with near-continual coverage at 30 m resolution or finer dating back to the early 1980s. Analysis using this dataset has demonstrated its capacity to provide temporally rich information on historical morphological changes in large braided rivers (Henshaw *et al.*, 2013) but new metrics are required that can successfully characterise morphodynamic behaviour in a way that preserves spatial linkages between different parts of the channel network. This chapter begins by examining the characteristics of braided channels from a network perspective, highlighting commonalities with other systems and phenomena, in order to define a set of universal properties. Through a critical review of literature from a wide range of network research disciplines, a collection of graph theory metrics has been identified that are particularly well suited to the study of braided river graphs. The metrics identified have been chosen based on the typology of braided river networks, which places limitations on braided river network structure and thus the array of graph theory metrics that are relevant to braided river

topologies. Following a description of these metrics, they are explored to proffer potential applications of this new toolbox to key gaps in knowledge.

3.2 Braided rivers as networks

Graphs represent systems as networks of N nodes, connected by m edges and described mathematically by a square, $N \times N$ adjacency matrix A (Newman, 2010). This data structure can be intuitively applied to the planform of a typical braided river network (e.g. Marra *et al.*, 2013; Figure 3.2). Bifurcations and confluences are represented as numbered nodes and connecting channels represent edges. Pairs of nodes can be connected by more than one edge (e.g. where a channel splits around a medial bar or island) and all edges are necessarily unidirectional (i.e. traversed downstream) due to the nature of water and sediment flux in rivers. In the adjacency matrix, positive numbers denote the presence of a directed edge or edges between two nodes ("from" nodes identified by row number, "to" nodes identified by column number) and zero values are used in the absence of a connection. Thus, in an unweighted, directed graph, an element of A, $a_{ij} = 1$, represents a connection between nodes i and j and the matrix is asymmetric (Phillips *et al.*, 2015). In most natural systems, it is unusual for all connections to have equal significance. This can be represented in a graph by applying weights to nodal connections to reflect their properties (Barrat *et al.*, 2004; Newman, 2010). Edge weights in the example shown in Figure 3.2 are based on an arbitrary, equal division of flow at each node, but more physically meaningful weights can be applied in braided channel networks. For example, Marra *et al.* (2013) propose the use of channel width (as a proxy for discharge) and the inverse of channel length (as a proxy for channel slope) due to their association with sediment transport capacity.

In addition to being directed, all braided river networks have a number of other common properties. Firstly, they are inherently spatial in their nature, with nodes embedded in two- or three-dimensional space. Spatial embedding alters concepts related to paths, which are measured by the number of edges on a path between two nodes, termed geodesic distance, in non-spatial networks (Rubinov & Sporns, 2010). The physical length of these paths, or route distance, and the "as-the-crow-flies", or Euclidean distance, between nodes are additional properties in spatial networks (Barthélemy, 2011). A network's topology describes the interrelations and arrangement of network components that result in certain patterns of connections. The spatial nature of braided systems has important implications for their topological properties, with the probability of direct links between two neighbouring nodes declining with distance. Secondly, braided river networks can be considered to be acyclic in that

they contain no self-edges (edges that connect a node to itself) or directed cycles (closed loops of directed edges that start and finish at the same node; Newman, 2010). For the practical purpose of computing potentially useful cycle-related metrics (see section 4), the directionality of edges can be removed, but most graphical representations will reflect the true nature of flow and sediment routing through braided reaches. Finally, all graphs of braided river networks are characteristically planar, meaning they can be drawn on a plane without having any edges cross and nodes are present wherever two edges intersect (Cardillo *et al.*, 2006; Newman, 2010; Barthélemy, 2011).

The wiring of complex networks can appear random, but their topological properties are a consequence of network evolution, fundamental design principles and limitations (Maslov *et al.*, 2004). As such, complex networks ranging from neural pathways in the brain, to transport links and food webs, have shown similarities in functional and structural patterning that have been identified using graph theory-based metrics. Many of these networks also share common topological features with braided river channels. For example, structural connections in brain networks form around a highly connected, central "rich-club" backbone (van den Heuvel *et al.*, 2012; Binicewicz *et al.*, 2016). Anatomically, this is more costly than alternative configurations, e.g. a larger number of shorter connections. However, although the neural "rich-club" pathways represent a relatively small element of the total wiring length of the brain, they carry a disproportionately large amount of information flow due to their enhanced topological efficiency, enabling faster, higher-level cognitive activity (van den Heuvel *et al.*, 2012; Alexander-Bloch *et al.*, 2013; Nicosia, Vértes *et al.*, 2013). This type of configuration, where a distinct dominant branch or branches from which secondary channels divide off, linking distal areas of the network, is commonly observed in braided rivers (Ashmore, 2013). This pattern emerges as a result of 1) topographic asymmetry and instability of bifurcations which, in turn, results in an unequal division of discharge and sediment transport that propagates downstream following the most efficient pathway (Bertoldi, Ashmore *et al.*, 2009; Schuurman & Kleinhans, 2015); and 2) non-linear relationships between shear stress and sediment transport rates (Dade, 2000; Church, 2006), such that small changes in discharge and slope can generate large changes in sediment transport rate along different pathways.

	68	67	66	65	64	63	62	61	60	59	58	57	56	55	54	53	52	51
68	0	0.5	0.5	0	0	0	0	0	0	0	0	0	0	0	0	0	0	0
67	0	0	0	0.5	0	0	0	0	0.5	0	0	0	0	0	0	0	0	0
66	0	0	0	0	0.5	0	0.5	0	0	0	0	0	0	0	0	0	0	0
65	0	0	0	0	0	0.5	0	0.5	0	0	0	0	0	0	0	0	0	0
64	0	0	0	0	0	0.5	0.5	0	0	0	0	0	0	0	0	0	0	0
63	0	0	0	0	0	0	0	0	0	1	0	0	0	0	0	0	0	0
62	0	0	0	0	0	0	0	0	0	0	0	0	0	0	0	0	1	0
61	0	0	0	0	0	0	0	0	0.5	0	0.5	0	0	0	0	0	0	0
60	0	0	0	0	0	0	0	0	0	0	0	1	0	0	0	0	0	0
59	0	0	0	0	0	0	0	0	0	0	0.5	0	0.5	0	0	0	0	0
58	0	0	0	0	0	0	0	0	0	0	0	1	0	0	0	0	0	0
57	0	0	0	0	0	0	0	0	0	0	0	0	0	1	0	0	0	0
56	0	0	0	0	0	0	0	0	0	0	0	0	0	0.5	0.5	0	0	0
55	0	0	0	0	0	0	0	0	0	0	0	0	0	0	0	0	0	1
54	0	0	0	0	0	0	0	0	0	0	0	0	0	0	0	1	0	0
53	0	0	0	0	0	0	0	0	0	0	0	0	0	0	0	0	1	0
52	0	0	0	0	0	0	0	0	0	0	0	0	0	0	0	0	0	0
51	0	0	0	0	0	0	0	0	0	0	0	0	0	0	0	0	0	0

Figure 3.2: The graph for a small subnetwork (middle), with an extract of the associated adjacency matrix (top). Node numbers reflect their position in the wider network and decrease in a streamwise direction, indicating flow direction. The adjacency matrix could not be included in full and is weighted to reflect an equal division of flow at each node. The legend highlights two types of shortest path, Euclidean and geodesic (see text) and the boxes (bottom) visually describe the graph theory metrics of node degree and cycles (cycle shown as grey channels; see text for descriptions).

Road networks also tend to form around central backbones of major highways, from which secondary roads branch off (de Arruda *et al.*, 2016). The topology of road networks is heavily influenced by spatial constraint, in particular planarity (Cardillo *et al.*, 2006; Barthélemy, 2011). Spatial planar networks have important characteristics that limit, for example, the number of connections to a single node (Cardillo *et al.*, 2006; Lämmer *et al.*, 2006), thereby placing

particular importance on certain types of junctions in road networks (Strano *et al.*, 2012). This is also true of braided channel networks, with bifurcations comprising a single incoming channel and two outgoing channels, and confluences usually comprising two (but occasionally more) incoming channels and a single outgoing channel (Ashmore, 2013). Road networks incorporating T-junctions provide a direct topological analogue to the majority of bifurcations and confluences in braided rivers (Figure 3.2).

The pattern of structural (physical) connectivity is an important control of function in many types of network, however system behaviour can also depend on the degree of synchronicity between clusters, or modules, of nodes (Cabral *et al.*, 2011). For example, synchronicity of electrical activity in brains has found functional connections between modules that act as a key control on pathological brain dynamics (Chavez *et al.*, 2010), with this analytical approach recently being proposed as a means to map functional connectivity in hydrological systems (Rinderer *et al.*, 2018). Modules are abstractions of sub-networks of neurons and intriguingly, it appears that the morphological structure of these modules can determine the degree of synchronicity and thus functional connectivity, rather than any direct linkage between them (Nicosia, Valencia *et al.*, 2013). In braided rivers, this is analogous to non-proximal reaches that possess similar morphological configurations displaying similar behavioural responses to stimuli such as flood events of a given magnitude, changes in sediment supply or channel management (e.g. Surian & Rinaldi, 2003).

The structural and functional similarities braided rivers share with the complex networks presented above indicates that graph theory-based metrics applied in other fields should be both transferable and, potentially, useful. However, when selecting measures and determining how they should be applied, it is also important to consider some of the differences between braided rivers and other forms of complex networks. Some of these are relatively subtle. For example, transport networks generally facilitate the efficient transfer of people between places, with their movement governed, in part, by the spatial extent and properties of different network elements (Tang *et al.*, 2016). People drive on roads, not through buildings or fields, and any given road can only accommodate a certain number of cars. Likewise, material transfers through braided river networks are also governed, to a certain degree, by the spatial properties of network elements, from the micro-scale morphology of individual channels, through the meso-scale positions of channels within the braidplain, to the macro-scale morphological configuration of the entire braidplain. However, the spatial properties of braided river networks are far less constrained than those of road networks. The spatial constraints imposed on single

junctions (nodes) and roads (edges), for example, limits their capacity to evolve, regardless of the traffic flow they receive. By contrast, in braided rivers the morphology of a bifurcation/confluence (node) or channel (edge) adjusts to the flow of water and sediment it receives, with subsequent effects on the wider braided network.

Other differences between types of complex networks and braided rivers are more striking. Networks ranging from the climate to the internet have been shown to demonstrate small-world or scale-free characteristics (Faloutsos *et al.*, 1999; Sen *et al.*, 2003; Abe & Suzuki, 2006; Kühnert *et al.*, 2006; Tsonis *et al.*, 2006; Bullmore *et al.*, 2009; Beauguitte & Ducruet, 2011). Small-world networks (SWNs) are characterised by topologies that facilitate efficient information transfer between densely interconnected sub-networks through a relatively small number of long-range connections between pairs of nodes, evidenced by high values of the *clustering coefficient* and low shortest path lengths (see section 4.2; Watts & Strogatz, 1998). Scale-free networks (SFNs) are characterised by node degree distributions that follow scale-free power-law decay, i.e. there are many nodes with few connections and few nodes with many connections (Barabási & Albert, 1999). This network property results from new nodes preferentially attaching to nodes that already have many connections. However, the development of SWN and/or SFN topologies are restricted when a network is both spatial and planar (Cardillo *et al.*, 2006; Barthélemy, 2011; Beauguitte & Ducruet, 2011). As braided rivers are spatial planar networks, certain graph theory-based metrics, for example the *clustering coefficient* (see section 4), used to characterise/discriminate between SWNs and SFNs are unlikely to be applicable in this context. Furthermore, in most braided rivers, pathways diverge and converge before eventual convergence of all paths on a single outlet node. This property will affect the transferability of certain measures designed for use with "tree" networks, which are reliant on either the convergence of multiple pathways (e.g. drainage networks; Rodriguez-Iturbe *et al.*, 1994) or largely divergent pathways (e.g. river deltas; Passalacqua *et al.*, 2013; Tejedor *et al.*, 2015a, 2015b; Passalacqua, 2017).

3.3 Graph theory-based metrics for the analysis of braided channel networks

The following sections outline a toolbox of potentially useful graph theory-based metrics that have scope to quantify the character of braided rivers at multiple spatial scales. This list is not exhaustive (for various metrics not included here see Hernandez & Van Mieghem, 2011; Newman, 2010; Rubinov & Sporns, 2010; but note the array of available metrics is extensive). The selection of metrics presented below was guided by the preceding discussion of the

characteristic features of braided channel networks. These features, particularly the spatial planar nature of braided rivers, place limitations on the relevance of various metrics to braided river graphs. As such, a critical analysis of different metrics was required to assess their theoretical applicability to studies of braided river morphodynamics. The metrics presented below form part of wider longlist of metrics, which is not described here in full due to weaker theoretical potential or presently unrealistic data requirements of certain metrics. The metrics chosen are organised by relevance to the scale at which the metric is applied (from local to reach/global) and the nature of the network property described by the metric. Note that certain metrics that are not relevant to braided river topologies but are widely used in other network studies have been included to reinforce the above comments on the transferability of metrics.

It should also be noted that network elements can be weighted to account for the properties of nodes and edges. Graph theory metrics calculated on weighted graphs are subsequently weighted, which can modify the equations (Rubinov & Sporns, 2010). The unweighted versions of metrics are presented below, with the exception of *strength*, for which edge weights are integral. The choice of node and edge weights in braided rivers will depend on the source of data from which a graph is derived. For graphs derived from satellite and aerial imagery, weights will be 2-D geometric variables, e.g. channel width, length etc., or parameters such as vegetated area, due to its effect on erosion and deposition (Corenblit *et al.*, 2014). The choice of edge weights will reflect both the specifics of research questions and the availability of weighting data.

3.3.1 Local-scale metrics

3.3.1.1 Basic metrics

The simplest way of describing the character and significance of a given node in a network is by examining the number of edges that are connected to it (Rubinov & Sporns, 2010). This property is known as node degree (k_i)

$$k_i = \sum_{j \in N} a_{ij}$$

(3.1)

where N is the set of all nodes in the network and a_{ij} is the connectivity between nodes i and j. $a_{ij} = 1$ when edge *(i,j)* occurs and 0 otherwise. In directed networks, degree can be decomposed to in-degree, the number of ingoing edges to a node, and out-degree, the number of outgoing

edges (Figure 3.2; Newman, 2010). Degree is an intuitively important measure of a node's connectedness that is often analysed in a global sense by looking at its probability distribution, often termed the degree distribution (e.g. Barabási & Albert, 1999). Degree could be a useful tool in identifying particular morphological features, for example disconnected channels where $k_i = 1$, or confluence-bifurcation meeting points where $k_i = 4$. In weighted networks, a simple extension of degree is node *strength* (S_i; de Arruda *et al.*, 2016) with the *strength* for each node i as

$$S_i = \sum_{j \in r_i} w_{ij} \tag{3.1}$$

Where r_i is the set of neighbours of i and w_{ij} is the weight of the edge connecting i to j. This metric will represent the spatial distribution of whichever morphological variable is used to weight edges.

Similarly, the number of triangles around a node i is a fundamental structural property of most networks (Rubinov & Sporns, 2010)

$$t_i = \frac{1}{2} \sum_{j,h \in N} a_{ij} a_{ih} a_{jh} \tag{3.2}$$

where a represents connectivity between node pairs (i,j), (i,h) and (j,h). This metric is integral to measuring segregation of a network into subnetworks (Rubinov & Sporns, 2010). The slender, chain-like and directed nature of braided river networks (Marra *et al.*, 2013) will limit the utility of t_i, even if the network is treated as undirected for the purpose of calculating structural metrics.

3.3.1.2   Metrics of centrality

Metrics of centrality are more complex and can be used to quantify the role of individual nodes or edges in facilitating interaction between regions of networks and fostering resilience to disturbance (Rubinov & Sporns, 2010). *Betweenness centrality* (*BC*) is perhaps the most well used centrality metric, having been applied to networks as diverse as roads (Lämmer *et al.*, 2006), prairie wetlands (Wright, 2010), artificial drainage networks (Poulter *et al.*, 2008) and,

indeed, braided rivers (Marra *et al.*, 2013). A node *i* has high *BC* if it is on many shortest paths between a pair of nodes

$$BC_i = \frac{1}{(n-1)(n-2)} \sum_{\substack{h,j \in N \\ h \neq j, \ h \neq i, \ j \neq i}} \frac{\rho_{hj}(i)}{\rho_{hj}} \tag{3.3}$$

where ρ_{hj} is the number of shortest paths between nodes *h* and *j*, and $\rho_{hj}(i)$ is the number of shortest paths between these nodes that cross *i*. The first term in the equation normalises a node's *BC* to account for the number of nodes in a network (Freeman, 1977). Node *BC* can be generalised to edges, with *edge betweenness centrality* (*eBC*) measuring the number of shortest paths between pairs of nodes that run along an edge (Girvan & Newman, 2002). Marra *et al's* (2013) application of weighted *BC*, using channel width and length as edge weights (see above), found that channels on the Jamuna River with high *BC* showed little variation in spatial position through time, being deemed morphodynamically more important to the network based both on size and high levels of connectivity to other channels.

BC and other centrality metrics quantify an abstract property of network topology, namely the role of a node in shortest paths between other nodes (Freeman, 1977). These metrics are based on geodesic paths and thus do not account for space. Combining Euclidean distance between node pairs and the sum of "physical" edge lengths on shortest geodesic paths between a pair of nodes led to the formulation of *straightness centrality $C^s(i)$* (Barthélemy, 2011)

$$C^s(i) = \frac{1}{N-1} \sum_{j \neq i} \frac{d_E(i,j)}{d_R(i,j)} \tag{3.4}$$

where $d_E(i, j)$ is the Euclidean distance between nodes *i* and *j*, and $d_R(i, j)$ is the route distance on the shortest path between *i* and *j*. Developed in the study of spatial networks, $C^s(i)$ provides a measure of the tortuosity of all shortest paths that cross node *i*. As the value of the metric approaches one, these paths become increasingly straight. Furthermore, by restricting *i* and *j* to adjacent nodes (connected by a single edge), the ratio $d_E(i, j)/d_R(i, j)$ provides a measure of the sinuosity of all single channels in a braided river network. High sinuosity is generally associated with lower channel slope, as straighter channels tend to follow paths of steeper slope, thus having greater stream power (van den Berg, 1995; Knighton, 1998). $C^s(i)$ and its single channel derivative can provide a detailed characterisation of sinuosity in braided rivers and are deemed

an improvement on classic sinuosity indices that produce a single value of sinuosity for an often arbitrarily defined reach length (Egozi & Ashmore, 2008).

3.3.1.3   Network motifs and cycles

Motifs are small, characteristic patterns of nodes and edges that repeat in different parts of the network (Binicewicz *et al.*, 2016). Functional motifs are a measure of these patterns (Rubinov & Sporns, 2010) which have been used to show that nodes representing different brain areas participated more strongly in certain patterns of connection (Binicewicz *et al.*, 2016). Whilst not explicitly using graph theory, a very similar approach has also been applied to the classification of landforms, using patterns of elevation change (Jasiewicz & Stepinski, 2013). "Path motifs" have also been used to show that certain ordered sequences of nodes exist in brains to facilitate communication between less well connected "local" nodes by routing information transfer through highly connected "rich-club" nodes that form the network's central backbone (van den Heuvel *et al.*, 2012). It is not clear whether subnetworks in braided rivers will show enough variation in their patterns of connections to calculate functional motifs. However, existence of these patterns would suggest a degree of local self-organization driven by the interaction between large-scale forcing variables, such as discharge and sediment supply, and more localised factors relating to the morphology of the braidplain.

Patterns that should be identifiable in braided river networks are cycles (closed loops of edges that start and finish at the same node). These have been used in the study of road networks as a means of showing differences in road layout that exist between urban areas (Cardillo *et al.*, 2006). Specifically, a cycle of four, for example, indicates a typical "block", such as those associated with road networks designed on a grid system. Indeed, Cardillo *et al.* (2006) found that American cities (which are often built on grid systems) tended to have the greatest proportion of cycles of four in the sample of cities analysed. Cycles are a less sophisticated metric than functional motifs, but as they consist of closed patterns, they will be present in braided river networks. The directionality of the network will need to be removed in order to permit their identification, but the metric should enable identification of bar types of varying complexity (compare the cycle of 2 between nodes 54-53 and the cycle of 6 in the expanded box in Figure 3.2).

3.3.2   Reach/global-scale metrics

3.3.2.1 Metrics of integration

Integration describes the capacity of different regions of a network to communicate rapidly with one another based around the concept of paths (Rubinov & Sporns, 2010). Shorter, more direct paths between pairs of nodes will, in general, facilitate more efficient transfer of information between these nodes. Employed in studies of both spatial and non-spatial networks, shortest path length d_{ij} is a descriptor of geodesic distance, in terms of number of nodes a_{uv} on a shortest path $g_{i \leftrightarrow j}$ between a node pair ij (Latora & Marchiori, 2001)

$$d_{ij} = \sum_{a_{uv} \in g_{i \leftrightarrow j}} a_{uv} \tag{3.5}$$

The characteristic path length of a network can be calculated by averaging the shortest path lengths between all pairs of nodes (e.g. Watts & Strogatz, 1998). In spatial networks, $d_R(i, j)$ defines the physical length of this path (Barthélemy, 2011).

Latora & Marchiori (2001) analysed networks using the metric *efficiency* (ϵ_{ij}). *Efficiency* of communication between two nodes *i* and *j* is defined as inversely proportional to the shortest path (d_{ij}) between these nodes. The average *efficiency* of a graph **G** is defined as

$$E(\mathbf{G}) = \frac{\sum_{i \neq j \in \mathbf{G}} \epsilon_{ij}}{N(N-1)} = \frac{1}{N(N-1)} \sum_{i \neq j \in \mathbf{G}} \frac{1}{d_{ij}} \tag{3.6}$$

E(**G**) measures the *global efficiency* of the graph (E_{glob}). *Local efficiency* E_{loc} is defined as the average efficiency of subgraphs **G**$_i$ of a node *i*

$$E_{loc} = 1/N \sum_{i \in \mathbf{G}} E(\mathbf{G_i}) \tag{3.7}$$

Applied to braided rivers, these metrics describe complexity at either the reach- or network-scale. Low values of E_{glob} or E_{loc} indicate a reach or network that is heavily bifurcating. Most bifurcations in braided systems are asymmetrical, with one distributary becoming dominant and

causing a possible destabilisation of the bifurcation (Ashworth, 1996; Schuurman *et al.*, 2016). Consequently, low efficiency network configurations may tend towards small-scale instability related to the dynamics at single bifurcations, whereas high efficiency networks may be more stable but with a greater probability of large-scale morphological change propagating from a point of disturbance.

Analysing sub-networks within river delta channel networks, Tejedor *et al.* (2015a, 2015b) defined *resistance distance* (*RD*), based on the theory of electrical circuits. Instead of focusing on the shortest path between a pair of nodes, *RD* quantifies the number of disjoint paths, paths not containing the same edges, between a node pair. As *RD* increases, so do the number of disjoint paths between a pair of nodes. Braided rivers exhibit longitudinal fluctuations in the number of parallel channels, which should manifest as subnetworks with varying *RD*. Simply looking at *RD* at a snapshot in time would give a variable describing the complexity of a reach at that time. However, multi-temporal analysis may provide insight into how this important aspect of a braided channel network varies in response to different stimuli, such as changes in flow or sediment supply.

3.3.2.2   Metrics of segregation

These metrics describe the presence of densely interconnected groups of nodes (Rubinov & Sporns, 2010). The clustering coefficient of the network (*C*) is one of the most widely used measures of segregation. Networks with a high *C* and low ‹d_{ij}› are classed as small-world (see section 2; Sen *et al.*, 2003; Watts & Strogatz, 1998). *C* is not well suited to planar graphs but the meshedness coefficient *M* is a promising alternative (Buhl *et al.*, 2004)

$$M = \frac{F}{F_{max}}$$
(3.8)

where *F* is the number of internal faces, regions of a planar graph bounded by edges, and F_{max} is the number of internal faces in the maximally connected version of the same graph, e.g. the version of the graph where each node is connected to as many neighbours as possible without breaking planarity. For any planar graph, *F* and F_{max} can be defined as (Buhl *et al.*, 2004)

$$F = m - n + 1$$
(3.9)

$$F_{max} = 2n - 6 \qquad\qquad (3.10)$$

where m and n are the number of edges and nodes in the graph. Cardillo *et al.* (2006) used M to assess the structure of urban road networks, with low values (≤ 0.1) of M being more tree-like and networks tending towards a regular lattice as M approaches 1. Variation in M in braided rivers would show network-scale fluctuations in complexity, with higher values being associated with rivers that that maximise possible connections between nodes.

3.3.2.3 Metrics to assess network sensitivity

Sensitivity is of paramount importance in networks such as infrastructure (Scott *et al.*, 2006; Jenelius, 2009; Sullivan *et al.*, 2010), supply (Wagner & Neshat, 2010; Kim *et al.*, 2015; Herrera *et al.*, 2016) and the internet (Newman, 2010). Approaches to sensitivity often utilise degree distributions. For example, SFN degree distributions (Barabási & Albert, 1999) result in networks that are sensitive to targeted attacks on high k nodes, but relatively insensitve to random attacks with higher probability of affecting low k, poorly connected nodes (Newman, 2010). Given that k is expected to have a limited range in braided rivers, examination of degree distributions in isolation is unlikely to provide much insight on network sensitivity. However, other measures designed to quantify the relative abundance of particular features based on k may be more instructive. For example, studying road networks, Strano *et al.* (2012) defined r_N

$$r_N = \frac{N_1 + N_3}{\sum_{k \neq 2} N_k} \qquad\qquad (3.11)$$

here N_k is the sum of nodes of degree k, thus measuring the relative abundance of dead ends (N_1) and T-junctions (N_3) in the network. Strano *et al.* (2012) did not consider nodes with $k = 2$, as they are not proper road junctions. Adapting this metric to consider only nodes of either in- or out-degree = 2 quantifies the number of either bifurcations or confluences in the sample of nodes of N_k. Weighting a directed version of r_N with, for example, bifurcation angle may quantify the relative abundance of morphological features prone to instability, e.g. high-angle bifurcations (Bertoldi, 2012).

3.4 Applications of graph theory to braided river research

The manifold elements and processes active in braided rivers result in their complex and spatially variable planform. Graph representations of braided rivers allow characterisation of braided planforms across nearly the full range of morphological unit scales. The preceding section has isolated a range of metrics that allow analysis across this range of scales and the following discussion will suggest some possible applications of graph theory to three different but complementary aspects of braided river research; 1) 2-D structural characterisation of braided channel networks, 2) graph theoretical analysis of braided river morphodynamics, 3) validating numerical models using graph theory.

3.4.1 Graph theory: a new, multi-scale framework for the morphological characterisation of braided rivers

At the smallest scale that can be resolved in graph representations of a braided channel network, single nodes represent bifurcations and confluences. The changing spatial distribution of different *strength* nodes (de Arruda *et al.*, 2016) will show how the physical properties of channels vary at discrete locations across the braidplain. Reformulation of r_N (Strano *et al.*, 2012) to analyse in- and out-degree on weighted networks would characterise the relative abundance of either bifurcations or confluences that have certain properties. Methods have also been proposed for deltas that use upstream channel properties to make probabilistic estimates of water or sediment flux routing to downstream neighbour nodes (Tejedor *et al.*, 2015b), though this method is fraught with large assumptions on flux routing controls and would be best applied to numerical models where flux routing is known. Characterisation of single network elements can likewise be applied to edges. The topological importance of single edges could be assessed using *eBC* (Girvan & Newman, 2002) to show areas where channel closure may disconnect part of a network. A similar approach has been applied to Norwegian road networks to ascertain edges (roads) at risk of closure from debris flows and the subsequent cost (in route distance) of the next shortest path between disconnected nodes (Meyer *et al.*, 2015). Edges may also be declared "homogenous" if the nodes connected to them share properties (Del Vicario *et al.*, 2016). The spatial distribution of "homogenous" edges would help to characterise areas of the braidplain that show local changes in physical properties.

Edge properties can also be used at the reach-scale to characterise planform. Figure 3.3 presents an example of two reaches, A and B, from the same instance of the Fiume Tagliamento's braided channel network. These reaches have visibly different planforms but very similar braiding intensity as quantified using a traditional braiding index (Egozi & Ashmore 2008), with values of 4.8 and 4.3, respectively. Reach A does not have a dominant main channel, being

characterised by roughly equally sized parallel channels that support areas of complex bar dissection. Reach B is clearly dominated by a main channel, with sequential loci of more intense bar dissection and longer avulsion channels branching from the main channel before rejoining downstream. Analysis of spatially distributed metrics such as *BC* that quantifies the properties of single nodes or edges may be able to characterise these differences and, indeed, chapter 6 of this thesis presents a multi-spatial analysis of *BC* to highlight patterns of planform change in response to flood events, showing how different areas of the network evolve over various spatial scales. Other approaches to reach-scale characterisation of braided planforms could apply network motifs or cycles to analyse how channel pattern changes between reaches. Visual assessment of the network skeletons overlain on reaches A and B in Figure 3.3 suggests that the frequency distribution of cycles in each reach may show some differences with, perhaps, a heavier right tail in reach B due to a greater number of large bars bordered by multiple bifurcations and confluences. Whilst this suggestion is hypothetical, it is indicative of the kind of characteristic information that can be extracted from braided rivers at the reach-scale; information that is missed by spatially averaged braiding indices.

At greater than the reach-scale, graph theory offers metrics applicable to network-scale characterisation of braided rivers. These include structural metrics such as E_{glob} (eq. 3.7) and *M* (eq. 3.9-3.11). It is possible that limitations placed on node degree in braided rivers may limit the range of values these metrics can take, which is observed for E_{glob} in chapter 6. However, variation of E_{glob} or *M* within small limits will be showing a change in the network's structural organisation. In particular, changes to E_{glob} will reflect differences in the average level of connectedness between node pairs based on the length of the shortest paths that connect them. Whether potentially subtle variations in these properties of global network structure can be used as broad discriminators between different types of braided river or as indicators of large-scale change in a single river over time is an open question, but it seems likely that these metrics will provide more detailed quantitative information on the reorganisation of braided river network structure than changes to a simple average of the number of wetted channels.

Whilst graph theory can be applied to multi-scale characterisation of braided river morphologies, it may also have the potential to quantitatively define reaches. The reach is one of the key spatial units in braided river studies, but is often defined arbitrarily (e.g. Ashmore *et al.*, 2011; Fotherby, 2009; Henshaw *et al.*, 2013; Liébault *et al.*, 2013). Topological metrics may provide a quantitative means to segment a braided river into reaches. *NN(h)* defines the average size of a neighbourhood (number of nodes) of *h* hops (along edges) from a given node (Faloutsos

et al., 1999). For a low *h*, *NN(h)* should scale with network complexity, which fluctuates along the length of a braided river. Calculating *NN(h)* for subsamples of nodes in a downstream direction should capture this fluctuating complexity, which may also serve as a basis for defining reach boundaries. Combining *NN(h)* with sequence zonation algorithms that use longitudinal variation in input parameters to define boundaries in a sequence (Parker *et al.*, 2012) could provide a quantitative method for defining reaches on braided rivers. Alternatively, algorithms designed to detect communities, e.g. highly connected groups of nodes, within networks may also provide a means to objectively define reaches. One such algorithm, *edge betweenness clustering* (Newman & Girvan, 2004), is trialled in chapter 5 with promising results that highlight how spatial scaling in braided rivers may show dynamics related to flood magnitude.
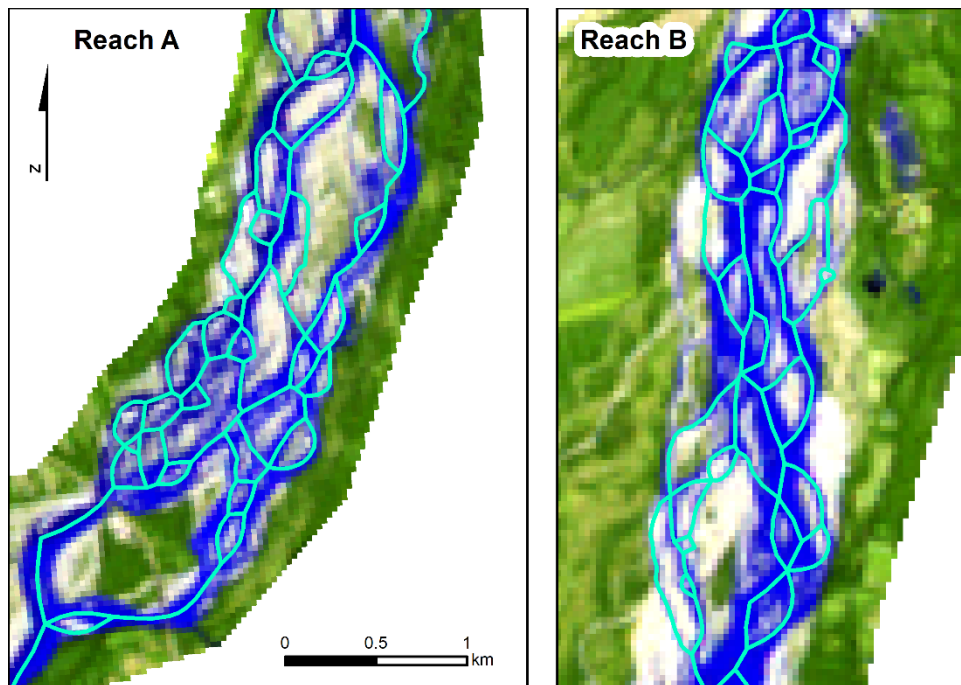
Figure 3.3: Comparison of two reaches with similar total braiding indices (A = 4.8, B = 4.3) but different planform structures.

It is apparent that graph theory may hold great potential for detailed characterisation of braided river planforms. However, planform is known to show considerable stage-dependence that relates to the complexities of braided river topography (Redolfi *et al.*, 2016), such that the complexity of braided river networks is greatest at intermediate stages when most channels are connected and higher bar surfaces are not inundated (Van Der Nat *et al.*, 2002, 2003). As with braiding indices (Egozi & Ashmore, 2008), this property of braided planforms will have considerable effects on certain graph theory metrics. Pattern-based metrics, such as *motifs* and *cycles*, will vary considerably with stage, likely showing minimal variation at high stage when few bars are exposed. Similarly, path-based metrics that assess alternate paths on subnetworks, e.g.

RD, will likely show maxima at intermediate stage when the number of wetted channels is also at a maximum. However, certain graph theory metrics, such as those based on the analysis of shortest paths, may show less stage dependency, especially in weighted networks where channel size and thus persistence over variable stage can be incorporated into the metric (e.g. Marra *et al.* 2013). Stage dependency in the spatial distribution of unweighted *BC* is considered further in chapter 6 of this thesis.

3.4.2 Network approaches to studying braided river dynamics

The evolution of a braided system is broadly driven by the interplay between sediment supply, discharge and, where it is prevalent, vegetation (Gurnell *et al.*, 2001; Bertoldi *et al.*, 2010; Charlton, 2010). In rivers with variable discharge regimes, floods are a major driver of morphodynamics that create considerable problems for analysing braiding behaviour under formative conditions. Inundation of the braidplain during flood events decreases network complexity and increases morphodynamic activity (Van Der Nat *et al.*, 2002; Bertoldi, Ashmore *et al.*, 2009; Ashmore *et al.*, 2011). Thus, we are left with something akin to Labov's (1972) "observer's paradox": when a braided river is at its most outspoken, it is also at its least observable! Network analysis of remotely sensed data may help to get around this problem.

Whilst stage-dependent network complexity undoubtedly causes problems for network analyses, it may also present opportunities. Where temporally rich datasets provide imagery over the course of a flood event, mapping the channel network and how its topology evolves with rising stage may allow inference of 3-D properties from 2-D analysis. For example, $C^s(i)$-type metrics may indicate the order in which channels of different slope magnitudes begin to convey flow. The temporal frequency for such analyses would likely come from aerial surveys or fixed position cameras (e.g. Bertoldi, 2012; Bertoldi *et al.*, 2010). These survey methods also avoid the inherent issue of cloud cover in satellite imagery around the time of floods. Multispectral satellite imagery does, however, provide temporal depth. Datasets such as Landsat, which spans 35 years with global, 16-day repeat coverage enable multi-temporal analysis of the evolution of braided river networks (Henshaw *et al.*, 2013). Again, it is important to recognise the limitations of braided river network analysis using satellite data. The entire network structure of braided rivers may be reset during large floods (Bertoldi *et al.*, 2010; Belletti *et al.*, 2015) and the length of time between cloud-free imagery can exceed the temporal persistence of single nodes and small bars. Although network elements will be georeferenced, it is unwise to try and track all but the largest of channels and bars over periods of variable hydrological conditions or without high temporal resolution observations.

The limitations posed by remote sensing datasets can be overcome with numerical models, which provide the ability to "observe" the unobservable, outputting detailed changes in morphometric variables and sediment transport rates across the model domain (Nicholas, 2000; Ziliani *et al.*, 2013; Church & Ferguson, 2015; Schuurman & Kleinhans, 2015). Network analysis of numerical models could use sediment transport data to weight nodes and edges, a similar approach to which has been taken in tributary networks, with results highlighting hotspots of geomorphic change (Czuba & Foufoula-Georgiou, 2014, 2015). Applying these weights to *BC*, for example, would show channels that are central to the network from both a topological and process-based perspective.

Numerical models will provide a ready source of variables with which to weight braided river graphs, however the reliance on 2-D datasets for graph analysis of natural systems means that consideration should be given to the morphodynamic behaviours that can be gleaned from unweighted networks. In this respect, concepts and behavioural analogies arising from studies of network dynamics in different fields may stimulate dynamic approaches to braided river research. In human brain networks, resting-state oscillation of electrical signals (Cabral *et al.*, 2011) are analogous to the constant, small-scale morphological adjustments that occur in braided rivers during periods of lower, yet competent, flows (Bertoldi *et al.*, 2010). These small-scale adjustments may be part of the evolution of a braided network towards a self-organised critical state (Sapozhnikov & Foufoula-Georgiou, 1997, 1999), priming the system for a certain response to a stimulus, e.g. a large flood. Given that responses to stimuli in complex, natural systems are often mediated by the propagation of a stimulus through a network's nodes (Bar-Yam & Epstein, 2004), it will be interesting to see whether the unweighted topology of braided rivers has any relationship with the response of the system over longer time-series and if system responses are better represented by weighted topologies. How to analyse dynamics using topological relations is an open question, to which some ideas are offered below.

Time-series analysis of braided river topologies is likely to be a key tool in probing responses to stimuli and long-term evolutionary trajectories. Methods based around the analysis of fractals have used time-series data to show that braided rivers scale dynamically, e.g. the evolution of network elements can be scaled in time such that rates of evolution are the same for elements across different spatial scales (Sapozhnikov & Foufoula-Georgiou, 1997). Sapozhnikov & Foufoula-Georgiou (1997) note that dynamic scaling is indicative of a system at a critical state and that in order to assess whether a braided river has established self-organised criticality, it would be necessary to track parameters that affect critical behaviour, for example slope. *$C^z(i)$-*

type (Barthélemy, 2011) sinuosity metrics may provide a surrogate for slope (see section 4), at scales ranging from single channels to the whole network. Combining analysis of dynamic scaling and $C^s(i)$-type metrics may provide a means to show whether a braided system is in a critical state and how it might react to further forcing. Responses to forcing also depend on antecedent conditions, with braided river evolution suggested to occur along trajectories (Ziliani & Surian, 2012). Autoregressive modelling of graph theory metrics, whereby the value (y_t) of a time-series at time t is modelled as a function of previous values ($y_{t-1}...y_{t-n}$; Harvey & Clifford, 2009) could investigate the presence of such trajectories, though the issues of tracking network elements over time (see above) may complicate the derivation of time series data. Cross-correlation analysis, which has shown time-dependent correlations between morphodynamic variables in a flume environment (Ashmore, 1991a), may also provide insight into relationships between graph theory metrics over time. Given that morphological instabilities can propagate downstream in braided rivers (Ashmore, 1987; Takagi *et al.*, 2007; Schuurman *et al.*, 2016), cross-correlation of, for example, reach-averaged *cycles* may show how different reach configurations propagate downstream over time, or show the periodicity with which a reach returns to a certain configuration.

Propagation of certain reach configurations could also be thought of in terms of continuation in what Thibaud *et al.* (2013) refer to as filial relations. This concept is based on ancestry and descendance between entities. An entity is a geomorphic feature, identified by one or more attributes that distinguish it from others present at the same time. If an entity persists from one timestep to the next, it perpetuates its identity. Changes to an entity may derive descendants, possibly by amalgamation with other entities. These two modes of filiation are termed "continuation" and "derivation" (Thibaud *et al.*, 2013). In braided rivers, entities could be defined by reaches, or sub-reach-scale *motifs* or paths, with their identities defined by attributes such as graph theory metrics and physical properties. Setting thresholds for change in the attributes of an entity shows continuation of the entity, or derivation. Analysis of the continuation or derivation of entities is performed in the lens of variables that drive morphodynamics (floods, sediment input etc.). Thus, filiations could provide a framework to assess the risk of morphodynamic change in response to driving variables at the reach-scale and, the aforementioned problems with tracking nodes and edges notwithstanding, at sub-reach scales.

Unlike remote sensing or field-based datasets of braided rivers, network elements can be tracked in numerical models of braided rivers and application of detailed morphometric or rate-

based model outputs will improve the capacity for weighting graphs derived from these models. Subsequently, time-series or filiation analyses could be extended to smaller spatio-temporal scales. The detailed representation of morphodynamic processes in numerical models may also enable agent-based modelling (ABM), whereby nodes (agents) are in one of various states, represented by a suite of different physical and graph theoretical metrics, and changes to these states occur based on dynamical rules or the state of neighbouring nodes (Barrat *et al.*, 2013). Dynamical rules could be developed through present knowledge of braided river processes. An ABM then probes the relative importance of different processes by iteratively changing rules to increase or decrease the importance of certain processes, with the response of the ABM checked against that of the numerical model. Barrat *et al.* (2013) note that difficulties in discriminating the effects of assumptions or parameters in ABMs grows with the number of parameters used. Given the spatial and temporal complexity of even a single braided river process, for example sediment transport (Ashworth & Ferguson, 1986; Nicholas, 2000; Kasprak *et al.*, 2015), there will be limitations on how detailed an ABM of a braided river could be, but ABMs may provide new insight into how certain parameters and processes affect braided river dynamics.

3.4.3 Does my model talk the talk and walk the walk? Graph theoretical approaches to numerical model validation

There has been considerable development in analytical and numerical modelling of braided rivers, with models now able to generate realistic braided morphologies of large braided rivers (Murray & Paola, 1994, 2003; Yang *et al.*, 2015; Schuurman *et al.*, 2016; Williams *et al.*, 2016). However, simplifying assumptions are inevitable, for example applying uniform roughness coefficients across the model domain or simplifying the effects of vegetation (Church & Ferguson, 2015). As such, datasets from natural systems are needed against which to validate the output of numerical models. There is, however, a lack of both laboratory and natural datasets that can be used to support model development (Williams *et al.*, 2016). Datasets that do exist for natural systems, either remote sensing planform-based or field-based, often only cover short time intervals or are of low temporal resolution for repeat surveys. Further limitations are placed on using planform-based datasets due to the low discriminatory power of classic methods, e.g. braiding indices, used to characterise such data (see above).

By representing natural braided rivers as a graph, much of their inherent complexity is assimilated into the graph's nodes and edges, whilst still representing the structure and behaviour of the network. Graph theory could, therefore, offer a novel approach to validating numerical models of braided river morphodynamics. The temporal depth and resolution of

satellite imagery provides datasets at spatial and temporal scales that capture both long-term and event-based morphodynamic responses in braided rivers. With datasets that can assess network change before and after discrete events *and* network behaviour of natural systems through time, it would also be possible to closely examine the behaviour of a numerical model.

Adapting graph theory as a tool to better understand model sensitivity and the mechanistic behaviour of models could take various approaches that utilise graph theory metrics to quantify properties of natural systems and use them as novel sources of reference data. Global properties of the network quantified with, for example, E_{glob} (eq. 3.7), M (eq. 3.9-3.11) or average BC (eq. 3.4) account for a variety of different structural properties of the network (see section 3.3) that cannot be captured using traditional braiding indices. Deriving these global network metrics for natural systems over time and before and after flood events would provide an overall measure of how modelled braided rivers replicate the structure of their natural counterparts. At smaller scales, both processes and forms may show spatial scaling in braided rivers (Sapozhnikov & Foufoula-Georgiou, 1996; Ashmore, 2013; Reitz *et al.*, 2014; Kasprak *et al.*, 2015). If it is found that, for example, channel length correlates with BC or that nodes of a given *BC* have a typical spacing within the network, then these could be used as model validation parameters by assessing whether a model recreates the same spatial scaling of network metrics seen in natural systems.

Alternative approaches to scaling in network research often utilise scale in the frequency or probability distribution of a metric (Barabási & Albert, 1999; Chen *et al.*, 2002; Beygelzimer *et al.*, 2005). Initial analysis of the distributions of *eBC* for braided river graphs at low, medium and high discharge appear to show patterns in their frequency distributions (Figure 3.4). Lower discharge seems to be associated with heavier tailed distributions. Visual assessment of *BC* maps for the Jamuna River (Marra *et al.*, 2013) suggest a similar pattern may be seen in these data, reflecting what is likely the effect of a relatively high number of more central channels at low flow, which diminishes at higher flows as more channels and new paths become active. Whilst more analysis is needed to confirm this relationship, it indicates that the distribution of *BC,* or other metrics, may have typical scaling for a given discharge in a natural river. Thus, the scaling of metric distributions in natural rivers could provide a reference against which to test a similarly parameterised model.

There is also potential for validating internal behavioural responses in models using graph theory. Schuurman *et al.* (2016) found that bifurcation instabilities cascaded downstream in their model of a large, sand-bed braided river. With graph datasets of natural systems at

sufficient temporal resolution, tracking metrics such as weighted r_N (Strano *et al.*, 2012) through time and space in both real and modelled rivers may show the propagation of these instabilities and whether the spatio-temporal properties of modelled propagation are corroborated by real-world observations. This would provide a dynamic measure of whether numerical models of braided rivers match the behaviours seen in modelled systems.
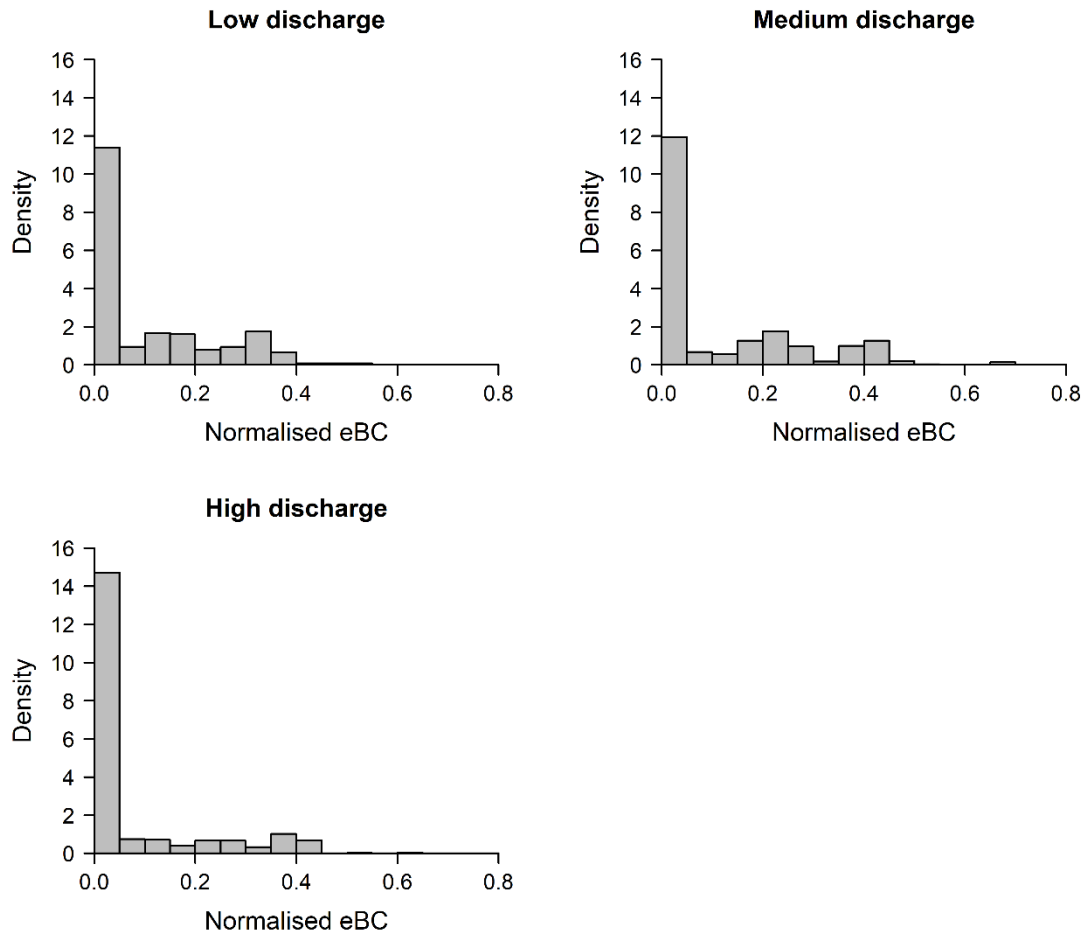
Figure 3.4: Plots of normalised eBC density functions for graphs derived at times of low, medium and high discharge on a medium sized braided river. Note that the y axes exceed 1 as the total integral of the bars sums to 1, with the plots showing the relative frequency of eBC in each bin.

3.5 Summary

Network analysis is a key tool for understanding the behaviour of natural and anthropogenic systems in a wide range of disciplines. This chapter sought to highlight how the topologies of braided river networks have striking similarities with networks as diverse as roads and brains, providing a rationale for the application of network analysis to braided river geomorphology. The study of network analyses across a range of disciplines has identified a suite of graph theory

metrics that may be of relevance to braided river morphodynamics. These metrics are applicable at nearly the full range of scales relevant to braided river processes and can also account for connectivity between geomorphic units within braided river networks. The *raison d'être* for network analysis of braided river systems can be pleasingly summarised by Boulding (1956: p. 207), who described the knowledge attained from systems approaches as "like, shall we say, the 'knowhow' of the gene as compared with the knowhow of the biologist."

Marra *et al.* (2013) have shown the potential of network analysis for studying braided river morphodynamics. To date, this is the only example of detailed research applying network methods and graph theory to braided rivers, despite a recent upsurge in geoscientific applications (Poulter *et al.*, 2008; Wright, 2010; Phillips, 2011; Heckmann & Schwanghart, 2013; Czuba & Foufoula-Georgiou, 2015; Heckmann *et al.*, 2015; Phillips *et al.*, 2015; Tejedor *et al.*, 2015a, 2015b; Masselink *et al.*, 2016; Passalacqua, 2017). The graph theory toolbox presented herein provides a suite of new metrics that can describe a multitude of topological properties, how these topological properties are affected by physical properties and new ways of showing the spatial distributions of these physical properties. Taken together, this toolbox provides a powerful new approach to quantitative descriptions of braided river morphologies, which can be linked to morphodynamic processes. There will be many approaches to graph theory-based analysis of braided river morphodynamics, of which some ideas have been offered here. Time-series analysis of braided river graphs is likely to be pivotal, whilst more experimental approaches, e.g. ABMs, could be facilitated by numerical modelling. Dynamical study of network behaviour is a growing field in network research (Boccaletti *et al.*, 2006), which may produce exciting possibilities for braided river research. Graph theory may also provide metrics that can test the response of numerical models of braided rivers, assessing whether the gross-scale structure and function of a modelled braided river matches its natural counterpart.

There is exciting theoretical potential in the application of network analysis to braided rivers that is supported by the recent increase in availability of temporally rich and relatively high-resolution satellite imagery such as Landsat (Roy *et al.*, 2014), providing a means to generate multi-temporal network datasets of medium to large braided rivers, globally. With the availability of datasets for network analysis of braided rivers, there is also the question of which metrics will actually be interpretable from a geomorphic perspective? This review has aimed at a theoretical overview of possible interpretations of graph theory metrics in the context of braided river morphodynamics. It is now down to thorough testing to look for statistical

patterns in metrics and their relationships with drivers of braided river behaviour and the behaviours themselves.

It is hoped that the applications of graph theory in the proceeding chapters of this thesis will provide a foundation for continued exploration of these methods within braided river research. The basis of this chapter and the wider approach to this thesis is interdisciplinary. Collaboration with researchers in other network disciplines and with those taking field- and modelling-based approaches to braided river research will be essential to the development of novel insights into the structure and function of braided rivers networks using graph theory, and how these insights may relate to other networks.

4. Application of novel image classification techniques to support braided river network extraction

Chapter synopsis

For the graph theory-based approach to braided river research advocated in this thesis to be viable, there is a need for methods to extract network representations of braided river systems with minimal data requirements. This chapter present an application of novel, Object Based Image Analysis (OBIA) techniques for the classification of braided channel networks from satellite remote sensing data. The performance of OBIA classification is assessed against traditional, "per-pixel" methods of landcover classification, finding that OBIA is as, or more accurate than traditional methods and faster to apply. A semi-automated workflow is then presented for the vectorisation of classified rasters of the channel network, which derives a network of channel centrelines with their associated topology representing the direction of connections and flow of water and sediment through the network. The geometrical properties of the channel network extraction are tested against reference data, showing that the Landsat derived channel networks replicate channel lengths in the reference dataset strongly but spatial resolution hampers accurate representation of channel width.

4.1 Introduction

The core aim of this thesis is to tackle the spatial and temporal limitations of current approaches to braided river research through the application of network analysis and graph theory. This aim is underpinned by the requirement for datasets that allow analysis of braided river network graphs at multiple spatial and temporal scales. In order to treat a braided river as a graph, a topological representation of the network must be extracted. However, for the analytical approaches applied in this thesis to be spatially and temporally scalable across multiple instances of one river, or across different rivers, there is a need to develop an approach to braided river graph extraction with minimal data requirements. Given the size of many braided rivers and the rapidity with which they evolve (Ashmore, 2013), satellite remote sensing provides, at present, the only data source that allows for multi-spatial and multi-temporal analysis of medium to large braided river networks (e.g. Henshaw *et al.,* 2013; Takagi *et al.,* 2007). The application of graph theory and network analysis to braided rivers is therefore

contingent on a methodology for extracting braided river networks from a single satellite or other remote sensing image input (Figure 4.1).

Extraction of a network representation of a braided river network requires the vectorisation of the channel network from the raster input image (Marra *et al.*, 2013). Vectorisation is contingent on image classification to isolate the areas of the input image that need to be vectorised, which in the present case are wetted channels. The array of available classification techniques is multifarious and spans orders of magnitude in terms of the complexity of their application (Lu & Weng, 2007). The majority of studies applying satellite-based remote sensing to braided river or delta research have applied traditional, pixel-based classification approaches (e.g. Takagi *et al.*, 2007; Bertoldi *et al.*, 2011; Edmonds *et al.*, 2011; Henshaw *et al.*, 2013; Ashraf *et al.*, 2016). However, developments in image classification techniques now recognise that classification using Object-Based Image Analysis (OBIA) generally provide more accurate results than pixel-based methods (Phiri & Morgenroth, 2017). Thus, this chapter reports a novel application of OBIA for the classification of braided river channels and provides an assessment of its accuracy relative to traditional, per-pixel classifiers.

After classification of a remotely sensed image to isolate the channel network and other landcovers of interest, the next stage of the network extraction process requires vectorisation of channel centrelines in a format that captures the connectivity between different channels. A simple workflow to derive channel centrelines with topology from a classified raster channel network has been developed using geoprocessing tools available in ArcGIS (ESRI Inc., Redlands, USA). The workflow is semi-automated, requiring some manual correction to remove artefacts created during vectorisation of the input raster and to correctly assign the direction of flow along an edge, but provides a fast and accurate means to derive braided river channel networks with topology that can be used for graph analysis.

The following sections provide a brief overview of different approaches to image classification in remote sensing. More detail is provided on the different types of image classification scheme applied herein and the techniques used to assess the classification accuracy of the different schemes. Results of the accuracy assessment are presented, followed by a description of the workflow used for extracting channel networks from classified imagery and an accuracy assessment of certain geometric properties of the extracted network.

4.1.1 Image classification methods: a brief overview

Three groups of image classification methods are described here: 1) per-pixel methods, 2) OBIA methods, 3) machine learning approaches. The latter is used as a catch-all grouping for more sophisticated methods that can be applied within object-based or per-pixel frameworks. Per-pixel image classification utilises the spectral properties of single pixels belonging to different landcovers to classify remote sensing imagery (Lillesand *et al.*, 2008). In a multi-spectral image, different landcovers reflect different wavelengths of the electromagnetic spectrum at varying magnitudes. Chlorophyll pigmentation in vegetation, for example, reflects light heavily in the near-infrared (NIR) band of the spectrum and absorbs light in the red band (Bertoldi, Drake *et al.*, 2011). These properties will be shown in the reflectance values of vegetated pixels and can thus be used to differentiate and classify landcovers.

Per-pixel classification techniques can be classed as supervised and unsupervised (Li *et al.*, 2014). Unsupervised techniques are automatic and operate by finding natural groupings of pixel values under the assumption that these groupings will reflect a landcover class. Supervised classifiers require training data, whereby the image analyst selects training samples that are representative of given landcovers. The spectral properties of all pixels in the image are then compared to these training samples and assigned a class based on decision rules (Li *et al.*, 2014). There are clear advantages and disadvantages to both unsupervised and supervised classifiers. Key advantages of unsupervised methods are their speed of implementation and objectivity, as an image is classified without *a priori* interventions by the analyst. This second point is also a disadvantage, as it is necessary to determine which landcovers the classes found by an unsupervised classification actually refer to. Unsupervised classifications are also more prone to error in heterogeneous landscapes than supervised methods, as the latter can be trained to detect landcovers with more ambiguous spectral properties. Selection of training data is the main pitfall of supervised classifiers, as it places a significant burden of labour on the image analyst when analysing large samples of imagery.

As the spatial resolution of satellite remote sensing data has increased above the size of the objects in the imagery, calls for taking an object-based approach to image classifications have increased (Blaschke *et al.*, 2014). The basic premise of OBIA is to initially segment an image's pixels into "image-objects" based on spectral similarity and adjacency (Kressler *et al.*, 2005; Blaschke, 2010). Grouping pixels into objects accesses more spectral information than single pixel values, such as mean values per band and statistical properties of the objects reflectance values, as well as spatial information including object dimensions and neighbourhood relations

(Blaschke, 2010). As with per-pixel methods, supervised and unsupervised classification can be applied whereby the image objects essentially take the place of single pixels. An alternative approach is also proposed, in which the classification procedure is iterative, from the original segmentation of the image to progressive classification of image objects based on a system of rules that utilise properties of image objects typical to that landcover class (Blaschke *et al.*, 2014). This rule-based approach to OBIA provides the framework within which OBIA classifications are developed in commercial-grade OBIA software such as eCognition Developer (Trimble Inc., Sunnyvale, USA) and Erdas Imagine (Hexagon Geospatial, Madison, USA). These platforms also allow for the integration of data from different sensor types, e.g. 2-D aerial or satellite imagery with 3-D LiDAR data, further increasing the amount of information that can be used in a classification relative to per-pixel methods. Fusion of 2-D multi-spectral and 3-D topographic data within an OBIA framework has recently been applied to regional scale classification of hydromorphological units from remotely sensed data (Demarchi *et al.*, 2016, 2017). Other examples of OBIA applications within fluvial geomorphology are limited, though Belletti *et al.* (2015) used OBIA classification routines to delineate the active channel area in multiple braided rivers in France.
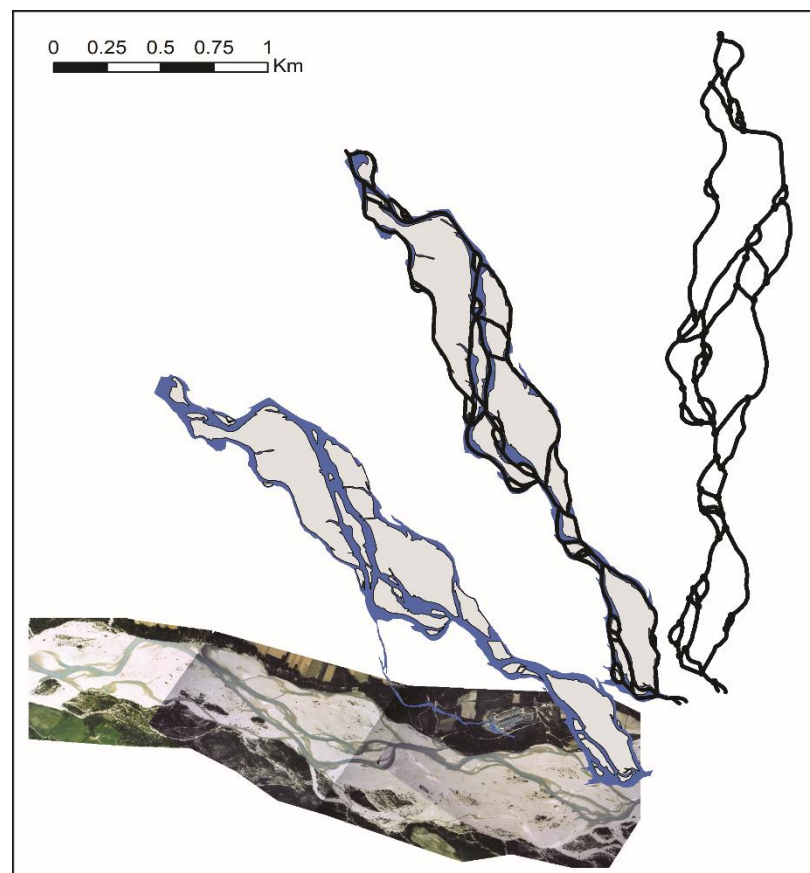
Figure 4.1: Schematic representation of the extraction of a braided river graph, from a raw remotely sensed image to a network skeleton capturing channel network connectivity.

Finally, a brief mention should be given to machine learning approaches to image classification. These are a special class of supervised classification methods, as they require training data from which algorithms can learn to partition pixels or image objects into different classes (e.g. Support Vector Machines (SVM); Mountrakis *et al.,* 2011). The attraction of machine learning approaches is the prospect of being able to train an algorithm on the possible variations seen in the spectral properties of landcover classes and then have it operate quasi-autonomously to generate classified imagery. However, Ma *et al.* (2017) caution that the performance of a machine learning algorithm may be predicated on the study area, with traditional classification methods potentially outperforming machine learning approaches in certain environments. The applicability of machine learning techniques, which are often complex, may also somewhat limit their application by non-specialists in remote sensing and computer vision. Nonetheless, applications of machine learning to image classification directly aimed at classifying and extracting complex river network patterns have shown significant promise for automatic delineation of whole river networks and channel centrelines from satellite imagery (Isikdogan *et al.*, 2015, 2018). The ability to accurately and automatically delineate channel centrelines in this manner would hugely facilitate global-scale graph analysis of multi-channel rivers systems and, indeed, Isikdogan *et al.* (2015) note that this underlies the motivations for their line of research.

4.2 Image classification methods

The workflow presented in this chapter has four broad steps:

1. Image pre-processing;

2. Image classification;

3. Skeletonise and vectorise classified images;

4. Construct graph models using dedicated software.

The satellite imagery used in this study is from the Landsat Surface Reflectance (SR) collection, which are atmospherically corrected data products (Masek *et al.*, 2006). Co-registration of the Landsat imagery was also not necessary, due to difficulties in tracking channels and nodes over time in Landsat data that preclude time series analysis of change in their positions. As such, step 1 was not required. The following methodology describes step 2, image classification, to test an OBIA classification of water, gravel and vegetation landcovers in a braided river environment. Results of from the OBIA classification were compared with classifications of the same three

landcover classes using two of the most widely used per-pixel classification schemes: Otsu's method (Otsu, 1979) and Maximum Likelihood Classification (MLC; Otukei & Blaschke, 2010). Image classification techniques were tested using Landsat imagery of the River Tagliamento, Italy, though the image classification techniques described here, and the general network extraction workflow, are not site specific and should be applicable to any river for which multi-spectral remote sensing data is available, provided the data's spatial resolution is high enough to resolve the wetted channel network.

4.2.1 Data acquisition and pre-preparation

NASA's Landsat (Woodcock *et al.*, 2008) and ESA's Sentinel (Berger *et al.*, 2012) missions provide freely available satellite imagery with near-continual coverage of the terrestrial Earth's surface from the early 1980s at 30 m resolution or finer. The imagery is multispectral, with images consisting of visible, infrared (IR), thermal IR bands and specific bands for the analysis of aerosols and clouds. Only the visible and non-thermal IR bands were used for landcover classification in this study. Furthermore, despite the higher spatial resolution of the Sentinel data (10-20 m, depending on the band; Berger *et al.* 2012), this mission was only launched in 2015, whereas the Landsat record has significantly greater temporal depth. As later analysis was aimed at braided river network evolution over multi-decadal timescales, only Landsat data has been employed for consistency, as the spatial resolution of Landsat imagery (30 m) is still detailed enough to resolve all but the smallest channels on the Tagliamento. Landsat data were acquired from the USGS Earth Explorer portal (USGS, 2017). Sentinel data can be acquired though the Copernicus Open Access Hub (ESA, 2017).

The swath width of Landsat means that a lot of extraneous land is captured in each image tile. In order to improve processing time during classification, it is necessary to remove these areas. The following processing steps are performed using geoprocessing tools within ArcGIS. A polygon image mask was created covering the length of the active braidplain and a small riparian border (hereafter the area of interest, AOI). The specific width of the riparian border is arbitrary, however a series of images spanning the length of the Landsat record (1980s to present) were assessed to ascertain a suitable width of the border that ensured variation in width of the braidplain over time would not result in the image mask removing relevant data. Each spectral band for each image tile is provided as a separate georeferenced raster file. For per-pixel classification methods that utilise spectral indices (see below), it is necessary to keep the bands as separate rasters for subsequent calculations. Thus, the image mask was used to extract data

from each of the bands relevant to the suite of indices applied. For the OBIA classification, composite images, images containing all bands in one raster file, were used. Composites of all bands were made using the Composite Bands function in the Image Analysis Window of ArcGIS. The image mask was then used to extract the AOI from the composite imagery. It should be noted that Landsat Surface Reflectance (SR) pixel values range from 0-20 000. The documentation for these data recommends applying a scale factor (0.001) to the data, which brings pixel values into a smaller range without affecting their spectrographic properties. However, for an unknown reason this stops the data rendering in the eCognition Developer OBIA software, precluding analysis. Given the scale factor appears only to function as a means of reducing the pixel value range in SR data, it was not applied.

4.2.2 Water and vegetation indices

Images classified with Otsu's method require the calculation of spectral indices and these indices also provide useful data that can be incorporated into OBIA classifications. The indices use the distinct spectral reflectance properties of different landcovers to differentiate between, for example, vegetated and non-vegetated surfaces. Three indices were used in this study: 1) the Normalised Difference Vegetation Index (NDVI), 2) the Modified Normalised Difference Water Index (MNDWI) and 3) the Automated Water Extraction Index (AWEI). Although other vegetation indices exist, NDVI was selected as it the most widely applied vegetation index in remote sensing studies and has been shown to be sensitive to the presence of low density vegetation typical of braided river corridors (Bertoldi, Drake *et al.*, 2011; Henshaw *et al.*, 2013). It is defined as (Rouse *et al.*, 1974)

$$NDVI = \frac{NIR - R}{NIR + R} \tag{4.1}$$

where NIR and R represent pixel values in the NIR and red bands of the multi-spectral image. The index is normalised, with a range of [-1, 1]. Vegetated pixels should have values > 0, with thresholds for vegetated pixels often set at > 0.1 for sparse vegetation and > 0.2 for dense vegetation (e.g. Bertoldi, Drake, *et al.,* 2011).

The MNDWI aims to differentiate water from other surfaces by manipulating its strong absorption of energy in the shortwave infrared (SWIR) wavelengths and high reflection of green wavelengths, relative to the high reflection of SWIR by terrestrial surfaces (Xu, 2006). It is defined as

$$MNDWI = \frac{Green - SWIR}{Green + SWIR} \qquad (4.2)$$

Values of MNDWI range between [-1, 1] and should be positive for water pixels and negative for non-vegetated terrestrial pixels.

MNDWI is one of the most widely applied water indices, however it has been criticised for performing poorly at discriminating water from shadowed and low albedo surfaces (Feyisa *et al.*, 2014). Thus, Feyisa *et al.* (2014) proposed a new water index, AWEI, which uses a combination of four or five bands and introduces coefficients designed to force non-water pixel values below 0 and water pixels above, even in the presence of dark or shadowed surfaces. They propose two versions of the index, one utilising four bands in areas where shadows are not a problem and using five bands designed to counter shadowing. As shadows are not normally a problem in the study area, the four-band index was applied, which is defined as:

$$AWEI = 4 \times (Green - SWIR_1) - (0.25 \times NIR + 2.75 \times SWIR_2) \qquad (4.3)$$

where *SWIR$_1$* and *SWIR$_2$* are shortwave infrared bands.

4.2.3 Per-pixel classification methods

The two trialled per-pixel classification methods, Otsu's method and MLC, are available as tools within ArcGIS. Otsu's method is an unsupervised binary classification procedure that seeks a threshold to maximise the inter-class variance (Otsu, 1979). It is well suited to the classification of images characterised by a bi-modal histogram, e.g. images to which a water or vegetation index has been applied forcing two peaks in the histogram for water/vegetation and non-water/non-vegetation pixels (Yang *et al.*, 2014). As such, input to the Otsu classification in this study is a raster in which pixel values represent a water or vegetation index. An advantage of Otsu's method in relation to unsupervised methods is that the binary output, e.g. each cell in the output raster has a value of 0 or 1, aids unambiguous definition of which class a pixel has been given.

MLC is one of the most well-used supervised classification methods (Otukei & Blaschke, 2010). It operates on multiband raster images and thus can utilise the spectral response of pixels in all six of the optical and IR bands in a Landsat image. The algorithm is fed with training samples that are delineated with polygons over areas of the image that clearly belong to the target

landcover classes, but that also try to capture the variability in spectral response of the different landcovers. MLC assumes the pixel values in the training samples are normally distributed and then assigns unclassified pixels to a given class based on the minimum distance to a class mean, which is scaled by a Bayesian probability rule. The output is a classified raster where pixels are assigned an integer value representing a landcover class, or a "No Data" value if the pixel could not be assigned to a class.

4.2.3.1 Object-based image analysis classification

OBIA groups pixels with similar spectral properties together into objects, which opens up a raft of other properties not present at the pixel level that can be used to classify objects. The power of OBIA classification methods has seen a consistent upsurge in OBIA applications within Geographic Information Science (Blaschke *et al.*, 2014), though a lack of applications to braided rivers leaves questions as to OBIA's performance relative to traditional per-pixel methods in the present context. OBIA classification routines were developed in the OBIA software environment, eCognition Developer (hereafter eCognition), to build rulesets; chains of in-built algorithms that iteratively classify image objects. An overview of the development of rulesets in eCognition is shown in Figure 4.2. Of most importance conceptually are the "feature values" (Figure 4.2a) and the "process tree" Figure 4.2b). Feature values include an array of different properties that describe the image objects (Table 4.1). The process tree is where rulesets are built, starting with image segmentation. An image segmentation algorithm divides up the raw, multi-band image into image objects. There are various segmentation algorithms available in eCognition, of which "multiresolution segmentation" was found to perform best on Landsat data in terms of segmenting the image into image objects that provide strong differentiation between water, gravel and vegetation. Multiresolution segmentation aims to create image objects that minimise internal spectral heterogeneity. It offers control of parameters that weight different bands in a multispectral image, giving more importance to bands with higher weight values. In the present study, it was found that a significant increase on the weighting of $SWIR_1$ and $SWIR_2$ bands relative to the other bands resulted in the best performance based on visual assessment. This is sensible, given water's high absorption of light in the $SWIR$ wavelengths (Xu, 2006). Other parameters include "scale", which determines the size of the resulting image objects. It's best to try and find a maximum value for the scale parameter, otherwise the remaining classification may essentially be working at or near the pixel scale, eschewing the benefits of an object-based approach. The other two key parameters are "colour" and "shape", which control the relative importance given to spectral homogeneity over the spatial homogeneity of image objects.

a)

Feature	Value
Image Object Related Features	
Object features	**Customized**
AWEI	0.4304
MNDWI	-0.1700
NDVI	0.1500
Layer values	**Mean**
Blue	1223.69
Brightness	1361.45
Green	1424.27
NIR	2008.69
Red	1484.54
SWIR1	2007.73
SWIR2	1373.23
Pixel-based	**Border contrast**
NIR	-66.83
SWIR1	-84.22
SWIR2	-99.25
Pixel-based	**Contrast to neig…**
NIR (0)	-51.27
SWIR1 (0)	-45.25
SWIR2 (0)	-79.12

b)

Process Tree
- Type 3 HighFlow_Bright
  - 1st Segmentation
  - Remove Classification
  - Stage 1 Classification
    - Deep and Shallow Water
    - Merge water classes
    - High NDVI Veg
      - unclassified with NDVI > 0.3 at New Level: Veg
    - Low NDVI Veg
    - Bright Gravel
  - Connect channels

Figure 4.2: Overview of the main steps in creating classification rulesets in eCognition Developer. Insets a) showing a selection of feature values for an image object, including customised features calculating spectral indices; and b) the "Process Tree" where rulesets are built. Each sub-group within the ruleset contains classification algorithms, such as the NDVI classifier shown, which assigns all unclassified image objects with the customised feature value "NDVI > 0.3" to the vegetation class.

Following segmentation, classification algorithms (rules) are added to the ruleset. Once built, a ruleset can be run in one go, outputting a classified Landsat image. Processing time is negligible on an area covering the braided extent of the Fiume Tagliamento (~200 km^2). An initial attempt was made to develop a "one-size-fits-all" ruleset that could be applied to any image, rapidly producing a classified image that accurately delineates the wetted channel network, exposed

gravel and vegetation. Classification algorithms, which assign image objects to classes based on whether an image object meets criteria defined by feature values (Figure 4.2b), were applied to develop a classification routine that first targeted image objects that were easily identifiable as belonging to a specific class. Given that, with the exception of small vegetated patches, the landcovers of interest are present as contiguous areas, classification of the most readily identifiable image objects of all classes was intended to provide seed areas. From these seed areas, classification of adjacent objects with properties less redolent of a specific landcover could bring to bear feature values based on neighbour relations. These feature values are a powerful aspect of the OBIA approach, enabling classification of image objects based on, for example, the spectral response of an image object relative to neighbouring image objects. However, despite the capacity for differentiation between landcover classes using neighbour relations, a problem that arose from classifying areas of gravel before classifying all water image objects was seen in areas of clear, shallow water (common on smaller side channels and channel margins on the Tagliamento) that have very similar spectral properties to bare gravel (high reflectance in all bands) and thus were classified as gravel. This caused gaps in the classified channel network that had to be dealt with by convoluted "clean-up" processes that targeted previously misclassified image objects.

Whilst problems of misclassification were present in the initial classification ruleset, the larger problem faced by the one-size-fits-all approach was temporal variation in the spectral characteristics of different landcovers. In images taken at times of higher flow, channels are larger and deeper. The larger size of channels means that the initial segmentation algorithm can use a larger scale parameter, which in turn creates larger initial image objects that still differentiate landcovers well. Larger image objects contain more pixels and thus their feature values are more representative of a given landcover (assuming the segmentation is accurate). It is therefore preferable to begin a classification by segmenting an image into the largest possible image objects. The second confounding problem with a one-size-fits-all ruleset was due to the depth of channels at higher flow and the subsequent increases in *IR* energy absorbance by water. Rules aimed at classifying areas of shallow water in lower flow images used neighbourhood relations to exploit the small differences in *SWIR* reflectance and MNDWI values between shallow water and gravel image objects. At higher flows, these rules tended to result in marked over-classification of gravel as water and a non-representative channel network.

Testing different iterations of a one-size-fits-all ruleset made apparent that variation of ruleset performance was systematic and largely related to flow conditions. Thus, rulesets were versioned based on visual assessment of classification results relative to a visual assessment of flow conditions. It should be noted that whilst linking ruleset versions to quantitative flow data would have been desirable, there is a paucity of flow data available for the Tagliamento, especially at the low flows when all imagery available to this study was captured (cloud cover precludes images captured at higher flows during rainfall events). Long-term stage records exist for the Tagliamento from gauging stations at Villuzza and Venzone (Bertoldi, Gurnell *et al.*, 2009; Ziliani & Surian, 2012), however all cloud-free imagery found for this study was captured at stages ≤ 0.7 m at Venzone. Below this level, stage measurements are affected by the changing morphology of the braidplain and thus there is no correlation between the observed extent of the channel network in Landsat imagery and the stage record.

These limitations notwithstanding, a collection of four rulesets that could be applied across the range of flow conditions that were visually observable on the Tagliamento were developed. These rulesets were divided into two categories that targeted: 1) channel networks with observably smaller and shallower channels; 2) channel networks with observably larger and deeper channels. Note that channel depth is qualitatively inferred by visual assessment of the spectral reflectance of areas of water using false-colour composites displaying red, blue and green as the red, NIR and SWIR$_2$ bands of a Landsat image. Due to the strong absorption by water of IR wavelengths, rendering an image in this way shows deeper areas of water as being notably darker, as can be seen in Figure 4.3a.

The core structure of the four rulesets is the same. After segmenting the image into image objects, classification targets objects identifiable as deep water at channel centres. Once classified, these unambiguous areas of water provide seeds from which rules utilising neighbour relations (Table 4.1) can be applied. Combining neighbour relations and the spectral properties of image objects enables the classification of shallower areas of water that have spectral properties that can intersect with the spectral properties of gravel. For example, areas of clear shallow water tend to absorb SWIR wavelengths more than adjacent bare gravel. Thus, the difference in SWIR absorption between neighbouring image objects can be used differentiate them. After the application of these first water classifiers, the bulk of the channel network is classified and contiguous areas of water are merged together, subsequently enabling the use of the larger area of water objects as a further means of discrimination against vegetation and gravel objects. Following the initial classification of water, vegetation is classified based on the

NDVI values of unclassified image objects. Once vegetation and water have been classified, the remaining image objects should mostly represent the gravel class, which is targeted by classifiers focussing on the high reflectance of gravel in the SWIR wavelengths. Finally, rules are applied to target image objects within specific classes where visual inspection has shown systematic misclassification.

Versioning of the rulesets focused primarily on maximising small spectral differences between shallow water and adjacent gravel image objects at times of lower flow and gave reduced importance to these differences at times of higher flow. This avoided the aforementioned problems of overclassifying water at times of higher flow due to the initial use of rules designed to classify shallow channels using small differences in SWIR reflectance between neighbouring water and gravel image objects. The rulesets designed for larger channels were also able to use a larger scale factor in the initial segmentation, which creates larger initial image objects and aids classification. Within the two ruleset categories, the differences between rulesets were subtle and had to be employed due to inconsistencies in the reflectance characteristics between different Landsat scenes where the size and depth of channels appeared similar. Roy *et al.* (2016) note that these inconsistencies can arise for various reasons, including differences in radiances recorded for the same landcovers by the various Landsat sensors (note different sensors are mounted on the Landsat 5, 7 and 8 satellites); coupling between atmospheric state and surface reflectance; and imperfections in the Landsat atmospheric correction algorithms that convert top of atmosphere reflectance to surface reflectance values. These inconsistencies manifested broadly as scenes that appear visually brighter or visually duller and hazy. Subsequently, rules targeting shallow water in a brighter scene tended to overclassify water in a hazier scene. Thus, by slightly varying, for example, MNDWI thresholds and relative differences between neighbouring objects in SWIR bands between rules in the shallow water and deep water rulesets, versions of these rulesets were created that visually increased classification performance. From brief testing of one or two of the ruleset versions based on visual interpretation of the flow conditions and the brightness of a scene, a raster image with near-complete classification of the contiguous braided channel network visible along a ~70 km stretch of the Tagliamento was possible in minutes (Figure 4.3). However, visual assessment of these results is not sufficient as either a standalone method of testing classification accuracy, nor for comparisons to be made between OBIA and per-pixel classification methods.

Table 4.1: Selected classes of "feature values" which define the properties of image objects. There is an extensive array of feature value classes available in eCognition, with only the most relevant to braided river landcover classification described here. Note class names match eCognition reference material and each class contains multiple types of feature value.

Feature value class	Description
Layer values	■ Feature values based on the spectral properties of image objects. ■ Includes statistical properties of an image object's reflectance in a given band, such as the mean, standard deviation and skewness. ■ Other feature values describe image object spectral properties relevant to neighbour objects or image object border properties.
Geometry	■ Measures of extent, shape and branching. ■ Extent includes image object area, length, width and certain ratios of these measures. ■ Shape feature values describe various measures of the conformity of image objects to idealised shapes, the properties of minimum bounding polygons around image objects and the orientation of image objects.
Texture	■ Feature values based on variation in spectral properties of an image object's sub-objects. ■ Other feature values account for differences in the form of sub-objects. ■ Texture is also described by a suite of feature values based on variation of grey scale values within image objects.
Class-related	■ These feature values can be used once some image objects within a scene have been assigned to a class. ■ They define neighbour relations to objects of different classes, such as distance to an object class m, length of shared border with m, or distance to an image object of class m.
Customised	■ Customised feature values are arithmetic or relational. ■ Custom arithmetic feature values works as a raster calculator for image objects, enabling calculation of spectral indices which are applied at the image object, rather than pixel level. ■ Custom relational features allow for building bespoke queries on in-built feature values of image objects and relative to their neighbours of a specific class or classes.

4.2.1 Image classification accuracy assessment

Testing the accuracy of an image classification requires reference data. These can either be field measurements that geolocate reference points within areas of the landcovers in the classification or georeferenced, remotely sensed data of higher resolution than the classified image that can be used to determine reference areas of specific landcovers (Lillesand *et al.*, 2008). In the present study, reference data was a mosaic of very high-resolution (1 m) aerial images covering a 21 km reach of the Tagliamento. These images were georeferenced in ArcGIS

using the georeferencing toolbar and a 3rd order polynomial transformation. Root mean squared error (RMSE) of the transformations for all 16 images was < 10 m, which is less than half the width of the narrowest channels on the Tagliamento (~25 m; Ziliani *et al.*, 2013).   Errors associated with georeferencing of the aerial imagery are therefore considered to have a minimal impact on positional inaccuracies between Landsat and reference data. The aerial imagery was captured on 23/05/2005, two days prior to the Landsat image. Stage data at Venzone indicates almost no fluctuation in flow between 23/05/2005 and 25/05/2005, with any impact of the time difference on the extent of the wetted channel network assumed to be negligible.
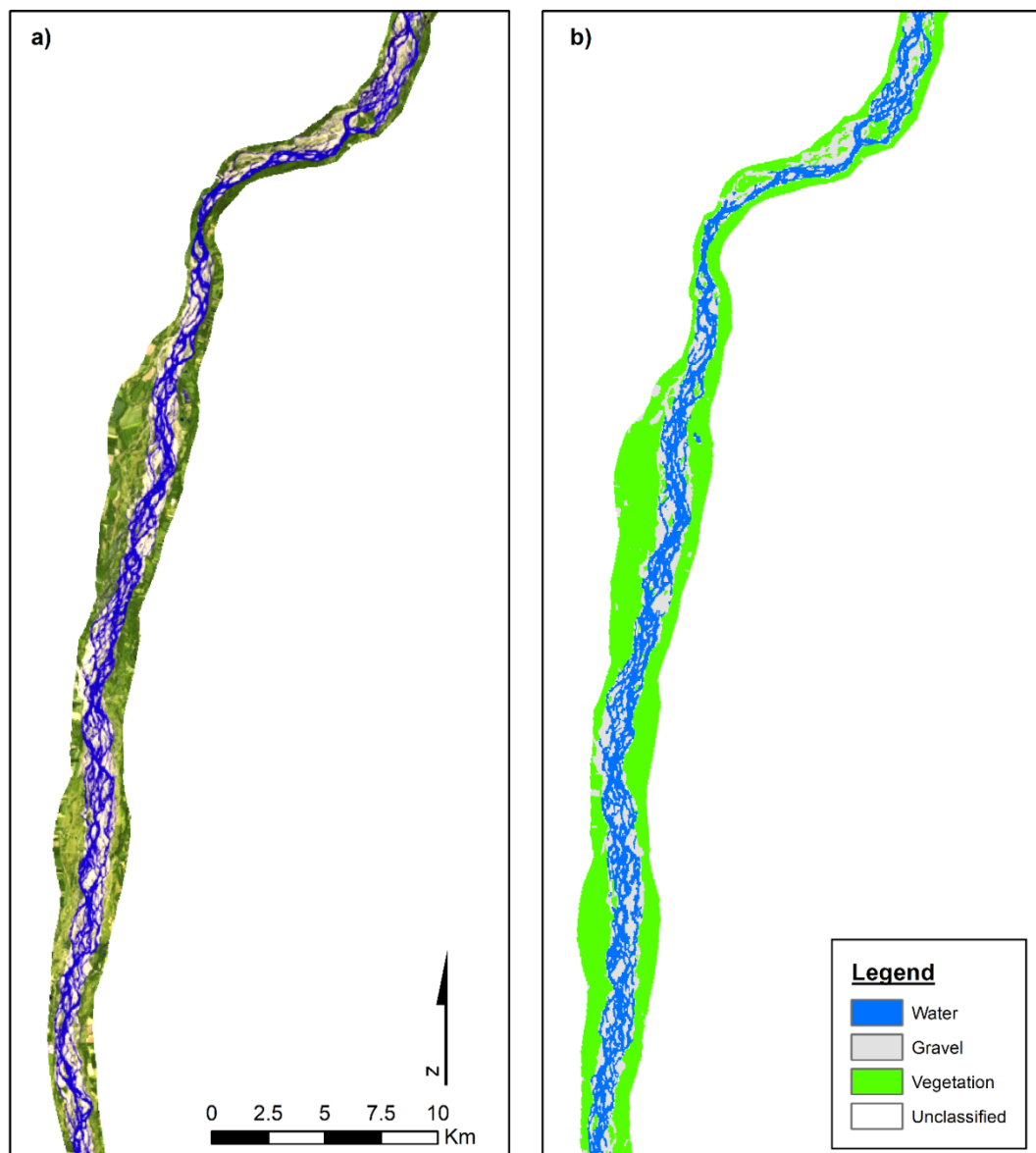
Figure 4.3: a) False-colour composite image of a ~56 km section of the braided River Tagliamento, Italy; b) The image classified using an OBIA ruleset. Note the contiguity of the channel network. Flow is from north to south.

Samples of reference data representing the landcovers in the classified image need to be collected to minimise bias in ensuing statistical measures of classification accuracy (Congalton, 1991). Congalton (1991) recommends either a random or stratified random sampling routine for selection of reference data. In the present case, the area under study was too big for random sampling to guarantee samples being collected from all sub-types of water, gravel and vegetation classes, e.g. deep and shallow water, sparse and dense vegetation etc. Similarly, stratified random sampling may still miss certain small but important features, such as patches of pioneer vegetation. As such, a stratified pseudo-random approach was adopted, whereby reference samples were collected from areas covering the range of different landcover class sub-types observed in the reference imagery and with no knowledge of locations of landcover classes in the classified image. 50 reference data samples were collected for each landcover class, resulting in final reference datasets of the order of 50-90,000 pixels per class. Extraction of reference data and class samples from the classified image was done by polygon mask extraction and counting the pixels within each polygon. Differences in sample size are caused by sample polygons falling on areas of unclassified pixels. In order to ensure the sample sizes of classified image data matched those in the reference data, the classified rasters were resampled from their native 30 m pixel size to 1 m using the Resample tool in ArcGIS with a nearest neighbour interpolation. It is assumed that error due to interpolation of the resampled pixel values is negligible to zero, as each 30 m cell will be equally divided into 1 m pixels.

Statistical analysis of classification accuracy was conducted using an error matrix and the associated Kappa statistic, which is a standard approach for image classification accuracy assessment (Congalton, 1991; Lillesand *et al.*, 2008). The error matrix (Table 4.2) shows the number of pixels in each class that were correctly classified (the diagonal). It also shows errors of commission, pixels in the reference data that were wrongly included in a given class (off-diagonal rows), and omission, pixels in the reference data that are wrongly excluded from a given class (off-diagonal columns). Statistics in the error matrix show user's accuracy, which quantifies errors of commission as the percentage of correctly classified pixels relative to all pixels in the reference sample for that class (the row total) and describes the probability that a classified pixel is representative of the landcover class on the ground. Producer's accuracy, quantifying errors of omission, is calculated in the same way as user's accuracy but uses column totals and shows the probability of a classified pixel of a given class being of that class in the reference data. Other accuracy measures derivable from the error matrix include the total accuracy of the classification (sum of the diagonal divided by total pixels in the matrix) and *kappa* statistic. *Kappa* (*K*) is defined as (Congalton, 1991)

$$K = \frac{N \sum_{i=1}^{r} x_{ii} - \sum_{i=1}^{r}(x_{i+} * x_{+i})}{N^2 - \sum_{i=1}^{r}(x_{i+} * x_{+i})} \qquad (4.4)$$

where r is the number of rows in the matrix, x_{ii} is the number of observations in row i, column i, x_{i+} and x_{+i} are total observations for row and column i, respectively. This metric provides a measure of chance assignment of a pixel in the classified image to the correct class, with a value of 0 indicating that the classification is essentially no better than a random assignment of pixels to different classes and a value of 1 suggesting that the classification should be accurate in all cases (Lillesand *et al.*, 2008).

Table 4.2: Example of the error matrix for the object-based image analysis classification.

	Reference data				
Pixels	*Water*	*Gravel*	*Vegetation*	*Row Total*	*User's accuracy (%)*
Water	50099	7887	1384	59370	84.4
Gravel	4068	61195	8834	74097	82.6
Vegetation	0	44	46746	46790	99.9
Column Total	54167	69126	56964	180257	
Producer's accuracy (%)	92.5	88.5	82.1		

4.3 Results

Table 4.3 presents the error matrix statistics used to assess the different classification routines. It is clear that Otsu's method performed worst. Of particular note is the low user's accuracy (52.7%) of the water class, suggesting significant commission errors that would have large impacts on subsequent network extraction from the classified raster of the channel network, with channels being inaccurately located in areas that are not actually water. Very poor producer's accuracy for vegetation (37.2%) also shows this method struggling to correctly classify areas of vegetation, which are very important for the morphodynamics of braided rivers (Gurnell & Petts, 2006; Bertoldi, Drake *et al.*, 2011; Corenblit *et al.*, 2014). Total accuracy of Otsu's method was also poor (66.6%) and a *Kappa* value of 0.52 suggests that the probability of correct classification of pixels is only just greater than 50-50.

Table 4.3: Comparison of different accuracy measures for the three trialled classification methods, Otsu's method (Otsu), Maximum Likelihood Classification (MLC) and object-based image analysis (OBIA).

	Producer's accuracy (%)			User's accuracy (%)			Total accuracy (%)	Kappa
	Water	Gravel	Vegetation	Water	Gravel	Vegetation		
Otsu	91.6	85.9	37.2	52.7	68.4	100	66.6	0.52
MLC	96.5	79.5	88.7	75.9	90.2	99.6	87.5	0.81
OBIA	92.5	88.5	82.1	84.4	82.6	99.9	87.7	0.81

Overall performance of MLC and OBIA classifications was near identical, as seen from the total accuracy and *Kappa* statistics (Table 4.3). However, these statistics may mask some important differences between each classification. Both OBIA and MLC had very high producer's accuracy for water (92.5% and 96.5%, respectively). However, MLC's user's accuracy was nearly 10% lower than that of the OBIA classification (Table 4.3), indicating that MLC is overclassifying areas of water. This will have three effects on subsequent extraction of information from the classified image: 1) areas erroneously classified as water will increase artefacts from automatic channel centreline vectorisation (see below); 2) overclassification of water may obscure important features, such as mid-channel bars, that are picked out in the OBIA classification (Figure 4.4); 3) extraction of channel width (see below) uses the channel network raster, thus over-classification of water will result in systematic mis-measurement of channel width. Very high (> 99%) user's accuracy was seen for vegetation in all three classifications, suggesting little overclassification of this class. Producer's accuracy shows MLC slightly outperformed OBIA in terms of finding areas of vegetation, but the difference is relatively small, and both classifications performed well (Table 4.3). In the gravel class MLC outperforms OBIA in user's accuracy, with the reverse seen for producer's accuracy (Table 4.3). Commission errors in the gravel class for OBIA were greatest for vegetation, indicating that the OBIA classification is classifying areas of vegetation as gravel, whereas omission errors in the MLC are driven by misclassification of gravel as water. Given the importance vegetation to braided river morphodynamics, misclassification of vegetation as gravel by OBIA is not ideal, though these misclassified pixels accounted for a relatively small proportion of the overall reference sample (12%). OBIA vegetation classification used simple NDVI thresholds taken from the literature (e.g. Bertoldi, Drake, *et al.*, 2011; Henshaw *et al.*, 2013). Future applications of OBIA to braided rivers could apply a more sensitive approach to vegetation classification.

Whilst the overall performance of OBIA and MLC are approximately equal, the overclassification of water by MLC would reduce the ease of network extraction from the resulting channel

network rasters. Furthermore, OBIA has the advantage of being significantly faster to run. This opens up the possibility to generate multiple braided river networks showing change over long time periods without being limited by data generation time.
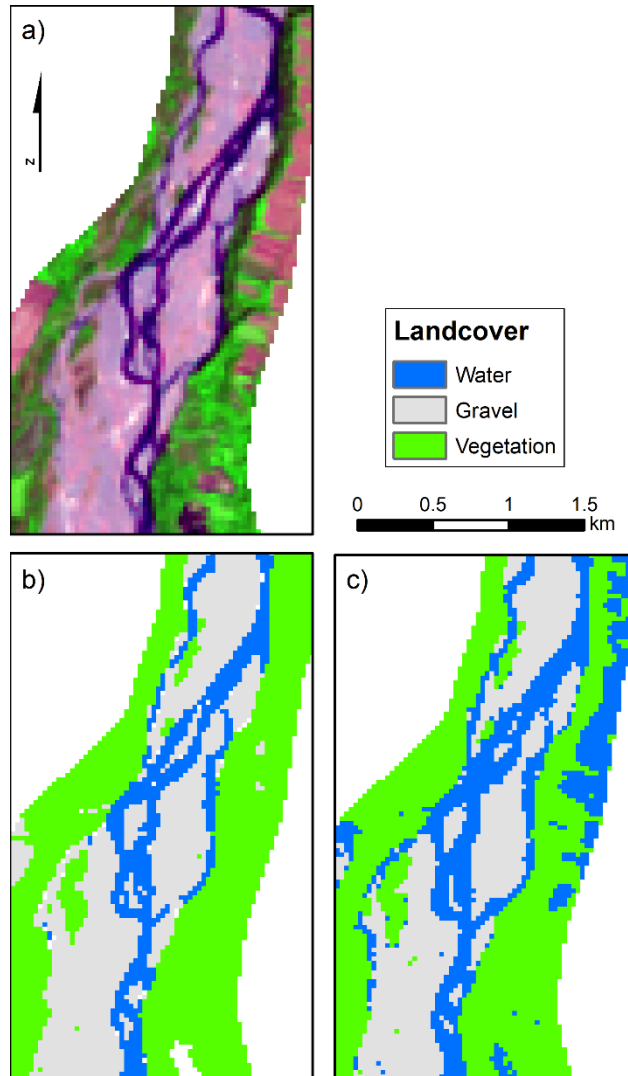
Figure 4.4: a) Landsat false-composite of a section of the Fiume Tagliamento; b) OBIA classification of the section shown in a). Note the separation of bars in the middle of the image; c) MLC classification of a), showing less precise classification of channels and bars and greater misclassification of water.

4.4 Network extraction from classified imagery

Once an accurate classification of the landcovers of interest has been achieved, a network skeleton of the channel network needs to be extracted. The network extraction process is presented as a simple workflow using ArcGIS to convert a binary raster mask of the channel network, e.g. water cells = 1, all other cells = 0, to channel centrelines. This network skeleton is defined as a set of intersecting lines, where any intersection (bifurcation or confluence) creates

a node and the order of the connections needs to preserve the direction of flow through the network. Each node will also have a physical distance from its neighbouring nodes. In essence, the problem is to create a spatial planar network representation of a braided river network from only a binary raster input, where the classified channel network is represented by a non-zero number and all other areas of the raster have a zero value. To the author's knowledge, only one technique has previously been developed, which is detailed in an unpublished Master's thesis (Marra, 2010). This method, which was originally applied to the much larger Jamuna River and provided the data for Marra *et al*'s (2013) application of graph theory to the Jamuna, involves thinning of the raster channel network to preserve only a single pixel chain that tracks the centreline of channels. The single pixel network skeleton is then vectorised, the orientation of channel centrelines is determined and connectivity information extracted. Application of this method requires only geoprocessing tools in ArcGIS. It was trialled on raster channel networks of the Tagliamento and works to an extent, however certain key features such as medial bars on narrower channels are not preserved in the thinning process. It is likely that the method is better suited to large channels, such as the Jamuna, where even side channels are multiple pixels in width.

An alternative network extraction workflow that was sensitive to the smaller size of channels on the Tagliamento was developed in ArcGIS, utilising geoprocessing tools and other native functionality. The workflow is semi-automated and, depending on the complexity of the channel network (which is itself dependent on stage), takes between 1-2 hours to derive a complete network representation of the channel network. Figure 4.5 shows the processing steps applied to extract the network and begins with vectorisation of the raster channel network using the ArcScan extension in ArcGIS. ArcScan is a vectorisation toolbar that provides automatic raster vectorisation functionality. Automatic vectorisation can trace the centrelines of contiguous raster cells with the same, non-zero value in a binary raster and thus is capable of automatically finding the centrelines of a rasterised braided channel network.

ArcScan automatic vectorisation is controlled by various user defined settings that control different aspects of the resulting centreline geometry. Of particular importance is "compression tolerance", which controls the number of feature vertices[4] comprising each channel centreline. A higher value of compression tolerance results in fewer feature vertices and a less complex geometry of the channel centreline. The default value of this parameter is sufficiently low to

---

[4]Feature vertices are points between line segments that build curved lines and bear no relation to graph vertices, the latter being largely referred to as nodes in this research.

not simplify channel centrelines. Iterative changes to other settings controlling the maximum width of raster cells to vectorise, line smoothing and how to resolve sharp corners were also found to operate well with default values. Settings that needed changing from defaults were noise level, which was set to 0 to avoid treating small groups of disconnected raster cells on side channels, where the classification had found only deeper water cells (pools in riffle-pool sequences), as noise. ArcScan automatic vectorisation can also close gaps between centrelines, with the size of gaps controlled by a "gap tolerance" setting. This setting has some utility for closing small gaps between channels that are disconnected in the raster channel network, however setting it too high results in erroneously connected channel centrelines by jumping gaps over bars to misconnect channels. The angle through which gap tolerance searches for connections can also be constrained using "fan angle". Whilst a fan angle of 180°, e.g. gaps can be jumped at right angles to the end of line segments, may seem unrealistic, at small scales such as chute channels dissecting complex bars, near 90° bifurcation and confluences have been observed in the raw Landsat data and thus the fan angle was set to 180°. These high angle bifurcations and confluences may be a consequence of the relatively coarse resolution of Landsat data relative to the size of channels on the Tagliamento, e.g. chute channels may be a few pixels long (~150-200 m) and one pixel (~30 m) wide and thus their true geometry cannot be resolved. Nevertheless, they are important aspects of the network topology and should be represented, though with caveats over geometric information that can be extracted at these points in the network.

The channel centrelines output by ArcScan vectorisation are not free from artefacts (Figure 4.5). These artefacts are in the general form of misconnected, disconnected and erroneous channels that cause inaccuracies in the network topology. Certain artefacts are systematic, such as bar heads and tails which appear as single pixels connected at the corners, rather than edges, of pixels within a larger pixel cluster representing a bar. These corner connections are not recognised by ArcScan and effectively treated like medial bars around which a channel centreline is split. Many artefacts are found in areas of highly dissected complex bars, where a combination of Landsat spatial resolution and classification errors cause inaccuracies in the classified raster and misconnected channel centrelines. Other artefacts are simply random, caused by combinations of classification inaccuracies and apparent inabilities of ArcScan to resolve certain aspects of the complex geometries of a braided channel network. No automated method could be found to accurately remove all artefacts, so they are removed by manual deletion and digitisation where necessary. After the network of centrelines has been cleaned, geoprocessing tools are used to ensure that centrelines end at all intersections with other lines.

This is necessary to create nodes wherever channels intersect. Centrelines are also dissolved so that no single channel comprises two separate lines.

Once a clean channel network skeleton has been derived, the direction of the channels must be corrected so that all channels are connected in a downstream direction. Marra (2010) applied a coordinate shift and rotation to channels and nodes on the Brahmaputra, orientating all network elements in the general flow direction. This allowed simple differencing of *y* coordinates to ascertain which channels and nodes were downstream of one another. In the case of the Tagliamento, which flows generally towards the south-south-west but has a section where flow direction is notably closer to the west, it was not possible to transform the coordinates of channels and nodes to ensure negative coordinate differences between nodes as a basis of determining channel direction. Extraction of connectivity between channels and nodes utilises ArgGIS' Coverage data model (ESRI Inc., 2016), which adds "FNODE" and "TNODE" fields to the channel attribute tables in a Coverage dataset. These fields describe the nodes that the channel connects from and to (Figure 4.5). Many of the upstream orientated channels can be found automatically by querying channels with "TNODE" > "FNODE" (note that node numbering is automatic and node numbers decrease in a downstream direction) and then flipping the direction of the selected lines. A final check is necessary as not all lines will be reoriented correctly. In cases where channel direction has to be amended manually, this can be done unambiguously by considering bifurcation and confluence angles and orientation and size of inflowing branch channels.

After removal of artefacts and reorientation of misoriented channels, the final problem is to remove short and very wide channels, which are present at larger confluences and bifurcations, often at multi-channel confluence-diffluences. Removal of overwide channels requires 1) extraction of channel width, 2) assessment of which channels are wide enough to constitute artefacts, 3) deletion of these channels and amendment of network connectivity to ensure no gaps are left in the network. To these ends, 1) and 3) were automated using Model Builder in ArcGIS. For task 2), a script was written in the statistical programming language R (R Core Team, 2017) that identifies overwide channels and flags them for deletion by the task 3) model.

Channel width extraction utilised a method after Marra (2010). A width raster is created using the Euclidean Distance tool in ArcGIS, which measures the distance from each cell to a "source area", in this case non-water cells reclassified with a NoData value. Multiplying the width raster by 2 results in a channel network raster in which centreline pixels approximate the channel width. High density points generated along each centreline act as cross-sections by extracting

the values of centreline pixels from the width raster. Widths are then averaged along each channel segment. Marra's (2010) width extraction method was also partially devised to deal with the same issue of overwide artefact channels. He suggests a threshold for deletion of channels that are twice as wide as they are long. This threshold was trialled in the present study and proved suitable based on visual assessment. The R width script thus takes in the width values for the cross-sections on each channel and the channel length, computing the average width and standard deviation and adding a flag to overwide channels, e.g. width ≥ (length*2). The output from the script is then fed into the task 3) model, which selects overwide channels, deletes them and then snaps together the ends of channels that previously connected to the deleted channel. After a final visual check to ensure the snapping procedure has not left any gaps in the network or caused any topological errors, the connectivity of the network is regenerated using another Coverage dataset and can be exported for use in dedicated graph analysis software.

4.4.1 Validating the extracted channel network

The channel network extraction workflow produces a set of channel centrelines derived from imagery that is at the lower limit of the spatial resolution capable of resolving the majority of the braided Tagliamento's channel network. There is an inevitable simplification of the network that will result from using Landsat data on a river the size of the Tagliamento, both in terms of the number of channels that are captured and their geometry. To compare how datasets from flume and natural rivers captured channel length scaling, Hundey and Ashmore (2009) plotted cumulative frequency distributions of channel length, normalised by the mean channel length in each sample. This approach is used here to assess whether the Landsat channel network captures similar distributions of channel length when compared to the network of channel centrelines derived from a digitisation of the channel network in the high-resolution (1 m) reference imagery. The digitised channel network was converted to a binary raster and the channel network extraction workflow described above was applied to derive the network skeleton.

Figure 4.6a shows the cumulative frequency distributions of the channel length/mean channel length ratios for the channel network derived from reference data and for the same channel network derived from Landsat data. The distributions show that the Landsat channels deviates only slightly from distributions of channel lengths found in the more detailed network. Deviations are most prominent in the tail of the distributions below the mean, which is caused

by the reference data channel network capturing shorter chute channels over smaller bars and a great many more short, upstream or downstream disconnected channels. Another slight deviation in the curves is seen just above the mean, which is indicative of the lower limit of channel size that is captured in the Landsat imagery negating a certain proportion of larger chute channels over complex bars that are of medium length. However, despite these slight variations in the channel length distributions, Figure 4.6a shows that the Landsat derived channel networks capture this essential aspect of channel geometry very effectively. The same analysis was performed for channel width (Figure 4.6b), however the large disparity in spatial resolution between the Landsat and reference data results in a very different distribution. This highlights the inaccuracies that would result from analysis using widths derived from Landsat classifications of medium sized braided rivers, for example weighting of networks using channel width.

4.5 Conclusion

A workflow has been presented that enables the extraction of topological representations of braided river networks from a single input, namely a multi-spectral remotely sensed image of sufficient spatial scale and resolution to resolve a braided channel network. The workflow begins with image classification to extract landcovers of interest: water, exposed gravel and vegetation. Image classification methods are multifarious, though the most commonly applied methods in studies of braided rivers and other similar settings are per-pixel approaches. Proposed as an advance on per-pixel methods, OBIA is a powerful alternative that maximises the information that can be obtained from higher resolution remotely sensed imagery. To test the performance of per-pixel methods against OBIA, two commonly applied per-pixel classifications, the unsupervised Otsu's method and the supervised MLC, and an OBIA classification were used to produce classified raster maps of the three landcovers under study along the full braided length of the River Tagliamento. OBIA classification routines require rulesets based around the properties of image objects to build a final classified raster map. Initial attempts to develop a one-size-fits-all ruleset that could be applied to any Landsat image of the Tagliamento were confounded by differences in the spectral properties of the channel network at different stage, due to the greater absorption of light by deeper water. Versioning of rulesets based on assessment of flow conditions resulted in four rulesets that, when matched to flow, could produce a classified raster map of landcovers of interest within minutes.
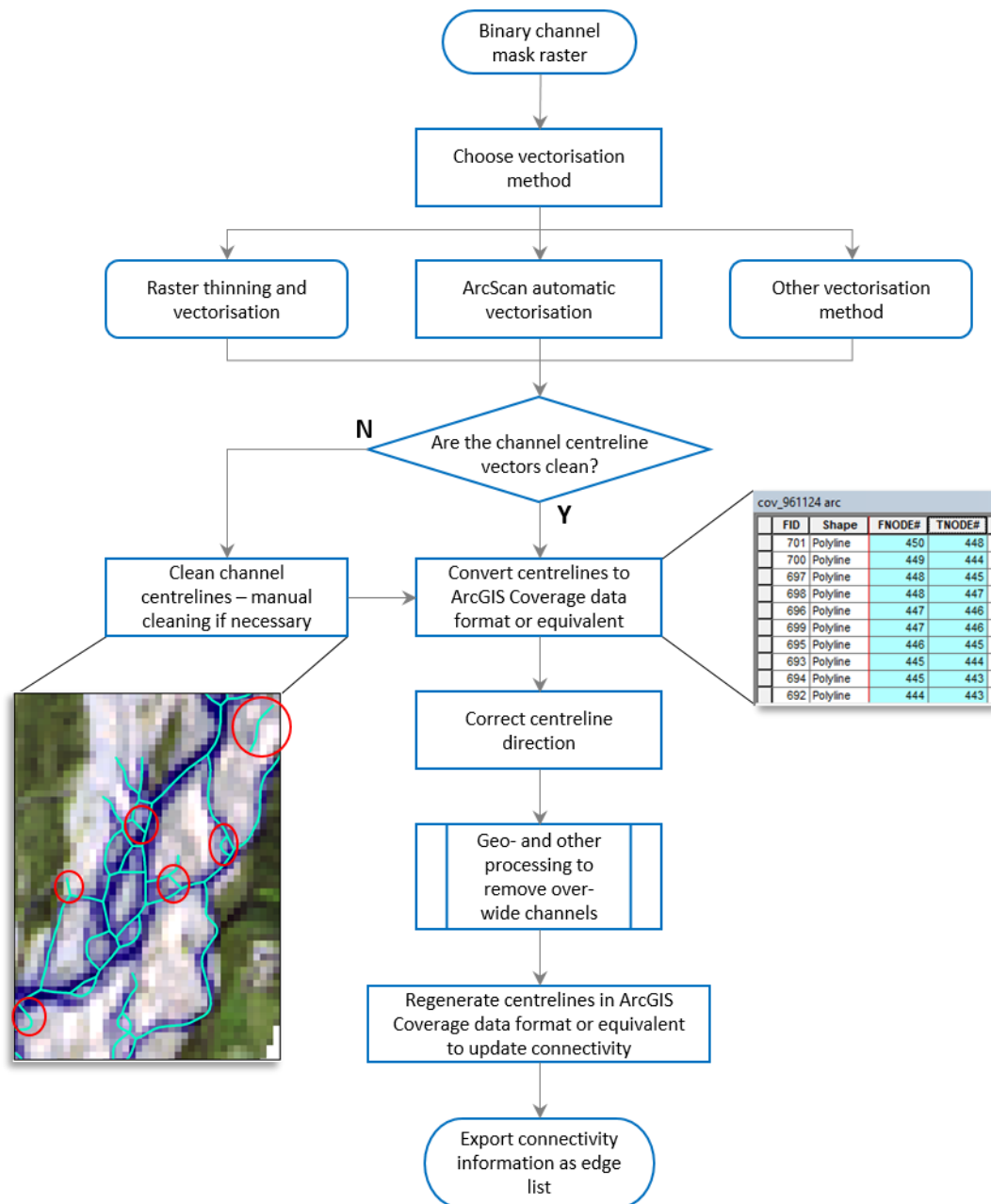
Figure 4.5: Flowchart showing general steps required for extraction of channel networks from a binary raster channel mask and extraction of connectivity. Insets show examples of artefacts (circled in red) in an uncleaned, automatically vectorised channel network (bottom left) and an example of a Coverage attribute table with the FNODE and TNODE fields highlighted, illustrating capture of network connectivity (middle right).

In order to test the accuracy of the trialled classification methods, a single Landsat image was classified using Otsu's method, MLC and OBIA. The results were compared to reference data derived from a mosaic of very high resolution (1 m) aerial images that were captured at approximately the same time as the Landsat image, to avoid any variation in the channel network that may invalidate the reference data. Analysis of classification errors showed that

Otsu's method clearly performed worse than MLC and OBIA. Particular issues were seen in commission (over-classification) and omission (under-classification) of water and vegetation, respectively. The *Kappa* statistic also suggests that the overall chance of correctly classifying pixels with Otsu's method in this environment is not much better than 50%. Little difference was observed in the performance of MLC and OBIA. Both approaches performed better with water and vegetation classification than gravel, though OBIA slightly outperformed MLC on omission errors in the gravel class. OBIA also was slightly higher in terms of total classification accuracy and *Kappa*, though both methods performed well. The slightly better performance of OBIA is more important in the context of time taken to perform a classification. Once rulesets for a given river have been established, classification is at least an order of magnitude faster than using the supervised MLC approach. Furthermore, the broader aims of this research were not to fully explore the potential of OBIA classification methods for applications to braided river network extraction and braided research more generally. It is likely that further investigation of the capabilities of eCognition or similar software will yield further improvements in classification accuracy and may offer the potential to automate classification routines without needing extensive knowledge in remote sensing and image analysis.
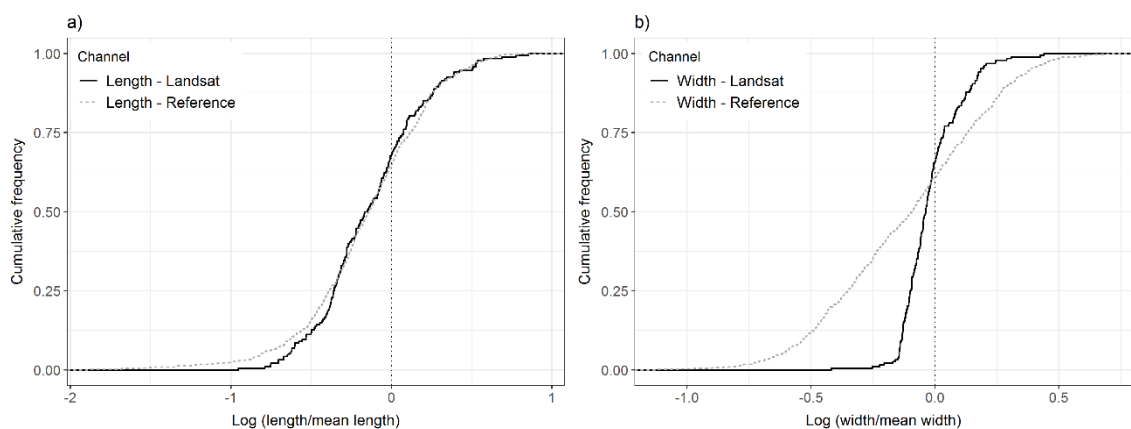
Figure 4.6: Cumulative distribution functions showing a) the range of channel lengths relative to the mean channel length and b) the range of channel widths relative to the mean channel width in the Landsat derived channel network and the channel network derived from high-resolution reference data.

The binary raster mask of the wetted channel network that is output from the image classification process is used as input to a semi-automated workflow that extracts channel centrelines and the associated topology and length scaling of the braided channel network. This workflow is, unfortunately, not devoid of manual correction of the channel network skeleton, though the requirement for manual cleaning of errors in the network are minimal. As such, a full graph representation of a medium sized braided river can be extracted in 1-2 hours. This

processing time is not restrictive in terms of generating datasets with sufficient temporal depth to look at braided river network evolution over decadal time scales at low temporal resolutions, e.g. annual to biannual. However, it does somewhat limit the ability to look at change at high temporal resolutions over long time periods, e.g. network change over the course of multiple floods over multiple years. The need for manual removal of artefacts after automatic vectorisation of the channel network is largely due to the accuracy of the channel network classification. Improvements in classification accuracy would beget reductions in time taken to remove artefacts, or potentially make automatic vectorisation capable of deriving a clean network skeleton. A fully automated process of retrieving a braided river's network topology is, ultimately, the end goal of this line of enquiry. Likely the biggest issue in generating the topology automatically is establishing the direction of channels and flow through the network. Achieving this without topography in rivers that deviate from a general flow direction is challenging and is, indeed, an objective and open research question being pursued by other workers looking to apply graph analysis to multi-channel rivers systems (e.g. Isikdogan *et al.* 2018).

5. Under or overreaching: (re)defining reaches in braided rivers

Chapter synopsis

Few studies of braiding provide explicit reasoning to their choice of reach length, despite length scaling in braided rivers indicating that reach length is likely integral to capturing a representative sample of planform or morphology. This chapter presents an analysis of the sensitivity of braiding index (*BI*) measurements under different spatial reach frameworks and over periods with highly variable flow conditions. Bivariate relationships between physical controls on braiding and *BI* provide further evaluation of the performance of the reach frameworks. The reach frameworks are 1) arbitrary, 1 km reaches after many previous studies of the Fiume Tagliamento; 2) fixed-distance reaches scaled on measures of average wetted width at two formative flow stages; 3) a novel approach to reach definition based on network topology that defines reaches of variable length. Results indicate that whilst the topological reach framework had the weakest relationships between *BI* and physical controls, this framework shows dynamic length scaling in response to flood events that suggests the underlying network topology responds to the magnitude of formative flood events. Furthermore, directions of change in the strength of the *BI*-physical control relationships indicate that these reaches may show greater sensitivity to previous flow conditions. Whether adopting a fixed reach length based on width scaling or variable lengths defined by topology, this chapter show clearly that short and arbitrary reach lengths are likely misrepresenting braided planforms and morphology.

5.1 Introduction

The reach is one of the most ubiquitous and fundamental units within fluvial geomorphology, used to sample different properties of rivers and describe aggregate form and behaviour. Despite the ubiquity of the reach in river science, their lengths are largely defined on what Parker *et al.* (2012) calls "operational" terms, e.g. a fixed-distance that is either arbitrary or perhaps scaled on some property of channel geometry such as width. Parker *et al.* (2012) note that whilst an operational reach definition may be useful for consistency of unit scales, the heterogeneity of fluvial forms and processes and their associated length scaling may mean operational reaches map onto fluvial morphodynamics more by luck than judgement and also miss important discontinuities that mark changes in morphodynamic behaviour. In studies of braiding, reaches

tend to be defined at either an arbitrary fixed-distance (e.g. Zanoni *et al.,* 2008; Ziliani & Surian 2012; Henshaw *et al.,* 2013), or at a distance that encompasses morphological features of interest and is practicable for field data collection, though rarely with explicit consideration of the chosen reach length (e.g. Van Der Nat *et al.*, 2002; Ashmore *et al.*, 2011; Wheaton *et al.*, 2013; Mueller & Pitlick 2014). Analysis of sampling considerations when conducting planform analysis of braided rivers has suggested that an operational reach definition should, at the minimum, be scaled by the average wetted width of the channel network at formative flow, such that bar-scale variability in channel pattern does not influence measures of braiding intensity (Egozi & Ashmore, 2008). However, recent research has shown that a statistically representative sample of morphological variability is contingent on a reach length that captures the intrinsic length scaling of braided rivers, which is in turn dependent on the width of the main (largest) channels (Redolfi *et al.*, 2016) and thus will vary longitudinally. This suggests that instead of operational reach definitions, functional definitions of variable reach lengths based around a consistent set of morphologically- and/or process-based properties may better capture morphodynamics in fluvial systems (Parker *et al.*, 2012).

Linked to the requirement for a more functionally representative method of reach definition in braided rivers is work within network research to define subnetworks, or communities, of nodes that are more closely connected with each other than with the wider network (e.g. Girvan & Newman 2002). This is a significant area of network science that has elucidated certain large-scale properties of *non-spatial* networks, such as the small-world network (SWN) phenomenon (see chapter 3, section 3.2) that plays a significant role in the dynamics of many types of network (Watts & Strogatz, 1998; Sen *et al.*, 2003; Beauguitte & Ducruet, 2011). In braided rivers, reaches are analogous to subnetworks and they provide a fundamental unit at the level of organisation above that of single network elements, e.g. bifurcations, confluences and channels. Definition of fundamental units at different hierarchical scales is an open question in various fields of connectivity and network research and has been identified as a particular challenge within geomorphic systems (Turnbull *et al.*, 2018). A robust method for the definition of reaches (subnetworks) is of particular interest in the context of this thesis, as it would unlock the possibility of applying an array of graph theory metrics best suited for the analysis of subnetworks that have great theoretical potential for the analysis of braided river morphodynamics (see chapter 3; Connor-Streich *et al.*, 2018).

Whether an approach to defining fundamental units (reaches) in braided rivers uses an operational, fixed-distance framework or a functional, variable length framework, the length of

a reach will considerably impact the planform or morphological properties it samples. The aforementioned links between channel width and representative reach lengths (Egozi & Ashmore, 2008; Redolfi *et al.*, 2016) stem from length scaling relationships between channel width and bar wavelengths that are in turn linked to the spacing of bifurcations and confluences and thus variations in channel pattern (Ashmore, 2009). Scaling reach lengths based on average wetted width should therefore encapsulate local planform variability caused by bar-scale processes such as chute channel erosion, but will still result in a fixed-distance, operational reach definition.

In attempting to define variable length, functional reaches in a meandering river, Parker *et al*. (2012) partitioned a continuous, longitudinal series of sediment transport capacity by finding partitions that minimise local variance. This approach in braided rivers has various difficulties. Firstly, deriving a reliable longitudinal series of any hydraulic variable at the network scale is a considerable challenge and would also rely on width averaging, which, in the context of defining functional reaches, may defeat the object of the exercise. Other longitudinal series of, for example, geometric properties of single channels or nodes may not show sufficient variation longitudinally, as a range of different channel geometries will normally be found at any given cross-section along a braided river. There is thus a need for an objective measure of the channel network that does not assume a particular length scale. Here, the topology of network may provide a possible solution, as local variations in the complexity of channel pattern will impact the connectivity of channels and nodes, which can be captured with graph theory metrics like *betweenness centrality* (*BC*; see chapter 3, section 3.3.1.2).

This chapter addresses the question of what is an appropriate length scale for capturing fluctuations in braiding intensity and its associated morphologies, and should these lengths be variable? To answer this question, an analysis of the sensitivity of a simple, channel-count *BI* to changes in spatial analytical framework is conducted. These spatial frameworks are defined as 1) arbitrary 1 km reaches as used in numerous studies of the Fiume Tagliamento; 2) two fixed-distance reach lengths scaled on average wetted width (*AWW*) at two formative flow stages; 3) a novel, graph theory-based approach using a community finding algorithm that partitions graphs based on *BC*. The sensitivity of these frameworks is analysed both in terms of spatial variation in *BI* at a point in time but also through time, in response to different magnitude flow events. Performance of each reach framework is then evaluated by analysis of bivariate relationships between known physical controls and reach-averaged *BI*. The physical controls are extractable from satellite remote sensing data and also include braid wavelength (*BW*).

Although not a physical control on braiding *per se* and normally being reported as an average parameter of whole channel networks (Ashmore, 2009; Bertoldi, Zanoni *et al.*, 2009), *BW* reflects the spacing of nodes within the channel network and thus should show an inverse relationship with braiding intensity, e.g. in reaches where *BW* is low, the average spacing of nodes is small and thus braiding intensity should be high. In a river such as the Tagliamento, which has transitional sections between braided and wandering planforms at lower flow stage, with concomitant impacts on channel length, *BW* will vary between reaches. This novel application of *BW* should serve as check on whether the reach framework is capturing internal variability in node spacing that will in turn impact braiding intensity.

Analysis presented in this chapter is aimed at answering the following research questions:

1. Do reach lengths defined by the network topology vary in space and over time and if so, are variations systematic?

2. Do flexible reach boundaries determined by the underlying network topology better characterise changes in braiding intensity?

3. If not, do fixed-length reaches scaled on *AWW* better capture changing braiding intensity?

4. Does reach framework impact on the strength of relationships between braiding intensity and reach-scale physical controls?

To answer these questions, different approaches to defining spatial reach frameworks are described. An assessment of the changes observed in reach length using the topological reach framework is presented, followed by an analysis of the sensitivity of *BI* under each framework and between frameworks. The bivariate relationships between physical controls and *BI* are then analysed, both in the context of the general strength of relationships under different reach frameworks and in terms of change in these relationships over time. Findings indicate that arbitrarily defined reach lengths that are short relative to the length scale of the network (e.g. 1 km in this case) introduce extraneous longitudinal fluctuations in braiding intensity, show little variation in their longitudinal patterns of *BI* over time, regardless of intervening flow conditions, and do not capture the negative *BI-BW* relationship seen in the other reach frameworks. Most intriguingly, the topological reach framework may show the first evidence of a braided channel network altering its length scale in response to discharge and the change, or lack thereof, in the positions of topological reach boundaries provides compelling evidence for the adoption of a

variable length reach framework in braided river research, with the general findings showing that reaches should, at a minimum, be scaled on a measure of *AWW*.

5.2 Methods

5.2.1 Data selection

For the wider purposes of this research, the channel network of the River Tagliamento has been extracted (using the method detailed in chapter 4) from 28 Landsat scenes spanning a period from 1996-2014. Various metrics, e.g. channel width, length and a range of graph theory metrics, have been computed for these networks. For the following analysis, a subset of 5 networks has been selected based on the flood conditions that separate the networks and a consideration of the number of edges (*m;* note edges and channels used interchangeably) that are present in each network, with *m* used as a rough proxy for stage. Use of a stage proxy is necessary due to inaccuracies of the Venzone stage record at low flows, e.g. problems with negative stage readings, which combined with the spatial and temporal variability in depth to water table and its associated effects on the channel network (see section 1.7.2) means that at the scale of the network, stage readings from Venzone in the majority of the studied networks bears little relevance to the amount of water visible in the corresponding Landsat scene. It is recognised that the number of wetted channels in a braided river shows a bell-shaped relationship to flow, peaking at intermediate stages before inundation of lower relief bars (Welber *et al.*, 2012; Redolfi *et al.*, 2016). As the networks used in this study were all captured at flows considerably below the stage associated with drowning of low relief bars on the Tagliamento (Bertoldi, Gurnell *et al.*, 2009; Welber *et al.*, 2012), it is assumed that increases and decreases in *m* correspond approximately with stage at the time of network capture.

Although the Venzone stage record does not capture accurate data in respect of low flows, it does provide a useful time series of flood events. Figure 5.1 shows the hydrographs over the two periods during which the five networks analysed in this chapter were captured. These two periods encompass one short period of low flow activity, the "low flow period", with few flow pulses capable of supporting widespread sediment transport (see section 1.7.2) and a longer period of high flow activity, the "high flow period", where the 2011 and 2013 networks are separated by a series of 2-3 m (some near-bankfull) events that culminate in a 1-in-10 year flood in 2012, whilst the 2013 and 2014 networks are separated by a series of 2-3 m floods. The high flow period should thus capture significant morphological change between 2011-2013 and

widespread but lower magnitude morphological change between 2013-2014 networks (see section 1.7.2). Within each period, networks with similar *m* were chosen to ensure comparability of braiding intensity was not affected by stage (Table 5.1).
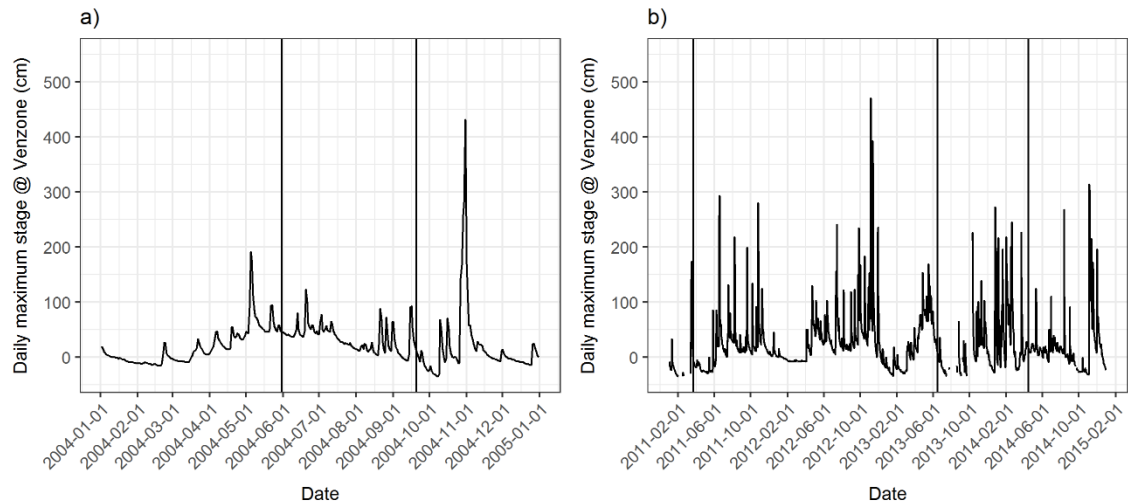
Figure 5.1: Hydrographs from the Venzone stage record for a) the low flow period and b) the high flow period. Horizontal lines in a) and b) show the dates of network capture.

5.2.2 Defining reaches

Studies on the Tagliamento have frequently employed a fixed-distance reach length of 1 km (e.g. Zanoni *et al.*, 2008; Ziliani & Surian 2012; Henshaw *et al.*, 2013), though as noted by Ziliani and Surian (2012), these are relatively short reaches given the braidplain width of the Tagliamento can exceed 1 km. Thus, an arbitrary, 1 km reach length provides the testcase of the standard approach to reach definition. Analysis of the effect of reach length on planform characterisation of braided rivers utilised a channel count *BI*. Whilst coarse, this index provides a robust and simple metric of variation in channel network complexity and braiding intensity. Egozi & Ashmore's (2008) analysis of sampling considerations when measuring braiding indices showed that sampling lengths should be at least 10 times the average wetted width (*AWW*) at channel forming flow. A distance scaled to channel forming *AWW* reduces the impact of bar-scale variability on channel pattern, which can skew index values.

Table 5.1: *m* for the different networks in each flow period.

	Low flow period		High flow period		
Date	*2004-05*	*2004-09*	*2011-03*	*2013-06*	*2014-04*
m	658	619	853	881	894

In the case of the River Tagliamento, there is a paucity of measurements of *AWW* at the scale of the channel network being employed in this study. However, the braided section of the Tagliamento flows through a small number of short, bedrock constrained reaches and is otherwise bordered by dense riparian woodland which acts as a significant width constraint at higher, channel forming flows. Bankfull discharge on the Tagliamento corresponds to a stage of ~3 m at Venzone (Bertoldi, Drake *et al.*, 2011), with flows of this magnitude inundating the width of the exposed gravel braidplain. Therefore, using a classified raster map of vegetation, gravel and water areas (see chapter 4) in an area limited to the river's riparian zone, it is possible to approximate bankfull *AWW* as the average width of exposed gravel and water areas. Polygons covering the exposed braidplain were reduced to lines tracking the right and left banks in ArcGIS. The distance to the banks was measured from points spaced 100 m apart along the centreline of the braidplain. Distance to each bank was measured using the Near tool in ArcGIS and aggregated, essentially providing the cross-sectional width of the braidplain at 722 cross-sections along the braided length of the Tagliamento. The average braidplain width of the 5 networks used in this chapter ranges from ~516 m to ~572 m and mean average braidplain width of the 5 networks is 543 m. Thus, an approximation of *AWW* at bankfull flow (AWW_{bf}) was taken as the mean average braidplain width rounded to the nearest 50 m, e.g. 550 m, with the AWW_{bf} scaled reach length set to 10 times this, e.g. 5.5 km. It should be noted that average widths mask significant width variation, with coefficients of variation (*CV*) ranging from 37 to 40%.

Previous research on the Tagliamento has found that the channel network can undergo significant reorganisation at flows that are less than bankfull (Bertoldi *et al.*, 2010). The threshold discharge for sediment erosion on the Tagliamento corresponds to a stage of 0.65 m at Venzone and stages above 2 m can begin to induce more widespread morphological change (see section 1.7.2). Using the estimate of *AWW* at a bankfull stage of 3 m and the 2 m stage threshold for the onset of large-scale change in channel planform, the bankfull *AWW* estimate was simply reduced by one third, e.g. 550 m · 0.66 = 363 m, resulting in an AWW_{2m} reach length of 3.6 km. It is recognised that this is a highly simplified approach to estimating *AWW*, but it was necessary due to the lack of data on *AWW* at different flows across the full length of the braided Tagliamento. As a check on the veracity of this estimate, the braid wavelength (*BW*) was also calculated as the number of bifurcations or confluences in a unit length of the river divided by the total length of channels within this reach, which gives a metric of the average spacing of nodes within the network (Ashmore, 2009). As the networks used in this study begin from and terminate in a single-thread channel, it is easy to calculate this metric for the whole network using the sum of edge lengths and the graph order

$$BW = \frac{\sum_{i=1}^{m} L_i}{N/2} \qquad\qquad (5.1)$$

where L_i is the length of edge i, m is the number of edges in the network and N is the graph order (number of nodes in the network). Egozi & Ashmore (2008) suggest that in the absence of data on *AWW* at channel-forming discharge, two to three times *BW* should provide an adequate sample length for calculating a braiding index. The mean of 3*BW* for the 5 instances of the river assessed in this chapter was 3 km (± 0.15, 1 SD) km, indicating that, whilst potentially a slight overestimate, the 3.6 km AWW_{2m} reach length is sufficient to incorporate multiple bifurcation-confluence units and reduce the effect of bar-scale variability in channel pattern on *BI*. Selecting reach lengths based on *AWW* also means reaches have a physical basis that reflects the spatial scaling of bifurcation-confluence units that, ultimately, determines channel patterns.

The third approach to defining reaches applied here uses the network topology, independent of any specific physical parameters. *Edge betweenness clustering* is a graph theory-based method for finding communities in networks that utilises the *edge betweenness centrality* (*eBC*) metric (Newman & Girvan, 2004). In a general sense, communities are groups of nodes that are more closely connected to each other than with other nodes in the wider network. Communication between nodes in different communities is normally facilitated by a small number of edges that form bridges between communities. Considering that a node or edge's *betweenness centrality* (*BC*) describes the number of shortest paths between pairs of nodes that traverse this node/edge (see chapter 3), nodes/edges within a community should have lower *BC* than the nodes/edges that connect communities and thus fall on more shortest paths. Many braided rivers exhibit a typical string-of-pearls planform structure, whereby the channel network expands and contracts longitudinally (Figure 5.2). This structure intuitively suggests that an algorithm capable of automatically dividing the network at high *BC* "bridges" may be able to find step changes in network complexity that result in transitions from multiple to one or two channels and *vice versa*. Thus, network topology may provide a means to define reaches at variable lengths that are determined by the complexity of the network planform, which should itself reflect longitudinal variation in morphodynamics. The *edge betweenness clustering* algorithm of Newman & Girvan (2004) has been implemented in the R (R Core Team, 2017) package igraph (Csárdi & Nepusz, 2006). It operates by:

1. Calculating *eBC* for all edges in the network;

2. Finding and removing the edge with the highest *eBC*;

3. Recalculating *eBC* for remaining edges;

4. Repeat from step 2.

The output lists which nodes/edges have been assigned to each community (reach). It should be noted that the implementation of *edge betweenness clustering* in igraph is for undirected networks but that in most cases, even in networks where edge direction is generally of high importance (such as braided rivers), the importance of connections between communities is unlikely to be affected by edge direction (Newman & Girvan, 2004). This is apparent in braided rivers as bridging channels between more complex sections of the river will have high *eBC* regardless of the direction in which they are traversed. This, as well as results typical of reach definition using *edge betweenness clustering,* is illustrated in Figure 5.3.

5.2.3 Braiding index calculation

Calculation of a channel count *BI* for each reach followed the methodology described in Egozi & Ashmore (2008). They recommend counting the number of channels at ≥ 10 cross-sections, equally spaced along the length of a reach. In the present study, 16 cross-sections were defined in each reach at equally spaced points along the braidplain centreline. Egozi & Ashmore (2008) found that increases above 10 cross-sections resulted in no increase in precision of measuring *BI* and thus the use of 16 cross-sections may introduce some redundancy. However, increasing the number of cross-sections above 10 had little impact on processing time and thus was done to reduce the probability of any short, intensely braided sections of a reach skewing *BI* values. 16 cross-sections were chosen as the maximum number that could fit, with equal spacing, into a 1 km reach without risk of double counting channels by overlapping cross-sections. Channels were represented by the network skeleton extracted from the classified water raster of the channel network (see chapter 4 for the full network extraction methodology). Channels were counted as the number of centrelines intersecting each cross-section, with *BI* defined as the mean of the channel counts at each cross-section in each reach.

Figure 5.2: The Jamuna River, Bangladesh (top, flow from right to left), the Waimakariri River, New Zealand (middle, flow from left to right) and the Toklat River, Alaska, USA (bottom, flow from right to left) are braided rivers of contrasting scale that all show a characteristic string-of-pearls configuration with expanding and contracting braiding intensity. (Image source: Google Earth, 2019)

5.2.1 Physical controls on braiding

As well as assessing variability in *BI* values between reach types, physical controls extractable from remotely sensed datasets were also analysed to determine whether reach spatial framework has an impact on any relationships between known physical controls on braiding and channel pattern. The following variables were either extracted directly from remotely sensed data or derived from other extracted variables: vegetation area, slope, braidplain width and wetted width. Vegetation is known to play a considerable role in the morphodynamics of the Tagliamento (Gurnell *et al.*, 2001; Bertoldi, Gurnell *et al.*, 2011; Corenblit *et al.*, 2014), whilst slope is associated with the conditions required for the onset of braiding (Ashmore, 2013). The importance of slope stems from its role in determining streampower, which has been suggested

as one of the dominant controls on braiding intensity (van den Berg, 1995; Ashmore, 2009). Width constraint has also been found to have a considerable influence on braided planforms, with the potential to force transitions from braided to single-thread channels (Mueller & Pitlick, 2014; Garcia Lugo *et al.*, 2015).
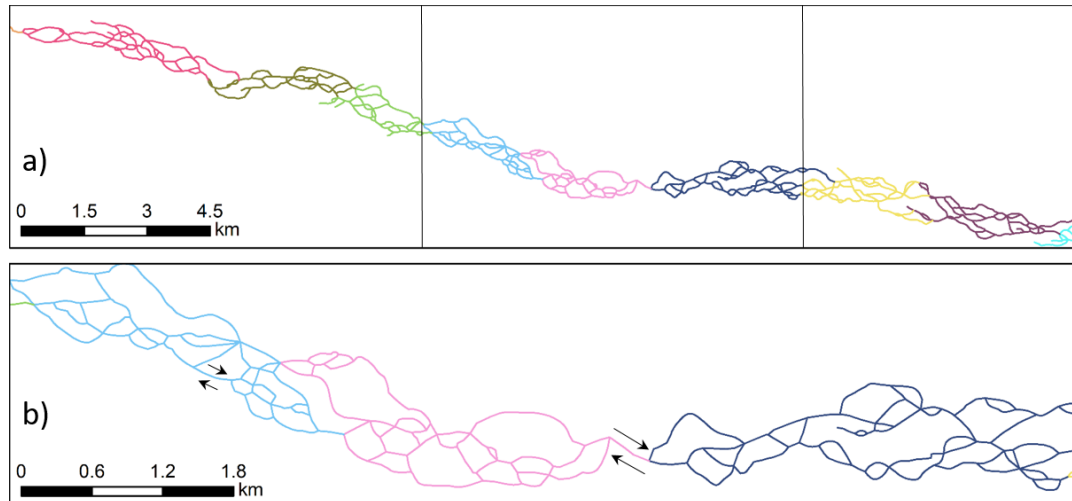
Figure 5.3: a) different colours represent reaches delineated automatically using the *edge betweenness clustering* algorithm in the R package *igraph*; b) close up of the area within the vertical lines in a). The arrows highlight two channels with quite different patterns of local connectivity that, regardless of the direction they are traversed, will be on the same number of shortest paths between upstream and downstream nodes and hence network direction can be neglected in the community finding algorithm.

Vegetation area for each reach was extracted from the vegetation classification produced during the process of channel network extraction (see chapter 4). Raster cells classified as vegetation were converted to polygons to enable areas of vegetation that cross reach boundaries to be split at respective boundaries, and to ease the extraction of vegetation areas. Polygons covering the braidplain in each reach were produced by splitting a polygon covering the whole exposed braidplain at the reach boundaries. The whole exposed braidplain polygon is derived by merging areas classified as water and gravel and filling "holes" left by vegetation. For the fixed-length reaches, positioning the reach boundaries is done simply by creating lines perpendicular to the main flow direction at the relevant fixed interval along the braidplain centreline. The *eBC* reaches do not have a fixed length, so the boundaries are situated at the most downstream node in any given reach. A method to automatically locate and create reach boundaries has been developed using geoprocessing tools in ArcGIS. This method largely performs well, though on occasion *eBC* reach boundaries were found to be located slightly upstream or slightly downstream of the most downstream node in a reach. These discrepancies are of the order of ≤ 90 m, which is less than an average channel width on the Tagliamento and thus will not have

a notable impact on the value of *BI* or other physical variables in an *eBC* reach. Once a set of polygons for each reach type has been produced for each instance of the river, the area of vegetation (m^2) in each reach is extracted and used to calculate percentage vegetation cover.

Analysis of the impact of width constraint on *BI* focussed on active width (*AW*), defined here as the average width of the unvegetated (gravel and water) areas of the braidplain. A key characteristic of the Tagliamento is the presence of vegetated islands within the braidplain (Gurnell *et al.*, 2001). Thus, this definition of *AW* assumes that areas of exposed gravel will have received sufficient disturbance by flood flows to remove or prevent the establishment of vegetated islands and may have been sites of sediment erosion, transport and deposition, subsequently being classified as 'active'. Whilst this is a relatively simple approach to the definition of active width that negates information on the actual locations of preferential vegetation establishment, erosion, deposition and bedload transport pathways, it gives a general measure of the width over which morphological change was capable of occurring during the last flood and is derivable from a single satellite image. *AW* for each reach was calculated by subtracting the sum of vegetation area in a reach from the total reach area and dividing by the reach length. This calculation is actually assessing the width of the minimum bounding rectangle of the irregular reach polygons and will thus slightly overestimate the *AW* of each reach. Comparing the average cross-sectional total braidplain width relative to the total braidplain width calculated by the area/length method, the area/length method results in a 10-13% increase in the average braidplain width compared to the cross-sectional method. However, given a *CV* of 37-40% for the cross-sectional method and the consistency of the overestimate of active width, indicating that reaches can still be compared relative to one another, this slight discrepancy is not considered to bias the results in any significant way. The total wetted width (*WW*) of channels in each reach was also computed using an area/length method, dividing the total water area by the sum of channel lengths in each reach. Again, this method is an oversimplification of *WW*, but for the same reasons as detailed for *AW*, it is assumed to not significantly misrepresent *WW* and reaches will still be comparable relative to one another.

The slope of each reach was extracted from the European Environment Agency (EEA) digital elevation model (DEM), EU-DEM, which provides a pan-European elevation dataset at 25 m resolution (EEA, 2014). Vertical root mean square error (RMSE) for the EU-DEM over Italy is reported as 2.2 m (EEA, 2014). RMSE values for the study area are not available. Elevations were extracted from the DEM raster at the mid-point of the braidplain at the upstream and downstream reach boundaries, with the elevation difference (Δz) and reach length used to

calculate reach slope (S, m m^{-1}). In the case of the *eBC* reaches, which are of variable length, the reach length is calculated as the difference between the downstream distance of the most upstream and downstream nodes. Where reach lengths are short, vertical errors on the DEM become more important as a reach's Δz is likely smaller. This problem caused one reach in the set of fixed-distance 1 km reaches to have negative S, with this reach excluded from further analysis involving S.

Statistical analysis of the relationships between *BI* and physical controls was conducted using linear regression. The regression relationships were analysed in terms of change in the estimates of the regression line slope coefficient (*b*) and the strength of the regression relationship (r^2) between reach frameworks and within the same framework over time relative to flow conditions. *BW* was also included as a physical variable due to its hypothesised relationship with *BI*. In order to analyse the *BW-BI* relationship using linear regression, it was necessary to log$_{10}$ transform the *BW* data to achieve a normal distribution. All statistical analysis was conducted in R (R Core Team, 2017).

5.3   Results

5.3.1   Visualising a variable length reach framework

The spatial and temporal heterogeneity visible in braided channel patterns suggests that change in morphology moving downstream may not conform to a fixed length scale, even at a single point in time. Figure 5.4 shows the variable lengths of the topologically defined "*eBC* reaches", which show a range of lengths at one point in time and change their length and the position of their boundaries over time. Reach boundaries over the low flow period show less variability than over the high flow period, with the boundaries in the 2004-05 and 2004-09 networks often falling in the same places or showing slight offsets. Boundary shifts are starker over the high flow period, with a notable offset of the reach boundaries between 2011-2013, followed by a smaller offset between 2013-2014, such that certain boundaries remain in similar positions whilst others return to positions closer to those seen in 2011 (Figure 5.4). Over the high flow period, there is also a reduction followed by an increase in the number of reaches. This change in the number of delineated reaches is accompanied by visible lengthening of reaches between 2011-2013, followed by an apparent retraction in length between 2013-2014 (Figure 5.4). The range of reach lengths seen in the high flow period networks shows this pattern quantitatively (Figure 5.5b). During the low flow period, reach lengths appear to become more homogenous

between 2004-05 and 2004-09 (Figure 5.4 & Figure 5.5a). This lengthening and shortening behaviour appears more strongly associated with certain locations, e.g. 20-25 km, 35-40 km and 45-55 km (Figure 5.4). It is also observed that the points around which these changes tend to be seen are also sites where reach boundaries are present in all networks in the low and high flow periods, e.g. at around 16 km, 26 km, 32.5 km and 45 km.
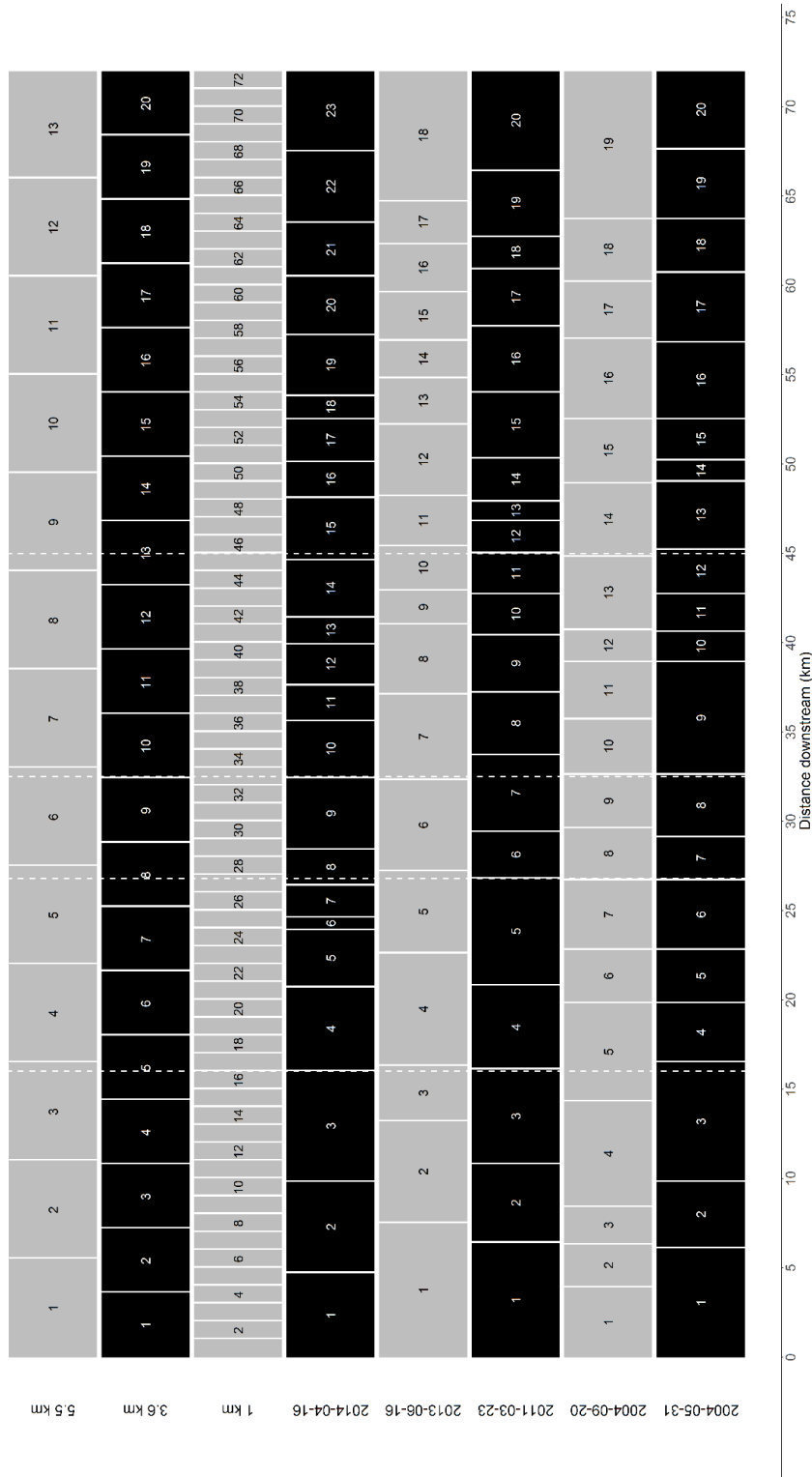
Figure 5.4: Change in the position of the boundaries of the *eBC* reaches over time. The positions of the fixed-distance reaches are included for reference. Dashed vertical lines show locations where *eBC* reach boundaries are relatively fixed over time.

117
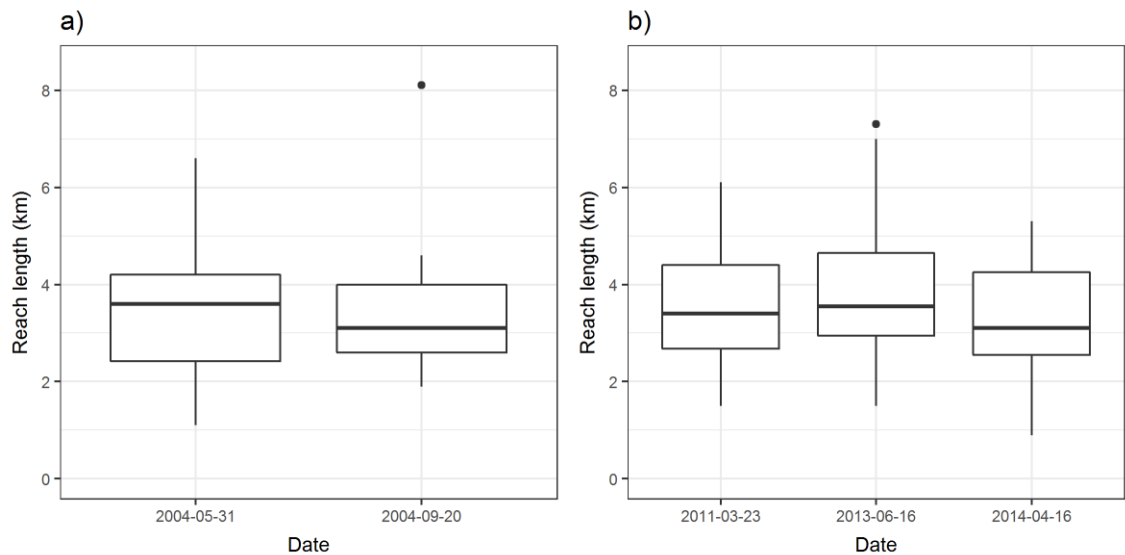
Figure 5.5: Boxplots showing the range of reach lengths for a) the low flow period and b) the high flow period. Lines in boxes represent the median, boxes the interquartile range (IQR), whiskers show 1.5IQR and dots represent outliers.

Variable lengths of the *eBC* reaches suggest that the scales over which morphological changes occur on the Tagliamento are also variable, both in time and space. Spatial variation in river planform can be visualised in Figure 5.6a and shown quantitatively using normalised *node betweenness centrality* (*nnBC*; see chapter 3, section 3.3.1.2) in Figure 5.6b. Changes to planform are clearly observable as areas where the channel network transitions from sections of single channels with central bars to areas of higher intensity braiding with channels dividing around multiple row bars, with these changes also reflected in the longitudinal variability in *nnBC*. Lengths of the network characterised by lower complexity, for example the first ~5 km visible in the top left corner of Figure 5.6a where the river transitions from a bedrock constrained single channel with occasional central bars, are characterised by nodes of only high *nnBC* (Figure 5.6b). Sections dominated by two parallel channels (15-20 km) have nodes of low to medium *nnBC* and are followed by a switch to a multiple bar-braided planform from ~20-27 km, which is characterised by an increase in both the density of nodes and the range of *nnBC* values present within the same area. Similar patterns are observable along the length of the braided Tagliamento. Notably, these patterns appear irregular in length, with areas that show different channel patterns (Figure 5.6a) and accompanying changes to the range of *nnBC* values tending to exceed a length of 1 km (Figure 5.6b).
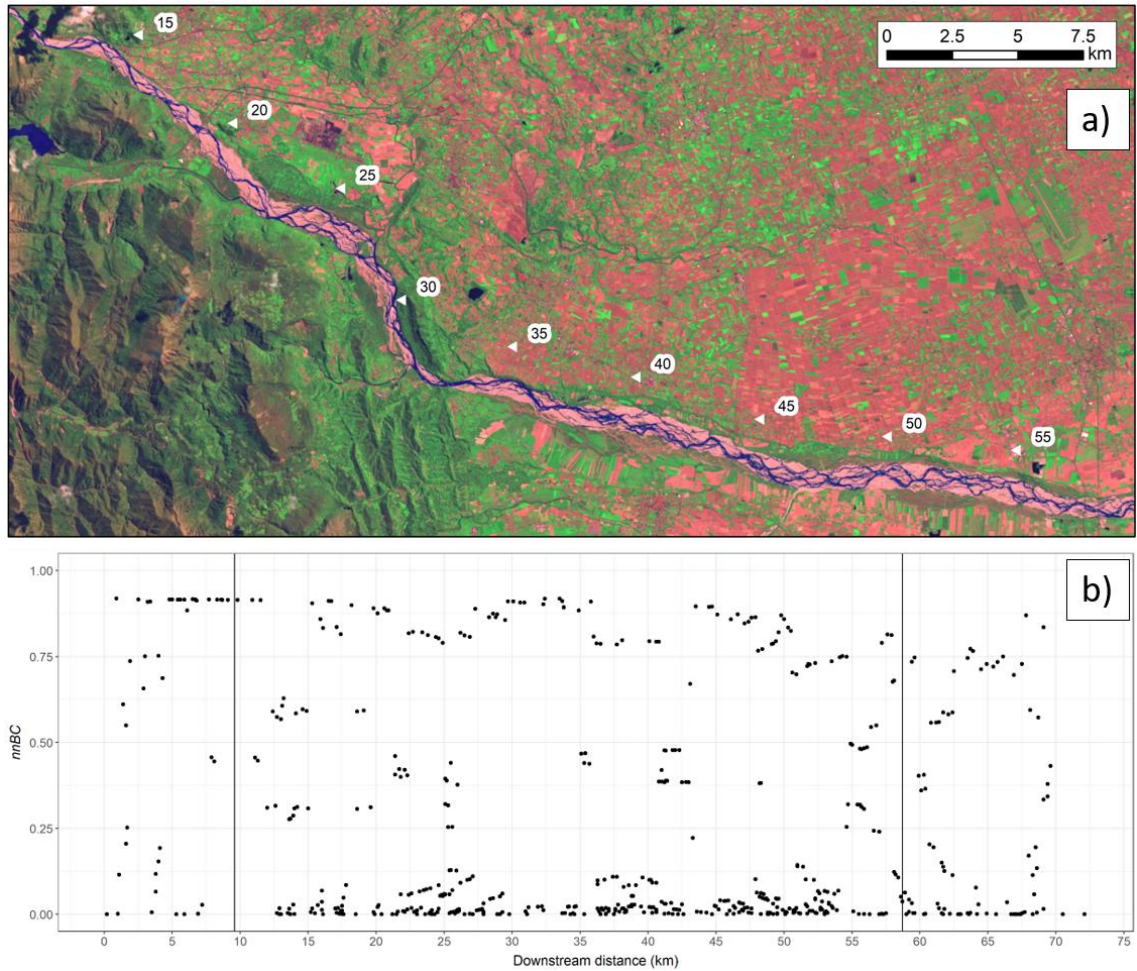
Figure 5.6: a) False-colour composite (bands 3, 4 and 6) of a Landsat scene covering a 49 km section of the River Tagliamento. Numbers mark 5 km distances moving downstream; b) Longitudinal variation in normalised *node betweenness centrality* (*nnBC*) for the channel network extracted from the Landsat scene in a). Vertical lines on the plot demarcate the section of the river shown in a).

5.3.2 Longitudinal variations in BI under different reach frameworks

To assess the impact of reach framework on the quantification of braiding intensity, longitudinal variation in *BI* for the variable length *eBC* reaches is shown against the fixed-distance reach frameworks for the low flow period (Figure 5.7) and high flow period (Figure 5.8). During the low flow period, the 1 km reaches show significant fluctuations in braiding intensity between adjacent reaches, although general trends in the longitudinal series are present. After the initial increase as the river begins to braid over the first 5 km, decreases in *BI* are seen to ~10 km (Figure 5.7). *BI* then shows an overall increasing trend over the next ~15 km, before decreasing between ~25 km and ~32 km. Downstream of 32 km, there is an initial spike in braiding at ~40 km, followed by around 20 km where the 1 km reaches fluctuate around a mean *BI* of 3.4 (2004-

09) and 3.5 (2004-05), before *BI* declines as the river transitions from braided to single-thread. *BI* is also variable between *eBC* reaches, though fluctuations are considerably less extreme (Figure 5.7). Indeed, *BI* values in the *eBC* reaches appear to track the general trends in *BI* seen in the 1 km reaches, appearing almost as a moving average, though with a variable window size. Highs and lows in braiding intensity in the *eBC* reaches are also largely in the same locations as the 1 km reaches but tend to be of lower magnitude, a pattern that is also seen in the 3.6 km and 5.5 km reaches.
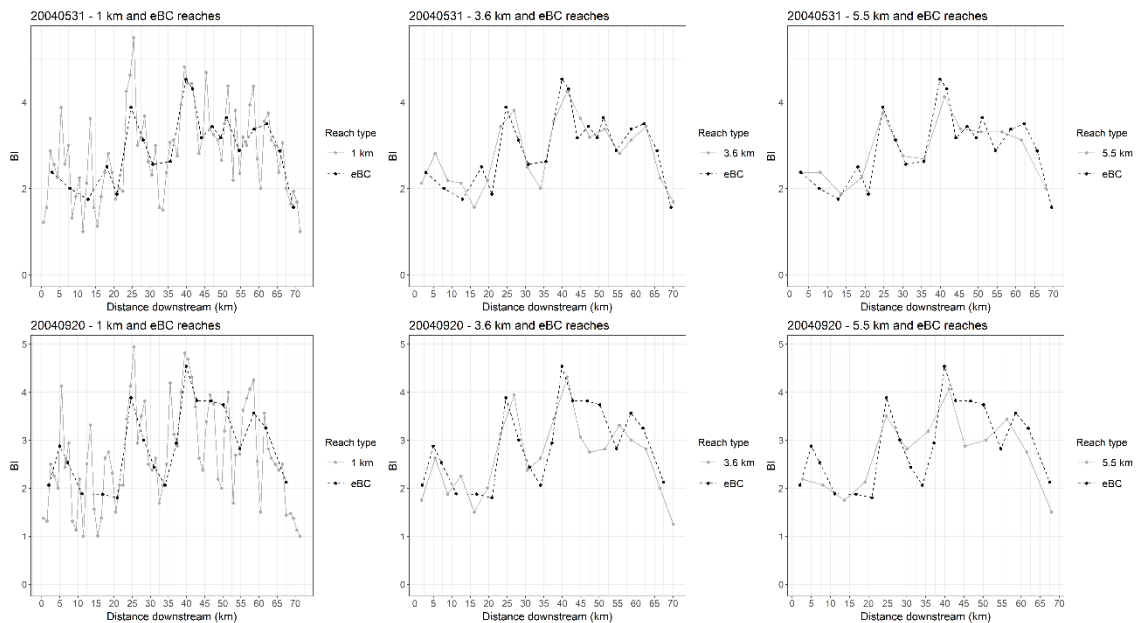
Figure 5.7: Longitudinal variation in *BI* of variable length, topologically defined *eBC* reaches and three fixed-distance reach types for two dates separated by a period of low flows on the River Tagliamento.

Comparing the *eBC* reaches and 3.6 km reaches, there is a remarkable concordance in the overall pattern of *BI* fluctuations moving downstream, especially in the 2004-05 network (Figure 5.7). The largest discordances are seen in the first 10-15 km and between ~40-60 km. It is interesting that, after a sharp drop between 40-45 km in the 2004-09 network *eBC* reaches, *BI* stabilises for around 7.5 km before declining again, whereas the decline in *BI* in the 3.6 km reaches is consistent over the same distance, a pattern that is also seen in the 5.5 km reaches. This suggests some difference in the channel patterns being sampled in each reach that relates to changes in the position of reach boundaries. The longitudinal variation in *BI* in the 5.5 km reaches relative to *BI* in the *eBC* reaches mirrors that of the *eBC* reaches relative to the 1 km reaches, acting to almost smooth out fluctuations in *BI* between adjacent reaches (Figure 5.7). This is particularly evident in the 2004-05 network downstream of 45 km and within the first 10 km of the 2004-09 network.

Figure 5.8 shows the longitudinal variation in *BI* values for different reach types for the high flow dates. Despite these networks having higher *m* (Table 5.1), and it is assumed stage and discharge, as well as being separated by periods of considerable hydrological variability, the broad patterns in terms of *BI* are still present. High and low BI reaches are still positioned in approximately the same locations regardless of reach type, however the extreme *BI* values observed at ~25 km in the 1 km reaches are evidence of both the effect of higher stage on *BI* and the subsequent impact of sampling shorter reaches through heavily braided sections of the river. As with the low flow dates, the *eBC* reaches approximate moving averages of the 1 km reaches, with the reverse seen in the 5.5 km reaches for the 2011 and 2014 networks. Longitudinal variation in *BI* between the *eBC* reaches and the 3.6 km reaches is also very similar for these dates, matching the patterns seen in the low flow dates (Figures 5.7 & 5.8). A notable exception is seen in comparison of the longitudinal variation in *BI* between the *eBC* reaches and the 3.6 and 5.5 km reaches in the 2013 network (Figure 5.8). This is the channel network formed by a series of 2-3 m stage flood pulses, including one bankfull event in June 2011 and a 1-in-10 year flood in November 2012 (Figure 5.1), and instead of the *eBC* reach *BI* values tracking similar trends to the 3.6 km reaches, they follow a remarkably similar pattern to the *BI* values observed for the 5.5 km reaches, both in terms of the position of the reaches and the value of *BI*, with this pattern being strongest over the first ~40 km.

5.3.3 Relationships between BI and physical controls under different reach frameworks

The longitudinal variation in *BI* seen for all reach types (Figures 5.7 & 5.8) is indicative of changing physical controls on braiding intensity along the length of the braided Tagliamento. Linear regression analysis of *BI* with reach-averaged physical controls has been used to test if different reach frameworks better capture relationships between *BI* and controlling variables. Regression relationships between reach vegetation percentage and reach slope yielded no significant relationships with *BI* for any of the reach frameworks and will not be discussed further. Figure 5.9 shows the relationship between *BI* and *AW* for the low and high flow periods. Regardless of reach framework and intervening flow conditions, there is a positive relationship between *BI* and *AW*. However, both the slope of the regression lines (b_{AW}) and the strength (r^2) of the relationship varies with reach type and over time. Values of b_{AW} range from 0.0015-0.0052, which equates to an estimated increase of 0.1-0.5 channels per 100 m increase in *AW* and, barring the 2004-09 *eBC* reaches, all relationships between *BI* and *AW* are significant at the 95% level or higher (Table 5.2). There is also a pattern of lower b_{AW} during the low flow period

under all reach frameworks, which is likely a reflection of the greater number of channels present in the 2011-2014 networks, given a lack of any significant increase in average *AW* between 2004 and 2014 (Table 5.2 & Table 5.4).
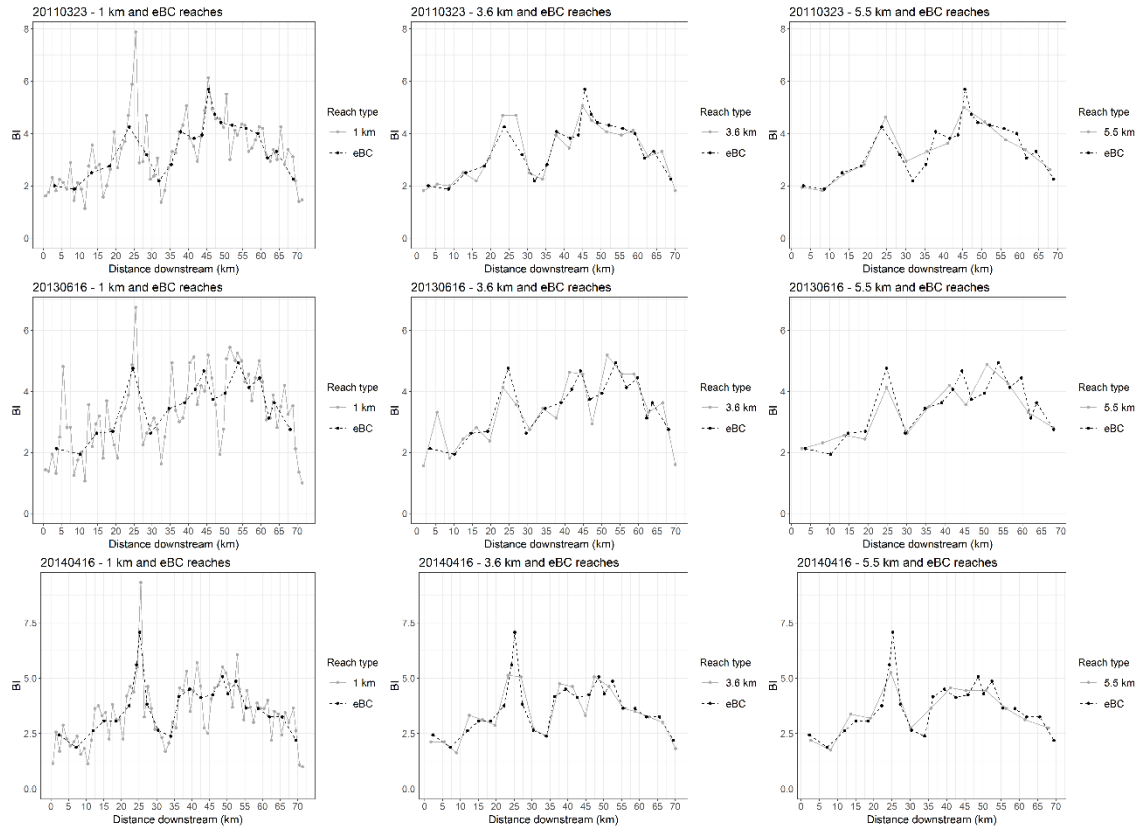
Figure 5.8: Longitudinal variation in *BI* of variable length, topologically defined *eBC* reaches and three fixed-distance reach types for three dates separated by periods of variable hydrological conditions. 2011-03-23 and 2013-06-16 are separated by various flood pulses of different magnitude, including a 1-in-10 year event in 2012. The 2013 and 2014 networks are separated by a smaller number of less than bankfull flood pulses.

Though all reach frameworks show a general pattern of b_{AW} over time, differences are seen in the size of b_{AW} and r^2. For the same networks, the *eBC* reaches have lower b_{AW} compared to any of the fixed-distance frameworks, whereas b_{AW} is comparable between the fixed-distance reaches (Table 5.2). Larger differences are observed in the strength of the regression relationships for the same networks when comparing the different fixed-distance reaches, with r^2 increasing with increasing fixed reach length (Figure 5.9, Table 5.2). As with b_{AW}, r^2 for the *BI-AW* relationships is lower for the *eBC* reaches when compared with the fixed-distance reaches for the same network (Table 5.2). Whilst the fixed-distance reaches may have higher b_{AW} and r^2 than the *eBC* reaches, analysis of the relative difference in b_{AW} and r^2 between paired dates over the low and high flow periods shows that the *BI-AW* relationship is more variable over time in

the *eBC* reaches when compared to the fixed distance reaches, both in terms of the size of the differences and their directions (Table 5.4). The direction of change in b_{AW} is negative over the low flow period in the *eBC* reaches and low but positive in the fixed-distance reaches. Directions of difference in b_{AW} are the same for all reach frameworks during the high flow period, with the change in b_{AW} between 2013-2014 in the *eBC* reaches being notable for being the only combination of physical control and date pair where the difference is smallest for the *eBC* reaches (Table 5.4). Relative differences in r^2 for the *BI-AW* relationships are greatest in the *eBC* reaches for all cases. There is also some degree of pattern in the directions of change in r^2 over the low and high flow periods, with generally negative differences in the low flow period (except in the 3.6 km reaches) and between 2011-2013 in the high flow period, and positive differences between 2013-2014 (except in the *eBC* reaches; Table 5.4).
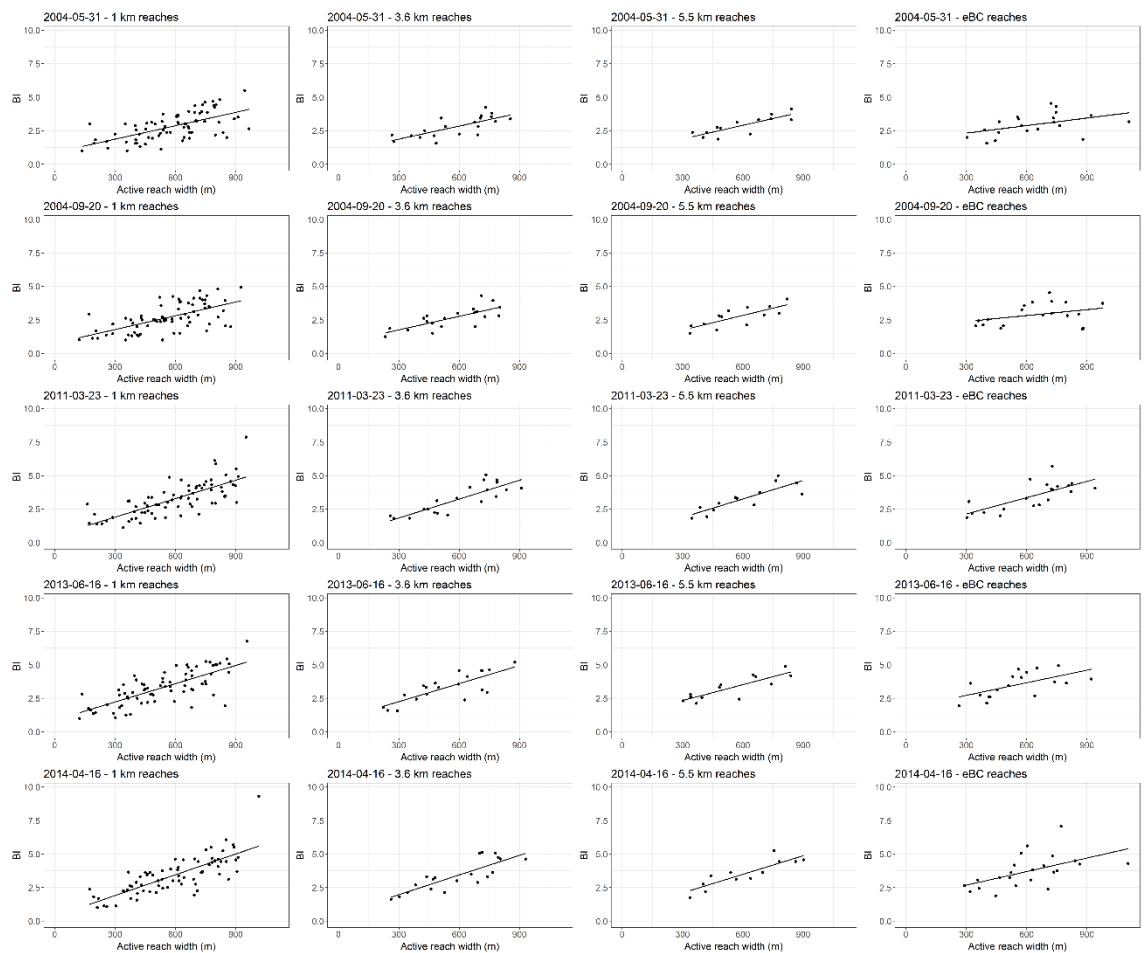
Figure 5.9: Braiding intensity (BI) Vs active width for 4 different reach types, across both the low flow (2004) and high flow (2011-2014) periods. Trend lines fitted using linear regression.

Strong positive relationships between *BI* and *WW* were seen for all reach frameworks (Figure 5.10), with moderate to high r^2 values and significant regression relationships at the 99% confidence level or higher in all cases (Table 5.2). The range of the *BI-WW* regression slope coefficient (b_{ww}) suggests that *BI* will increase by ~0.9-1.3 per 100 m increase in *WW*. These estimates are sensible given that average channel width from the larger sample of 28 networks (see section 2.1) is 95.4 m. There is not a particular pattern across the reach frameworks for change in the values of b_{WW} over the low flow periods, however over the high flow period all reach frameworks show an increase and then a decrease in b_{WW} (Table 5.2). The relative differences in b_{WW} and r^2 for the *BI-WW* relationships are perhaps more informative. Greater magnitude changes in b_{ww} and r^2 are seen in the *eBC* reaches across both flow periods, with the lowest changes generally seen in the 1 km and then 5.5 km reaches (Table 5.4). Directions of change in b_{WW} are the same for all reach types during the high flow period, increasing between 2011-2013 and then decreasing between 2013-2014, which is a plausible response to the high magnitude flood of 2012 followed by floods that are within the range of a more normal inter-annual flow regime (Table 5.4). In the low flow period, the 1 km and 5.5 km reaches suggest, albeit modest, increases in predicted *BI* as a function of *WW*, whereas the direction of the difference is reversed in the 3.6 km and *eBC* reaches (Table 5.2 & Table 5.4). Percent change in b_{WW} is also very similar between 2011 and 2013 in the 3.6 km and *eBC* reaches, however b_{WW} in the 3.6 km reaches is approximately half as sensitive to the lower magnitude floods between 2013-2014 and during the low flow period (Table 5.4, Figure 5.1). The greater variability in *BI* with *WW* in the *eBC* reaches is also clearly visible in Figure 5.10 and shown quantitatively in the lower values and large negative differences of r^2 seen on all dates when compared with the fixed-distance reaches (Table 5.2 & Table 5.3).

Table 5.2: Results from linear regression of braiding intensity against active width (*AW*, m), wetted width (*WW*, m) and $\log_{10}$ braid wavelength (BW_{log10}, m) for the slope coefficient (*b*), Std. error of *b*, the strength of the regression relationship (r^2) and the significance of the relationship (*p*).

Reach type	Date	b AW	b WW	b BW_{log10}	Std. error AW	Std. error WW	Std. error BW_{log10}	r^2 AW	r^2 WW	r^2 BW_{log10}	p AW	p WW	p BW_{log10}
1 km	20040531	0.0033	0.0111	-0.48	0.0005	0.0010	0.52	0.40	0.66	0.01	****	****	N.S.
	20040920	0.0034	0.0113	-0.47	0.0005	0.0008	0.55	0.39	0.76	0.01	****	****	N.S.
	20110323	0.0046	0.0101	-1.78	0.0005	0.0006	0.71	0.55	0.79	0.08	****	****	*
	20130616	0.0045	0.0123	-1.39	0.0005	0.0010	0.67	0.55	0.69	0.06	****	****	*
	20140416	0.0052	0.0116	-1.96	0.0005	0.0009	0.87	0.60	0.70	0.07	****	****	*
3.6 km	20040531	0.0032	0.0114	-2.18	0.0007	0.0014	1.14	0.56	0.78	0.17	***	****	N.S.
	20040920	0.0034	0.0103	-2.19	0.0007	0.0012	0.95	0.56	0.81	0.23	***	****	*
	20110323	0.0047	0.0101	-6.47	0.0007	0.0009	1.61	0.71	0.88	0.53	****	****	***
	20130616	0.0045	0.0127	-6.12	0.0008	0.0014	1.16	0.63	0.81	0.62	***	****	***
	20140416	0.0049	0.0112	-5.69	0.0008	0.0012	1.60	0.69	0.83	0.42	****	****	**
5.5 km	20040531	0.0034	0.0099	-2.37	0.0007	0.0015	1.22	0.68	0.79	0.26	***	***	N.S.
	20040920	0.0036	0.0107	-2.32	0.0009	0.0014	1.08	0.61	0.83	0.30	**	***	N.S.
	20110323	0.0046	0.0092	-7.85	0.0009	0.0012	2.28	0.72	0.85	0.53	***	****	**
	20130616	0.0040	0.0109	-5.19	0.0008	0.0013	1.94	0.72	0.87	0.41	***	****	*
	20140416	0.0046	0.0101	-4.77	0.0008	0.0012	1.74	0.77	0.87	0.41	***	****	*
eBC	20040531	0.0019	0.0103	-1.18	0.0009	0.0019	0.82	0.21	0.62	0.10	*	***	N.S.
	20040920	0.0015	0.0082	-2.70	0.0010	0.0023	1.20	0.12	0.43	0.23	N.S.	**	*
	20110323	0.0041	0.0088	-2.03	0.0009	0.0014	0.97	0.54	0.70	0.15	***	****	N.S.
	20130616	0.0031	0.0111	-6.53	0.0010	0.0022	1.67	0.37	0.62	0.58	**	***	***
	20140416	0.0034	0.0087	-4.17	0.0011	0.0021	0.96	0.30	0.44	0.38	**	***	**

***** = < 0.0001, **** = < 0.001, *** = < 0.01, * = < 0.05, N.S. = not significant

Table 5.3: Average active width (*AW*) of the braidplain during the low and high flow periods

	Low flow period		High flow period		
Date	*2004-05*	*2004-09*	*2011-03*	*2013-06*	*2014-04*
Average AW (m)	586	561	599	535	591
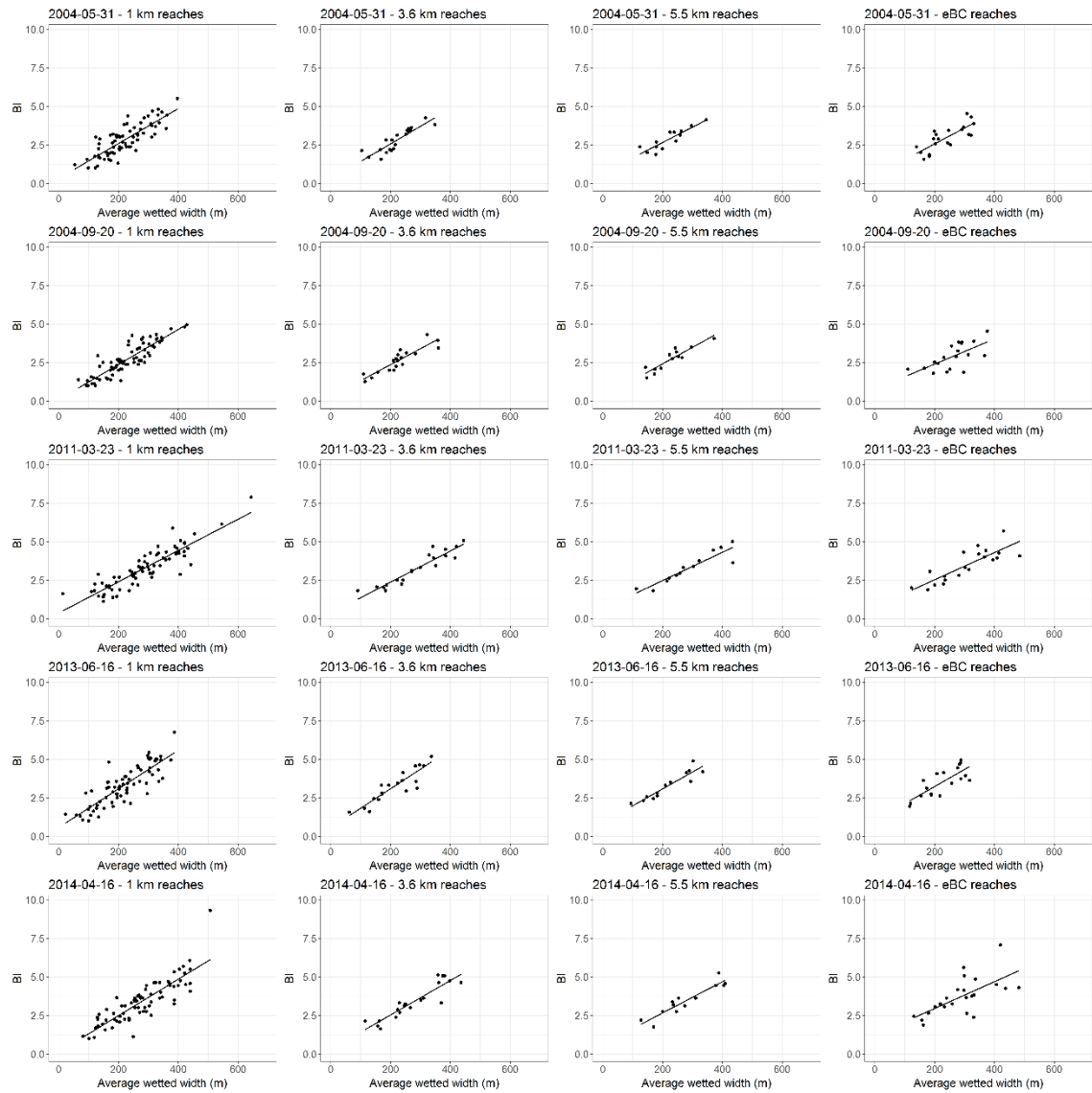
Figure 5.10: Braiding intensity (*BI*) Vs average wetted width for 4 different reach types, across both the low flow (2004) and high flow (2011-2014) periods. Trend lines fitted using linear regression.

Figure 5.11 shows the relationships between *BI* and BW_{log10} for each reach framework over the low and high flow periods. Note that the BI-BW_{log10} regression slope coefficient (b_{BW}) is considerably larger than for *AW* and *WW* due to the log_{10} transformation and describes the predicted change in *BI* for order of magnitude changes in *BW*. Negative b_{BW} in all cases also confirms the hypothesised inverse relationship between *BI* and *BW* (see section 5.1). The 1 km

reaches have weak to no relationship between BI and BW_{log10}, particularly in the low flow period networks. Values of b_{BW} (-0.48 to -1.96) and, in particular, r^2 (< 0.1) for all 1 km reaches emphasise the weakness of these relationships (Table 5.2). Figure 5.11 also shows a clear difference in the nature of the BI-BW_{log10} relationships between the low and high flow periods under all reach frameworks. These differences are highlighted in the large increases in b_{BW} and r^2 values between the low and high flow periods, as well as all-bar-one insignificant p-value being found in the low flow period networks (Table 5.2).

Table 5.4: Percentage change in the regression slope coefficients (b) within the low flow period and between different years in the high flow period.

| Reach type | Period | % change | | | | | |
| | | AW | | WW | | BW_{log10} | |
		b	r^2	b	r^2	b	r^2
1 km	**Low flow**						
	2004-05 - 2004-09	2.68	-2.72	2.04	13.35	-3.25[††]	-15.83[††]
	High flow						
	2011-2013	-0.99	-0.45	17.71	-12.55	-31.18	-27.65
	2013-2014	11.98	8.76	-5.72	1.00	48.67	11.29
3.6 km	**Low flow**						
	2004-05 - 2004-09	3.57	0.43	-9.37	3.68	0.78[†]	27.11[†]
	High flow						
	2011-2013	-4.44	-11.47	20.31	-7.70	-1.35	15.58
	2013-2014	8.18	8.11	-11.75	2.58	-8.80	-33.01
5.5 km	**Low flow**						
	2004-05 - 2004-09	6.64	-10.17	7.18	4.81	-1.88[††]	14.17[††]
	High flow						
	2011-2013	-13.89	-0.30	16.27	2.28	-51.90	-23.34
	2013-2014	14.45	7.52	-7.43	-0.70	-11.00	0.04
eBC	**Low flow**						
	2004-05 - 2004-09	-21.52[†]	-42.27[†]	-20.78	-30.32	128.80[†]	55.34[†]
	High flow						
	2011-2013	-22.77	-30.65	20.81	-10.94	125.91[†]	73.57[†]
	2013-2014	7.09	-20.89	-21.77	-29.25	-39.77	-34.08

[†] indicates that b for one date is not statistically significant at the 95% level.
[††] indicates that b for both dates is not statistically significant at the 95% level.

In the high flow period networks, much higher, statistically significant b_{BW} coefficients and r^2 values are observed for the 3.6 and 5.5 km networks in all years and in the *eBC* reaches in 2013 and 2014 (Table 5.2), suggesting that the BI-BW_{log10} relationship may have some dependence on stage. There is a lot of variation in the relative differences in regression statistics between the different reach frameworks over each flow period (Table 5.4). The 1 km reaches will not be

considered, due to the weakness of their *BI-BW* relationships. Over the low flow period, the 3.6 and 5.5 km reaches show little change in b_{BW} and although percentage changes in r^2 values are higher, these relationships remain weak and largely insignificant (Table 5.2 & Table 5.4). Over the high flow period, all changes in b_{BW} are negative in the 3.6 and 5.5 km reaches, though these changes are larger in the 5.5 km reaches, especially between 2011-2013, which suggests the 5.5 km reach framework decouples the *BI-BW* relationship during periods of high flow (Table 5.4). Conversely, in the *eBC* reaches there is a switch to a much stronger and significant trend between 2011 and 2013, before the strength of this relationship relaxes between 2013-2014 (Figure 5.11, Table 5.2 & 5.4). A similarly large percentage increase in b_{BW} and r^2, as well as a switch to statistical significance, is seen over the low flow period in the *eBC* reaches, however b_{BW} and r^2 are very low for the 2004-05 *eBC* reaches and this relative increase does not result in strong *BI-BW* relationships.
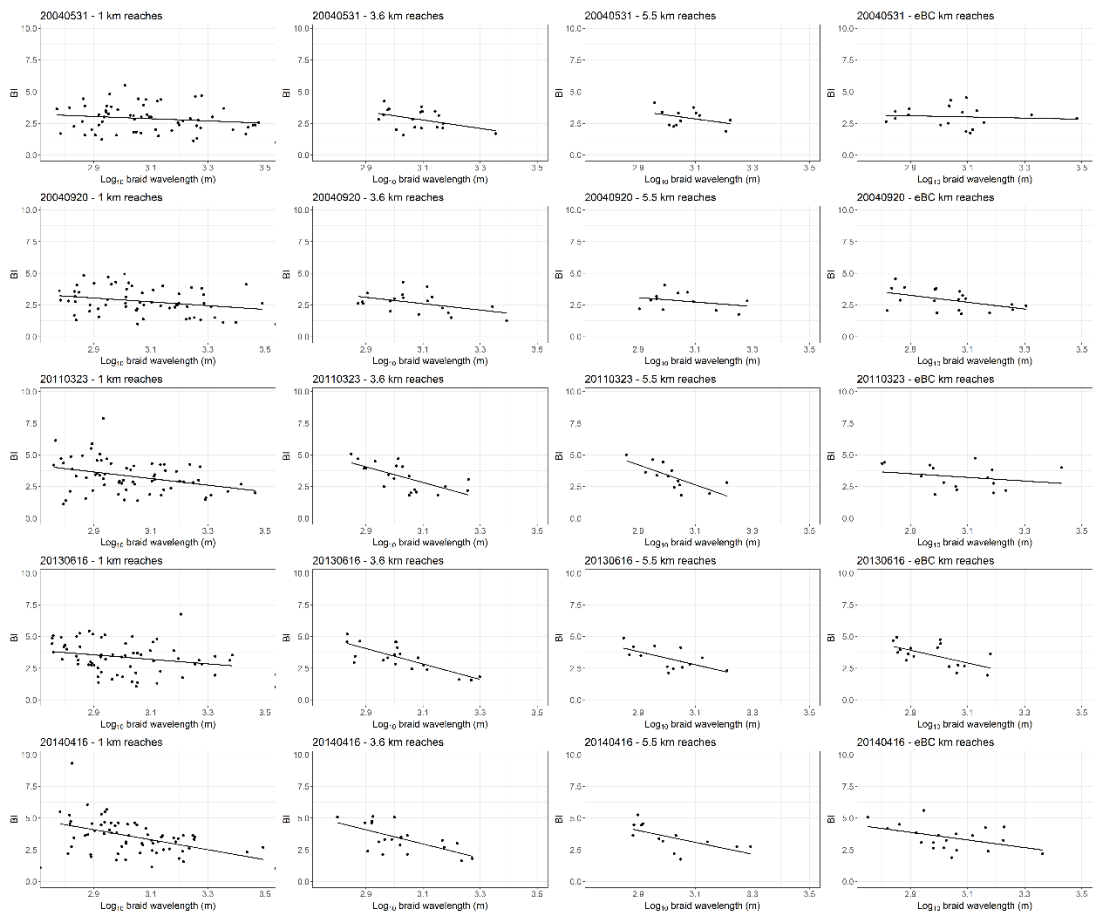
Figure 5.11: Braiding intensity (BI) Vs $\log_{10}$ braid wavelength for 4 different reach types, across both the low flow (2004) and high flow (2011-2014) periods. Trend lines fitted using linear regression.

5.4 Discussion

5.4.1 Spatial and temporal variation in BI under different reach frameworks

Regardless of reach framework, flow stage and intervening flow conditions, certain key features of the Tagliamento and their impact on braiding intensity can be identified in the longitudinal series of *BI* (Figure 5.7 & Figure 5.8). More detail on these features is provided in Chapter 1, section 1.7.3, with a summary provided here. Bedrock constraints at ~10 and 32.5 km cause decreases in braiding intensity as the channel is forced to become single-thread. From around 20 km the river enters two well studied reaches, Cornino and Flagogna. Cornino (from ~22-27 km) is a bar-braided and unconfined reach that tends to exhibit high braiding intensity. This is reflected in peaks in *BI* for all reach types at ~25 km. At the downstream end of Cornino, a large bedrock island (visible as a large patch of vegetation in the middle of the braidplain between 25-30 km in Figure 5.6a) constrains braidplain width, with concomitant decreases in braiding intensity. This island marks the transition into the Flagogna reach (~28-32 km), which terminates at Pinzano Gorge and is laterally constrained by floodplain topography and high vegetation growth. This set of controls is seen as declining *BI* through Flagogna to Pinzano Gorge (32.5 km), before the braidplain widens downstream of Pinzano and another peak in *BI* is observed between 35-45 km in all cases. Behaviour of BI downstream of this peak is then more dependent on reach type but follows a general declining trend as the river transitions to single thread (Figure 5.7 & Figure 5.8).

Whilst these key features are present in the longitudinal *BI* series for the 1 km reaches, the variation in *BI* between adjacent reaches does not appear to follow a particular pattern (Figure 5.7 & Figure 5.8). It is recommended to scale reach lengths with river size to avoid sampling *BI* over lengths that do not capture bar-scale variability in channel pattern (Egozi & Ashmore, 2008). There is a wide range of reported bar wavelength-width ratios, which largely fall in the range 5-12*B*, where *B* is channel width (Ashmore, 2009). Taking the average channel width of 95.4 m (see section 3.3), bar wavelength would be in the region of 477 to 1145 m. Due to the inaccuracies of measuring channel width from Landsat data (see Chapter 4), these values should be taken as broad estimate, or perhaps a broad underestimate, as the sample of channel networks were all captured at low flow and mean channel width is also likely to be skewed downwards by the inclusion of side and chute channels that rarely support bar formation processes. However, even using this range, a 1 km reach may sample at most two bars and

possibly less than one. The length scaling of braided river planforms provides a reasonable explanation for the large longitudinal fluctuations in *BI* seen over short distances, where a reach may be capturing a single, highly dissected complex bar or a single section of the river which is close to single thread. This problem can be visualised in Figure 5.6a, where more heavily braided sections are separated by sections with less complex planforms, both of which are often greater than 1 km in length. Whilst *BI* in the 1 km reaches shows marked longitudinal fluctuations, this pattern of downstream change in *BI* is relatively invariant across all dates in this study.

As with the 1 km reaches, the longitudinal patterns in *BI* in the physically-based reaches reflect known controls moving downstream (see above). Between these controls, the different reach frameworks show different levels of concordance and discordance in terms of the spatial position of reaches of different braiding intensity (Figure 5.7 & Figure 5.8). A general pattern is seen in concordances between *BI* in the *eBC* and 3.6 km reach longitudinal series in the low flow period and in the 2011 and 2014 networks, especially upstream of Pinzano Gorge (~32 km; Figure 5.7 & Figure 5.8). This is less surprising when considering that the mean lengths of *eBC* reaches for the 4 networks analysed in this chapter, excluding 2013, range from 3.2-3.6 km. Indeed, from the larger sample of 28 networks, the average *eBC* reach length is 3.6 km ($n = 556$, 1 SD = 1.47 km). That the mean length of the *eBC* reaches matches the length of the AWW_{2m} scaled reaches exactly is perhaps serendipitous, as the latter were derived from an assumed average wetted width at a channel forming $Q < Q_{bf}$, which was approximated as two thirds of the braidplain width, assuming that the braidplain width represents the average wetted width at Q_{bf}. However, research has shown that the length of confluence-bifurcation units scales with the width of their connecting channels (Hundey & Ashmore, 2009) and the hydraulic geometry of single braid channels conforms to the classic hydraulic geometry relationships for single-thread rivers (e.g. Leopold & Maddock Jnr 1953), such that channel width should scale with discharge. Given the *eBC* reach boundaries tend to be placed in areas where the river goes close to single-thread and thus the *eBC* reaches should incorporate a series of confluence-bifurcation units, it appears possible that the network topology is capturing the length scale of the river that results from the dominant formative discharge, e.g. flood pulses between 2-3 m stage at Venzone (Bertoldi *et al.*, 2010). This interpretation is further supported by the shift to a closer match between the *eBC* reaches and the longitudinal pattern in *BI* of the 5.5 km reaches in the 2013 network (Figure 5.8), which is also accompanied by an increase in the average *eBC* reach length to 4 km. The 2013 network is a configuration partially determined by a 1-in-10 year flood, suggesting that the network topology is responding to flow conditions, e.g. when the dominant flows causing most change in the network are $\leq Q_{bf}$, we see topological reach lengths capture

braiding intensity variations at a similar scale to 10 times AWW_{2m}. Whereas when a flood large enough to activate the whole width of the braidplain occurs, we see the topology respond by capturing variations in *BI* at lengths that scale to the total average active width of the braidplain.

5.4.2 The impact of reach framework on relationships between BI and physical controls on braiding

Certain general properties of the relationships between *BI* and physical controls are seen for all reach frameworks. The positive *BI-AW* relationships (Figure 5.10, Table 5.2) fit with previous observations of decreased braiding intensity with increases in width constriction in both natural and laboratory rivers (Fotherby, 2009; Mueller & Pitlick, 2014; Garcia Lugo *et al.*, 2015; Redolfi *et al.*, 2016). Similarly, the strong positive relationships between *BI* and *WW* follow expected behaviour, as *WW* is known to increase with increasing braiding intensity at the reach-scale (Ashmore, 2013). The presence of these relationships across a range of fixed reach lengths is indicative of the strength of control width constriction has on braided planforms and the trait of braided rivers to increase average wetted width by the addition of new channels, rather than widening of existing channels (Bertoldi, Zanoni *et al.*, 2009). It is also interesting that, whilst the trends of *BI* with physical controls are generally weaker, they are present in most networks for the *eBC* reaches, suggesting that the topology of the network preserves these essential physical controls on braiding intensity. Unlike the *BI-AW* and *BI-WW* relationships, moderate to strong relationships between *BI* and physical controls were not seen in all cases for the *BI-BW$_{log10}$* relationships. Over both the low and high flow period, the 1 km reaches showed essentially no relationship between *BI* and BW_{log10}, suggesting that at this scale, the average spacing of nodes within a reach is not related to the intensity of braiding. A likely cause for this behaviour can be visualised by looking at the positions of the 1 km reach boundaries in relation to bifurcation-confluence units. By incorporating a single bifurcation-confluence unit and two short sections of parallel channels, the reach in Figure 5.12 has a small number of channels, resulting in a low total channel length and thus a low *BW and* low *BI*. This emphasises the problems associated with choosing a reach length that does not incorporate the fundamental length scaling properties of braided rivers, such as the scaling of *BW* with the square root of discharge (Egozi & Ashmore, 2008; Ashmore, 2009). However, it was also observed that the *BI-BW$_{log10}$* relationships showed considerable temporal variability in the physically scaled and topologically defined reaches (Table 5.4).

The nature of temporal variation in the *b* coefficients and r^2 differs considerably between the fixed-distance frameworks depending on the physical control, whilst the *eBC* reaches show a

consistent pattern of greater variability in terms of both the magnitude of changes in *b* and *r²* and also differences in the direction of changes. All fixed-distance reach frameworks show small but positive change in b_{AW} over the low flow period. Based on the flood record over the low flow period (Figure 5.1a), change in the channel network over the low flow period would have occurred without interactions of the channel network with bank constraints, being caused mainly by localised sediment transport and channel abandonment at lower flows (Van Der Nat *et al.*, 2002; Bertoldi *et al.*, 2010; Welber *et al.*, 2012). This could be hypothesised to weaken the *BI-AW* relationship, however all fixed-distance reach frameworks recorded small increases in b_{AW} and retained moderate to moderately strong *r²* (Table 5.2 & Table 5.4). Conversely, the *eBC* reaches saw considerable change in b_{AW}, r^2 and a loss of statistical significance over the low flow period, which suggests that braiding intensity in these reaches may be more sensitive to other physical controls on braiding that are more important over periods of lower flow.
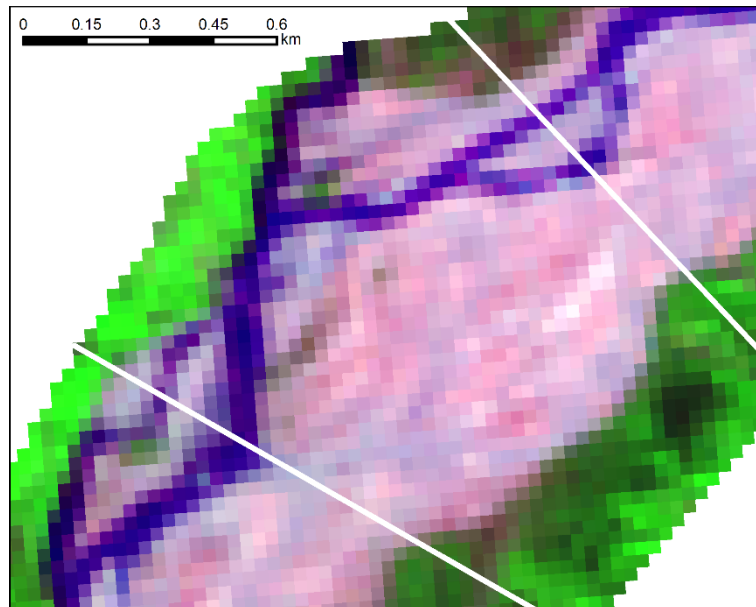
Figure 5.12: A 1 km reach (white lines indicate the reach boundaries) showing how this scale can sample bits of different morphological units, e.g. a single bifurcation confluence unit and some central bars, resulting in low braid wavelength (782 m; the mean for this network is 1403 m) and low *BI* (2).

Over the high flow period, negative differences in b_{AW} for all reach frameworks between 2011-2013 is a somewhat confounding result, given the 1-in-10 year flood that occurred in 2012. Again, the Tagliamento's flood history may provide a possible explanation of these differences. The period between 2008 and 2011 is characterised by a series of 2-3 m flood events, which would inundate the exposed gravels but not larger vegetated islands (Bertoldi, Gurnell *et al.*, 2009). The 2012 flood event peaked at 4.7 m (Figure 5.1b). On this basis, the network observed

in 2011 would be a network configuration constrained by the *AW* as measured in this study, e.g. the average width of exposed water and gravel areas, whereas the 2013 network would have been formed by a flood that would have inundated the whole braidplain and possibly some riparian areas. The resulting channel network may therefore be less constrained by the *AW* of the braidplain as defined in this study, resulting in negative b_{AW} differences. It is, therefore, potentially relevant that the larger negative differences in b_{AW} are seen for the *eBC* and 5.5 km reaches (Table 5.4), given the possible discharge related length scaling observed in the longitudinal variation in *BI* values. Support for this hypothesis of a decoupling of braiding intensity from *AW* during very high magnitude flood events can also be seen in the reversion to positive differences in b_{AW} in all reach types between 2013-2014 (Table 5.4), during which period a series of 2.1-2.7 m flow events occurred, e.g. flood magnitudes at which flow is most constrained by riparian banks and vegetated islands.

The nature of change in b_{WW} and the associated r^2 values shows more variation between reach frameworks than the *BI-AW* relationships over the low flow period. Again, the directions of change in b_{WW} provide some information about how each reach framework may be capturing change. *WW* estimates are derived from the water area in each reach and over the low flow period, there is almost no change in the area of water present in the whole network (15.9 km^2 on 2004-05 and 16 km^2 on 2004-09) and both networks have a very similar *m* (Table 5.1), which suggests that changes in *WW* will have been caused by local channel abandonment and local erosion and deposition that may change local braiding intensity but not substantially alter reach averaged *WW*. This hypothesis needs to be tested more thoroughly and would benefit from higher resolution data to derive more accurate measurements of *WW*, however it seems unlikely that the change in b_{WW} would be positive, as was observed for the 1 km and 3.6 km reaches (Table 5.2 & Table 5.4). Over the high flow period, the response of b_{WW} was more consistent between all reach frameworks, with the largest change again seen in the *eBC* reaches (Table 5.4). These responses in the *BI-WW* relationship are expected, given that both anabranch width and braiding intensity are known to scale with increased discharge (Ashmore, 2013) and thus positive followed by negative differences in b_{WW} reflect the flood magnitudes observed between 2011-2013 and 2013-2014 (Table 5.4, Figure 5.1b).

The greatest temporal change in relationships between *BI* and physical controls were seen in the *BI-BW$_{log10}$* relationships. Over the low flow period, trends are weak and largely insignificant for all reach types. This likely reflects the nature of the Tagliamento at low flow, when the network consists of sections that are more transitional between braiding and wandering

planforms due to loss of water to the river's alluvial aquifer (Henshaw *et al.*, 2013; Surian *et al.*, 2015). This behaviour fits with the known scaling relationship of *BW* with discharge (Ashmore, 2009), as the channel network at low flow is not characteristic of the channel network formed by formative discharges and thus is unlikely to replicate the node spacing that results from higher discharges. The behaviour of the *BI-BW$_{log10}$* relationships over the high flow period is particularly complex, with all reach frameworks capturing very different behaviour in response to different magnitude flood events (Figure 5.11, Table 5.2). The relatively small changes in b_{BW} over the high flow period in the 3.6 km reaches suggest that at this scale, node spacing has a fairly high strength relationship to braiding intensity that is relatively insensitive to flood magnitude across a range of formative events, though the increase and subsequent decrease in r^2 between 2011-2013 and 2013-2014 may indicate a slight effect of greater discharge on this relationship. Changes in b_{BW} in the 5.5 km and *eBC* reaches both show large changes in response to the high flows between 2011-2013, but the opposite direction change in b_{BW} somewhat confounds the suggestions that the topology of the network is changing its length scale in response to discharge. The very large change in b_{BW}, r^2 and the switch to significance of the relationship seen in the *eBC* reaches between 2011-2013 followed by a relaxation of the trend between 2013-2014 (Table 5.4) does suggest, however, that this reach framework is responding to high magnitude forcing by flood events by adjusting the spacing of nodes in relation to braiding intensity. The drivers of these changes require further investigation and should be analysed in the context of known scaling relationships between bifurcation-confluence unit length and anabranch width (Hundey & Ashmore, 2009; Kasprak *et al.*, 2015), which could serve as a check on whether a reach framework is capturing the spacing of nodes based on a more spatially variable measure of length scaling.

5.4.3 Dynamic boundaries or bounded dynamics: should reach lengths be flexible?

We have seen contrasting results in terms of the performance of the different reach frameworks in capturing longitudinal variations in braiding intensity and relationships between *BI* and physical controls. The question that stems from these results is whether the greater variability in the *BI* relationships is reflective of the *eBC* reaches not capturing key relationships between physical controls and braiding as strongly, or better capturing competing effects on braiding of an array of parameters not quantified here (e.g. stream power, grain size, sediment supply, channel slope etc.). More detailed analysis of local planform change is required to assess whether change in the lengths of the *eBC* reaches over the low flow period (Figure 5.5a) is a

response to small scale morphological change resulting from the few competent flood events over this period, or if it is an effect of stage variation and channel abandonment. However, the relatively static positions of reach boundaries between the 2004-05 and 2004-09 networks (Figure 5.4) indicates that the topological reach framework is not that sensitive to stage variation or low-level morphological change. Over the high flow period there is a much clearer response in both the lengths and position of the *eBC* reach boundaries to floods of varying magnitude (Figure 5.5b & Figure 5.4) that further supports the argument that the network topology is varying its length scale depending on flood magnitude and that, perhaps, reach lengths should vary depending on flow conditions. It is also apparent from the relatively static locations of certain *eBC* reach boundaries (e.g. at 16 km, 27.5 km, 32.5 km and 45 km; Figure 5.4) across both the low and high flow periods that a local control is forcing a change in braiding intensity at these points, which is picked up as a change in *eBC* and thus a reach boundary. Further analysis of the spatio-temporal variability in *eBC* (presented in Chapter 6) has shown these locations are "hinge points" in the network from which change in planform dynamics over the ensuing 5-10 km tends to be observed. Notably, downstream of these hinge points tend to be areas of more dynamic length changes in the *eBC* reaches (Figure 5.4).

The changing length of the *eBC* reaches and some of the resultant reach lengths and boundary positions do highlight some potential issues with the topological reach framework (Figure 5.3 & Figure 5.4). Certain reaches, e.g. reach 6 in the 2014 networks, are erroneously short (Figure 5.4), and overlap in the nodes and edges that are grouped into each reach can cause problems in reach boundary placement (Figure 5.3). The application of the *edge betweenness clustering* algorithm was done on an unweighted graph in this study, e.g. a graph that does not account for any physical properties of the channel network. Detailed analysis of the spatial distribution of *eBC* in Chapter 6 has revealed that the most central pathway through the network often tracks secondary channels. It is these channels that are "cut" by the clustering algorithm. These secondary channels do not drive variability in braiding intensity and are unlikely to participate strongly in setting the dominant length scale of bifurcation-confluence units, which has been shown to be related to the width of the main channels (Hundey & Ashmore, 2009). As such, weighting the network using channel width may improve the performance of the topological reach framework. This raises its own set of challenges due to the accuracy of width estimates using data of medium spatial resolution, e.g. the Landsat data used in this study, on a river where channels vary from around the width of single pixel to a few pixels (see Chapter 4). However, a more accurate variable length reach framework may address a potentially fundamental flaw in even a fixed-distance reach framework scaled on *AWW*; namely that braided river planform and

morphology has been shown to be fundamentally affected by width constriction (Garcia Lugo *et al.*, 2015; Redolfi *et al.*, 2016). Given that the braidplain width and thus AWW_{BF} of the networks analysed in this chapter had coefficients of variation between 37-40%, there is clearly significant longitudinal width variation that is going to locally impact planform change and thus also impact the validity of a reach length scaled on average width.

5.5 Conclusion

It is apparent that the 1 km reach framework introduces erroneous fluctuations into measures of braiding intensity. These results are not surprising, given the bar-wavelength of the Tagliamento is likely to be at least 0.5 km and braiding intensity in these reaches will be heavily affected by bar-scale variability in braiding processes. Furthermore, the 1 km reaches do not capture the *BI-BW* relationship seen in longer reaches regardless of a network's *m* and assumed stage or intervening flow conditions, further indicating that the 1 km reaches are decoupled from the length scale of the network. The moderate to strong *BI-AW* and *BI-WW* relationships seen in the 1 km reaches suggests that these controls on braiding are relevant even at small scales that do not adequately represent changes in braiding intensity. Stronger relationships seen in the physically scaled reaches suggest that these frameworks better capture the effects of physical controls on braiding.

Of all the reach frameworks, *BI* in the physically scaled reaches show the strongest relationships with physical controls, whereas the topological reach framework shows generally the weakest relationships between *BI* and physical controls. It is notable, however, that the topology of the network does result in reaches that still capture these essential physical controls on braiding intensity. Where the topological reaches differ markedly from the fixed-distance reach frameworks is in the temporal response to floods of varying magnitude. The *eBC* reaches show the largest fluctuations in the magnitude, e.g. the *b* coefficients of linear regression relationships, and in the strength, e.g. r^2, of the *BI*-physical control relationships. Over the high flow period, the *eBC* reaches match the general patterns in the direction of change in *b* for the fixed-distance frameworks in the *BI-AW* and *BI-WW* relationships. Changes in *b* coefficients over the high flow period have plausible physical mechanisms, e.g. a weakening of *AW* control due to the size of the 1-in-10 year flood in 2012 and the widening of channels due to greater discharge, with an associated effect on the *BI-WW* relationships. That the *eBC* reaches show the largest changes in *b* and r^2 in response to different magnitude flood events suggests that this reach framework is potentially more sensitive to changes in discharge. This conclusion is also

supported by the *eBC* reaches showing notable weakening of the *BI-AW* and *BI-WW* relationships over the low flow period, which fits the probable response of braiding intensity over a period where change in the channel network would have seen little interaction with width constraint and very little change in the total wetted area of the channel network was observed. However, the generally weaker relationships in the *BI*-physical control relationships may also point to the role of other controls. Further testing with a broader suite of physical controls is necessary to truly evaluate how different reach frameworks capture controls on braiding.

To the authors knowledge, the negative *BI-BW$_{log10}$* relationship reported herein is the first evidence linking variability in node spacing within the network to braiding intensity. For all reach frameworks, this negative relationship was seen mainly in the high flow period networks, which relates to the many transitional sections of the Tagliamento at low flow that exhibit wandering planforms and thus decouple node spacing and *BI*. It is not clear whether the *BI- BW$_{log10}$* relationship shows systematic responses to floods at different reach scales. Highly variable behaviour of the *BI-BW$_{log10}$* relationship over the high flow period in the physically based and topological reach frameworks indicates that this relationship needs to be tested further under a range of different flow conditions. It also suggests that braiding intensity as a function of average node spacing has some dependence on the length of the sampling window.

In the case of the *eBC* reaches, the lengths of the sampling windows show a more consistent response to discharge. It appears that the topology of the network responds to higher magnitude flood events by increasing the average length of clusters of nodes and edges that are less well connected to the rest of the network, and that these clusters tend to correspond to areas of the river with different magnitudes of braiding intensity. This is observed in the shifting longitudinal positions of reaches of varying braiding intensity under the *eBC* reach framework. Noting that the 5.5 km reaches are scaled on *AWW$_{bf}$*, it is intriguing that the shifts in the longitudinal pattern of *BI* move to more closely match *BI* in the 5.5 km reaches after a series of bankfull or larger floods and otherwise *eBC* reach *BI* tends to track patterns in *BI* in the 3.6 km reaches, ergo the reach length scaled on the more frequently occurring 2 m flow stage. It is also apparent that, whilst the *eBC* reach lengths and their associated boundary positions are variable, certain *eBC* reach boundaries are located in approximately the same positions in all networks, regardless of intervening flow conditions, showing that the topological reach framework captures fixed controls on braided planforms.

In summary, results from this chapter have highlighted that arbitrarily defined reach lengths, especially those that are short relative to the average width of a braided river's braidplain, are

unlikely to accurately capture the structure or dynamics of braided planforms. It seems that at the bare minimum, a reach length based on some consideration of the *AWW* over the last formative flow events should be chosen. This study has provided further evidence to suggest that reach lengths should actually be flexible, both over the course of a river at a single point in time and over time. The *edge betweenness clustering* algorithm provides an objective method for defining reach lengths. Further testing is now required to assess whether the behaviour of this algorithm is maintained over larger samples, on different rivers and if it improves with network weighting.

6. Beyond the reach: flood driven responses in braided river network structure and behaviour at multiple scales

Chapter synopsis

The complexities of braided river morphodynamics and the rapidity and magnitude of flood driven changes to braided river morphologies present significant barriers to their study. Satellite remote sensing may provide a solution to the difficulties of sampling braided river planforms and morphology over representative time and space scales, however we lack an analytical framework that is capable of maximising the information that can be extracted from network-scale analysis of braided rivers. This chapter presents a multi-spatial and multi-temporal analysis of planform evolution on the Fiume Tagliamento, using a spatially distributed measure of channel connectivity: *edge betweenness centrality* (*eBC*). It is shown that consistent, large-scale patterns of *eBC* and the temporal dynamics of these patterns can highlight planform change linked to varying magnitudes of flood event in a manner that would not be detected by traditional methods of planform analysis. Furthermore, "hinge points" from which planform change originates are seen to provide static loci of control over downstream morphodynamics at scales of up to 10 km. Analysis of two novel, global scale metrics of network structure and sinuosity are also presented. These metrics may provide a new means to classify different types of braided river and are related to each other in a manner that suggests changes in the network structure may be linked to changes in the sinuosity of highly connected, high *eBC* channels.

6.1 Introduction

Quantitative understanding of braiding in rivers has developed from the first empirical relationships between slope and discharge that discriminate between meandering and braided channels (Leopold & Wolman, 1957) to an advanced knowledge of the controls on the emergence and evolution of braiding. Discriminant functions have been proposed to explain transitions from single-thread to braided planforms based on thresholds of stream power (van den Berg, 1995; Kleinhans & van den Berg, 2011) and sediment supply (Mueller & Pitlick, 2014), though these thresholds tend to be somewhat fuzzy. Stream power and sediment supply combine at the bar-scale, resulting in erosion, deposition and core "mechanisms" that result in braiding (Ashmore, 1991b; Wheaton *et al.*, 2013). Instabilities in the geometries of bifurcations and confluences (Federici & Paola, 2003; Bertoldi & Tubino, 2007; Szupiany *et al.*, 2009; Marra

et al., 2014) and the migratory nature of sediment transport (Egozi & Ashmore, 2009) change the spatial distribution of erosion and deposition, resulting in the highly dynamic nature of braided rivers. Furthermore, in rivers where vegetation can establish in the braidplain, it has been shown to significantly affect braided morphologies (Kollmann *et al.*, 1999; Gurnell *et al.*, 2001; Zanoni *et al.*, 2008; Corenblit *et al.*, 2014; Mardhiah *et al.*, 2015). However, despite a well-developed understanding of the myriad controls on braiding, our capacity to predict the morphological evolution of braided rivers is still limited.

The complexities of braided river morphodynamics are compounded by the rapidity of change under certain forcings (Ashmore, 2013). Whilst physical and numerical models have shown discharge variability is not a prerequisite of braiding (Ashmore, 1991a; Murray & Paola, 1994), in most natural systems floods are the dominant driver of morphological change over short time-scales (Belletti *et al.*, 2015). Instantaneous morphological activity, e.g. the number of active channel branches, depends on stream power, which is itself dependent on discharge and slope (Bertoldi, Zanoni *et al.*, 2009). Thus, sediment transport and morphological activity will increase over the course of a flood event. Discharge fluctuations also impact the division of discharge at bifurcations, which tend to an asymmetrical discharge distribution at lower flows, becoming more symmetrical as flow increases (Kleinhans *et al.*, 2013). This change in the discharge distribution at a bifurcation will in turn affect stream power in the respective channel branches and thus change wider patterns of erosion and deposition. Greater change in erosion, deposition and sediment transport around the network also results in the migration of bars and evolution of bed morphologies that change the geometries of bifurcations and confluences (Bertoldi & Tubino, 2007; Ashworth *et al.*, 2011), further impacting the morphodynamics of braided rivers under high flows. It follows that the morphology left by previous formative events, combined with other factors such as changes to sediment supply, will affect the response of the network to further forcing by flood flows. The result is a system whose evolution is conditioned by both its memory of past events and instantaneous changes to morphodynamic processes.

With morphological evolution of braided rivers dependent on both antecedent conditions and present dynamics in response to discharge variation, capturing the complex, flood driven responses is a considerable challenge. The scale of morphological change to flood events is dependent on the event magnitude and can be widespread for higher flood magnitudes (Bertoldi, Gurnell *et al.*, 2009). This presents limitations for studying responses to flooding in the field, due to the practicalities of sampling over large spatial scales and the requirement for

repeat sampling. Physical models are limited by scaling considerations relative to the size of the modelling facility and can thus represent reach-scales at best (Young & Warburton, 1996). And numerical models are now capable of simulations at spatio-temporal scales relevant to flood mediated channel network evolution (Ziliani *et al.*, 2013; Schuurman *et al.*, 2016), but are limited by our capacity to validate their outputs and morphodynamic behaviours, especially at larger scales. The recent upsurge in the availability of satellite remote sensing data, e.g. the Landsat (Woodcock *et al.*, 2008) and Sentinel (Berger *et al.*, 2012) missions, may provide a possible solution to these problems. These datasets have spatial resolutions that allow analysis of 2-D braided river evolution at spatial scales ranging from single bifurcations to the whole network and, in the case of Landsat, have temporal depth that facilitates analysis of braided river evolution over multiple formative discharge events. Research has shown the potential of satellite-based approaches for studying braided rivers (Takagi *et al.*, 2007; Bertoldi, Drake *et al.*, 2011; Henshaw *et al.*, 2013; Marra *et al.*, 2013), but, with the exception of Marra *et al.*, these studies have lacked an analytical framework that facilitates analysis of the highly heterogeneous changes observed in braided river planforms over time.

Some previous research has used a graph framework to analyse bulk structural properties (Howard *et al.*, 1970; Webb, 1995) or reach-average connectivity in braided river networks (Lehotský *et al.*, 2018). However, the work by Marra *et al*. (2013) was the first detailed application of graph theory to braided river planform analysis. They derived the channel network of the Jamuna river, Bangladesh and analysed it using *betweenness centrality (BC)*, which measures the importance of a single node (bifurcation or confluence) or edge (channel) within the network based on how well connected it is to other nodes or edges in the network. *BC* operates on the concept of shortest paths and assumes that nodes or edges that are on lots of shortest paths between other node pairs are central to the network and thus more important. Marra *et al*. (2013) applied a weighted version of *BC*, using a ratio of width and length as a proxy for discharge and channel slope. They found that most networks were dominated by a highly central (high weighted *BC*) pathway that was associated with the network's main channel and was largely invariant in its spatial position within the network through some reaches, but much more dynamic in others. However, their analysis focussed mainly on global properties of the network and not on the local changes that are important for understanding how and when morphodynamic changes may occur in braided rivers. Furthermore, their time series of networks was relatively short and did not include a range of flood events that could induce different magnitudes of morphological change within the network.

To the authors knowledge, no previous research has analysed BC across a series of networks for a single river spanning a period longer than a decade and encompassing a range of formative flow events that are known to cause different magnitudes of morphological change. Furthermore, Marra *et al's.* (2013) previous application of BC to the Jamuna River did not assess what information the unweighted version of BC may be able to extract from the network. Weighted networks account for the fact that the simple existence of a connection between nodes may not sufficiently represent the nature of this connection (Barthélemy, 2011). As an example, a small chute channel across an alternate bar will have lower discharge and sediment transport capacity than the larger channel it has branched from, and thus an equal representation of the connections of these channels to their downstream nodes may do the larger channel a disservice in terms of its morphodynamic importance. However, an alternative view could look at the unweighted topology of the network as the imprint of self-organisation that results from complex interactions between the manifold processes that drive braided river morphodynamics. Thus, there may be intrinsic value to analysis of the unweighted network topology that captures the evolution of the network as a product of combined braiding processes. Furthermore, issues associated with spatial resolution and the extraction of channel width from medium sized braided rivers using Landsat imagery (see chapter 4) preclude accurate network weighting of rivers such as the Tagliamento with the present datasets. As such, this study has applied analysis of unweighted BC to 14 instances of the Fiume Tagliamento's braided channel network captured over an 18-year period.

The study period encompasses a wide range of flood events with pairs of networks separated by little to no significant flow activity up to separation by 1-in-10-year floods. The aim of this study is to assess the extent to which metrics derived from the unweighted topology of a braided river network can be used to describe planform changes at multiple spatial scales in response to varying magnitudes of formative flood events. It is hypothesised that 1) the unweighted topology will provide meaningful data on planform change that is more detailed than data derived from standard methods of planform analysis, e.g. braiding indices; 2) these data will also show a response to flooding that will increase in size with increasing flood magnitude. As well as analysis of the spatially distributed nature of BC, two novel metrics are applied to the network-scale characterisation of the Tagliamento. These metrics measure global network structure, E_{glob}, and the sinuosity of the most central (high BC) pathway through the network (CPS). They are hypothesised to show signatures of flood disturbance, with networks becoming temporarily less efficient (lower E_{glob}) and developing more sinuous central pathways (higher CPS) after higher magnitude flood events due to enhanced bank erosion and subsequent

sediment deposition and associated channel branching. As *BC* and the global metrics measure changes in planform configuration and traditional methods of planform analysis in braided rivers are prone to significant dependence on stage (Egozi & Ashmore, 2008), an assessment of possible stage dependence of these new metrics is conducted. It is shown that the graph metrics applied in this study have less stage dependence than traditional braiding indices. Responses of *BC* to varying levels of flood disturbance highlight changes in braided river planforms across multiple spatial scales and also identify locations within the network that may act as control points on the evolution of planform over distances up to 10 km downstream. Analysis of change over time and relationships between the global metrics show that they are responsive to forcing by flood events and indicate that changes to the sinuosity of highly central channels (*CPS*) may be related to variation in the global network structure (E_{glob}).

6.2 Methods

6.2.1 Hydrological conditions and network selection

Selection of different instances of the Tagliamento's braided channel network has been guided by analysis of the rivers flood record over a period ~20 years. Figure 6.1 presents the record of daily maximum stage from the Venzone hydrometer. As discussed in chapter 1, no accurate stage-discharge relationship has been derived for the Tagliamento, however previous analyses have indicated certain stage thresholds at which different magnitudes of morphological change are likely to occur. The earliest network analysed in this study was captured on 1996-11-24, which is slightly after the largest flood within the whole studied record (Figure 6.1), when stage peaked at 5 m on 1996-11-14. Figure 6.1 shows that 1996 was a year of hydrological extremes, with a second flood exceeding 4 m in June. As such, the network captured on 1996-11-24 should represent a point from which further change is occurring in the context of an extensively reworked, or "reset", morphology.

A total of 14 networks have been selected for analysis, covering a period of 18 years. These 14 networks were subdivided into groups representing sequences of networks separated by flows of different magnitudes. The flows separating the different dates are separated into four groups, based on the thresholds for different magnitudes of change detailed above: 1) no stage > 2 m, representing flows where only local morphological changes are expected; 2) stage between 2-3 m, representing flows where more widespread morphological changes are expected to occur; 3) bankfull floods, stage ≈3 m and capable of causing significant

reorganisation of morphology and planform; 4) stage >> 3 m, representing floods with 10 year return periods or greater. Table 6.1 details dates when the studied networks were captured, the intervening flow conditions and the number of edges (*m*) in each network. The latter is taken as a proxy for stage, as all networks within this study were captured at close to baseflow conditions when the stage record at Venzone does not correspond well with the stage or discharge that is visibly present in a Landsat scene. Where possible, networks have been paired to minimise the difference in *m*, as differences in *m* will affect the spatial distribution of *BC* when channels are abandoned at lower flows and the potential pathways are consolidated amongst fewer channels.
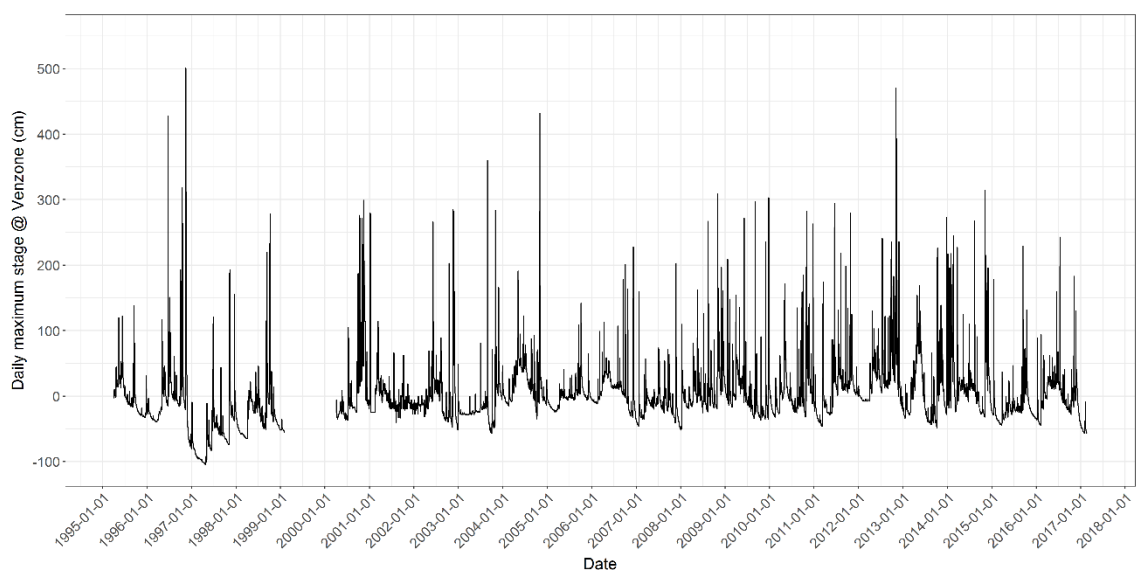
Figure 6.1: Long-term daily maximum stage record from the Venzone gauging station on the River Tagliamento. Note that negative values are negative relative to a local datum and can be taken as stage indicative of baseflow.

6.2.2 Graph extraction

The analysis described herein requires the extraction of network graphs braided channel networks. These graphs are extracted from a single, multi-spectral remote sensing image. A full description of the workflows required to derive braided river network graphs from remotely sensed imagery is provided in chapter 4 of this thesis. A synopsis of the processing will be provided here. The first stage is to classify the input image to isolate the landcovers of interest, which in the present case are water (river channels), bare gravel and vegetation. Landcover classification and image analysis of remotely sensed imagery is an extensive topic and interested readers are directed to Lillesand *et al*. (2008) and Lu & Weng (2007) for thorough overviews. Object-based image analysis (OBIA) is increasingly being used in landcover classification studies

and is generally regarded as providing improvements in classification accuracy over traditional, per-pixel classification methods (Blaschke *et al.*, 2014). In the present study, landcovers of interest were classified using an OBIA approach applied to multi-spectral Landsat imagery. The OBIA classification routines developed for this study have the advantage of being very quick to apply once developed, allowing ready classification of a large catalogue of Landsat images of the River Tagliamento spanning ~20 years and multiple flood events.

Table 6.1: Network pairs and intervening flow conditions. *m* is the number edges (channels) in the network and is taken as rough proxy for stage when the network was captured.

Date	*m*	Flow group (between paired dates)	Intervening flow events between date pairs	
			Date	*Stage (m)*
1996-11-24	701	< 2 m	Jun 1996	1.21
1997-06-29	781			
1997-11-20	411	< 2 m	Nov 1997	1.88, 1.93
1998-05-15	393	< 2 m	Dec 1997	1.55
1998-10-22	585	2-3 m	Sept 1998, Oct 1998	2.2, 2.79
2003-09-02	583	2-3 m	Nov 2003, May 2004	2.84, 1.91
2004-05-31	658			
2004-09-20	619	< 2 m	Jun 2006	1.23
2004-11-07	782	>> 3 m	Oct 2004	4.32
2005-05-25	502	< 2 m	Oct 2005, Apr 2006	1.42, 1.13
2006-05-12	530			
2011-03-23	853	>> 3 m	Jun 2011, Oct 2011, Nov 2012	2.94, 2.8, 4.71
2013-06-16	881	2-3 m	6 events	Max stage = 2.73
2014-04-16	894			

The output from the landcover classification process is a raster map, where each cell of the raster has an integer code that refers to one of the three landcovers of interest. Isolating the raster cells classified as the channel network results in a binary mask of the channel network, where all cells classified as water have the value 1 (or another non-negative integer value) and all non-water cells are classified with a value of 0. This binary channel mask serves as input to automatic vectorisation using the ArcScan toolbar within ArcGIS. Automatic vectorisation using ArcScan traces the centrelines of the contiguous raster channel network, providing a rapid tool for extraction of network skeletons from classified Landsat or other remotely sensed data. The

network skeletons extracted from the channel network masks are not free from artefacts, which require some manual cleaning. Directions of the centrelines also need to be correctly set, otherwise network connectivity will be misrepresented. By deriving the connectivity of the original, "misdirected" network, rules were applied to largely correct the direction of channels, e.g. so water flows downstream along edges. In some cases these rules did not apply and some manual correction of edge direction was necessary. The final processing step is to delete overwide channels, the majority of which are created at large anabranch junctions where multiple anabranches meet. These anabranch junctions create an enlarged area of water that is treated like a very short and wide channel by the automatic vectorisation process. Overwide channels were found and removed automatically, with the resulting gap in the network filled by snapping together the ends of the channels that connected to the deleted channel. Following a final visual check to ensure no gaps had been left by the snapping procedure, the channel network skeleton was converted to the ArcGIS Coverage data format (ESRI Inc., 2016). This format captures the networks connectivity within the resulting feature attribute table, from which it can exported as an "edge list"; a list that states which nodes (bifurcations or confluences) an edge (channel) connects from and to, which in turn forms the basis of building network graphs. Full details of the workflow summarised here can be found in chapter 4, section 3.2.

6.2.3 Computing, normalising and mapping betweenness centrality

The edge lists extracted from channel network skeletons were used as input to graph analysis using betweenness centrality. Graph models of 28 instances of the River Tagliamento's braided channel network were created using the *igraph* package (Csárdi & Nepusz, 2006) within the R programming environment (R Core Team, 2017). 14 of these graphs were chosen for in-depth analysis in this chapter (see above). The graph models are used as input to *igraph* functions for computing betweenness centrality (*BC*; see chapter 3, section 3.1.2. for a full description of this metric and how it is calculated). These functions have been implemented for computing unweighted and weighted node betweenness centrality (*nBC*; Freeman 1977) and it's generalisation to edges (*eBC*; Girvan & Newman 2002). These algorithms calculate, in the case of *nBC*, the sum of the number of shortest paths between a pair of nodes *h, j* that cross node *i* and, in the case of *eBC*, the number of these paths that traverse edge *e*. The higher the value of betweenness for *i* or *e*, the more well connected and likely central to the network this node or edge will be. As stated above, the focus of this research is on previously unassessed spatial patterns of unweighted *BC*.

The raw *BC* values for the network graphs of the Tagliamento range by orders of magnitude and will also clearly be much higher for nodes and edges that are, longitudinally, in the "middle" of the network, as these network elements will by default be on the highest number of shortest paths between nodes that are upstream and downstream. As a consequence, nodes and edges at the upstream and downstream ends of the network that lie on many shortest paths between network elements in other areas of the network will have proportionally much lower *BC*, despite being as important from a connectivity perspective as the nodes in the geographical middle of the network. As such, a normalisation proposed by Marra *et al.* (2013) was applied to the raw *BC* values. *BC* was normalised by the product of the number of nodes upstream and downstream of *i* or *e*

$$nnBC_i|neBC_e = \frac{nBC_i|eBC_e}{(N-i)(i-1)} \qquad (6.1)$$

where *nnBC$_i$|neBC$_e$* is the normalised *BC* for node *i* or edge *e*, *nBC$_i$|eBC$_e$* is the raw node or edge *BC* value for node *i* or edge *e* and *N* is the total number of nodes in the network. This equation assumes that all nodes with an index > *i* are downstream and all nodes with an index < *i* are upstream or *vice versa,* if, as was the case in the present study, node indices are automatically created and decrease in a downstream direction. The denominator should provide a potential maximum for *BC* under the assumption that (*N* - *i*)(*i* - 1) represents the maximum *BC* if *i*|*e* were on all shortest paths between its upstream and downstream nodes (Marra *et al.*, 2013). This assumption should mean *nnBC* and *neBC* values are in the range 0-1, however due to the irregular layout of braided river networks, there are some rare cases where nodes or edges with high raw *BC* values have an associated *i* that is lower than its relative position in the network. In these cases, the *nnBC* or *neBC* value can be > 1. Where this problem was encountered, these nodes or edges were given a value of the 99th percentile of *nnBC* or *neBC*, which assumes that these nodes or edges had a very high raw *BC* value and thus must be highly central to the network. A visual check of the position of a number of nodes and edges with *nnBC* or *neBC* > 1 confirmed this to be a fair assumption. Once *nnBC* or *neBC* has been calculated for the *N* nodes or *m* edges in each network, these data can be mapped back onto nodes and edges to allow analysis of the spatial patterns *nnBC* or *neBC* throughout the network. This mapping was performed in ArcGIS. The focus of this chapter is on patterns of *neBC*, which can be mapped onto edges by simply joining the *neBC* values to the network skeleton features from which the edge list was extracted using unique edge IDs that have been preserved through the previous processing steps.

6.2.4 Global metrics of network structure and sinuosity

Two novel metrics for the network-scale classification of braided river structure and sinuosity are proposed in this chapter. The metric of sinuosity measures the sinuosity of the most central pathway, the contiguous pathway of high $neBC$ channels that is observed as a key feature of all networks studied in this research. Sinuosity of river channels is a key parameter that is linked to channel slope and thus stream power (Knighton, 1998). Central path sinuosity (CPS) is defined here after Friend and Sinha (1993), who define sinuosity in multi-thread rivers as L_{cmax}/L_R, where L_{cmax} is the length of main channel and L_R is a reach length. In the present study, L_{cmax} is defined as the length of the contiguous most central pathway of high $neBC$ channels and L_R is the length of the braided Tagliamento (72 km). To isolate the central pathway, all channels within the top two quintiles of the range of $neBC$ for a given network were selected. This resulted in a near contiguous pathway through the network, though in places this pathway is broken where channels with lower $neBC$ divide around central bars, thus halving the $neBC$ in the bifurcates. In these cases, one of the bifurcates was manually selected, alternating between the left and right bifurcate at successive bifurcations to maintain an objective selection of channels in the central pathway.

A second global metric quantifying network structure, *global efficiency* (E_{glob}), has also been applied. Like metrics of centrality, E_{glob} is also based on the concept of shortest paths, however it differs from centrality metrics by describing the average inverse shortest path length of the whole network (Latora & Marchiori, 2001), as opposed to the connectedness of single networks elements. The full derivation of E_{glob} is provided in chapter 3, section 3.3.2.1 and a brief description of its interpretation is provided here. As E_{glob} increases, it shows that it takes on average fewer hops to traverse between pairs of nodes (e.g. the average shortest path length of the network is decreasing) and thus nodes are, on average, better connected. E_{glob} is applied here to assess it's potential to show a signal of channel network reorganisation in response to flood events.

For the purposes of timeseries analysis of *CPS* and E_{glob}, it was also necessary to assess their dependence on *m* as a proxy for stage. As a further check on possible stage dependence of these metrics, they were also compared to a channel count braiding index (*BI*) for the whole network, due to the known sensitivity of *BI* to stage at low flows on the Tagliamento (Welber *et al.*, 2012). Linear regression shows that *m* and *BI* have a very strong linear relationship ($r^2 = 0.95$, $p = < 0.0001$). Analysis found weak and insignificant relationships between *CPS* with *m* and *BI*

(*m*-CPS: r^2 = 0.22, *p* = > 0.05; *BI*-CPS: r^2 = 0.12, *p* = > 0.05). This indicates *CPS* may be stage-independent and that comparisons between networks with different numbers of channels should be valid. Regression analysis of E_{glob} with *m* and *BI* suggests that E_{glob} may show some dependence on stage, with moderate and significant E_{glob}-*m* relationship (r^2 = 0.49, *p* = 0.003), but a weak and insignificant (r^2 = 0.37, *p* = > 0.05) E_{glob}-*BI* relationship. The relatively low r^2 value for the E_{glob}-*m* relationship suggests that comparisons of E_{glob} between networks with different *m* will not be invalid but should be treated with caution.

6.3 Results

The following results show patterns observed in the spatial distribution of *neBC* seen across multiple instances of the River Tagliamento that are separated by a range of flow conditions. The results are described in terms of purely spatial patterns in *neBC*, e.g. patterns in the longitudinal variability of *neBC* that are present in all instances of the channel network, and in terms of the temporal variability of these spatial patterns. Both spatial and spatio-temporal patterns are broken down further to describe patterns that are observed at the scale of the network, global patterns, and patterns of *neBC* that show variation at scales that are analogous to the reach scale, local patterns, though without an explicit spatial framework used to define local scale change. Finally, analysis of temporal variability in novel descriptors of channel network structure and physical properties provides a first assessment of the potential of graph theory-based approaches to the characterisation of braided river networks, at the scale of the whole channel network.

6.3.1 Spatial patterns in neBC across multiple scales

6.3.1.1 Global spatial patterns

Figures 6.2-6.5 show *neBC* mapped to the 14 different instances of the braided Tagliamento analysed in this study. In all networks, there is a clear central pathway (*neBC* > 0.45) along the length of the river. These pathways are largely contiguous in all networks, though are not static in terms of their positions within the braidplain. There is a general pattern of the central pathway migrating from one side of the braidplain to the other in a downstream direction, almost as if in attenuated meanders. These migrations are most pronounced in areas where the braidplain widens, e.g. between 20-30 km and over ~20 km downstream of Pinzano Gorge (32.5 km). However, within this broad positional pattern of the most central pathway, the pathway is quite sinuous (Figure 6.2-6.5). The presence of such a well-defined central pathway in the

unweighted *neBC* data for each network begs the question of whether these central channels have particular characteristics?

Visual analysis of Landsat imagery reveals that the channels being tracked by the central pathway are, in general, side channels (Figure 6.6). For all dates, these side channels often appear as chute or avulsion channels that bypass areas of more complex channel branching and bar dissection. In bypassing the more complex areas of planform, these side channels provide more direct routes through the network and thus are on more shortest paths between their upstream and downstream nodes. Routing of the central pathway through side channels also results in these channels having a physical signature. Figure 6.7 shows that channels on the central pathway (CP channels) tend to be longer, with greater medians and interquartile ranges in all cases. This length pattern was observed across the range of *m* for the 14 networks in this study, suggesting that CP channels are, on average, longer than the non-CP channels, regardless of stage. The same analysis was also applied to channel straightness (or sinuosity), which calculated as the ratio between the Euclidean distance between a pair of nodes and the length of their connecting edge. Thus, as this metric tends to 1, channels are increasingly straight. Stage independence is less apparent in the straightness of channels, with the difference in the range of straightness between the CP and non-CP channels increasing slightly with increasing *m*. However, with the exception of the 1998-05-15 network (*m* = 393), the other networks in Figure 6.7 indicate that CP channels are slightly more sinuous than non-CP channels across a range of *m* and thus assumed stage.

Whilst the pattern of the central pathway tracking secondary channels is the dominant pattern across the studied networks, it is not always the case. Exceptions tend to be seen in two distinct planform styles. The first is where planform is not dominated by a single main channel, instead being characterised by two approximately equally sized parallel channels with a central pathway tracking the least branched of the two channels (Figure 6.8a). The second is seen in networks where the main channel goes close to single-thread, with these sections of the main channel also being the central path (Figure 6.8b). These patterns are largely seen in the lower *m* networks, which suggests that local deviations from the global pattern of high *neBC* can be stage-dependent. The other key control that forces the central pathway to track the main channel in all networks are the bedrock constraints at 10 and 32 km, which force the river into a single-thread channel with very high *neBC*.
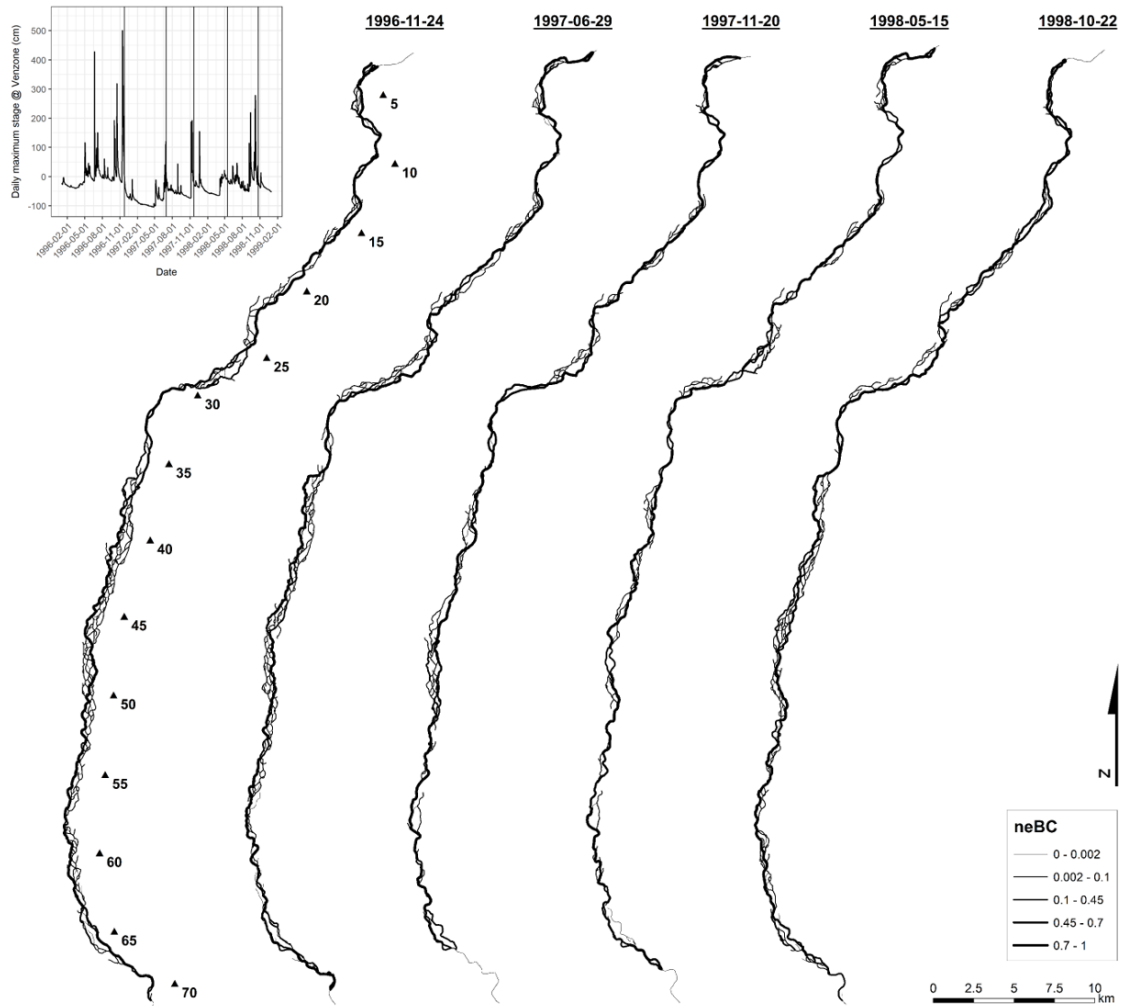
Figure 6.2: *neBC* mapped to the braided channel network of the River Tagliamento under variable flow conditions between 1996-11-24 and 1998-10-22. Markers against the left-most network show 5 km intervals. The inset hydrograph shows stage variation at the Venzone gauging station between 1996-1998. Vertical lines on the hydrograph show dates of the networks in the main figure.
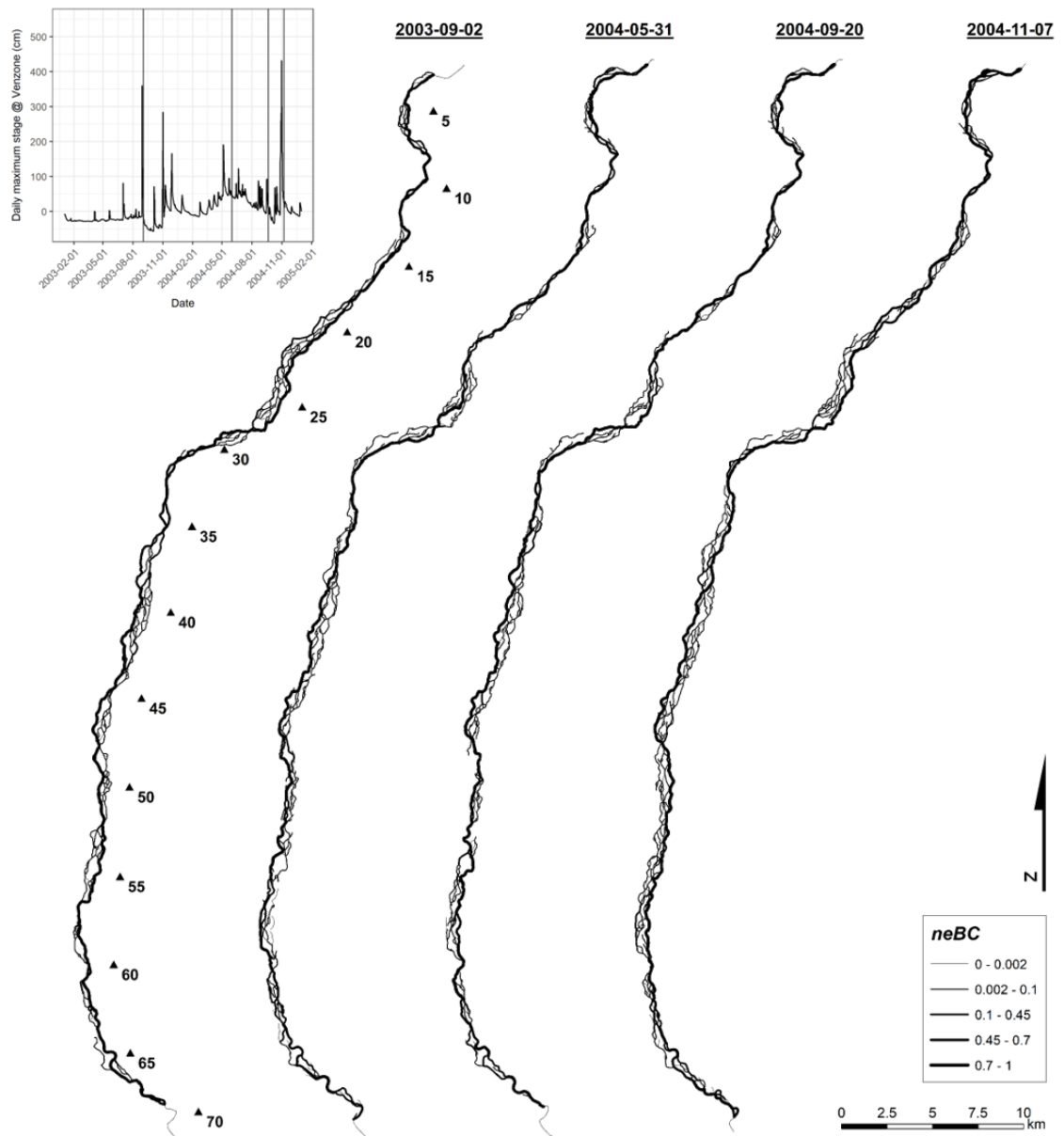
Figure 6.3: *neBC* mapped to the braided channel network of the River Tagliamento under variable flow conditions between 2003-09-02 and 2004-11-07. Markers against the left-most network show 5 km intervals. The inset hydrograph shows stage variation at the Venzone gauging station between 2003-2004. Vertical lines on the hydrograph show dates of the networks in the main figure.
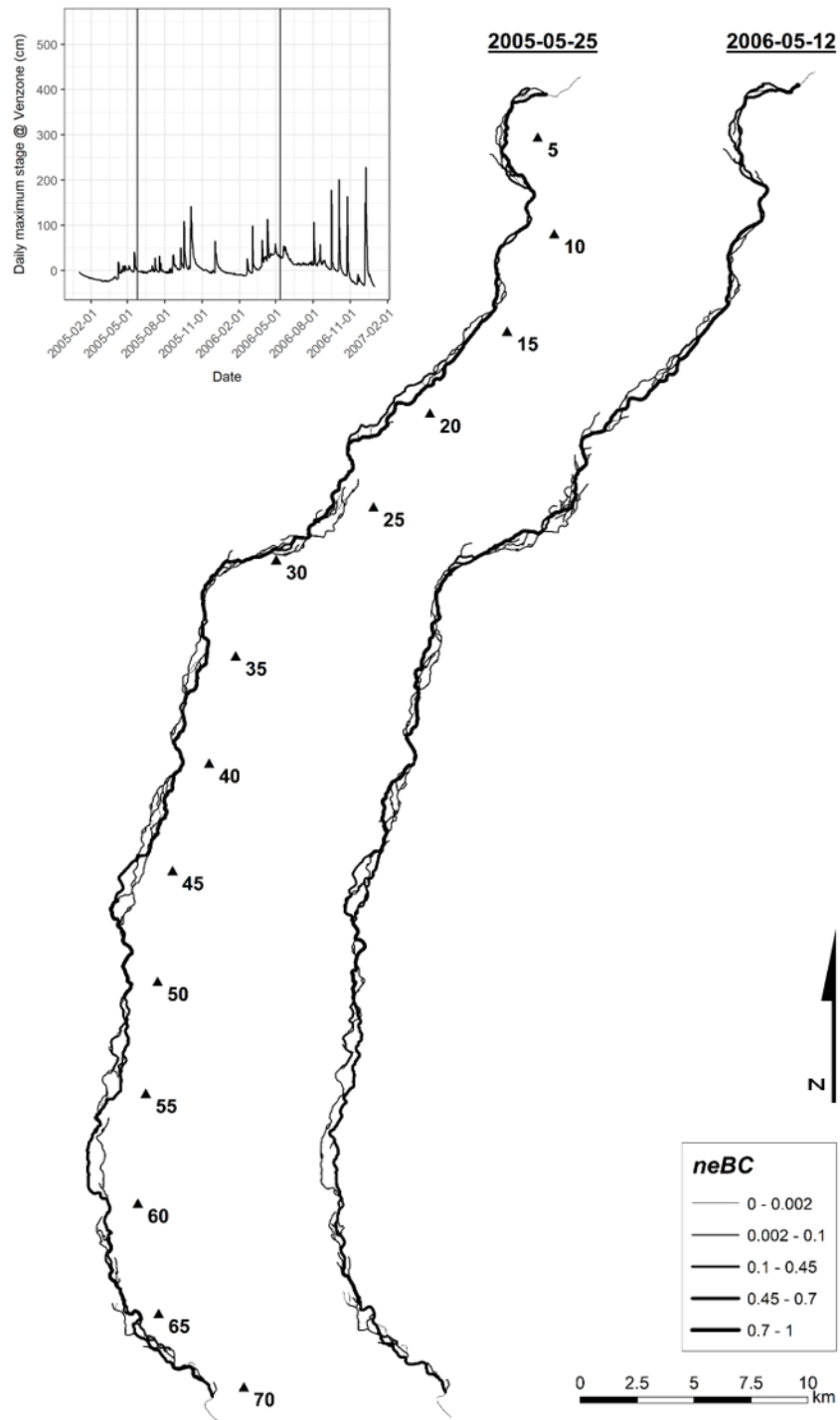
Figure 6.4: *neBC* mapped to the braided channel network of the River Tagliamento under variable flow conditions between 2005-05-25 and 2006-05-12. Markers against the left-most network show 5 km intervals. The inset hydrograph shows stage variation at the Venzone gauging station between 2005-2006. Vertical lines on the hydrograph show dates of the networks in the main figure.
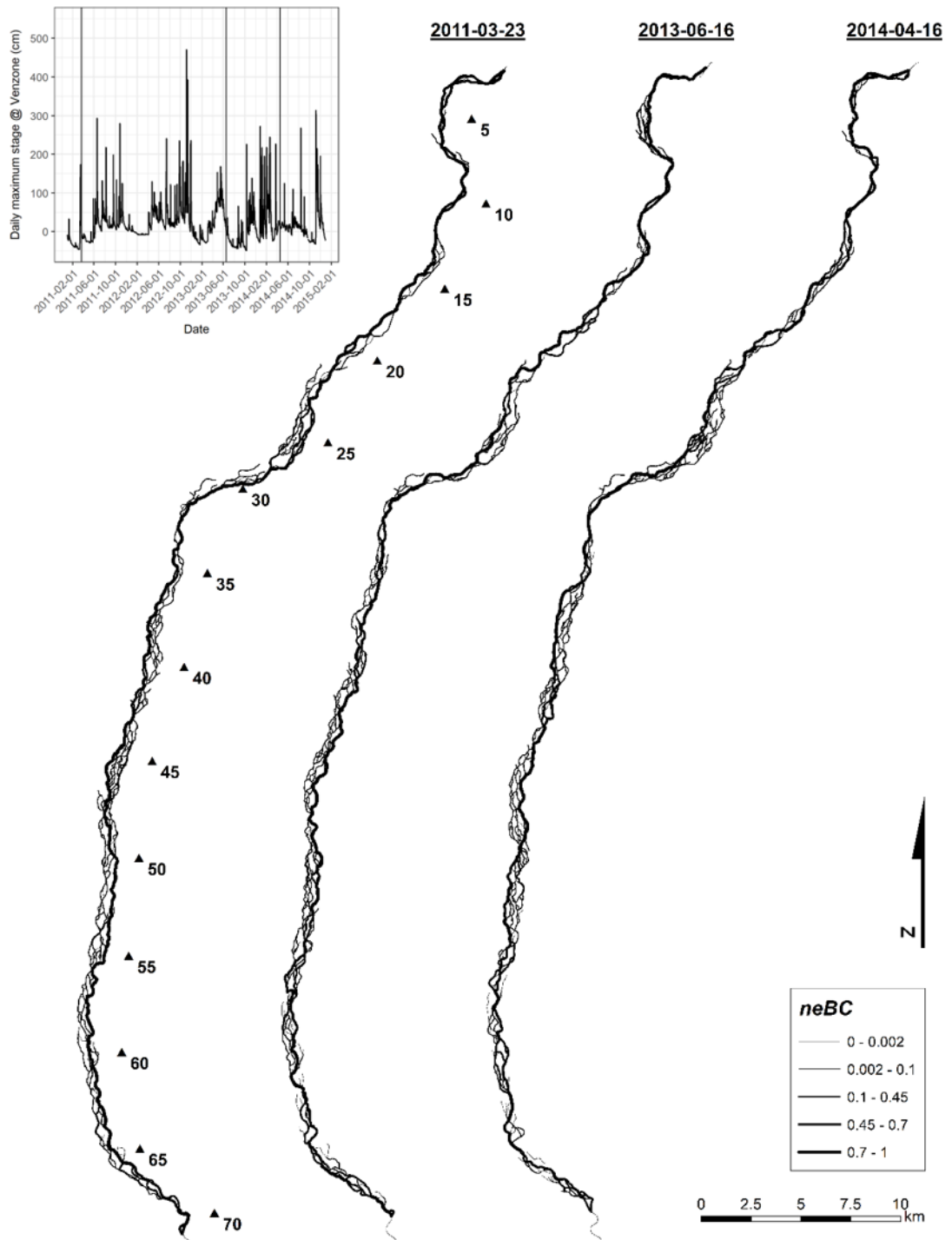
Figure 6.5: *neBC* mapped to the braided channel network of the River Tagliamento under variable flow conditions between 2011-03-23 and 2014-04-16. Markers against the left-most network show 5 km intervals. The inset hydrograph shows stage variation at the Venzone gauging station between 2011-2014. Vertical lines on the hydrograph show dates of the networks in the main figure.
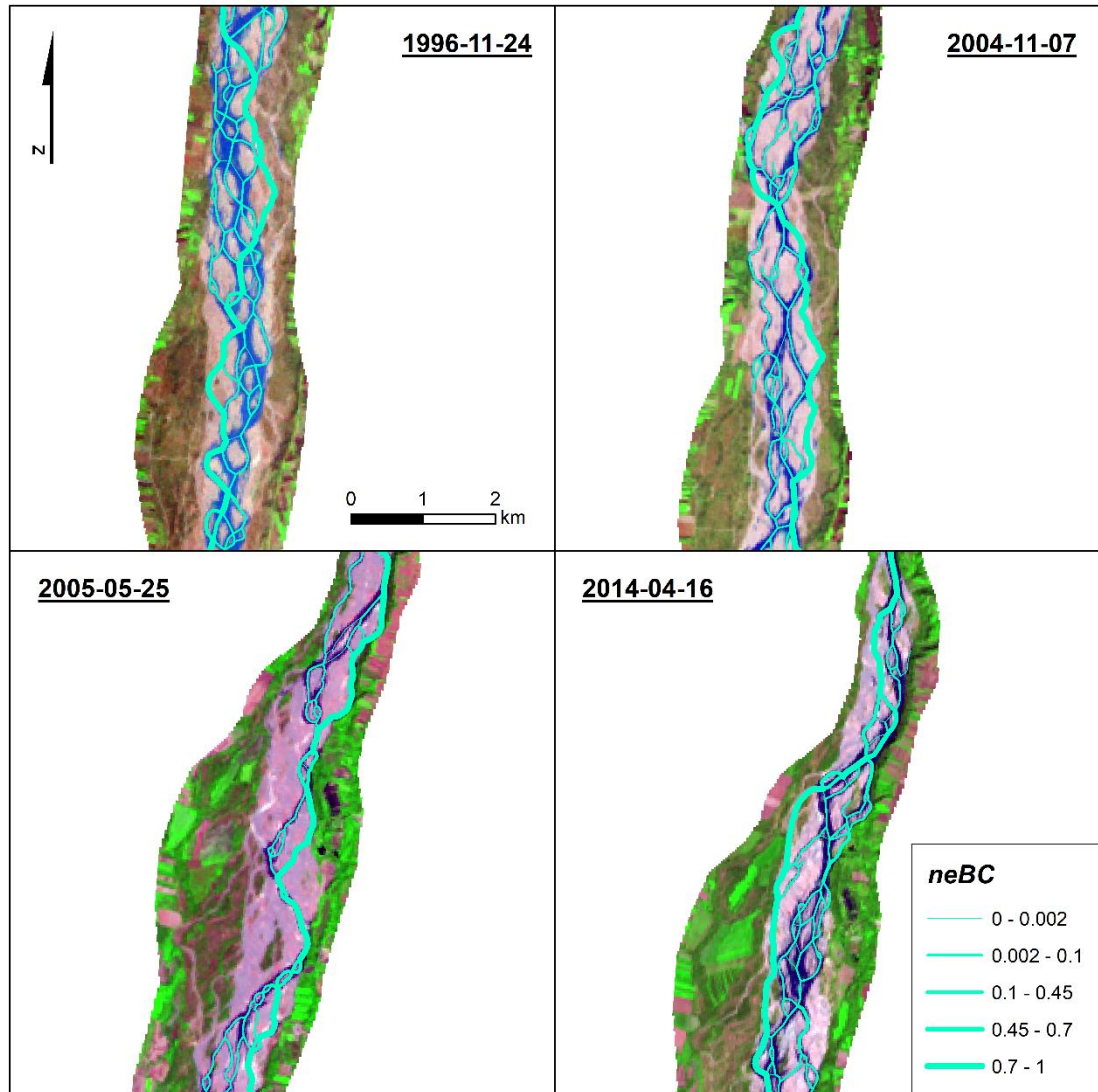
Figure 6.6: The *neBC* coded channel network skeleton imposed onto false-colour composites of two reaches on the Tagliamento for different dates across the study period. Flow is top to bottom.

6.3.1.2   Local spatial patterns

Local variability in the spatial distribution of *neBC* can, in many locations, be related to known controls moving downstream. From 20 km, the widening of the braidplain through the Cornino reach (see chapter 1, section 1.7.3) to the permanent island at ~27 km is apparent on all dates as a pattern of two parallel channels, one generally more heavily branched and with lower centrality (Figure 6.2-6.5). Following the pattern of the central pathway tracking secondary channels, the more heavily braided and complex areas of planform in Cornino are associated with the main channel and lower *neBC* values. Downstream of Cornino, the river flows into the Flagogna reach (see chapter 1, section 1.7.3) where a local deviation from the global CP channel

pattern is often observed. In the downstream half of this reach, the most central channel is against the true-left bank, with this channel being either equally sized or larger than the parallel, lower *neBC* channel. This distribution of *neBC* seems to reflect the dominant locations of vegetated islands on the right of the braidplain, which cause a greater number of bifurcations on the right-hand channel branch through this reach, subsequently lowering the *neBC* of these channels (Figure 6.9).
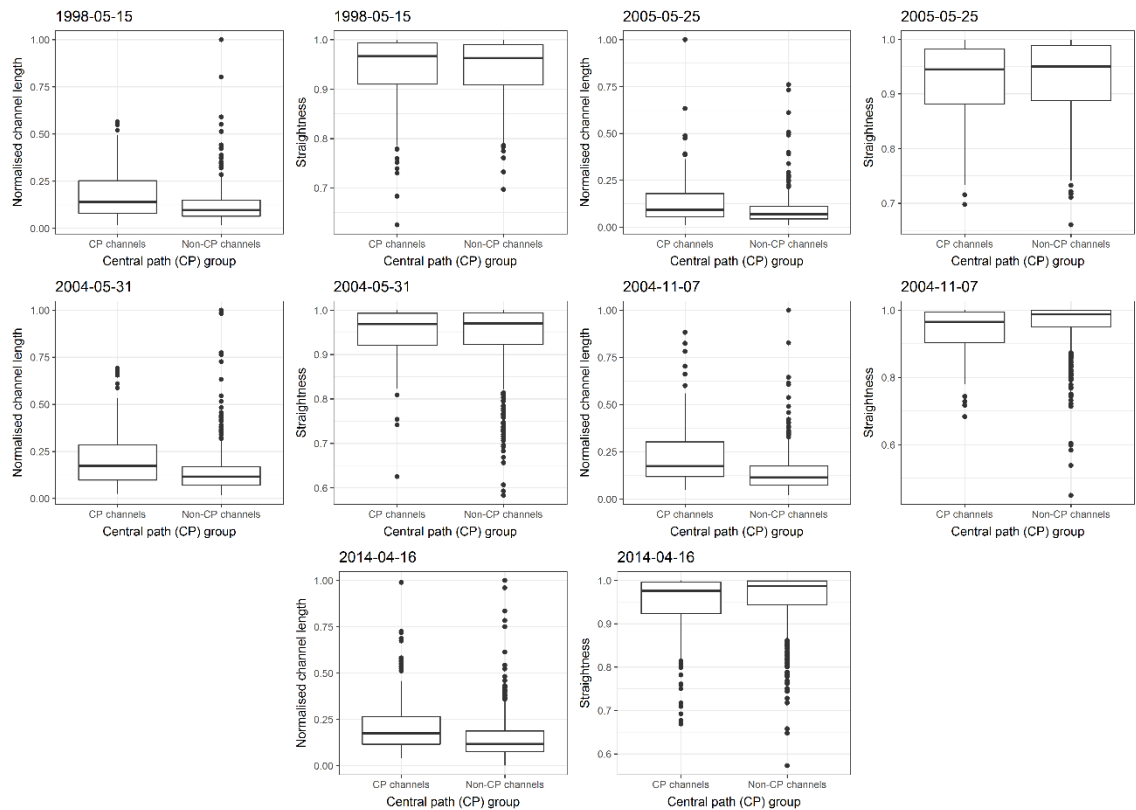
Figure 6.7: Boxplots showing the range of channel length and straightness for channels that comprise the central path group (CP channels) and those in the rest of the network (Non-CP channels). Dates represent the range of number of edges (*m*) across the 14 networks in this study and increase row-wise from the top right, from *m* = 393 to *m* = 894. Lines are the median, boxes represent the interquartile range (*IQR*), whiskers extend to ±1.5*IQR* and outliers are classified as <> 1.5*IQR*. Channel length is normalised by the longest channel in the network.

The downstream limit of Flagogna is marked by Pinzano Gorge (~32.5 km). As the braidplain widens downstream of this constriction, there is a general pattern of increased braiding and a larger ensemble of low *neBC* channels for 20-25 km which, in most cases, is bordered to the left or right by the central pathway of secondary channels (Figure 6.2-6.5). This 20-25 km stretch of the river presents the most extensive section of intense braiding, which begins to wane downstream of 50 km. In networks with lower *m*, this waning network complexity often

manifests as a transition to a largely single thread character where the main channel becomes the most central pathway (Figure 6.2-6.5). The decrease in the complexity of planform reflects the transitional nature of the lower reaches of the Tagliamento as it transitions into a meandering river. An exception to this trend is observed at ~65 km in all networks pre-2011, where the planform is dominated by two parallel channels, each supporting some minor branching around central bar bifurcations, with the least bifurcated channel supporting the most central pathway. The least bifurcated channel, and thus the most central pathway, does not show a tendency to follow the main or subordinate channel branch through this reach. In all cases these parallel branches are instigated by bifurcation around a large vegetated island in the middle of the braidplain. Between 2006 and 2011, this island has been heavily dissected, whilst notable establishment of vegetated islands on the left of the braidplain has forced the channel network to occupy the right of the braidplain from 2011 onwards and, by removing the parallel channels around this island, forced the central pathway to track the main channel through this reach (Figure 6.10). This is a clear example of how the competing temporal dynamics of flow and vegetation growth can cause a spatial rearrangement of planform and network topology.
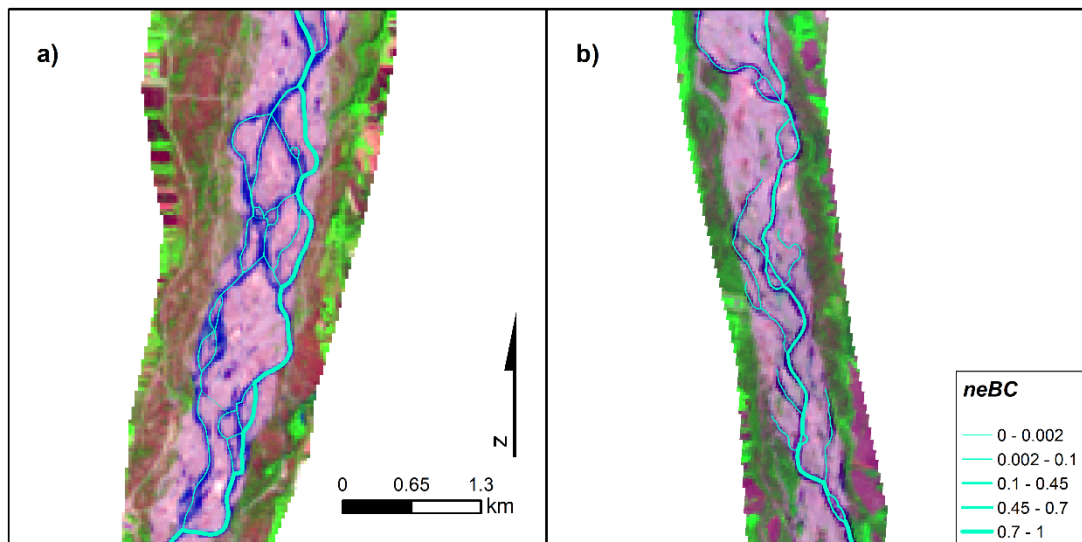
Figure 6.8: a) the central pathway tracking the least branched of two relatively equally sized, parallel channels; b) the central pathway tracking the main channel through a section where the river is close to single-thread. Flow is top to bottom.

6.3.2 Temporal variability in the spatial distributions of neBC

6.3.2.1 Global spatio-temporal patterns

Analysis of temporal variation in *neBC* is conducted through the lens of the recent flood history of the Tagliamento (Figure 6.1). Network scale change in *neBC* over time is seen in shifts in the position of the most central pathway (Figure 6.2-6.5). These positional changes in high *neBC* channels indicate movement in the position of the main channel and its associated planform, such that more intensely braided sections of the river are seen to switch from side to side over time. In general, these shifts in the most central pathway are less pronounced between periods of lower flow activity, e.g. between paired dates separated by flows < 2 m (Table 6.1), which are seen in the 1996-1998 networks (Figure 6.2), the 2004-05 and 2004-09 networks (Figure 6.3) and 2005-2006 networks (Figure 6.4). Between pairs of networks separated by larger flow events and with comparable *m*, large shifts in the position of the central pathway are generally instigated by flow events > 2 m. In the 2011-2013 networks, migration of the central pathway is seen between each date at various locations moving downstream and across downstream distances ranging from ~5-15 km (Figure 6.5). Notably, similar scales of change in the central pathway position are seen between networks separated by > 4 m floods, e.g. 2004-05 to 2004-11 and 2011 to 2013 (Figure 6.3 & Figure 6.5), and between other dates where central pathway switching is observed when intervening flows have been between 2-3 m stage (Table 6.1, Figure 6.2-6.5). However, this flood mediated behaviour is not seen universally. For example, a lesser degree of change is seen between the 2003-09 and 2004-05 networks, which are separated by 2.84 m and 1.91 m flood pulses (Figure 6.3).

With apparent relationships between the magnitude of network-scale change in the spatial distribution of *neBC*, there are also patterns that indicate switches in the position of the central pathway originate from hinge points that maintain similar locations over time. Some of these hinges have known controls, e.g. the widening of the braidplain and flow augmentation into Cornino (~20 km), the narrowing of the braidplain at the island boundary between Cornino and Flagogna (~27 km) and the sudden widening downstream of Pinzano (~32 km; Figure 6.2-6.5). The other major hinge point appears to be between 45-50 km. There is a notable width constriction at 45 km and a bridge spans the river at this point, after which the braidplain widens out and the central pathway is often observed to switch between alternate sides of the braidplain after periods of greater flow activity.
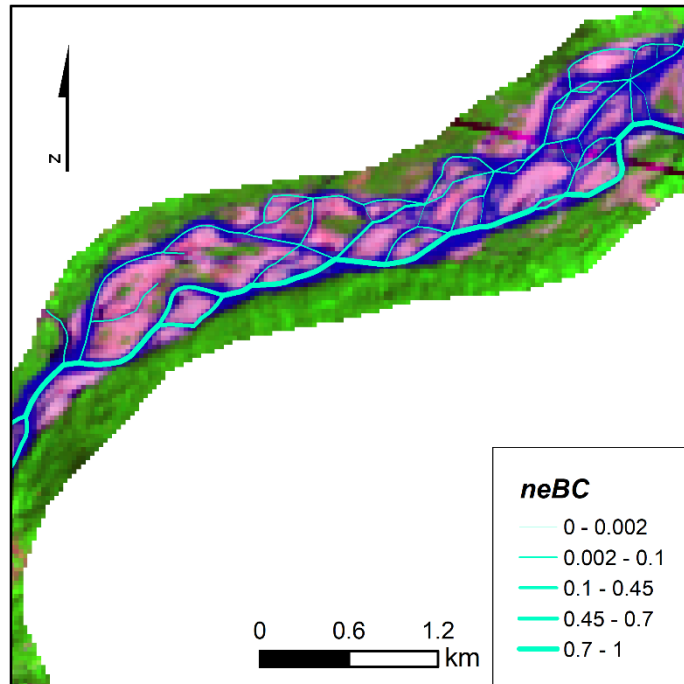
Figure 6.9: Channel division around vegetated islands in the River Tagliamento's Flagogna reach forces the high *neBC* central pathway to track the main channel along it's predominantly left-bank position. Flow is from top-right.

Temporal consistency is also seen in the general spatial patterning and physical characteristics of channels in the lower *neBC* groups (*neBC* < 0.45). The lower *neBC* channels tend to include the main channel and branch channels that contribute to the bulk of planform variation and therefore covers a wide range of channel sizes. As such, the ensemble of low *neBC* channels is consistent in its lack of consistency in terms of physical characteristics. Analysis of the relationships of the low *neBC* channels with channel length and straightness found no correlations. There were also no correlations between the high *neBC* group and *neBC* in general with these physical channel characteristics. The lack of correlations of unweighted *neBC* with physical variables is due to the topology of the unweighted network being somewhat agnostic in terms of the channels its central pathway will follow. Although the central pathway (high *neBC* channels) does have a dominant characteristic of following side channels, it also intersects the main channel at various points as well as sometimes following paths along chute channels dissecting bars. This can be seen in the range of length and straightness of the central pathway channels (Figure 6.7). Thus, the use of unweighted centrality, because this aspect of the network topology is apparently not related to the physical size of channels, provides a means of assessing

changes in planform character, whereas a weighted *BC* may allow analysis of specific drivers of planform evolution that are related to the chosen weighting.
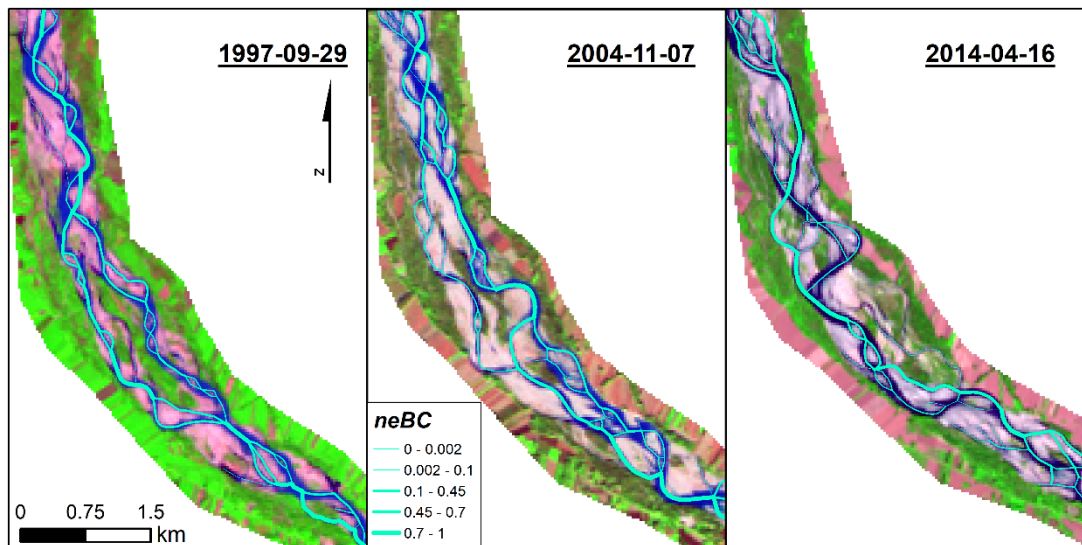
Figure 6.10: Dissection of the large, central vegetated island present in 1997 and establishment of dense vegetation to the left of the braidplain by 2014 shows feedbacks between vegetation development and removal, channel pattern and the resultant spatial distributions of *neBC*. Flow is from top-left.

6.3.2.2   Local spatio-temporal patterns

An initial note of caution should be given in respect of local temporal change in the spatial distribution of *neBC* related to changes in stage, especially when a change in the central pathway is observed over a period with minimal flow activity. This phenomenon is observed at Cornino between the 2004-11 and the 2005-05 networks, where the central pathway has switched from the left to the right side of the braidplain (Figure 6.3 & Figure 6.4). Over this period, which saw no flow events > 1 m (Figure 6.1), the main channel has not moved and changes in planform appear largely related to reductions in stage (Figure 6.12e & 6.12f). Upstream disconnection of the side channels that comprised the central pathway through Cornino in 2004-11 has reduced the number of shortest paths that traverse these edges, which in turn lowers their *neBC* and shifts the position of the central pathway to track the main channel in the 2005-05 network. The upstream disconnection of highly central channels is often responsible for a switch to the most central pathway tracking the main channel, rather than side channels, in networks with lower *m* and further indicates the potential benefits of using weighted *BC* which may be less sensitive to these stage-based effects on central pathway positions.

Although stage can have an impact on spatial distribution of *neBC*, local changes in central pathway position observed between 40-47 km over the 2005-2006 lower flow period show how even relatively small flow pulses (Table 6.1, Figure 6.1) can result in notable change in planform. Through this section, we see shifts in the position of the central pathway that reflect an opposite shift in the main channel from one side of the braidplain to the other (Figure 6.4 & Figure 6.11). This change appears related to migration and possible coalescence of a series of unit bars that choke the main channel, forcing a bifurcation to migrate upstream and direct a greater proportion of flow into the previously subordinate and higher *neBC* channel in the 2005-05 network. Change in the main channel position has resulted in a shift in the loci of channel branching and thus centrality between 40-45 km. At ~45 km, reorientation of the main channel in the area upstream has slightly reoriented the bifurcation seen at the 45 km hinge point; redistributing flow, reactivating channels and changing the distribution of *neBC* in the areas between ~45-47 km (Figure 6.11). This is a good example of small-scale changes that are active under lower flows that still exceed the sediment entrainment threshold affecting reach-scale, but not wider change and planform change cascading downstream, both of which are picked up quantitatively by the underlying network topology.
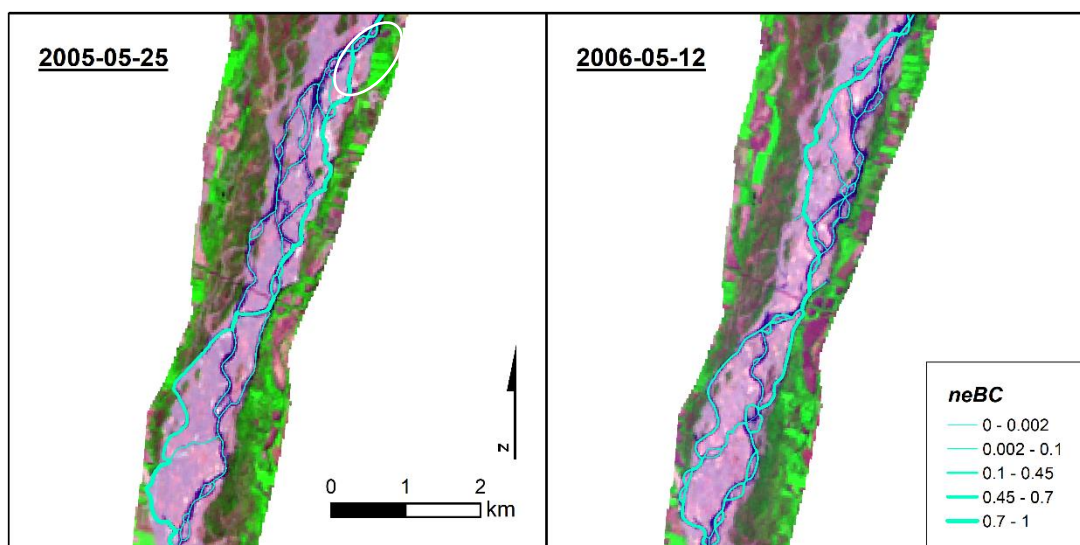
Figure 6.11: Local planform and *neBC* reorganisation after a period with two 1-1.5 m stage flood events. The ellipse in the 2005-05-25 image highlights a series of unit bars that may have migrated and coalesced to shift the location of the large bifurcation in this area upstream, changing the distribution of flow into this reach. Flow is from top to bottom.

Whilst planform change and associated spatial variation in *neBC* can occur in certain locations over periods with relatively low flow activity, the majority of planform and associated *neBC*

dynamics that are differentiable from stage-related effects result from larger floods. This can be seen in the evolution of channel pattern in the Cornino reach, which is visualised in Figure 6.12. In the 1996-1998 networks, Cornino is dominated by two parallel channel branches that originate from a bifurcation at ~25 km. This bifurcation appears asymmetric, based on the visible size of channels and the larger amount of bifurcation activity on the right branch, which manifests as lower centrality due to the increase in the length of geodesic pathways where the main channel branches around bars. Following a period of high flow activity between 2000-2003 (Figure 6.1), culminating in a > 3.5 m event shortly before imaging of the 2003-09 network, Cornino's channel pattern has changed markedly, though the position of a low planform complexity side channel has remained to the left of the braidplain and the main channel and its associated bar complexes remain to the right, which can be seen in the spatial distribution of *neBC*. The subsequent change in position of the most central pathway to the right side of the braidplain in 2005-2006 results from the aforementioned stage effects, but by 2011, after multiple bankfull or near-bankfull floods (Figure 6.1), the *neBC* distribution has changed to show only a slight elevation of *neBC* on Cornino's left channel branch. Through the 2013 and 2014 networks, separated from the 2011 network by a 1-in-10 year flood and from each other by a series of 2-3 m floods, the central pathway shifts to Cornino's right channel branch. This seems to relate to a reorientation and repositioning of the bifurcation at around 25 km that controls flow into Cornino, providing a strong example of a hinge point that controls morphodynamics and planform over the ensuing 3-5 km.

The length over which the hinge point at the upstream end of Cornino can control planform dynamics has a natural downstream boundary at the bedrock island that marks the transition from Cornino into Flagogna. Hinge points at Pinzano and the bridge at ~45 km tend to see more extended downstream reaches over which temporal change in the spatial distribution of *neBC* appears to capture switching behaviour of the main channel related to high flow events. In the proceeding 10-15 km downstream of these hinge points, the central pathway is seen to switch from side to side on the braidplain over time (Figure 6.2-6.5). These switches tend to be associated with periods of high flow activity. When comparing networks with similar *m,* central pathway switching is only observed when intervening flows have exceeded 2 m stage at Venzone. It is also notable that the two 1-in-10 year floods (2004 and 2012, Figure 6.1) do not seem to cause switching behaviour to be seen at a higher proportion of hinge points compared with the 2-3 m floods. In general, it appears a change in the central pathway and thus the position of the main channel is instigated from at least one hinge point in response to formative flow events (events > 2 m).
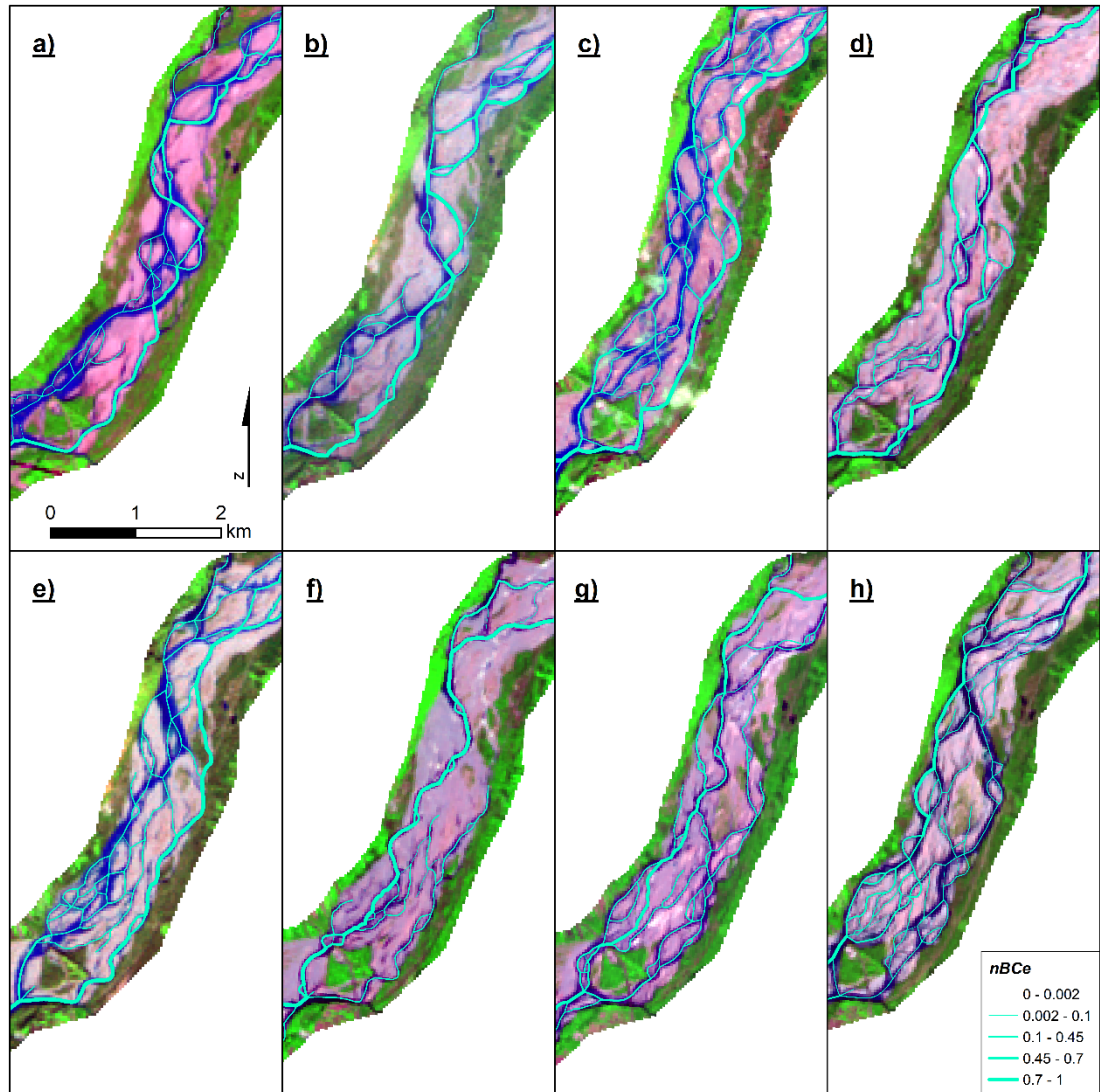
Figure 6.12: Evolution of the Cornino reach and temporal variation in the spatial distribution of *neBC* from over an 18-year study period. Panels show a) 1997-06-29, b) 1998-10-22, c) 2003-09-02, d) 2004-09-20, e) 2004-11-07, f) 2005-05-25, g) 2013-06-16 and h) 2014-04-16. Dates chosen to show change over intervening periods of variable flood conditions (see Table 1). Flow is from top-right.

6.3.3 Global metrics of physical and network structural change in braided rivers

The results presented in the previous two sections provide a largely qualitative analysis of spatio-temporal variation in *neBC* in a braided river network subject to a wide array of flow conditions. A well-defined central pathway of high *neBC* edges is a ubiquitous feature of the analysed networks. This central pathway has been isolated and its sinuosity, *CPS*, calculated. As it appears *CPS* is a stage-independent property of the network (see section 2.3), it is possible to compare trends in *CPS* across the ensemble of networks in this study. Figure 6.13a shows a time

series of variation in *CPS*, which shows that values of *CPS* do not vary markedly (by ~0.1) for the whole study period. However, within this range notable temporal fluctuations are observed. Between 1996-2004, *CPS* fluctuates considerably around the mean *CPS* for the whole study period. From 2005-2013, there is then a switch to a fairly consistent increasing trend in *CPS*, with all values over the long-term mean. At the end of the record, there is a slight decrease in *CPS* between 2013-2014.
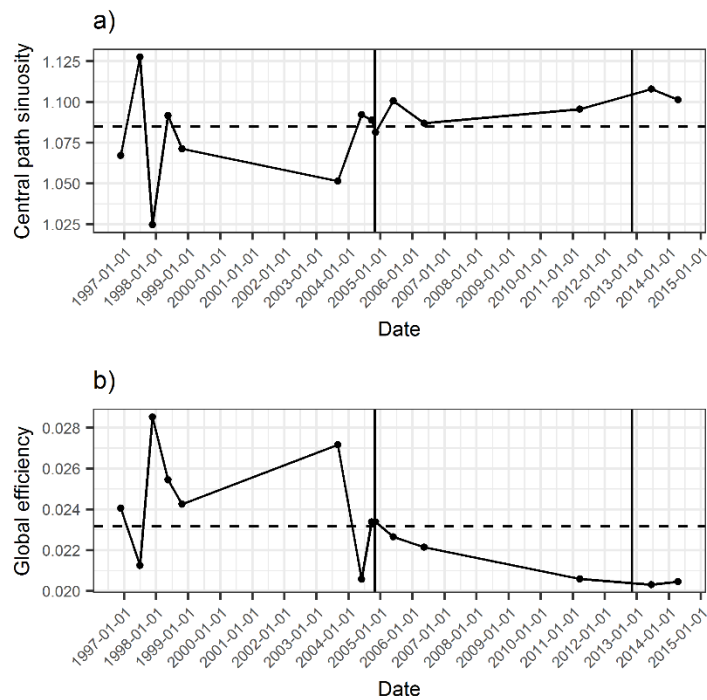
Figure 6.13: Time series of a) Central path sinuosity and b) E_{glob}. Dashed lines show the mean for each variable over the study period. Vertical solid lines show dates of 1-in-10 year flood events.

The E_{glob} time series shows very similar behaviour in terms of patterns of variation, which are much more extreme from 1996-2004, before beginning a steady declining trend from 2005-2013, with the declining trend ending between 2013-2014 (Figure 6.13b). This series also shows that whilst networks with lower m tend to have E_{glob} above the mean for the study period, relatively large changes in E_{glob} can be seen between networks with similar m (e.g. 2003-09 to 2004-05) and lower m networks, e.g. 2005-2006, have lower E_{glob} than earlier networks with higher m (Table 6.1). These patterns indicate the weak stage dependence of this metric and suggest that temporal comparisons of different m networks should not be invalid. Notably, the values of E_{glob} show a largely inverse relationship to *CPS*, which is confirmed with linear regression showing a strong negative relationship ($b = -8.4$, $r^2 = 0.7$, $p = < 0.001$, $n = 14$). This suggests that decreases in *CPS*, which quantifies a physical property of the channels that are on

164

the most "efficient" pathways through the network, are linked to decreases in the overall complexity of the network quantified as increases in E_{glob}. As E_{glob} is an average property of the network, whereas *CPS* is derived from a metric of the connectedness of single channels to the wider network (*neBC*), these results indicate that changes in the global topology (E_{glob}) of the network manifest physically in the properties of channels that track the shortest, or most "efficient", path through the network.

6.4 Discussion

6.4.1 Stage-(in)dependency in the unweighted topological analysis of a braided river network

A large pitfall in the traditional braiding indices used to study braided river planform is their considerable dependence on stage (Egozi & Ashmore, 2008). Braiding intensity measured using either sinuosity or channel count braiding indices have bell-curve shaped relationships with stage, peaking at water levels that have not yet drowned out bars and reduced planform complexity (Egozi & Ashmore, 2008; Welber *et al.*, 2012). As *neBC* is quantifying an aspect of how a braided planform is connected, it is important to consider whether *neBC* is also stage-dependent. Although all networks in the present study were captured at low flow, when stage at the Tagliamento's Venzone gauging station cannot be reliably linked to channel pattern, the use of *m* as a rough proxy for stage suggests the low flow networks in this study capture some variation in stage across the study period. Thus, it is notable that regardless of *m*, the spatial distribution of *neBC* shows a largely consistent pattern that is dominated by a central pathway of high *neBC* channels that tend to skirt much more complex areas of low *neBC* channels. This corroborates the findings of Marra *et al*. (2013) who found that *BC* on the Jamuna River, Bangladesh also showed less sensitivity to stage than traditional braiding indices. Assessment of the physical characteristics of high *neBC* channels have also shown that these channels are, on average, longer than lower *neBC* channels across the range of *m* analysed in this study (Figure 6.7). This pattern also largely holds for the straightness of these channels, with the only exception seen in the lowest *m* network (Figure 6.7). It follows from the differences seen in the length and straightness of high and low *neBC* channels that *CPS* for each network also appears unrelated to stage, based on weak and insignificant regression relationships between *CPS* with *m* and *BI*.

The global spatial patterns and physical characteristics of high *neBC* channels in relation to *m* and *BI* suggest that at the network scale, *neBC* has a degree of stage-independence not seen in traditional braiding indices. However, at local scales, *neBC* does show stage-dependence linked to the connection and disconnection of channels as stage rises and falls. The Tagliamento sees significant changes in channel network connectivity related to stage variation, where low stages are associated with a network of disconnected ponds, upstream or downstream disconnected channels and a connected low flow channel network (Van Der Nat *et al.*, 2002, 2003). *BC* is intrinsically related to a node or edge's connectivity to the wider channel network (Freeman, 1977). It is therefore clear that as stage changes, disconnection and reconnection of channels from the upstream and downstream channel network can trigger changes in the spatial distributions of *neBC*. If using *neBC* to analyse changes in braided river planform and morphology, it is important to recognise that the movement of high *neBC* channels around the network could be the result of channel disconnection or reconnection, rather than an actual change in planform driven by changes in bed morphology.

Local redistribution of high *neBC* due to changes in stage is also likely related to the central pathway through the Tagliamento largely tracking side channels, which are more likely to be disconnected at lower stage (Bertoldi, 2012). Weighting nodes and edges in a network changes the values of metrics calculated from that network's graph (Heckmann *et al.*, 2015). Analysis of the Brahmaputra's channel network using *BC* weighted by the channel width:length ratio of each channel found that the central pathway tracked the main channels more closely than was observed in this study, over both low and high flow periods (Marra *et al.*, 2013). The ensemble of low *neBC* channels in the present data are mainly comprised of the river's main channel and bifurcates resulting from the array of bar deposition and erosion processes that result in braided channel morphologies. This presents the intriguing prospect of being able use unweighted or weighted centrality analysis to probe different aspects of braided river behaviour. As shown in the present study, high unweighted *neBC* tracks secondary channels and the locations of these channels switch across the braidplain in response to flood events. It thus seems likely that these secondary channels may be loci of higher magnitude change over *proceeding* flood events and may provide an indicator of where larger morphodynamic changes are likely to occur in the future. An alternative use of *BC* could use node and edge weightings to analyse the specific responses of braided river planforms to processes that are linked to a given weighting parameter. This could be a particularly powerful method of analysis in numerical models, where both the parameters and process variables (e.g. sediment transport rates, anabranch discharge) that drive braided river morphodynamics can be extracted (Williams *et al.*, 2016). In the present

case, unweighted *neBC* was applied as a) braided river planforms have not previously been analysed with an unweighted topological metric and thus it is important to assess if the network's underlying topology manifests with certain physical characteristics and behaviours; b) at the scale of rivers such as the Tagliamento, where the smallest channels can be around the width of a single pixel in Landsat imagery, the spatial resolution of the data does not allow accurate enough extraction of channel width to be confident in its use as a weighting parameter. That the unweighted centrality of the network has shown detailed patterns of planform change that are, in most cases, linked to flood activity indicates the universality of this approach to braided rivers across a range of sizes.

6.4.2 Multi-scale patterns in the spatial distribution of betweenness centrality in a braided river network

Certain behaviours that are apparent in the present dataset suggest links between the spatial patterning of *neBC* and local factors that are known to affect the Tagliamento's morphology in specific reaches. The Flagogna reach is known to support conditions that promote the establishment of large vegetated islands (Gurnell *et al.*, 2001). The effect of vegetation on planform is complex and depends on the size of vegetated islands, with smaller patches associated with more complex planforms and denser vegetation associated with width constraint that can force a braided river into a simpler planform (Gran & Paola, 2001; Murray & Paola, 2003; Coulthard, 2005). It appears that both these effects are observed in Flagogna, with high vegetation density on the right of the braidplain forcing the main channel to be predominantly to the left of the braidplain and vegetated islands forcing secondary channels to bifurcate and thus reduce their *neBC*.

Vegetation is also observed to dominate planform character towards the downstream limit of the braided Tagliamento (at ~65 km), where a reach that supports a large mid-channel vegetated island around which the channel network is split through the majority of the study period (1996-2006) then sees a switch in the distribution of vegetation and thus the position of the main channel in the 2011-2014 networks. As in Flagogna, the impact of vegetation on planform in this reach has a concomitant impact on the spatial distributions of *neBC*, often forcing a departure from the dominant high *neBC* side channel pattern. Previous research has shown that vegetation on the Tagliamento causes a topographic signature by promoting accretion on vegetated islands (Bertoldi, Gurnell *et al.*, 2011). It seems vegetation may also result in a topological signature due to its effects on planform. Part of the impact of vegetation on planform in braided rivers stems from its capacity to reduce the active areas occupied by

channels. In reaches where the active area is less constrained, such as Cornino and the ~25 km downstream of Pinzano Gorge, braiding tends to be more intense and the spatial distribution of *neBC* is dominated by the global pattern of the central pathway tracking secondary channels. In these reaches, it is the dynamics of change in the location of the central pathway that suggests the temporal variation in local spatial distributions of *neBC* may provide information on the evolution of the channel network.

There is considerable fluctuation in the spatial distribution of *neBC* at different scales on the Tagliamento. A consistent, network-scale pattern of high *neBC* channels that appear as a contiguous pathway through the network is observed in almost all networks. These central pathway channels are generally not associated with the river's main channel and thus are less heavily bifurcated, which results in them providing shorter geodesic pathways through the network and causes their higher *neBC*. Field research has shown that the processes of sediment erosion, transport, deposition and associated bar building and dissection are most active on a braided river's main channel (Wheaton *et al.*, 2013), likely due to the strong association between sediment transport, stream power and discharge (van den Berg, 1995; Doeschl-Wilson & Ashmore, 2005). This provides something of a paradox, whereby high unweighted *neBC* may actually be showing an index of less morphologically active channels.

One of the issues inherent in interpreting change in braided rivers using the satellite record is that any index of change must be used to deduce morphodynamic processes *a posteriori*. The channel networks analysed in this study represent imprints of the Tagliamento's morphology shaped by the previous formative flow event(s). As such, the spatial distribution of the high *neBC* side channels suggests these are locations of channels that are large enough to persist at low stage, but their simpler planform when compared with the main channel and its branches implies that they may see significantly less sediment transport. We know that morphological activity in braided rivers migrates around the network and it is rare, especially in gravel-bed rivers, that all anabranches will be transporting sediment simultaneously (Egozi & Ashmore, 2009; Ashmore *et al.*, 2011; Reitz *et al.*, 2014; Leduc *et al.*, 2015). Furthermore, Egozi and Ashmore (2009) showed that active braiding, e.g. channels actively transporting sediment, increases with discharge. Bifurcation asymmetry is also known to decrease over flood events, as the subordinate channel branch captures more flow when discharge increases (Bertoldi, 2012; Kleinhans *et al.*, 2013; Marra *et al.*, 2013).

In the present study, the low *neBC* channel ensembles that are associated with the main channel depositing and dissecting bars appear likely to have certain properties that would reduce their

hydraulic efficiency over a flood event. Firstly, greater channel branching will increase the sinuosity of flow pathways through these channel ensembles, with concomitant decreases in channel slope and stream power (Knighton, 1998). Smaller branch channels tend to be associated with higher bifurcation angles, which can promote deposition in the subordinate bifurcate (Ashworth *et al.*, 2011) and as bars are inundated as main channel discharge increases, flow expansion will promote sediment deposition (Ashworth *et al.*, 2000). It is thus hypothesised that over a flood event, bifurcations that provide the loci from which the central pathway bypasses the main channel and its associated bar complexes will increase their symmetry, resulting in greater sediment transport in the secondary, central pathway channel. At the same time, increased sediment transport in the main channel and the lower hydraulic efficiency associated with the area downstream of this bifurcation will cause this channel to aggrade, reducing its efficiency further and potentially creating a slope advantage in the secondary channel. This, in turn, could result in the secondary channel capturing more discharge and sediment transport, eroding its banks to widen and become the main channel, and triggering the deposition of unit and lateral bars downstream. Bar deposition and subsequent coalescence and dissection would increase planform complexity in the now main (and previously subordinate) channel branch, which would manifest as a change in the spatial distribution of *neBC*. This process is conceptualised in Figure 6.14. A high temporal resolution sequence of networks with similar *m* that would allow an analysis of this hypothesised series of events is not available in the present dataset, however the switching behaviour of the central pathway does provide some support for this hypothesis. Higher temporal resolution remote sensing data of natural rivers and laboratory or numerical models could provide a means to probe these behaviours.

6.4.3 *Spatio-temporal evolution of a braided channel network in response to flood events*

At the network-scale, the pattern of *neBC* is, in a general sense, quite consistent over time. However, the spatial distribution of *neBC* shows considerable dynamism, with the high *neBC* central pathway and the ensemble of low *neBC* channels frequently switching across the braidplain (Figure 6.2-6.5). Given the central pathway in these unweighted networks may be showing an index of inactivity, or at least an index of lesser morphodynamic activity associated with secondary channels, a switch in the location of the central pathway may be indicative of an opposite switch in the location of the Tagliamento's main channel and the greater morphodynamic activity associated with it. Switches in central pathway position at multiple

locations within the network are associated with intervening periods where flood pulses have exceeded 2 m stage at Venzone (Figure 6.2-6.5), which is in accordance with previous research relating magnitudes of planform and morphological change to flow magnitude on the Tagliamento (Bertoldi, Gurnell *et al.*, 2009; Bertoldi *et al.*, 2010; Ziliani & Surian, 2012). Bertoldi *et al*. (2010) also found that, within the wider and more heavily braided Cornino reach, planform changes associated with main channel relocation of the order of 100-200 m could occur at stages > 1.5 m, but that this was not always observed when flood pulses of this magnitude were recorded. This behaviour is observed across all the wider and more intensely braided sections of the network in the present data in the form of central pathway switching, though does not appear to be more prevalent under higher flow conditions, such that the largest floods with 10 year return periods do not appear to cause significantly more central pathway switching to occur than over periods separated by smaller, more frequent flood pulses.

The locations from which this switching behaviour occurs remain relatively static through time and appear to create hinge points from which downstream change in planform originates. This phenomenon is seen clearly in the Cornino reach, where a predominantly asymmetric bifurcation at ~25 km controls the distribution of flow and thus the locations of varied braiding intensity and *neBC* throughout the reach (Figure 6.12). There is considerable reworking of planform along the dominant channel branch after periods with flood pulses > 2 m. This supports the large body of literature on the impacts of bifurcation asymmetry, which has shown how the larger channel branch at an asymmetric bifurcation captures more flow and has higher sediment transport (Bolla Pittaluga *et al.*, 2003; Bertoldi & Tubino, 2007; Hardy *et al.*, 2011; Kleinhans *et al.*, 2013; Marra *et al.*, 2014), which it is assumed will result in more complex planforms being developed downstream from the dominant branch of a large, main channel bifurcation. Over the 2011-2013 networks, there is a clear reorientation of the hinge bifurcation at the head of Cornino, resulting in a shift in main channel location that is reflected in the spatial redistribution of *neBC* . The temporal resolution of the present dataset does not allow for analysis of what may have caused the change in bifurcation location and orientation in the 2013-2014 networks, but the response is clear in the reorganisation of the network planform and topology, showing how changes at specific points in the network control the morphodynamics of areas downstream.
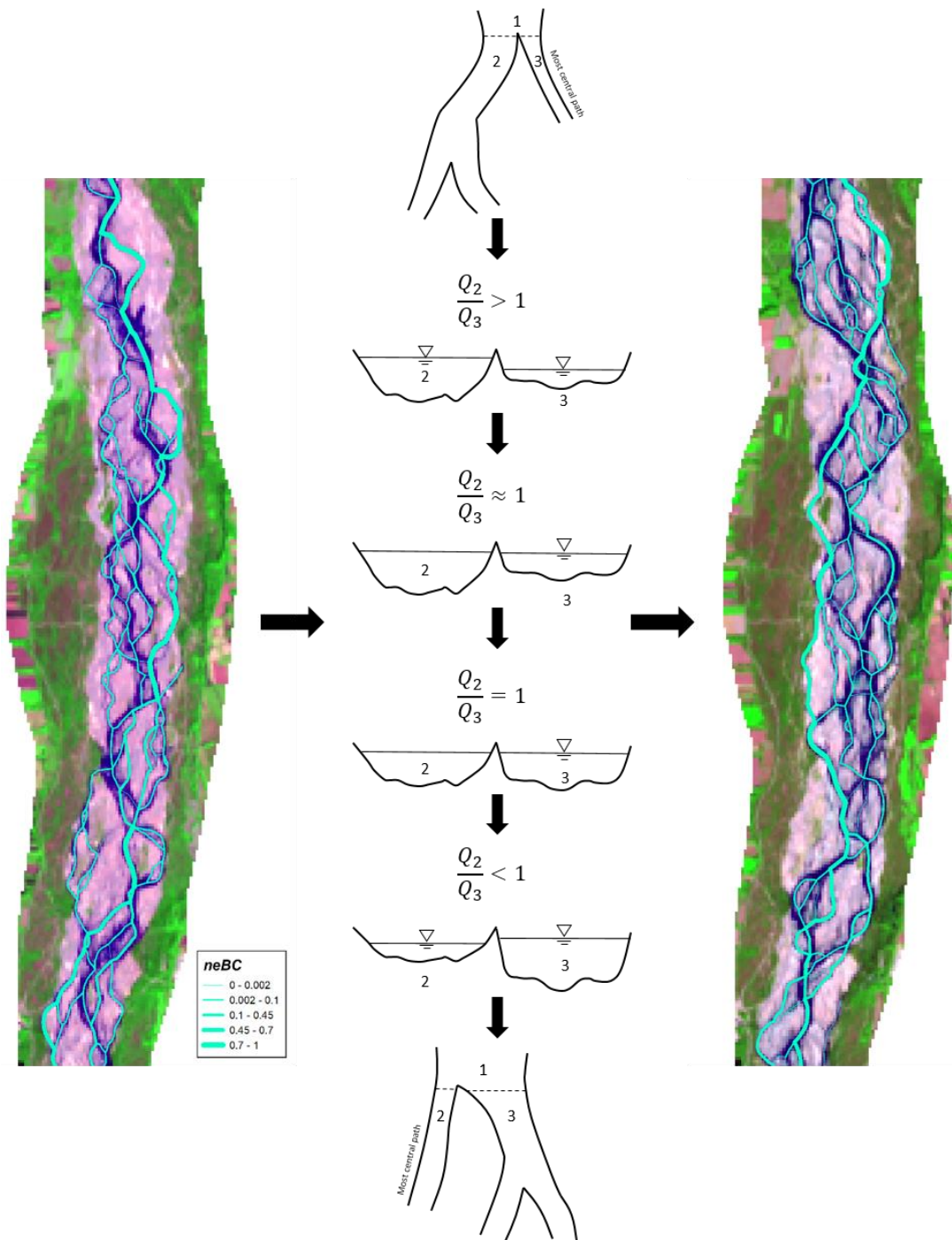
Figure 6.14: Conceptualisation of a potential mechanism of central pathway switching where, from the initial position of the high *neBC* central pathway in the 2013 network, the subordinate channels at bifurcations on the most central pathway, e.g. channel 3 in the top schematic, begin as asymmetric bifurcations with asymmetric discharge partitioning ($Q_2/Q_3 > 1$). These bifurcations symmetrise over the course of a flood event ($Q_2/Q_3 \approx 1 \rightarrow Q_2/Q_3 = 1$) as channel 3 captures flow from the dominant channel 2 and channel 2 aggrades. Finally, channel 3 becomes dominant ($Q_2/Q_3 < 1$), with greater sediment transport leading to a more complex planform downstream, a decrease in centrality on this branch and a switch in the most central pathway, c.f. the position of the central pathway in 2014. Note that 2013-2014 had a series of formative flood events between 2-3 m stage. The dashed lines in the top and bottom schematics indicate the positions of the hypothetical cross-sections.

Morphodynamic changes propagating from points of disturbance have been observed both in natural (Ashworth *et al.*, 2000) and numerically modelled braided rivers (Schuurman *et al.*, 2016), with these changes resulting from particular flow distributions at confluences or in anabranches of bifurcations that subsequently change downstream patterns of erosion and sedimentation. However, it has not been shown previously for the Tagliamento that large scale variation in planform seen in changes to the spatial distribution of *neBC* over distances up to ~10 km may propagate from fixed locations (Figure 6.2-6.5). It has also been suggested that planform instability at specific locations may be cyclical and that, through certain sections of a river, instabilities at a given location may cascade to adjacent downstream locations (Takagi *et al.*, 2007). To analyse this behaviour thoroughly in the present study, it is necessary to isolate changes in planform and the spatial distribution of *neBC* that occur in response to flood events, rather than local changes in *neBC* that result from channel abandonment as stage changes. In the present study this is achieved by comparing networks of similar *m*, using *m* as a proxy for stage. Gaps in the temporal sequence of networks with similar *m* limits a thorough analysis of cyclical destabilisation of certain areas of the channel network, however, it was observed that in the two sections where central path switching was most common (35-45 km and 45-55 km), the central path did not switch across the braidplain in both of these sections over the same time period, regardless of the magnitude of intervening flood events (Figure 6.2-6.5). The 2011-2014 networks provide the best series in which to analyse this behaviour more closely and it is seen that between 2011-2013, there is a switch in the central pathway from the left to the right of the braidplain over the 35-45 km reach, but no switch from 45-55 km, whereas between 2013-2014, there is a right-to-left switch of the central path originating at around 50 km, with the central path position being relatively similar over the upstream distance to Pinzano Gorge (~32.5 km). Whilst this is an isolated example of possible propagating cyclicity in planform change, it does suggest that in certain areas of the Tagliamento, morphological changes in one location may be determined by changes that occurred in areas upstream over the previous flood event, and that *neBC* may provide a means with which to quantify this change.

Central pathway switching may provide evidence of large-scale changes in planform in relation to larger flood pulses, but it also appears that more subtle planform changes can be detected over periods of lower flow by local reorganisation of *neBC*. Mao and Surian (2010) found that the Tagliamento shows considerable local variation in sediment transport under flood events of the same magnitude, with high sediment transport seen in areas associated with the main channel over low magnitude, high frequency flood events (< 1.1-year return period). This behaviour appears to be visible in changes to the spatial distribution of *neBC* between 40-47 km

in the 2005-2006 networks (Figure 6.4 & Figure 6.11), in response to minor flood pulse events (stage 1-2 m) that caused local reorganisation of the channel network. Capturing this behaviour shows how an analytical framework that is sensitive to change across spatial scales, from local reorganisation of the channel network up to global patterns of network structure, is capable of providing significant advances on data generated by traditional methods of planform analysis. In the only other previous research to apply *BC* to a braided river network, much of Marra *et al's*. (2013) analysis focussed on ways to use *BC* to assess average properties of the network, including a *BC* weighted braiding index. This approach neglects likely the most powerful aspect of the network approach: it's spatially distributed nature.

The challenge that arises from this finding is that in order to quantitatively analyse change in the spatial distribution of topological metrics, there is a need for methods than can analyse changes where present data limitations mean tracking single network elements, e.g. nodes and channels, is not reliable given the time periods between data capture and the highly dynamic nature of the system. Methods and concepts coming from the field of the spatial statistics may provide possible solutions. Regression models that can account for spatial and temporal autocorrelation (e.g. Gumpertz, Wu and Pye, 2000) may provide a way to assess whether certain areas of the braidplain have a greater association with higher values of *neBC*, though this example is used to analyse binary associations between a response variable and descriptor variables. An application to braided rivers would require models that can operate with continuous data. Other spatial statistical analyses, including hotspot analysis (Getis & Ord, 1992), have been trialled, with hotspot analysis providing a testcase of issues involving spatial statistics with the present dataset. Hotspots are defined as areas where spatial features that are either all of similar values or all of differing values are clustered within a certain distance of one another, suggesting a spatial pattern of either alike or unlike features. In braided rivers, whilst it would seem that these clusters of alike features, e.g. the high *neBC* channel groups, may provide hotspots, the constrained nature of the braidplain and length over which the groups of these features persist mean that the unlike, low *neBC* channels are inevitably too close to the groups of features from which they are trying to be differentiated. This presents a general issue with trying to spatially differentiate nodes and channels with different values of network metrics given the relatively constrained and directional nature of clustering; an issue that is compounded by an environment where the precise directions in which it is necessary to search for clustering of values will change in response to flood events. One possible solution could be to spatially discretise the active braidplain, giving discrete areas of the braidplain a value based on its occupation (or lack thereof) by a node or channel with a certain value of *BC*, for example.

This would allow analysis of how certain areas of the braidplain are changing and may be able to quantitatively show switches in the most central pathway as areas where a switch in the occupying values of *neBC* occur. This would in turn show a relocation of the main channel and its associated morphological activity.

6.4.4 Quantitative, network-scale characterisation of braided river networks

Much of the above analysis of *neBC* has been qualitative, due to the difficulties in quantitative analysis of such spatio-temporally heterogenous data. However, at the network-scale, E_{glob} and *CPS* have provided novel, quantitative description of braided river network structure and sinuosity, respectively. Comparison of the values of E_{glob} to those reported for transport, road and neurological networks, which are all spatial but not necessarily planar, reveal order of magnitude differences in E_{glob} between these graphs and graphs for the Tagliamento (Latora & Marchiori, 2001; Cardillo *et al.*, 2006; Alexander-Bloch *et al.*, 2013). The low efficiency (from a topological perspective) of the Tagliamento's channel network reflects high spatial constraint on braided river networks and the implications this has for their topology. In the context of E_{glob}, two aspects of braided river topology become important. Firstly, sections where braided rivers become single-thread or close to single-thread at specific points mean that shortest paths between more distal nodes are likely to have to pass along certain edges, removing the potential for more "efficient" paths through the network. Secondly, channel branching around dissected bars causes notable local increases in the potential number of channels that need to be traversed to connect a pair of nodes. These areas of bar dissection and more complex planform and topology are often associated with a braided network's main channel(s), which suggests that changes in E_{glob} will be determined more by changes to the intensity of local channel branching around the main channels. Hypothetically, increases in E_{glob} may reflect decreases in the intensity of local braiding processes and more direct connections between main channels. Whether braided river networks of different types (e.g. sand-bed, gravel-bed) or size would have different ranges of E_{glob} and thus show differences in network structure that may link to their dynamical behaviour is an open question, but this metric does provide a means of classifying braided rivers based on a property that, compared to traditional braiding indices, better describes the internal structure of the network.

The inverse relationship of E_{glob} with *CPS* is intriguing and suggests that reductions in sinuosity in the most well-connected (high *neBC*) channels results in a reduction in the overall complexity of the network. As channel slope is negatively related to sinuosity (Knighton, 1998), lower *CPS*

should indicate increases in channel slope along the central pathway channels. Greater channel slope increases stream power (Kleinhans & van den Berg, 2011) and thus the networks with lower *CPS* may be associated with formative conditions under which sediment transport was higher. It is somewhat counterintuitive that a network configuration formed under conditions with greater sediment transport also has greater E_{glob}, as it is assumed that greater sediment transport would result in more erosion and deposition, increasing the complexity of the network structure and the lengths of shortest paths between nodes, thus reducing E_{glob}. An alternative hypothesis could be that networks with higher *CPS* and thus lower channel slopes see greater rates of deposition on the falling limb of flood events, which in turns increases network complexity and reduces E_{glob}. Clearly this relationship requires more detailed analysis over a larger sample, not least due to the apparent relationship between the physical properties of largely secondary channels (the central pathway channels) and an abstract property of the global network structure.

Time series of E_{glob} and *CPS* shows the temporal variation in their inverse relationship and that the magnitude of change in each metric is relatively in step. It is intriguing that in the period from 1996-2004 where the greatest fluctuations in both variables are seen, E_{glob} is largely above the mean for the whole series. If networks with higher E_{glob} are considered to be better connected and thus more likely to propagate change, could the fluctuations in E_{glob} and *CPS* between 1996-2004 relate to network configurations that are more sensitive to perturbations by flood events? What is clear from the time series in Figure 6.13 is the remarkable switch in behaviour seen at the point of the 1-in-10 year flood in 2004, followed by another switch in the dominant 2005-2013 trend of both variables that coincides closely with the 1-in-10 year flood in 2012 (Figure 6.1). A recent analysis of factors that have contributed to a widening of the Tagliamento's braidplain since the 1990s suggested a large reduction in gravel mining combined with local increases in unit streampower due to historical narrowing of the braidplain to be the most important factors in the recent widening trend (Ziliani & Surian, 2012). It seems likely that widening of the braidplain combined with greater sediment supply could allow the development of more complex planforms as flow expansion decreases streampower on the falling limb of floods, resulting in greater *CPS* and lower E_{glob}. Proper assessment of whether the 1-in-10 year floods have tipped the behaviour of the channel network structure to more closely match a trajectory aligned to the recent braidplain widening trends requires a longer, higher resolution time series, but application of E_{glob} and *CPS* may provide a network-scale means to analyse these trends.

6.5 Conclusion

This chapter has presented the first in-depth, multi-spatial and multi-temporal analysis of braided river morphodynamics using a spatially distributed graph theory metric, namely *edge betweenness centrality*. Furthermore, two novel network-scale classifiers that describe physical and structural properties of braided channel networks have been proposed. A qualitative assessment of *neBC* against a proxy for flow stage in each network suggests that at the network-scale, patterns in the spatial distribution of *neBC* persists over varying stage. This finding is supported by a persistent pattern in the average value and range of values for channel length and straightness within the group of high *neBC* central pathway channels and the other, non-central pathway channels. These physical characteristics of the central pathway channels also results in apparent stage independence of a network's *CPS*, however E_{glob} shows weak dependence on the *m* number of edges is in the network, which should be considered when comparing results from networks with different *m* or stage. At a local scale, the spatial distribution of *neBC* does appear to show more dependence on stage (or *m*), as channel abandonment or reconnection causes a change in the upstream and downstream connectivity of a channel and thus its *neBC*. This should be a consideration when analysing spatial change in metrics based on node or channel connectivity. It is also noted that this research did not have access to an accurate stage record at the flows at which data was captured. Actual stage data is required to confirm the assertions about stage independence offered in this research. Further research should also assess whether local scale stage dependence persists in weighted networks, where the spatial distributions of the *neBC* will change depending on the node or edge weightings applied. This study has shown that the analysis of unweighted *neBC* can still provide valuable information on planform change.

Planform evolution on the Tagliamento is visible largely through the shifting position of a most central pathway of high *neBC* channels that is a ubiquitous feature of the networks studied here. This central pathway tends to largely track less heavily branched, secondary channels. It may thus provide something of an index of inactivity, though relocations of the central pathway are likely to show areas where the main channel has made an opposite shift in position and therefore can be used as a means to assess locations of morphological change. A possible mechanism that describes how these central pathway switches may occur has been conceptualised and it is now down to analysis with high temporal resolution and numerical model data to test this conceptualisation. It is also apparent that, in line with previous research on the Tagliamento, floods > 2 m in stage were needed to trigger large scale changes in the

spatial distribution of *neBC* and thus the locations of morphological change at multiple locations throughout the network. However, the hypothesised increase in the scale of planform change with increasing flood magnitude was not observed, with floods considerably over bankfull causing a similar amount of planform change than periods with successive floods between 2-3 m stage.   These results present the first time this behaviour has been observed at the scale of the whole braided Tagliamento channel network.

Change in the spatial distribution of *neBC* was also found to highlight local changes in channel pattern resulting from small floods (1-1.5 m) that exceed the threshold for sediment transport. These changes would not be picked up using traditional braiding indices. Furthermore, it was observed that large scale changes in the spatial distribution of channel planform may originate from hinge points in the networks that are relatively static over time. The propagation of change from specific locations supports results from numerical modelling and low temporal resolution satellite remote sensing studies, but using higher temporal resolution data here has shown that these changes result from floods over a certain magnitude. The analysis of spatial change in planform using *neBC* presented here has been largely qualitative, owing to the complex spatial nature of these data.   However, it has confirmed the hypothesis that meaningful data on planform change above that provided by traditional braiding indices can be extracted from the unweighted topology of a braided channel network. Suggestions have been offered for ways to quantitatively analyse change in braided rivers using fully distributed network metrics and developments in these methods will greatly strengthen network analysis of braided rivers in the future.

The application of two novel metrics of channel network structure and sinuosity have provided new opportunities for the classification of braided river networks. Comparison of E_{glob} against values from other networks suggest that braided rivers are intrinsically inefficient.   This highlights the chain-like nature of their topology whereby there are few shortcuts through the network. Owing to its quantification of changes in the global structure of braided river networks, changes in E_{glob} may relate to reorganisation of channels that increase or decrease connectivity between the wider channel network.   Thus, this metric may provide a new means to differentiate and classify braided rivers. It is now down to testing on a wide range of different rivers to fully assess the utility of E_{glob}. An intriguing relationship between *CPS* and E_{glob} was also observed that suggests we are seeing change in global-scale network properties (E_{glob}) linked to the sinuosity of channels that are on many shortest paths through the network (*CPS*). This relationship fits the hypothesis that lower E_{glob} will be associated with higher *CPS,* though more

work is needed to confirm that this relationship holds with larger datasets, in different rivers and to probe possible physical mechanisms that might underlie this behaviour. It is likely that this last question will benefit considerably from analysis using numerical models. E_{glob} and *CPS* did not show consistent responses with flood magnitude, as hypothesised, but their time series do appear to show changes in behaviour in relation to very high magnitude flood events. Further analysis with longer, higher resolution time series is also required to assess whether the temporal dynamics of *CPS* and E_{glob} are detecting what could be described as flood mediated changes in regime of the channel network structure and, moreover, whether these dynamics can be linked explicitly to different types of morphological change.

7. Conclusions and recommendations for further research

The core aim of this thesis was to use graph theory to investigate the potential of network research methods for tackling shortcomings in the spatio-temporal scope of current approaches to studying braided rivers. Chapter 2 identifies the knowledge gap in our current understanding of braided river behaviour, in the context of the reductionist paradigm within geomorphology. Graph theory and network analysis provide a complementary and more holistic approach to braided river geomorphology, which is outlined in chapter 3 and Connor-Streich *et al.* (2018). Chapter 4 outlines a methodology that is necessary for the derivation of braided river graphs and shows how using novel image classification techniques can assist in the extraction of braided river networks from remotely sensed data. The products of chapter 4 are used in chapter 5 to provide a quantitative analysis of different spatial frameworks for reach definition to answer a crucial question in braided river geomorphology: do arbitrarily defined reach lengths truly capture the complex nature of braided river networks or should reaches be scaled on a property of the network? Finally, in chapter 6, graph theory and network analysis are applied to show how the evolution of braided rivers is dependent on the dynamics of specific locations in the system that can manifest as large-scale change to network structure, with these behaviours controlled fundamentally by flood events. These outputs have contributed to meeting the core aim of this thesis, which was broken down to a set of research goals around which these concluding remarks are based.

Goal 1: Identify a toolbox of graph theory metrics relevant to braided river morphodynamics based on critical, inter-disciplinary analysis of network research across a range of sciences.

This goal was achieved through a critical review of network literature and literature on braided river geomorphology, resulting in the publication of Connor-Streich *et al*., (2018), which is presented in edited form in chapter 3 of this thesis. The main output from chapter 3 is the identification of a novel, graph theory-based toolbox of metrics with potential relevance to braided river morphodynamics. This toolbox was determined in the context of considerations on network structure in braided rivers, particularly the limitations on certain aspects of braided river topologies that are caused by the spatial planar nature of the network. The application of graph theory to braided rivers was framed by analogies between braided rivers and other types of network. From a theoretical perspective, this is a fascinating line of enquiry that should be pursued further. Universal properties of networks as diverse as disease transmission and air

transport routes have been found to optimise around certain topologies that facilitate ready communication between all parts of the network. Quantifiable similarities between braided rivers and other types of network may allude to some important aspects of braided river dynamics governed by as yet unobserved properties of connectivity. Potential applications of the graph theory toolbox were also proposed in chapter 3, highlighting how graph theory may offer new approaches to characterising braided rivers, understanding their dynamics and validating braided river numerical models.

Goal 2: Test the utility of OBIA for the classification and network extraction of braided river network graphs from satellite imagery.

This goal was achieved in chapter 4 and motivated by the need to develop a fast and accurate method for derivation of braided river graphs from a single input image. The method was developed on Landsat imagery and applied novel, Object-Based Image Analysis (OBIA) techniques to quickly and accurately delineate braided channel networks. It was found that OBIA classifications performed as well or better than traditional, per-pixel methods of image classification and, importantly, are faster to apply and provided better classification of water. The workflow described herein, which extracts the channel network skeleton and topology from the classified channel network, provides an effective method for acquisition of the network graphs of medium to large braided rivers. However, this methodology is hampered by being only semi-automated. Automatic extraction of multi-channel river networks with accurately represented network topology is an open area of research that will contribute greatly to network approaches to braided river research, as will continued improvements in the spatial resolution and availability of remote sensing datasets.

Goal 3: To address a key question in connectivity-based research: how to define fundamental units at different hierarchical levels of system organisation? Or in the case of braided rivers, how should we define a reach when working at the scale of the whole channel network?

What defines a fundamental unit is a key question in network research. In braided rivers, at the lowest level of planform organisation, bifurcations, confluences, channel and bars intuitively define the fundamental units. At the next level of organisation, we define the reach. Most previous research on braided rivers has defined reaches at arbitrary lengths that do not account for the intrinsic length scale of braided morphologies. This length scaling is linked to processes of erosion and deposition and thus reaches defined without consideration of an adequate length risk misrepresenting channel planform, morphology and the true nature of braided river morphodynamics. Chapter 5 assessed the sensitivity of a channel count braiding index (BI) and the relationships between BI and physical controls on braiding under three reach frameworks:

1) a traditional and arbitrarily defined 1 km reach length applied to many studies of the River Tagliamento; 2) a spatial reach framework of fixed-distance reaches defined by scaling relationships of bar-scale processes with average wetted width; 3) a framework defined by the topology of the network based around concepts of *betweenness centrality* and that allows reach lengths to be variable.

Results have shown that the arbitrary reach lengths were too short relative to dominant length scales of the Fiume Tagliamento and thus captured erroneous fluctuations in braiding intensity by sampling single bars or sections of single-thread channels. Furthermore, this reach framework was relatively insensitive to floods of various magnitude. The fixed-distance reaches defined by the physically scaled reach framework showed the strongest relationships between *BI* and physical controls on braiding. These reaches also showed greater sensitivity in the longitudinal variation of *BI* in response to flood events when compared with the 1 km reaches, confirming previous research that suggests reaches should at least be scaled based on a measure of average wetted width at channel forming flow. However, average wetted width fluctuates both along the length of a river at a single point in time and shows at-a-station variability over time due to varying flood magnitude. The novel, graph theory-based approach to reach definition applied in this chapter tried to account for these scaling heterogeneities. In a small sample of networks, the topological reach framework has shown a systematic response of reach length and longitudinal variation in braiding intensity to flood magnitude, suggesting that the topology of the network may respond to changes in discharge. This may provide the basis for a reach framework that can better capture local dynamics in braided rivers. It is now necessary to test the physically-scaled and topological reach frameworks over a larger sample from the Tagliamento and on different rivers, and to assess the performance of the topological reach framework using weighted networks.

Goal 4: Apply graph theory-based analysis to a multi-spatial, multi-temporal dataset encompassing a range of different flood magnitudes known to cause varying levels of morphological change to a reference braided river system.

Satellite data archives have huge potential for multi-spatial and multi-temporal analysis of change in braided river planforms that is beyond the scope of other survey methods. It has been proposed in this thesis that graph theory provides the analytical framework that is required to maximise the utility of satellite remote sensing. Chapter 6 uses graph theory to analyse the evolution of the Fiume Tagliamento's planform in response to a series of different magnitude flood events over a period of 18 years, using unweighted *edge betweenness centrality* (*eBC*) to analyse planform changes from local to network scales. This analysis found some unexpected

patterns in the spatial distribution of unweighted *eBC*, showing that the most central pathway through the network tracks secondary channels, providing an index of inactivity that highlights shifts in simpler, less branched areas of planform over time. However, highlighting changes in the locations of less active channels also highlights changes in the locations of the more active, main channel, which was observed to switch across the braidplain in response to floods over 2 m in stage. Notably, this switching activity did not become more widespread in response to higher magnitude flood events. It was also found that switching of the most central pathway often originated from locations that are relatively static through time. These "hinge points" may house critical bifurcations that control the downstream evolution of channel morphology over scales of 5-10 km on the Tagliamento.

At smaller scales, spatio-temporal analysis of the local redistribution of *eBC* highlighted local changes in channel pattern due to small-scale sediment transport processes, evidencing the sensitivity of braided planforms to smaller but competent flood events in a way that would not be seen in traditional braiding indices. At the other end of the scale, two novel metrics quantifying global network structure, E_{glob}, and sinuosity, *CPS*, have been proposed. Unlike traditional sinuosity indices, *CPS* appears to be stage-independent as the central pathway of channels from which it is derived is a ubiquitous feature of the Tagliamento's channel network, regardless of the *m* number of edges present in the network, with *m* being used as proxy for stage. E_{glob} provides a measure of network structure that is defined by the average strength of connectivity between different network nodes. The inverse relationship between *CPS* and E_{glob} shows evidence of structural rearrangement of a braided river network that may manifest as changes to the physical properties of the network's channels, whilst changes in the behaviour of these metrics in response to high magnitude, low frequency flood events may show flood triggered regime shifts in network behaviour. It is now necessary to test these metrics on data with higher temporal resolution and on other rivers, as well as using numerical models to probe the morphodynamics that may drive variation in these metrics. It is also necessary to develop methods that can quantitatively describe the spatio-temporal variation in *eBC* at multiple spatial scales.

7.1 Directions for further research

Each chapter from this thesis has resulted in the requirement and recommendations for further graph theory- and network-based research on braided rivers. Most of these recommendations

are complementary and aim to expand the overarching aim of the thesis. They are summarised under the following groups:

1. ***Remote sensing and methods for the extraction and analysis of braided river networks***

There is an extensive and ever-growing archive of remotely sensed planform imagery of braided rivers. To fully exploit these data sources for network analysis, there is a need to develop automated methods for the extraction of network skeletons that capture the network's topology, e.g. the direction of flow through the network. This is an open area of research in which developments are being made in the extraction of multi-channel river delta networks and their associated topology (Jarriel *et al.*, no date; Isikdogan *et al.*, 2015, 2017, 2018). Application of the methods detailed in these studies may yield results that could greatly advance the prospects of network studies of braided rivers.

A key issue highlighted in this thesis is the inability of optical remote sensing datasets to capture braided river networks at higher flows in environments when flooding is often pluvial and thus the river is obscured by cloud during flood events. Synthetic Aperture Radar (SAR) data is not sensitive to cloud cover and recognition of its potential for studying braided rivers in environments with cloud cover problems is not new (e.g. Smith *et al*. 1995), though the lack of freely available SAR data at adequate spatial resolutions is likely to have limited applications to braided river research. The Sentinel-1 satellites are now providing freely available global SAR data at 20 m spatial resolution (Berger *et al.*, 2012), e.g. at a resolution capable of capturing channels on medium to large braided rivers. Recent work has shown the potential for SAR-based inundation mapping in near-real time (e.g. Shen *et al*. 2019) and SAR data seems likely to provide the missing piece of the puzzle in terms of capturing braided river networks over the full range of flow conditions. Other work using satellite altimetry is seeking to derive global datasets of water surface slope to support space-based discharge estimation (Garambois *et al.*, 2017). These efforts may provide invaluable sources of weighting data for deriving weighted graphs of braided rivers, further strengthening the network approach.

2. ***Defining reaches and applying subnetwork analysis***

This thesis has shown that current approaches for defining reaches using arbitrary spatial frameworks do not accurately represent braided rivers planforms. More testing is required to assess whether the physically-scaled or topological reach frameworks proposed in this thesis provide better reach-scale characterisation of braided rivers, including testing the topological

183

method with weighted networks. The critical review of metrics presented in chapter 3 and Connor-Streich *et al*. (2018) identified various metrics with great potential for braided river research, but that are applied at a subnetwork (reach) level. Application of these metrics requires an adequate framework for defining subnetworks, which is further motivation to conclusively determine a method for defining reaches on braided rivers.

3. *Quantitative classifications of network structure and behaviour*

This research has shown the potential of graph theory for studying braided river behaviour using qualitative observations of *eBC* at multiple scales. We now need new methods to quantitatively describe the spatio-temporal variability in metrics that are fully spatially distributed throughout all channels or nodes in a network, with these methods needing to account for our inability to track single network elements over time. There is also a need for deeper testing of the behaviour of network scale classifiers like *CPS* and E_{glob}, to analyse whether they show systematic changes across multiple river networks that can be linked to catchment-scale physical controls or autogenic processes. Determining if the latter may be driving changes in network-scale classifiers will likely require analysis using numerical models, where detailed observations of small-scale morphodynamics are possible.

As well as network analysis of braided rivers benefitting from the use of numerical models, chapter 3 proposed that graph theory may provide potential solutions for validating numerical models. Possible approaches could include analysis of a model's capacity to replicate global-scale network structure using metrics like E_{glob} or *M*; replication of the length scaling of distributed metrics like *BC*, assuming that these metrics show a typical length scale; scaling of frequency distributions of spatially distributed metrics that would show if a numerical model is replicating statistical properties typical of a prototype braided river system; and analysis of internal behaviours of numerical models by comparison of high temporal resolution data showing the spatio-temporal evolution of weighted node or edge characteristics, which could be supported by the use of SAR data to capture change over flood events.

Analysis of network dynamics using numerical models may also open up the potential for highly experimental approaches to graph-based analysis of braided rivers, such as agent-based models (ABMs). Whilst ABMs may be somewhat limited in scope by the complexity of braided river morphodynamics, they could provide a parsimonious approach to elucidating key controls on braided river behaviour. At sub-reach to reach scales, dynamic analysis using filial relations may provide a framework within which to analyse thresholds for change in particular local

morphological configurations of the network, based on graph and physical properties. Taken together, the graph theoretic approach proposed in this thesis has great potential to provide fundamental developments in our knowledge of braided rives and our ability to predict their evolution.

8. Bibliography

Abe, S. and Suzuki, N. (2006) 'Complex-network description of seismicity', *Nonlinear Processes in Geophysics*, 13, pp. 145–150.

Alexander-Bloch, A. F. *et al.* (2013) 'The anatomical distance of functional connections predicts brain network topology in health and schizophrenia', *Cerebral Cortex*, 23(1), pp. 127–138. doi: 10.1093/cercor/bhr388.

de Arruda, H. F., Comin, C. H. and da Fontoura Costa, L. (2016) 'Minimal paths between communities induced by geographical networks', *Journal of Statistical Mechanics: Theory and Experiment*, 2016(2), p. 023403. doi: 10.1088/1742-5468/2016/02/023403.

Ashmore, P. (1987) 'Bed load transfer and channel morphology in braided streams', in *Erosion and Sedimentation in the Pacific Rim, Proceedings of the Corvallis Symposium, August 1987. International Association of Hydrological Sciences Publication*, pp. 333–341.

Ashmore, P. (1991a) 'Channel morphology and bed load pulses in braided, gravel-bed streams', *Geografiska Annaler. Series A. Physical Geography*, 73(1), pp. 37–52.

Ashmore, P. (1991b) 'How do gravel-bed rivers braid?', *Canadian Journal of Earth Sciences*, 28(3), pp. 326–341. doi: 10.1139/e91-030.

Ashmore, P. (2009) 'Intensity and characteristic length of braided channel patterns', 36, pp. 1656–1666. doi: 10.1139/L09-088.

Ashmore, P. (2013) 'Morphology and dynamics of braided rivers', in Shroder, J. F., Wohl, E. (ed.) *Treatise on geomorphology*. San Diego: Academic Press, pp. 289–312.

Ashmore, P., Bertoldi, W. and Gardner, J. T. (2011) 'Active width of gravel-bed braided rivers', *Earth Surface Processes and Landforms*, 36(11), pp. 1510–1521. doi: 10.1002/esp.2182.

Ashraf, M., Bhatti, M. T. and Shakir, A. S. (2016) 'River bank erosion and channel evolution in sand-bed braided reach of River Chenab: role of floods during different flow regimes', *Arabian Journal of Geosciences*, 9(2), pp. 1–10. doi: 10.1007/s12517-015-2114-y.

Ashworth, P. J. *et al.* (1994) 'The physical modelling of braided rivers and deposition of fine-grained sediment', in Kirkby, M. J. (ed.) *Process models and theoretical geomorphology,*. John Wiley & Sons, Ltd, pp. 115–139.

Ashworth, P. J. (1996) 'Mid-Channel Bar Growth and its Relationship to Local Flow Strength and Direction', 21, pp. 103–123. doi: 10.1002/(SICI)1096-9837(199602)21:2<103::AID-ESP569>3.0.CO;2-O.

Ashworth, P. J. *et al.* (2011) 'Evolution and sedimentology of a channel fill in the sandy braided South Saskatchewan River and its comparison to the deposits of an adjacent compound bar', *Sedimentology*, 58, pp. 1860–1883. doi: 10.1111/j.1365-3091.2011.01242.x.

Ashworth, P. J., Best, J. L. and Bristow, C. S. (2000) 'Morphological evolution and dynamics of a large, sand braid-bar, Jamuna River, Bangladesh', *Sedimentology*, 47, pp. 533–555. doi: 10.1046/j.1365-3091.2000.00305.x.

Ashworth, P. J., Best, J. L. and Jones, M. A. (2007) 'The relationship between channel avulsion, flow occupancy and aggradation in braided rivers: Insights from an experimental model', *Sedimentology*, 54, pp. 497–513. doi: 10.1111/j.1365-3091.2006.00845.x.

Ashworth, P. J. and Ferguson, R. I. (1986) 'Interrelationships of Channel Processes, Changes and Sediments in a Proglacial Braided River', *Geografiska Annaler. Series A, Physical Geography*. Taylor & Francis, Ltd.Swedish Society for Anthropology and Geography, 68(4), p. 361. doi: 10.2307/521527.

Bagnold, R. A. (1935) 'The transport of sand by wind', *The Geographical Journal*, 89(5), pp. 409–438. doi: 10.2307/1774538.

Baki, A. B. M. and Gan, T. Y. (2012) 'Riverbank migration and island dynamics of the braided Jamuna River of the Ganges-Brahmaputra basin using multi-temporal Landsat images', *Quaternary International*. Elsevier Ltd and INQUA, 263, pp. 148–161. doi: 10.1016/j.quaint.2012.03.016.

Bar-Yam, Y. and Epstein, I. R. (2004) 'Response of complex networks to stimuli.', *Proceedings of the National Academy of Sciences of the United States of America*, 101(13), pp. 4341–4345. doi: 10.1073/pnas.0400673101.

Barabási, A.-L. and Albert, R. (1999) 'Emergence of Scaling in Random Networks', *Science*, 286(5439), pp. 509–512.

Barrat, A., Barthelemy, M. and Vespignani, A. (2013) *Dynamical processes on complex networks*. Cambridge, UK: Cambridge University Press.

Barrat, A., Barthélemy, M. and Vespignani, A. (2004) 'Weighted evolving networks: Coupling topology and weight dynamics', *Physical Review Letters*, 92(22), pp. 228701–1. doi: 10.1103/PhysRevLett.92.228701.

Barthélemy, M. (2011) 'Spatial networks', *Physics Reports*. Elsevier B.V., 499(1–3), pp. 1–101. doi: 10.1016/j.physrep.2010.11.002.

Beauguitte, L. and Ducruet, C. (2011) 'Scale-free and small-world networks in geographical research: A critical examination', in *17th European Colloquium on Theoretical and Quantitative Geography*. Athens, pp. 663–671.

Belletti, B., Dufour, S. and Piégay, H. (2015) 'What is the relative effect of space and time to explain the braided river width and island patterns at a regional scale?', *River Research and Applications*, 31(1), pp. 1–15. doi: 10.1002/rra.2714.

van den Berg, J. H. (1995) 'Prediction of alluvial channel pattern of perennial rivers', *Geomorphology*, 12(4), pp. 259–279. doi: 10.1016/0169-555X(95)00014-V.

Berger, M. *et al.* (2012) 'ESA's sentinel missions in support of Earth system science', *Remote Sensing of Environment*. Elsevier Inc., 120, pp. 84–90. doi: 10.1016/j.rse.2011.07.023.

Von Bertalanffy, L. (1950) 'An outline of general system theory.', *British Journal for the Philosophy of science*, 1, pp. 134–165. doi: 10.1093/bjps/I.2.134.

Bertoldi, W., Gurnell, A., *et al.* (2009) 'Understanding reference processes: Linkages between river flows, sediment dynamics and vegetated landforms along the Tagliamento River, Italy', *River Research and Applications*, 25(5), pp. 501–516.

Bertoldi, W. (2012) 'Life of a bifurcation in a gravel-bed braided river', *Earth Surface Processes and Landforms*, 37(12), pp. 1327–1336. doi: 10.1002/esp.3279.

Bertoldi, W. *et al.* (2014) 'A flume experiment on wood storage and remobilization in braided river systems', *Earth Surface Processes and Landforms*, 39, pp. 804–813. doi: 10.1002/esp.3537.

Bertoldi, W., Ashmore, P. and Tubino, M. (2009) 'A method for estimating the mean bed load flux in braided rivers', *Geomorphology*. Elsevier B.V., 103, pp. 330–340. doi: 10.1016/j.geomorph.2008.06.014.

Bertoldi, W., Drake, N. A. and Gurnell, A. M. (2011) 'Interactions between river flows and colonizing vegetation on a braided river: Exploring spatial and temporal dynamics in riparian vegetation cover using satellite data', *Earth Surface Processes and Landforms*, 36(11), pp. 1474–1486. doi: 10.1002/esp.2166.

Bertoldi, W., Gurnell, A. M. and Drake, N. A. (2011) 'The topographic signature of vegetation development along a braided river: Results of a combined analysis of airborne lidar, color air photographs, and ground measurements', *Water Resources Research*, 47(6), pp. 1–13. doi: 10.1029/2010WR010319.

Bertoldi, W. and Tubino, M. (2007) 'River bifurcations: Experimental observations on equilibrium configurations', *Water Resources Research*, 43(10), pp. 1–10. doi: 10.1029/2007WR005907.

Bertoldi, W., Zanoni, L. and Tubino, M. (2009) 'Planform dynamics of braided streams', *Earth Surface Processes and Landforms*. John Wiley & Sons, Ltd, 34(4), pp. 547–557. doi: 10.1002/esp.1755.

Bertoldi, W., Zanoni, L. and Tubino, M. (2010) 'Assessment of morphological changes induced by flow and flood pulses in a gravel bed braided river: The Tagliamento River (Italy)', *Geomorphology*. Elsevier B.V., 114, pp. 348–360. doi: 10.1016/j.geomorph.2009.07.017.

Best, J. L. *et al.* (2003) 'Three-Dimensional Sedimentary Architecture of a Large, Mid-Channel Sand Braid Bar, Jamuna River, Bangladesh', *Journal of Sedimentary Research*, 73, pp. 516–530. doi: 10.1306/010603730516.

Best, J. L. and Roy, A. G. (1991) 'Mixing-layer distortion at the confluence of channels of different depth', *Nature*, 350, pp. 411–413. doi: 10.1038/350411a0.

Beygelzimer, A. *et al.* (2005) 'Improving network robustness by edge modification', *Physica A: Statistical Mechanics and its Applications*, 357(3–4), pp. 593–612. doi: 10.1016/j.physa.2005.03.040.

Binicewicz, F. Z. M. *et al.* (2016) 'Graph analysis of the anatomical network organization of the hippocampal formation and parahippocampal region in the rat', *Brain Structure and Function*. Springer Berlin Heidelberg, 221(3), pp. 1607–1621. doi: 10.1007/s00429-015-0992-0.

Blaschke, T. (2010) 'Object based image analysis for remote sensing', *ISPRS Journal of Photogrammetry and Remote Sensing*. Elsevier B.V., 65(1), pp. 2–16. doi: 10.1016/j.isprsjprs.2009.06.004.

Blaschke, T. *et al.* (2014) 'Geographic object-based image analysis–towards a new paradigm', *ISPRS Journal of Photogrammetry and Remote Sensing*. International Society for Photogrammetry and Remote Sensing, Inc. (ISPRS), 87, pp. 180–191. doi: 10.1016/j.isprsjprs.2013.09.014.

Boccaletti, S. *et al.* (2006) 'Complex networks: Structure and dynamics', *Physics Reports*, 424(4–5), pp. 175–308. doi: 10.1016/j.physrep.2005.10.009.

Bolla Pittaluga, M., Repetto, R. and Tubino, M. (2003) 'Channel bifurcation in braided rivers: Equilibrium configurations and stability', *Water Resources Research*, 39(3), pp. 1–13. doi: 10.1029/2001WR001112.

Boulding, K. (1956) 'General systems theory - the skeleton of science', *Management science*, 2(3), pp. 197–208.

Bracken, L. J. *et al.* (2013) 'Concepts of hydrological connectivity: Research approaches, pathways and future agendas', *Earth-Science Reviews*. Elsevier B.V., 119, pp. 17–34. doi: 10.1016/j.earscirev.2013.02.001.

Bracken, L. J. and Croke, J. (2007) 'The concept of hydrological connectivity and its contribution to understanding runoff-dominated geomorphic systems', *Hydrological Processes*, 21(13), pp. 1749–1763. doi: 10.1002/hyp.6313.

Brasington, J., Langham, J. and Rumsby, B. (2003) 'Methodological sensitivity of morphometric estimates of coarse fluvial sediment transport', *Geomorphology*, 53, pp. 299–316. doi: 10.1016/S0169-555X(02)00320-3.

Brasington, J. and Richards, K. (2007) 'Reduced-complexity, physically-based geomorphological modelling for catchment and river management', *Geomorphology*, 90(3–4), pp. 171–177. doi: 10.1016/j.geomorph.2006.10.028.

Brasington, J., Vericat, D. and Rychkov, I. (2012) 'Modeling river bed morphology, roughness, and surface sedimentology using high resolution terrestrial laser scanning', *Water Resources Research*, 48, pp. 1–18. doi: 10.1029/2012WR012223.

Bravard, J. (2010) 'Discontinuities in braided patterns: The River Rhône from Geneva to the Camargue delta before river training', *Geomorphology*. Elsevier B.V., 117(3–4), pp. 219–233. doi: 10.1016/j.geomorph.2009.01.020.

Bristow, C. S. (1987) 'Brahmaputra River: Channel Migration and Deposition', *Recent Developments in Fluvial Sedimentology*, (SP39), pp. 63–74. doi: 10.2110/pec.87.39.0063.

Bristow, C. S. and Best, J. L. (1993) 'Braided rivers: perspectives and problems', in Best, J. L. and Bristow, C. S. (eds) *Geological Society, London, Special Publications*. Geological Society London Special Publication, pp. 1–11. doi: 10.1144/GSL.SP.1993.075.01.01.

Brown, H. I. (1996) 'The methodological roles of theory in science', in *The Scientific Nature of Geomorphology; Proceedings of the 27th Binghampaton Symposium in Geomorphology, 27-29 September*, pp. 3–20.

Buhl, J. *et al.* (2004) 'Efficiency and robustness in ant networks of galleries', *European Physical Journal B*, 42, pp. 123–129. doi: 10.1140/epjb/e2004-00364-9.

Bullmore, E. T., Sporns, O. and Solla, S. A. (2009) 'Complex brain networks: graph theoretical analysis of structural and functional systems.', *Nature reviews. Neuroscience*, 10(3), pp. 186–98. doi: 10.1038/nrn2575.

Burton, I. (1963) 'THE QUANTITATIVE REVOLUTION AND THEORETICAL GEOGRAPHY', *The Canadian Geographer/Le Géographe canadien*. Wiley/Blackwell (10.1111), 7(4), pp. 151–162. doi: 10.1111/j.1541-0064.1963.tb00796.x.

Cabral, J. *et al.* (2011) 'Role of local network oscillations in resting-state functional connectivity', *NeuroImage*. Elsevier Inc., 57(1), pp. 130–139. doi: 10.1016/j.neuroimage.2011.04.010.

Cardillo, A. *et al.* (2006) 'Structural properties of planar graphs of urban street patterns', *Physical Review E - Statistical, Nonlinear, and Soft Matter Physics*, 73(6), pp. 1–8. doi: 10.1103/PhysRevE.73.066107.

Charlton, R. (2010) 'Channel form And behaviour', in *Fundamentals of Fluvial Geomorphology*.

Oxford, pp. 117–156.

Chavez, M. *et al.* (2010) 'Functional modularity of background activities in normal and epileptic brain networks', *Physical Review Letters*, 104(11), pp. 1–4. doi: 10.1103/PhysRevLett.104.118701.

Chen, Q. C. Q. *et al.* (2002) 'The origin of power laws in Internet topologies revisited', *Proceedings.Twenty-First Annual Joint Conference of the IEEE Computer and Communications Societies*, 2(c), pp. 608–617. doi: 10.1109/INFCOM.2002.1019306.

Chorley, R. (1962) 'Geomorphology and general systems theory', *Geological Survey Professional Paper 500-B*, pp. 1–9.

Church, M. (2006) 'Bed Material Transport and the Morphology of Alluvial River Channels', *Annual Review of Earth and Planetary Sciences*, 34(1), pp. 325–354. doi: 10.1146/annurev.earth.33.092203.122721.

Church, M. (2010) 'The trajectory of geomorphology', *Progress in Physical Geography*, 34(3), pp. 265–286. doi: 10.1080/00343404.2010.509128.

Church, M. and Ferguson, R. I. (2015) 'Morphodynamics: Rivers beyond steady state', *Water Resources Research*, 51(4), pp. 1883–1897. doi: 10.1002/2014WR016862.

Congalton, R. G. (1991) 'A review of assessing the accuracy of classifications of remotely sensed data', *Remote Sensing of Environment*, 37, pp. 35–46. doi: 10.1016/0034-4257(91)90048-B.

Connor-Streich, G. *et al.* (2018) 'Let's get connected: A new graph theory-based approach and toolbox for understanding braided river morphodynamics', *Wiley Interdisciplinary Reviews: Water*, 5, p. e1296. doi: 10.1002/wat2.1296.

Corenblit, D. *et al.* (2014) 'The biogeomorphological life cycle of poplars during the fluvial biogeomorphological succession: A special focus on Populus nigra L.', *Earth Surface Processes and Landforms*, 39(4), pp. 546–563. doi: 10.1002/esp.3515.

Coulthard, T. J. (2005) 'Effects of vegetation on braided stream pattern and dynamics', *Water Resources Research*, 41, pp. 1–10. doi: 10.1029/2004WR003201.

Crosato, A. and Saleh, M. S. (2011) 'Numerical study on the effects of floodplain vegetation on river planform style', *Earth Surface Processes and Landforms*, 36(6), pp. 711–720. doi: 10.1002/esp.2088.

Csárdi, G. and Nepusz, T. (2006) 'The igraph software package for complex network research', *InterJournal, Complex Systems*, 1695.

Czuba, J. A. and Foufoula-Georgiou, E. (2014) 'A network-based framework for identifying potential synchronizations and amplifications of sediment delivery in river basins', *Water Resources Research*, 50, pp. 3826–3851. doi: 10.1002/ 2013WR014227.

Czuba, J. A. and Foufoula-Georgiou, E. (2015) 'Dynamic connectivity in a fluvial network for identifying hotspots of geomorphic change', *Water Resources Research*, 51(3), pp. 1401–1421. doi: 10.1002/2014WR016139.

Dade, W. B. (2000) 'Grain size, sediment transport and alluvial channel pattern', *Geomorphology*, 35(1–2), pp. 119–126. doi: 10.1016/S0169-555X(00)00030-1.

Davies, T. *et al.* (2013) 'Recent behaviour and sustainable future management of the Waiho River, Westland, New Zealand', *Journal of Hydrology (NZ)*, 52, pp. 27–42.

Davis, W. (1899) 'The geographical cycle', *The Geographical Journal*, 14(5), pp. 481–504.

Demarchi, L., Bizzi, S. and Piégay, H. (2016) 'Hierarchical object-based mapping of riverscape units and in-stream mesohabitats using lidar and VHR imagery', *Remote Sensing*, 8(2). doi: 10.3390/rs8020097.

Demarchi, L., Bizzi, S. and Piégay, H. (2017) 'Regional hydromorphological characterization with continuous and automated remote sensing analysis based on VHR imagery and low-resolution LiDAR data', *Earth Surface Processes and Landforms*, 42(3), pp. 531–551. doi: 10.1002/esp.4092.

Dewan, A. *et al.* (2017) 'Assessing channel changes of the Ganges-Padma River system in Bangladesh using Landsat and hydrological data', *Geomorphology*, 276, pp. 257–279. doi: 10.1016/j.geomorph.2016.10.017.

Dixon, S. J. *et al.* (2018) 'The planform mobility of river channel confluences: Insights from analysis of remotely sensed imagery', *Earth-Science Reviews*, 176, pp. 1–18. doi: 10.1016/j.earscirev.2017.09.009.

Doeschl-Wilson, A. B. and Ashmore, P. E. (2005) 'Assessing a numerical cellular braided-stream model with a physical model', *Earth Surface Processes and Landforms*, 30(5), pp. 519–540. doi: 10.1002/esp.1146.

Edmonds, D. A. *et al.* (2011) 'Quantitative metrics that describe river deltas and their channel networks', *Journal of Geophysical Research: Earth Surface*, 116(4), pp. 1–15. doi: 10.1029/2010JF001955.

EEA (2014) *EU-DEM Statistical Validation*. Copenhagen. Available at: https://land.copernicus.eu/user-corner/technical-library/eu-dem-v1.0 (Accessed: 4 January 2019).

Egozi, R. and Ashmore, P. (2008) 'Defining and measuring braiding intensity', *Earth Surface Processes and Landforms*, 2138(14), pp. 2121–2138. doi: 10.1002/esp.

Egozi, R. and Ashmore, P. (2009) 'Experimental analysis of braided channel pattern response to increased discharge', *Journal of Geophysical Research*, 114, pp. 5183–5205. doi: 10.1029/2008JF001099.

Engelund, F. and Skovgaard, O. (1973) 'On the origin of meandering and braiding in alluvial streams', *Journal of Fluid Mechanics*, 57(2), pp. 289–302. doi: 10.1017/S0022112073001163.

ESA (2017) *Copernicus Open Access Hub*. Available at: https://scihub.copernicus.eu/ (Accessed: 31 October 2017).

ESRI Inc. (2016) *Coverage topology—Help | ArcGIS for Desktop*. Available at: http://desktop.arcgis.com/en/arcmap/10.3/manage-data/coverages/coverage-topology.htm (Accessed: 19 February 2018).

Faloutsos, M., Faloutsos, P. and Faloutsos, C. (1999) 'On Power-Law Relationships of the Internet Topology', *ACM SIGCOMM computer communication review*, 29(4), pp. 251–262.

Federici, B. and Paola, C. (2003) 'Dynamics of channel bifurcations in noncohesive sediments', *Water Resources Research*, 39(6). doi: 10.1029/2002WR001434.

Ferguson, R. I. (1993) 'Understanding braiding processes in gravel-bed rivers: progress and unsolved problems', in Best, J. L. and Bristow, C. S. (eds) *Braided Rivers*. Geological Society London Special Publication, pp. 73–87. doi: 10.1144/GSL.SP.1993.075.01.03.

Feyisa, G. L. *et al.* (2014) 'Automated Water Extraction Index: A new technique for surface water mapping using Landsat imagery', *Remote Sensing of Environment*. Elsevier Inc., 140, pp. 23–35. doi: 10.1016/j.rse.2013.08.029.

Fotherby, L. M. (2009) 'Valley confinement as a factor of braided river pattern for the Platte River', *Geomorphology*. Elsevier B.V., 103(4), pp. 562–576. doi: 10.1016/j.geomorph.2008.08.001.

Freeman, L. C. (1977) 'A Set of Measures of Centrality Based on Betweenness', *Sociometry*, 40, p. 35. doi: 10.2307/3033543.

Friend, P. F. and Sinha, R. (1993) 'Braiding and meandering parameters', *Geological Society, London, Special Publications*, 75, pp. 105–111. doi: 10.1144/GSL.SP.1993.075.01.05.

Garambois, P. A. *et al.* (2017) 'Hydraulic visibility: Using satellite altimetry to parameterize a hydraulic model of an ungauged reach of a braided river', *Hydrological Processes*, 31, pp. 756–767. doi: 10.1002/hyp.11033.

Garcia Lugo, G. A. *et al.* (2015) 'The effect of lateral confinement on gravel bed river morphology', *Water Resources Research*, 51(9), pp. 7145–7158. doi: 10.1002/2015WR017081.

Getis, A. and Ord, J. K. (1992) 'The Analysis of Spatial Association', *Geographical Analysis*, 24, pp. 189–206. doi: 10.1111/j.1538-4632.1992.tb00261.x.

Gilbert, G. K. (1877) *Report on the geology of the henry mountains*.

Gilbert, G. K. (1895) 'Sedimentary measurement of Cretaceous time', *The Journal of Geology*, 3(2), pp. 121–127.

Girvan, M. and Newman, M. E. J. (2002) 'Community structure in social and biological networks.', *Proceedings of the National Academy of Sciences of the United States of America*, 99(12), pp. 7821–6. doi: 10.1073/pnas.122653799.

Gran, K. and Paola, C. (2001) 'Riparian vegetation controls on braided stream dynamics', *Water Resources Research*, 37(12), pp. 3275–3283. doi: 10.5194/esurf-3-577-2015.

Gumpertz, M. L., Wu, C.-T. and Pye, J. M. (2000) 'Logistic regression for southern pine beetle outbreaks with spatial and temporal autocorrelation', *Forest Science*, 46, pp. 95–107.

Gupta, N., Atkinson, P. M. and Carling, P. A. (2013) 'Decadal length changes in the fluvial planform of the River Ganga: Bringing a mega-river to life with Landsat archives', *Remote Sensing Letters*, 4, pp. 1–9. doi: 10.1080/2150704X.2012.682658.

Gurnell, A. M. *et al.* (2000) 'Wood storage within the active zone of a large European gravel-bed river', *Geomorphology*, 34, pp. 55–72.

Gurnell, A. M. *et al.* (2001) 'Riparian vegetation and island formation along the gravel-bed Fiume Tagliamento, Italy', *Earth Surface Processes and Landforms*. John Wiley & Sons, Ltd., 26(1), pp. 31–62. doi: 10.1002/1096-9837(200101)26:1<31::AID-ESP155>3.0.CO;2-Y.

Gurnell, A. M., Blackall, T. D. and Petts, G. E. (2008) 'Characteristics of freshly deposited sand and finer sediments along an island-braided, gravel-bed river: The roles of water, wind and trees', *Geomorphology*, 99(1–4), pp. 254–269. doi: 10.1016/j.geomorph.2007.11.009.

Gurnell, A. and Petts, G. (2006) 'Trees as riparian engineers: the Tagliamento river, Italy', *Earth Surface Processes and Landforms*. John Wiley & Sons, Ltd, 31(12), pp. 1558–1574. doi: 10.1002/esp.1342.

Gurnell, A., Surian, N. and Zanoni, L. (2009) 'Multi-thread river channels: A perspective on

changing European alpine river systems', *Aquatic Sciences*, 71, pp. 253–265. doi: 10.1007/s00027-009-9186-2.

Hardy, R. J., Lane, S. N. and Yu, D. (2011) 'Flow structures at an idealized bifurcation: A numerical experiment', *Earth Surface Processes and Landforms*, 36(15), pp. 2083–2096. doi: 10.1002/esp.2235.

Harvey, G. L. and Clifford, N. J. (2009) 'Microscale hydrodynamics and coherent flow structures in rivers: Implications for the characterization of physical habitat', *River Research and Applications*, 25(2), pp. 160–180. doi: 10.1002/rra.1109.

Heckmann, T. *et al.* (2018) 'Indices of sediment connectivity: opportunities, challenges and limitations', *Earth-Science Reviews*. Elsevier, 187, pp. 77–108. doi: 10.1016/J.EARSCIREV.2018.08.004.

Heckmann, T. and Schwanghart, W. (2013) 'Geomorphic coupling and sediment connectivity in an alpine catchment - Exploring sediment cascades using graph theory', *Geomorphology*. Elsevier B.V., 182, pp. 89–103. doi: 10.1016/j.geomorph.2012.10.033.

Heckmann, T., Schwanghart, W. and Phillips, J. D. (2015) 'Graph theory—Recent developments of its application in geomorphology', *Geomorphology*. Elsevier B.V., 243, pp. 130–146. doi: 10.1016/j.geomorph.2014.12.024.

Henshaw, A. J. *et al.* (2013) 'An assessment of the degree to which Landsat TM data can support the assessment of fluvial dynamics, as revealed by changes in vegetation extent and channel position, along a large river', *Geomorphology*. Elsevier B.V., 202, pp. 74–85. doi: 10.1016/j.geomorph.2013.01.011.

Hernandez, J. M. and Van Mieghem, P. (2011) 'Classification of graph metrics', *Delft University of Technology: Mekelweg, The Netherlands*, pp. 1–20.

Herrera, M., Abraham, E. and Stoianov, I. (2016) 'A Graph-Theoretic Framework for Assessing the Resilience of Sectorised Water Distribution Networks', *Water Resources Management*, 30, pp. 1685–1699. doi: 10.1007/s11269-016-1245-6.

van den Heuvel, M. P. *et al.* (2012) 'High-cost, high-capacity backbone for global brain communication', *Proceedings of the National Academy of Sciences of the United States of America*, 109, pp. 11372–11377. doi: 10.1073/pnas.1203593109.

Hong, L. B. and Davies, T. R. H. (1979) 'A study of stream braiding', *Bulletin of the Geological Society of America*, 90(Part II), pp. 1839–1859. doi: 10.1130/GSAB-P2-90-1839.

Horton, R. (1945) 'Erosional development of streams and their drainage basins; hydrophysical approach to quantitative morphology', *Geological society of America bulletin*, 56(3), pp. 275–370.

Howard, A. D., Keetch, M. E. and Vincent, C. L. (1970) 'Topological and Geometrical Properties of Braided Streams', *Water Resources Research*, 6(6), pp. 1674–1688. doi: 10.1029/WR006i006p01674.

Huggett, R. J. (1988) 'Dissipative systems: implications for geomorphology', *Earth Surface Processes and Landforms*, 13(1), pp. 45–49. doi: 10.1002/esp.3290130107.

Hundey, E. J. and Ashmore, P. E. (2009) 'Length scale of braided river morphology', *Water Resources Research*, 45, pp. 1–9. doi: 10.1136/acupmed-2015-011012.

Isikdogan, F., Bovik, A. and Passalacqua, P. (2015) 'Automatic Channel Network Extraction From Remotely Sensed Images by Singularity Analysis', *IEEE Geoscience and Remote Sensing*

Letters, 12, pp. 2218–2221. doi: 10.1109/LGRS.2015.2458898.

Isikdogan, F., Bovik, A. and Passalacqua, P. (2017) 'RivaMap: An automated river analysis and mapping engine', *Remote Sensing of Environment*. Elsevier Inc., 202, pp. 88–97. doi: 10.1016/j.rse.2017.03.044.

Isikdogan, F., Bovik, A. and Passalacqua, P. (2018) 'Learning a River Network Extractor Using an Adaptive Loss Function', *IEEE Geoscience and Remote Sensing Letters*, 15(6), pp. 813–817. doi: 10.1109/LGRS.2018.2811754.

Jarriel, T. *et al.* (no date) 'Automatic extraction of distributary networks and their variation through time', *Journal of Geophysical Research - Earth Surface*.

Jasiewicz, J. and Stepinski, T. F. (2013) 'Geomorphons-a pattern recognition approach to classification and mapping of landforms', *Geomorphology*, 182, pp. 147–156. doi: 10.1016/j.geomorph.2012.11.005.

Jenelius, E. (2009) 'Network structure and travel patterns: explaining the geographical disparities of road network vulnerability', *Journal of Transport Geography*. Elsevier Ltd, 17(3), pp. 234–244. doi: 10.1016/j.jtrangeo.2008.06.002.

Kasprak, A. *et al.* (2015) 'The relationship between particle travel distance and channel morphology: Results from physical models of braided rivers', *Journal of Geophysical Research F: Earth Surface*, 120(1), pp. 55–74. doi: 10.1002/2014JF003310.

Kidová, A., Lehotský, M. and Rusnák, M. (2016) 'Geomorphic diversity in the braided-wandering Belá River, Slovak Carpathians, as a response to flood variability and environmental changes', *Geomorphology*, 272, pp. 137–149. doi: 10.1016/j.geomorph.2016.01.002.

Kim, Y., Chen, Y. S. and Linderman, K. (2015) 'Supply network disruption and resilience: A network structural perspective', *Journal of Operations Management*. Elsevier B.V., 33–34, pp. 43–59. doi: 10.1016/j.jom.2014.10.006.

Kleinhans, M. G. *et al.* (2008) 'Bifurcation dynamics and avulsion duration in meandering rivers by one-dimensional and three-dimensional models', *Water Resources Research*, 44(8), pp. 1–31. doi: 10.1029/2007WR005912.

Kleinhans, M. G. (2010) 'Sorting out river channel patterns', *Progress in Physical Geography*, 34, pp. 287–326. doi: 10.1177/0309133310365300.

Kleinhans, M. G. *et al.* (2013) 'Splitting rivers at their seams: Bifurcations and avulsion', *Earth Surface Processes and Landforms*, 38(1), pp. 47–61. doi: 10.1002/esp.3268.

Kleinhans, M. G. *et al.* (2015) 'Swiftness of biomorphodynamics in Lilliput- to Giant-sized rivers and deltas', *Geomorphology*. Elsevier B.V., 244, pp. 56–73. doi: 10.1016/j.geomorph.2015.04.022.

Kleinhans, M. G. and van den Berg, J. H. (2011) 'River channel and bar patterns explained and predicted by an empirical and a physics-based method', *Earth Surface Processes and Landforms*, 36(6), pp. 721–738. doi: 10.1002/esp.2090.

Knighton, D. (1998) *Fluvial Forms and Processes: A New Perspective*. Routledge.

Kollmann, J. *et al.* (1999) 'Interactions between vegetation development and island formation in the Alpine river Tagliamento', *Applied Vegetation Science*, 2(1), pp. 25–36. doi: 10.2307/1478878.

Kressler, F. P., Steinnocher, K. and Franzen, M. (2005) 'Object-oriented classification of

orthophotos to support update of spatial databases', *International Geoscience and Remote Sensing Symposium (IGARSS)*, 1(C), pp. 253–256. doi: 10.1109/IGARSS.2005.1526155.

Kühnert, C., Helbing, D. and West, G. B. (2006) 'Scaling laws in urban supply networks', *Physica A: Statistical Mechanics and its Applications*, 363(1), pp. 96–103. doi: 10.1016/j.physa.2006.01.058.

Labov, W. (1972) 'Some principles of linguistic methodology', *Language in Society*. Cambridge University Press, 1(01), p. 97. doi: 10.1017/S0047404500006576.

Lämmer, S., Gehlsen, B. and Helbing, D. (2006) 'Scaling laws in the spatial structure of urban road networks', *Physica A: Statistical Mechanics and its Applications*, 363(1), pp. 89–95. doi: 10.1016/j.physa.2006.01.051.

Lane, S. N. and Richards, K. S. (1997) 'Linking river channel form and process: time, space and casuality revisited', *Earth Surface Process and Landforms*, 22(3), pp. 249–260.

Lane, S. N., Westaway, R. M. and Hicks, D. M. (2003) 'Estimation of erosion and deposition volumes in a large, gravel-bed, braided river using synoptic remote sensing', *Earth Surface Processes and Landforms*, 28, pp. 249–271. doi: 10.1002/esp.483.

Latora, V. and Marchiori, M. (2001) 'Efficient behavior of small-world networks.', *Physical review letters*, 87(19), p. 198701. doi: 10.1103/PhysRevLett.87.198701.

Leduc, P., Ashmore, P. and Gardner, J. T. (2015) 'Grain sorting in the morphological active layer of a braided river physical model', *Earth Surface Dynamics*, 3(4), pp. 577–585. doi: 10.5194/esurf-3-577-2015.

Lehotský, M. *et al.* (2018) 'Multitemporal assessment of coarse sediment connectivity along a braided-wandering river', *Land Degradation and Development*, 29(4), pp. 1249–1261. doi: 10.1002/ldr.2870.

Leopold, L. B. and Maddock, T. (1953) 'The Hydraulic Geomtry of Stream Channels and Some Physiographic Implications', *Geological Survey Professional Paper 252*, p. 57.

Leopold, L. B. and Wolman, M. G. (1957) 'River channel patterns: braided, meandering, and straight', *USGS Professional Paper*, p. 51.

Leopold, L. and Langbein, W. (1962) 'The concept of entropy in landscape evolution', *U.S. Geol. Survey Prof.*, (Paper 500-A), pp. A1–A20. doi: 10.1080/01426399808706533.

Lewin, J. and Brewer, P. A. (2001) 'Predicting channel patterns', *Geomorphology*, 40(3), pp. 329–339. doi: 10.1016/S0169-555X(01)00061-7.

Li, M. *et al.* (2014) 'A review of remote sensing image classification techniques: The role of Spatio-contextual information', *European Journal of Remote Sensing*, 47(1), pp. 389–411. doi: 10.5721/EuJRS20144723.

Liébault, F. *et al.* (2013) 'Long profile responses of alpine braided rivers in SE France', *River Research and Applications*, 29(10), pp. 1253–1266. doi: 10.1002/rra.2615.

Lillesand, T. M., Kiefer, R. W. and Chipman, J. W. (2008) *Remote sensing and image interpretation*. 7th edn. Hoboken, NJ, USA.

Lu, D. and Weng, Q. (2007) 'A survey of image classification methods and techniques for improving classification performance', *International Journal of Remote Sensing*, 28, pp. 823–870. doi: 10.1080/01431160600746456.

Luchi, R. *et al.* (2007) 'Monitoring and predicting channel change in a free-evolving, small

Alpine river: Ridanna Creek (North East Italy)', *Earth Surface Processes and Landforms*. John Wiley & Sons, Ltd., 32(14), pp. 2104–2119. doi: 10.1002/esp.1511.

Lunt, I. A., Bridge, J. S. and Tye, R. S. (2004) 'A quantitative, three-dimensional depositional model of gravelly braided rivers', *Sedimentology*. Wiley/Blackwell (10.1111), 51(3), pp. 377–414. doi: 10.1111/j.1365-3091.2004.00627.x.

Ma, L. *et al.* (2017) 'A review of supervised object-based land-cover image classification', *ISPRS Journal of Photogrammetry and Remote Sensing*. The Authors, 130, pp. 277–293. doi: 10.1016/j.isprsjprs.2017.06.001.

Mao, L. and Surian, N. (2010) 'Observations on sediment mobility in a large gravel-bed river', *Geomorphology*. Elsevier B.V., 114, pp. 326–337. doi: 10.1016/j.geomorph.2009.07.015.

Mardhiah, U., Rillig, M. C. and Gurnell, A. (2015) 'Reconstructing the development of sampled sites on fluvial island surfaces of the Tagliamento River, Italy, from historical sources', *Earth Surface Processes and Landforms*, 40(5), pp. 629–641. doi: 10.1002/esp.3658.

Marra, W. A. *et al.* (2014) 'Near-bed and surface flow division patterns in experimental river bifurcations', *Water Resources Research*, 50(2), pp. 1506–1530. doi: 10.1002/2013WR014215.

Marra, W. a (2010) *Dynamic Channel Network Extraction from Satellite Imagery of the Jamuna River*. Utrecht University.

Marra, W., Kleinhans, M. G. and Addink, E. A. (2013) 'Network concepts to describe channel importance and change in multichannel systems: test results for the Jamuna River, Bangladesh', *Earth Surface Processes and Landforms*, 39(6), pp. 766–778. doi: 10.1002/esp.3482.

Masek, J. G. *et al.* (2006) 'A Landsat Surface Reflectance Dataset for North America, 1990-2000', *IEEE Geoscience and Remote Sensing Letters*, 3, pp. 68–72. doi: 10.1109/LGRS.2005.857030.

Maslov, S., Sneppen, K. and Zaliznyak, A. (2004) 'Pattern Detection in Complex Networks: Correlation Profile of the Internet', *Physica A: Statistical Mechanics and its Applications*, 333, pp. 529–540. doi: 10.1016/j.physa.2003.06.002.

Masselink, R. J. H. *et al.* (2016) 'A network theory approach for a better understanding of overland flow connectivity', *Hydrological Processes*, 31, pp. 207–220. doi: 10.1002/hyp.10993.

McSaveney, E. (2015) *Landscapes – overview - Central South Island*, *Te Ara - the Encyclopedia of New Zealand*. Ministry for Culture and Heritage Te Manatu Taonga. Available at: https://teara.govt.nz/en/photograph/13049/waimakariri-river (Accessed: 7 February 2019).

Mertes, L. A. K. (2002) 'Remote sensing of riverine landscapes', *Freshwater Biology*. John Wiley & Sons, Ltd (10.1111), 47, pp. 799–816. doi: 10.1046/j.1365-2427.2002.00909.x.

Meyer, N. K. *et al.* (2015) 'Roads at risk: Traffic detours from debris flows in southern Norway', *Natural Hazards and Earth System Sciences*, 15, pp. 985–995. doi: 10.5194/nhess-15-985-2015.

Mountrakis, G., Im, J. and Ogole, C. (2011) 'Support vector machines in remote sensing: A review', *ISPRS Journal of Photogrammetry and Remote Sensing*. Elsevier B.V., 66(3), pp. 247–259. doi: 10.1016/j.isprsjprs.2010.11.001.

Mueller, E. R. and Pitlick, J. (2013) 'Sediment supply and channel morphology in mountain river systems: 1. Relative importance of lithology, topography, and climate', *Journal of Geophysical Research: Earth Surface*, 118(4), pp. 2325–2342. doi: 10.1002/2013JF002843.

Mueller, E. R. and Pitlick, J. (2014) 'Sediment supply and channel morphology in mountain river systems: 2. Single thread to braided transitions', *Journal of Geophysical Research: Earth Surface*, 119(7). doi: 10.1002/2013JF003045.

Murray, A. B. and Paola, C. (1994) 'A cellular model of braided rivers', *Nature*, 371(6492), pp. 54–57. doi: 10.1038/371054a0.

Murray, B. A. and Paola, C. (2003) 'Modelling the effect of vegetation on channel pattern in bedload rivers', *Earth Surface Processes and Landforms*, 28(2), pp. 131–143. doi: 10.1002/esp.428.

Van Der Nat, D. *et al.* (2002) 'Inundation Dynamics in Braided Floodplains: Tagliamento River, Northeast Italy', *Ecosystems*, 5, pp. 636–647. doi: 10.1007/s10021-002-0170-0.

Van Der Nat, D. *et al.* (2003) 'Habitat change in braided flood plains (Tagliamento, NE-Italy)', *Freshwater Biology*, 48(10), pp. 1799–1812. doi: 10.1046/j.1365-2427.2003.01126.x.

Newman, M. (2010) *Networks: An Introduction*. Oxford: OUP Oxford.

Newman, M. E. J. and Girvan, M. (2004) 'Finding and evaluating community structure in networks', *Physical review E*, (69), p. 026113. doi: 10.1103/PhysRevE.69.026113.

Nicholas, A. P. (2000) 'Modelling bedload yield braided gravel bed rivers', *Geomorphology*, 36, pp. 89–106. doi: 10.1016/S0169-555X(00)00050-7.

Nicosia, V., Vértes, P. E., *et al.* (2013) 'Phase transition in the economically modeled growth of a cellular nervous system.', *Proceedings of the National Academy of Sciences*, 110(19), pp. 7880–7885. doi: 10.1073/pnas.1300753110.

Nicosia, V., Valencia, M., *et al.* (2013) 'Remote synchronization reveals network symmetries and functional modules', *Physical Review Letters*, 110(17), pp. 1–5. doi: 10.1103/PhysRevLett.110.174102.

Otsu, N. (1979) 'A threshold selection method from gray-level histograms', *IEEE Transactions on Systems, Man, and Cybernetics*, 9, pp. 62–66.

Otukei, J. R. and Blaschke, T. (2010) 'Land cover change assessment using decision trees, support vector machines and maximum likelihood classification algorithms', *International Journal of Applied Earth Observation and Geoinformation*, 12(SUPPL. 1), pp. 27–31. doi: 10.1016/j.jag.2009.11.002.

Parker, C., Clifford, N. J. and Thorne, C. R. (2012) 'Automatic delineation of functional river reach boundaries for river research and applications', *River Research and Applications*. John Wiley & Sons, Ltd, 28, pp. 1708–1725. doi: 10.1002/rra.1568.

Passalacqua, P. *et al.* (2013) 'Geomorphic signatures of deltaic processes and vegetation: The Ganges-Brahmaputra-Jamuna case study', *Journal of Geophysical Research: Earth Surface*, 118(3), pp. 1838–1849. doi: 10.1002/jgrf.20128.

Passalacqua, P. (2017) 'The Delta Connectome : A network-based framework for studying connectivity in river deltas', *Geomorphology*. Elsevier B.V., 277, pp. 50–62. doi: 10.1016/j.geomorph.2016.04.001.

Peirce, S., Ashmore, P. and Leduc, P. (2018) 'The variability in the morphological active width: Results from physical models of gravel-bed braided rivers', *Earth Surface Processes and Landforms*, 43(11), pp. 2371–2383. doi: 10.1002/esp.4400.

Petts, G. E. *et al.* (2000) 'Longitudinal variations in exposed riverine sediments: a context for

the ecology of the Fiume Tagliamento, Italy', *Aquatic Conservation: Marine and Freshwater Ecosystems*. John Wiley & Sons, Ltd, 10(4), pp. 249–266. doi: 10.1002/1099-0755(200007/08)10:4<249::AID-AQC410>3.0.CO;2-R.

Phillips, J. D. (1992) 'Nonlinear dynamical systems in geomorphology: revolution or evolution?', *Geomorphology*, 5(3–5), pp. 219–229. doi: 10.1016/0169-555X(92)90005-9.

Phillips, J. D. (2011) 'Predicting modes of spatial change from state-and-transition models', *Ecological Modelling*, 222, pp. 475–484. doi: 10.1016/j.ecolmodel.2010.11.018.

Phillips, J. D. (2015) 'Badass geomorphology', *Earth Surface Processes and Landforms*, 40, pp. 22–33. doi: 10.1002/esp.3682.

Phillips, J. D., Schwanghart, W. and Heckmann, T. (2015) 'Graph theory in the geosciences', *Earth-Science Reviews*. Elsevier B.V., 143, pp. 147–160. doi: 10.1016/j.earscirev.2015.02.002.

Phiri, D. and Morgenroth, J. (2017) 'Developments in Landsat Land Cover Classification Methods : A Review', *Remote Sensing*, 9(967). doi: 10.3390/rs9090967.

Picco, L. *et al.* (2013) 'Evaluating short-term morphological changes in a gravel-bed braided river using terrestrial laser scanner', *Geomorphology*. Elsevier B.V., 201, pp. 323–334. doi: 10.1016/j.geomorph.2013.07.007.

Poulter, B., Goodall, J. L. and Halpin, P. N. (2008) 'Applications of network analysis for adaptive management of artificial drainage systems in landscapes vulnerable to sea level rise', *Journal of Hydrology*, 357, pp. 207–217. doi: 10.1016/j.jhydrol.2008.05.022.

R Core Team (2017) 'R: A language and environment for statistical computing.' R Foundation for Statistical Computing, Vienna, Austria. Available at: https://www.r-project.org/.

Redolfi, M. *et al.* (2016) 'Analysis of reach-scale elevation distribution in braided rivers: Definition of a new morphologic indicator and estimation of mean quantities', *Water Resources Research*. John Wiley & Sons, Ltd, 52(8), pp. 5951–5970. doi: 10.1002/2015WR017918.

Reid, H. E. *et al.* (2018) 'Geomorphological effectiveness of floods to rework gravel bars: insight from hyperscale topography and hydraulic modelling', *Earth Surface Processes and Landforms*. Wiley-Blackwell. doi: 10.1002/esp.4521.

Reitz, M. D. *et al.* (2014) 'Diffusive evolution of experimental braided rivers', *Physical Review E*, 89(5), pp. 1–6. doi: 10.1103/PhysRevE.89.052809.

Rhoads, L. (2006) 'The dynamic basis of geomorphology reenvisioned', *Annals of the Association of American Geographers*, 96(1), pp. 14–30.

Richardson, W. R. and Thorne, C. R. (2001) 'Multiple thread flow and channel bifurcation in a braided river: Brahmaputra-Jamuna River, Bangladesh', *Geomorphology*, 38(3–4), pp. 185–196. doi: 10.1016/S0169-555X(00)00080-5.

Rinderer, M., Ali, G. and Larsen, L. G. (2018) 'Assessing structural, functional and effective hydrologic connectivity with brain neuroscience methods: State-of-the-art and research directions', *Earth-Science Reviews*. Elsevier, 178, pp. 29–47. doi: 10.1016/j.earscirev.2018.01.009.

Robertson-Rintoul, M. S. E. and Richards, K. S. (1993) 'Braided-channel pattern and palaeohydrology using an index of total sinuosity', in Best, J. L. and Bristow, C. S. (eds) *Braided Rivers*. London: The Geological Society, pp. 113–118. doi: 10.1144/GSL.SP.1993.075.01.06.

Rodrigues, S. *et al.* (2007) 'In-channel woody vegetation controls on sedimentary processes and the sedimentary record within alluvial environments: A modern example of an anabranch of the River Loire, France', *Sedimentology*, 54(1), pp. 223–242. doi: 10.1111/j.1365-3091.2006.00832.x.

Rodriguez-Iturbe, I. *et al.* (1994) 'Self-organized river basin landscapes: Fractal and multifractal characteristics', *Water Resources Research*, 30(12), pp. 3531–3539. doi: 10.1029/94WR01493.

Rouse, J. W. *et al.* (1974) 'Monitoring vegetation systems in the Great Plains with ERTS', in *Third ERTS Symposium, NASA SP-351*. Washington, DC, pp. 309–317.

Roy, D. P. *et al.* (2014) 'Landsat-8: Science and product vision for terrestrial global change research', *Remote Sensing of Environment*. Elsevier B.V., 145, pp. 154–172. doi: 10.1016/j.rse.2014.02.001.

Roy, D. P. *et al.* (2016) 'Characterization of Landsat-7 to Landsat-8 reflective wavelength and normalized difference vegetation index continuity', *Remote Sensing of Environment*. The Authors, 185, pp. 57–70. doi: 10.1016/j.rse.2015.12.024.

Rubinov, M. and Sporns, O. (2010) 'Complex network measures of brain connectivity: Uses and interpretations', *NeuroImage*. Elsevier Inc., 52(3), pp. 1059–1069. doi: 10.1016/j.neuroimage.2009.10.003.

Sack, D. (2002) 'The educational value of the history of geomorphology', *Geomorphology*, 47(2–4), pp. 313–323. doi: 10.1016/S0169-555X(02)00091-0.

Sambrook Smith, G. H. *et al.* (2006) 'The sedimentology and alluvial architecture of the sandy braided South Saskatchewan River, Canada', *Sedimentology*, 53, pp. 413–434. doi: 10.1111/j.1365-3091.2005.00769.x.

Sapozhnikov, V. B. and Foufoula-Georgiou, E. (1997) 'Experimental evidence of dynamic scaling and indications of self-organized criticality in braided rivers', *Water Resources Research*, 33(8), pp. 1983–1991. doi: 10.1029/97WR01233.

Sapozhnikov, V. B. and Foufoula-Georgiou, E. (1999) 'Horizontal and vertical self-organization of braided rivers toward a critical state', *Water Resources Research*, 35(3), pp. 843–851. doi: 10.1029/98WR02744.

Sapozhnikov, V. and Foufoula-Georgiou, E. (1996) 'Self-affinity in braided rivers', *Water Resources Research*, 32(5), pp. 1429–1439. doi: 10.1029/96WR00490.

Sarker, M. H. *et al.* (2014) 'Morpho-dynamics of the Brahmaputra-Jamuna River, Bangladesh', *Geomorphology*. Elsevier B.V., 215, pp. 45–59. doi: 10.1016/j.geomorph.2013.07.025.

Sarker, M. H. and Thorne, C. R. (2006) 'Morphological Response of the Brahmaputra–Padma–Lower Meghna River System to the Assam Earthquake of 1950', in Sambrook Smith, G. H. *et al*. (eds) *Braided Rivers*. Oxford, UK: Blackwell Publishing Ltd., pp. 289–310. doi: 10.1002/9781444304374.ch14.

Schumm, S. A. and Lichty, R. W. (1965) 'Time, space, and causality in geomorphology', *American Journal of Science*, pp. 110–119. doi: 10.2475/ajs.263.2.110.

Schuurman, F. and Kleinhans, M. G. (2015) 'Bar dynamics and bifurcation evolution in a modelled braided sand-bed river', *Earth Surface Processes and Landforms*, 40(10), pp. 1318–1333. doi: 10.1002/esp.3722.

Schuurman, F., Kleinhans, M. G. and Middelkoop, H. (2016) 'Network response to disturbances in large sand-bed braided rivers', *Earth Surface Dynamics*, 4(1), pp. 25–45. doi: 10.5194/esurf-

4-25-2016.

Scott, D. M. *et al.* (2006) 'Network Robustness Index: A new method for identifying critical links and evaluating the performance of transportation networks', *Journal of Transport Geography*, 14(3), pp. 215–227. doi: 10.1016/j.jtrangeo.2005.10.003.

Sen, P. *et al.* (2003) 'Small-world properties of the Indian railway network', *Physical review E*, 67(3), p. 036106. doi: 10.1103/PhysRevE.67.036106.

Sendrowski, A. and Passalacqua, P. (2017) 'Process connectivity in a naturally prograding river delta', *Water Resources Research*. John Wiley & Sons, Ltd, 53(3), pp. 1841–1863. doi: 10.1002/2016WR019768.

Shen, X. *et al.* (2019) 'Near-real-time non-obstructed flood inundation mapping using synthetic aperture radar', *Remote Sensing of Environment*. Elsevier, 221, pp. 302–315. doi: 10.1016/j.rse.2018.11.008.

Smith, L. C. *et al.* (1995) 'Estimation of Discharge From Braided Glacial Rivers Using ERS 1 Synthetic Aperture Radar: First Results', *Water Resources Research*, 31, pp. 1325–1329. doi: 10.1029/95wr00145.

Smith, L. C. (1997) 'Satellite remote sensing of river inundation area, stage, and discharge: a review', *Hydrological Processes*, 11, pp. 1427–1439. doi: 10.1002/(SICI)1099-1085(199708)11:10<1427::AID-HYP473>3.0.CO;2-S.

Strahler, A. (1952a) 'Dynamic basis of geomorphology', *Geological Society of America Bulletin*, 63(9), pp. 923–938. doi: 10.1130/0016-7606(1952)63.

Strahler, A. (1952b) 'Hypsometric (area-altitude) analysis of erosional topography', *Geological Society of America Bulletin*, 63(11), pp. 1117–1142.

Strahler, A. (1957) 'Quantitative analysis of watershed geomorphology', *Eos, Transactions American Geophysical Union*, 38(6), pp. 913–920.

Strahler, A. N. (1950) 'Davis' Concepts of Slope Development Viewed in the Light of Recent Quantitative Investigations', *Annals of the Association of American Geographers*, 40(3), p. 209. doi: 10.2307/2561058.

Strano, E. *et al.* (2012) 'Elementary processes governing the evolution of road networks', *Scientific Reports*, 2, pp. 1–8. doi: 10.1038/srep00296.

Sullivan, J. L. *et al.* (2010) 'Identifying critical road segments and measuring system-wide robustness in transportation networks with isolating links: A link-based capacity-reduction approach', *Transportation Research Part A: Policy and Practice*. Elsevier Ltd, 44, pp. 323–336. doi: 10.1016/j.tra.2010.02.003.

Surian, N. (1999) 'Channel changes due to river regulation: the case of the Piave River, Italy', *Earth Surface Processes and Landforms*. John Wiley & Sons, Ltd., 24(12), pp. 1135–1151. doi: 10.1002/(SICI)1096-9837(199911)24:12<1135::AID-ESP40>3.0.CO;2-F.

Surian, N. *et al.* (2015) 'Vegetation turnover in a braided river: Frequency and effectiveness of floods of different magnitude', *Earth Surface Processes and Landforms*, 40, pp. 542–558. doi: 10.1002/esp.3660.

Surian, N. and Rinaldi, M. (2003) 'Morphological response to river engineering and management in alluvial channels in Italy', *Geomorphology*, 50, pp. 307–326. doi: 10.1016/S0169-555X(02)00219-2.

Szupiany, R. N. *et al.* (2009) 'Morphology, flow structure, and suspended bed sediment transport at two large braid-bar confluences', *Water Resources Research*, 45(5), pp. 1–19. doi: 10.1029/2008WR007428.

Takagi, T. *et al.* (2007) 'Channel braiding and stability of the Brahmaputra River, Bangladesh, since 1967: GIS and remote sensing analyses', *Geomorphology*, 85(3–4), pp. 294–305. doi: 10.1016/j.geomorph.2006.03.028.

Tang, J. *et al.* (2016) 'Estimating the most likely space-time paths, dwell times and path uncertainties from vehicle trajectory data: A time geographic method', *Transportation Research Part C: Emerging Technologies*. Elsevier Ltd, 66, pp. 176–194. doi: 10.1016/j.trc.2015.08.014.

Tejedor, A. *et al.* (2015a) 'Delta channel networks: 1. A graph-theoretic approach for studying connectivity and steady state transport on deltaic surfaces', *Water Resources Research*, 51(6), pp. 3998–4018. doi: 10.1002/2014WR016259.

Tejedor, A. *et al.* (2015b) 'Delta channel networks: 2. Metrics of topologic and dynamic complexity for delta comparison, physical inference, and vulnerability assessment', *Water Resources Research*. Blackwell Publishing Ltd, 51(6), pp. 4019–4045. doi: 10.1002/2014WR016604.

Tejedor, A. *et al.* (2017) 'Entropy and optimality in river deltas', *Proceedings of the National Academy of Sciences*, p. 201708404. doi: 10.1073/pnas.1708404114.

Tejedor, A. *et al.* (2018) 'Multiplex Networks: A Framework for Studying Multiprocess Multiscale Connectivity Via Coupled-Network Theory With an Application to River Deltas', *Geophysical Research Letters*, 45, pp. 9681–9689. doi: 10.1029/2018GL078355.

Thibaud, R. *et al.* (2013) 'A Spatio-temporal graph model for marine dune dynamics analysis and representation', *Transactions in GIS*, 17, pp. 742–762. doi: 10.1111/tgis.12006.

Thomas, R. E. *et al.* (2011) 'An experimental study of discharge partitioning and flow structure at symmetrical bifurcations', *Earth Surface Processes and Landforms*, 36, pp. 2069–2082. doi: 10.1002/esp.2231.

Thorne, C. R. and Soar, P. (1996) 'R. A. BAGNOLD: A BIOGRAPHY AND EXTENDED BIBLIOGRAPHY', *Earth Surface Processes and Landforms*. Wiley-Blackwell, 21(11), pp. 987–991. doi: 10.1002/(SICI)1096-9837(199611)21:11<987::AID-ESP699>3.0.CO;2-D.

Trigg, M. A. *et al.* (2012) 'Floodplain channel morphology and networks of the middle Amazon River', *Water Resources Research*, 48, pp. 1–17. doi: 10.1029/2012WR011888.

Tsonis, A. A., Swanson, K. L. and Roebber, P. J. (2006) 'What do networks have to do with climate?', *Bulletin of the American Meteorological Society*, 87(5), pp. 585–595. doi: 10.1175/BAMS-87-5-585.

Turnbull, L. *et al.* (2018) 'Connectivity and complex systems: learning from a multi-disciplinary perspective', *Applied Network Science*. Applied Network Science, 3, p. 11. doi: 10.1007/s41109-018-0067-2.

USGS (2017) *EarthExplorer*. Available at: https://earthexplorer.usgs.gov/ (Accessed: 31 October 2017).

Del Vicario, M. *et al.* (2016) 'The spreading of misinformation online', *Proceedings of the National Academy of Sciences*, 113(3), pp. 554–559. doi: 10.1073/pnas.1517441113.

Wagner, S. M. and Neshat, N. (2010) 'Assessing the vulnerability of supply chains using graph

theory', *International Journal of Production Economics*. Elsevier, 126, pp. 121–129. doi: 10.1016/j.ijpe.2009.10.007.

Watts, D. J. and Strogatz, S. H. (1998) 'Collective dynamics of "small-world" networks.', 393(6684), pp. 440–442. doi: 10.1038/30918.

Webb, E. K. (1995) 'Simulation of Braided Channel Topology and Topography', *Water Resources Research*, 31, pp. 2603–2611. doi: 10.1029/95WR01952.

Welber, M., Bertoldi, W. and Tubino, M. (2012) 'The response of braided planform configuration to flow variations, bed reworking and vegetation: the case of the Tagliamento River, Italy', *Earth Surface Processes and Landforms*, 37(5), pp. 572–582. doi: 10.1002/esp.3196.

Westoby, M. J. *et al.* (2012) '"Structure-from-Motion" photogrammetry: A low-cost, effective tool for geoscience applications', *Geomorphology*. Elsevier B.V., 179, pp. 300–314. doi: 10.1016/j.geomorph.2012.08.021.

Wheaton, J. M. *et al.* (2010) 'Accounting for uncertainty in DEMs from repeat topographic surveys: Improved sediment budgets', *Earth Surface Processes and Landforms*, 35, pp. 136–156. doi: 10.1002/esp.1886.

Wheaton, J. M. *et al.* (2013) 'Morphodynamic signatures of braiding mechanisms as expressed through change in sediment storage in a gravel-bed river', *Journal of Geophysical Research: Earth Surface*, 118(2), pp. 759–779. doi: 10.1002/jgrf.20060.

Williams, R. D. *et al.* (2013) 'Hydraulic validation of two-dimensional simulations of braided river flow with spatially continuous aDcp data', *Water Resources Research*, 49(9), pp. 5183–5205. doi: 10.1002/wrcr.20391.

Williams, R. D. *et al.* (2015) 'Linking the spatial distribution of bed load transport to morphological change during high-flow events in a shallow braided river', *Journal of Geophysical Research: Earth Surface*, 120, pp. 604–622. doi: 10.1002/2014JF003346.

Williams, R. D., Brasington, J. and Hicks, D. M. (2016) 'Numerical Modelling of Braided River Morphodynamics: Review and Future Challenges', *Geography Compass*, 10(3), pp. 102–127. doi: 10.1111/gec3.12260.

Wohl, E. *et al.* (2019) 'Connectivity as an emergent property of geomorphic systems', *Earth Surface Processes and Landforms*, 44, pp. 4–26. doi: 10.1002/esp.4434.

Wohl, E., Magilligan, F. J. and Rathbun, S. L. (2017) 'Introduction to the special issue: Connectivity in Geomorphology', *Geomorphology*. Elsevier B.V., 277, pp. 1–5. doi: 10.1016/j.geomorph.2016.11.005.

Woodcock, C. E. *et al.* (2008) 'Free Access to Landsat Imagery', *Science*, 320, pp. 1011–1012. doi: 10.1126/science.320.5879.1011a.

Wright, C. K. (2010) 'Spatiotemporal dynamics of prairie wetland networks : power-law scaling and implications for conservation planning Spatiotemporal of prairie wetland networks : dynamics and implications for conservation scaling planning', *Ecology*, 91, pp. 1924–1930.

Wu, X. *et al.* (2018) 'Response of the downstream braided channel to Zhikong Reservoir on Lhasa River', *Water*, 10, pp. 1–18. doi: 10.3390/w10091144.

Xu, H. (2006) 'Modification of normalised difference water index (NDWI) to enhance open water features in remotely sensed imagery', *International Journal of Remote Sensing*, 27(14), pp. 3025–3033. doi: 10.1080/01431160600589179.

Yang, H., Lin, B. and Zhou, J. (2015) 'Physics-based numerical modelling of large braided rivers dominated by suspended sediment', *Hydrological Processes*, 29(8), pp. 1925–1941. doi: 10.1002/hyp.10314.

Yang, K. *et al.* (2014) 'River delineation from remotely sensed imagery using a multi-scale classification approach', *Journal of selected topics in applied earth observations and remote sensing*, 7(12), pp. 4726–4737.

Young, W. J. and Warburton, J. (1996) 'Principles and practice of hudraulic modelling of braided gravel-bed rivers', *Journal of Hydrology (NZ)*, 35(2), pp. 175–198.

Zanoni, L. *et al.* (2008) 'Island dynamics in a braided river from analysis of historical maps and air photographs', *River Research and Applications*. John Wiley & Sons, Ltd., 24(8), pp. 1141–1159. doi: 10.1002/rra.1086.

Ziliani, L. *et al.* (2013) 'Reduced-complexity modeling of braided rivers: Assessing model performance by sensitivity analysis, calibration, and validation', *Journal of Geophysical Research: Earth Surface*, 118, pp. 2243–2262. doi: 10.1002/jgrf.20154.

Ziliani, L. and Surian, N. (2012) 'Evolutionary trajectory of channel morphology and controlling factors in a large gravel-bed river', *Geomorphology*. Elsevier B.V., 173, pp. 104–117. doi: 10.1016/j.geomorph.2012.06.001.